SILICON CARBIDE ALLOYS

A thesis submitted for the degree of

Doctor of Philosophy

of the University of Newcastle upon Tyne

by

Margaret MacDonald Patience, B.Sc.

The Crystallography Laboratory

Department of Metallurgy and Engineering Materials

University of Newcastle upon Tyne

September, 1983

Preface

This thesis describes original work which has not been submitted for a degree at any other university.

The investigations were carried out in the Crystallography Laboratory, Department of Metallurgy and Engineering Materials of the University of Newcastle upon Tyne during the period October 1979 to September 1982 under the supervision of Professor K.H. Jack F.R.S. and Dr D.P. Thompson.

The thesis describes (i) the structure of calcium α'-sialon and (ii) the formation of the 2H polytype of silicon carbide by alloying with nitrogen or with aluminium nitride. Scanning electron microscopy coupled with chemical analyses are used to characterize the prepared alloys. The mechanism of the 2H→3C transformation which occurs when 2H is heated at higher temperatures is deduced from high resolution electron microscopy observations and by use of lattice imaging techniques.

Acknowledgements

I wish to thank Professor K.H.Jack F.R.S. and Dr D.P.Thompson for many enlightening discussions, advice and encouragement during the supervision of this work.

I also thank:

The Science Research Council for the provision of a research studentship;

The technical staff of the electron-optic unit for assistance with scanning electron microscopy and chemical analysis;

Dr P. Ferguson for electron probe micro-analyses;

The technical staff of the Crystallography Laboratory;

Many colleagues, past and present, for stimulating discussion particularly Dr P. Korgul for his encouragement, help and advice in learning electron microscopy;

Mrs C.Ward and Mrs M.Walsh for typing the script.

I am also grateful to my parents for their continued support throughout my studies and last but not least to Gary for his patience and understanding during the last two years.

September, 1983

Abstract

Structure determination of a calcium α'-sialon containing 1.8 calcium atoms per unit cell shows that these atoms occupy the two large interstitial sites in the structure. The carbothermal reduction of α'-sialons results in silicon carbide-aluminium nitride alloys with the wurtzite-type structure. A more direct method of firing powder mixtures of silicon nitride, aluminium nitride, carbon and calcium oxide in the temperature range 1650-2100°C is explored. Phase relationships in the silicon carbide-aluminium nitride system have been determined up to 2100°C and contrary to previous reports there is a miscibility gap extending from about 40 m/o to 84 m/o aluminium nitride at 1800°C. 2H-SiC formed at the silicon carbide-rich end of the system by the reaction of silicon nitride with carbon at 1650°C contains up to 12 a/o nitrogen which stabilizes it relative to other polytypes. At higher temperatures, 2H transforms to 3C which is itself stabilized by nitrogen and, unlike nitrogen-free 3C, does not transform to 6H below 2100°C.

The phases produced by high-temperature reaction and heat-treatment are characterized by X-ray diffraction, scanning electron microscopy and chemical analysis. High resolution electron microscopy is used to examine structural details and particularly to follow the 2H→3C transformation in silicon carbide alloys.

CONTENTS

I. INTRODUCTION

I.1 High-temperature engineering ceramics

Research over the last ten years on high-performance materials has been concerned with those which can replace metals in high-temperature engineering applications. The decreasing supply of metals such as Cr, Co, Ni and Ti and the increasing emphasis on energy conservation accompanied with the desire to use that energy more efficiently has made high-temperature structural ceramics leading contenders as engineering materials. For example, the gas turbine engine using nickel-based superalloys runs at 1100°C but the necessity for a cooling fluid adds design complexity and weight, which in turn results in increased power consumption. Future development of heat engines requires higher temperatures at acceptable costs but although ceramic materials undoubtedly offer improved temperature performance and efficiency, the limiting factor at present is the difficulty in fabricating precise shapes made to complex designs.

A desirable engineering material is one in which high stress can be tolerated at a low strain, i.e. one with a high elastic modulus, E. A more useful parameter is the elastic modulus divided by the specific gravity - the specific modulus - that is, the usable strength per unit weight (see Table I.1). Other desirable properties of an engineering ceramic include high-temperature strength, chemical stability and low thermal expansion together with good thermal shock resistance. The highest values of elastic modulus occur where the interatomic bond strengths are high and for a low density, the structure must be comprised

TABLE I.1

Potential high-temperature engineering materials

material	specific modulus 10^4 MNm^{-2}	melting or decomposition temperature, ^oC
SiC	17.2	2600
AlN	10.3	2450
Si_3N_4	11.7	1900
Al_2O_3	9.0	2050
BeO	12.4	2530
BN	4.8	2700
carbon fibres	42.0	3500
vitreous SiO_2	3.1	1710
steel (typical)	3.8	1500
aluminium	3.0	660

of low atomic weight elements which also have low coordination numbers. Likely engineering ceramics will therefore be covalently bonded with low molecular weights. Thermal stability is also associated with strong covalent bonds.

Of the materials listed in Table I.1 with acceptable melting temperatures and high specific moduli, AlN is easily hydrolysed, BN is anisotropic and difficult to fabricate, Al_2O_3 has poor thermal shock resistance, BeO is toxic and C is easily oxidized. Thus, SiC and Si_3N_4 remain as suitable contenders for high-temperature engineering applications.

I.2 Silicon nitride ceramics

Unlike the traditional ceramic materials based on silicates and aluminosilicates, pure silicon nitride, like silicon carbide, cannot be sintered to high density because of its highly covalent bonding and low self-diffusivity. However, two methods have been developed for fabricating silicon nitride namely hot-pressing and reaction bonding.

In the hot-pressing process, α-silicon nitride powder is mixed with a densifying additive such as MgO or Y_2O_3 and inductively heated to 1650 - 1750°C in a graphite die under 15 - 40 MPa to give fully dense high strength β-silicon nitride. The product has excellent thermal shock resistance, erosion and corrosion resistance as well as good strength up to ∿ 1000°C. However, it is difficult to machine, making the process costly, and hence is restricted to simple shapes. In addition, a grain-boundary oxynitride glass is formed on cooling because the densifying additive (MgO) reacts with the surface layer of silica on the silicon nitride particles. These materials exhibit poor

creep resistance between 1200° - 1350°C when the glass softens. A more viscous grain-boundary glass can be formed with yttria but crystalline yttrium silicon oxynitrides can also occur and materials containing these phases suffer extensive cracking on oxidation at 1000°C due to large changes in specific volume as the oxides are formed.

An alternative material - reaction bonded silicon nitride - is readily formable, requires little machining and thus is relatively inexpensive. The required shape is fabricated from compacted silicon metal powder which is then nitrided in molecular nitrogen to give mixed α and β silicon nitrides without changing the original dimensions of the compact; the product has 18-25% porosity.

I.3 Silicon carbide ceramics

At present, silicon carbide based ceramics are available commercially in a range of forms prepared either by hot-pressing, sintering, reaction-bonding or chemical vapor deposition (CVD). Each group has different properties which are a direct result of the variation in the fabrication route. Some typical properties of these materials are listed in Table I.2 but until ten years ago it was widely accepted that SiC could not be pressureless sintered to high densities because of the strongly covalent nature of the Si-C bond and the high activation energy for self diffusion. However, Prochazka (1973) demonstrated that submicron SiC powder could be sintered to high densities between 1950° - 2100°C by small additions of boron and carbon. The three factors of ultrafine grain size, an additive to promote volume diffusion and control of surface chemistry are considered to be the key requirements for producing other pressureless sintered, single-phase covalent compounds such as silicon carbide and silicon nitride.

TABLE I.2

Typical properties of silicon carbide ceramics

type	Young's modulus 10^4 MNm^{-2}	coefficient of thermal expansion $\alpha(10^{-6}\ ^oC^{-1})$	thermal conductivity $K(wm^{-1}\ ^oC^{-1})$
sintered (α-phase)	407	4.8	100 - 50
reaction-bonded (20 v/o free Si)	345	4.4	100 - 50
SiC fiber - Si composite	340	-	70
CVD	414	-	-
REFEL SiC	413	4.3	84 - 39
sintered Si_3N_4 (alumina additive)	276	3.2	28 - 12

Sintered silicon carbide is made into simple shapes by slip-casting, die pressing and extrusion but more complex shapes can be formed by a reaction-bonding process. This involves the production of a mouldable body from silicon carbide powder, graphite and a plasticizer which is then pressed, extruded, injection moulded or otherwise formed into the required shape. The plasticizer is then converted to a porous char by pyrolysis before silicon liquid or vapour is infiltrated to react *in situ* with the graphite to give a reaction-bonded product. However, this only has a reasonable strength up to the melting point of silicon ($\sim$ 1400^{o}C) but has the advantage of retaining the original geometry of the compact, thus requiring little machining and hence keeping the component cost relatively low.

The United Kingdom Atomic Energy Authority (U.K.A.E.A.) have recognised the versatility of the reaction bonding process and have produced a fine-grained homogeneous material (designated REFEL* SiC) that is used as a cladding material in high-temperature gas-cooled reactors. The ceramic is fully dense, impermeable to gases, resistant to oxidation and dimensionally stable under neutron irradiation. However, it is in a non-nuclear engineering field that the major exploitation of REFEL SiC is currently being pursued. REFEL SiC has found applications as an engineering ceramic in two major areas: for components operating at high temperature in oxidising atmospheres and at low temperature in abrasive environments. There is also the well-established use of silicon carbide as heating elements. Figure I.1 shows a selection of REFEL SiC components which include mechanical seals, bearings, radiant heater tubes, gas turbine parts and chemical

---

* REFEL (Reactor Fuel Element Laboratories) is a registered trademark of U.K.A.E.A.

Figure I.1

REFEL SiC components

(courtesy of U.K.A.E.A.)

plant components.

Dense SiC materials can also be produced without additives by chemical vapour deposition but the strength, which in most cases is high, is unpredictable because of the non-uniform microstructure. Complex engineering shapes have been produced by this method but it is expensive and the most probable application for CVD material may be as an erosion and oxidation resistant coating for SiC ceramics formed by more conventional routes.

I.4 Ceramic alloys

One of the most exciting developments in recent years was the discovery of a new class of ceramics based on silicon nitride and similar in diversity to the mineral silicates. Indeed, β-silicon nitride has the same atomic arrangement as that of beryllium silicate, Be_2SiO_4. The new "sialons" (Jack, 1976) are derived from the nitride by applying the simple principles of silicate chemistry, except that the wide variety of phases are built-up of $(Si,Al)(O,N)_4$ tetrahedra as opposed to SiO_4 or $(Si,Al)(O)_4$ tetrahedra in the case of silicates and aluminosilicates respectively. The first of these sialons were reported concurrently by Oyama & Kamigaito (1971) and Jack & Wilson (1972) and had a structure based on that of β-silicon nitride but with nearly three-quarters of the silicon replaced by aluminium and the corresponding amount of nitrogen replaced by oxygen. Because of its structure the resulting β'-sialon has physical and mechanical properties similar to silicon nitride and its chemical composition results in chemical properties approaching those of alumina. The material has a lower coefficient of thermal expansion and better oxidation resistance than silicon nitride; see Table I.3.

Other sialons are now known which have structures based on α-silicon nitride. These are similar to the "stuffed" derivatives of quartz in which Al^{3+} replaces Si^{4+} and positive valency deficiencies are compensated by "stuffing" Li^{+} or Mg^{2+} into interstitial sites.

Recently the concurrent discovery at Newcastle and Utah Universities (Cutler, et al., 1978) that, like silicon nitride, silicon carbide could be "alloyed", in this case, with aluminium nitride, was of considerable interest. It seemed likely that with further research the electrical and semi-conducting properties of silicon carbide could be tailored by alloying in this way.

TABLE I.3

Typical properties of silicon nitride based ceramics

type	Young's modulus (GPa)	coefficient of thermal expansion $\alpha(10^{-6}\ ^{o}C^{-1})$	thermal conductivity $K(Wm^{-1}\ ^{o}C^{-1})$
hot-pressed (MgO additive)	317	3.0	30 - 15
sintered (Y_2O_3 additive)	276	3.2	28 - 12
reaction-bonded	165	2.8	6 - 3
β' - sialon (sintered)	297	2.7	22

II PREVIOUS INVESTIGATIONS

II.1 Silicon nitride

Silicon nitride was first reported by Deville & Wohler (1857) who noted its excellent thermal and chemical stability but it was not until one-hundred years later that Hardie & Jack (1957) established that silicon nitride existed as two polymorphs, α and β, both having hexagonal unit cells with similar a dimensions, but with the c dimension of α almost twice that of β, i.e.

$$a_\alpha = 7.752\ \text{Å}, \quad c_\alpha = 5.620\ \text{Å},$$

$$a_\beta = 7.608\ \text{Å}, \quad c_\beta = 2.911\ \text{Å}$$

The cell volume of α-silicon nitride is double that of β and contains twice the number of atoms, $Si_{12}N_{16}$ as compared to Si_6N_8. The same workers also found that β was isostructural with the silicate phenacite, Be_2SiO_4, the structure being built up of (SiN_4) tetrahedra sharing corners, with each N common to three tetrahedra. β is built up of Si-N atom layers arranged in an ABAB... sequence whereas in α the arrangement is ABCD...; see Figures II.1 and II.2. Anomalies in the structure determination and also the low density of 3.167 gcm^{-3} for α compared with 3.192 gcm^{-3} for β (Wild et al., 1972b) were accounted for by assuming α to be a defect structure with partial replacement of nitrogen by oxygen and a composition $Si^{4+}_{11.5}N^{3-}_{15}O^{2-}_{0.5}$ or $Si^{4+}_{10}Si^{3+}_{2}N^{3-}_{15}O^{2-}_{0.5}$. This was supported by thermodynamic investigations in the Si-O-N system (Wild et al., 1972b; Colquhoun et al., 1973) which confirmed that up to 1 in 30 nitrogens were replaced by oxygen. Despite extensive further investigations, the exact nature of α-Si_3N_4 remains unclear since, for example, chemically vapour deposited (CVD)α can be prepared without

Figure II.1

The crystal structure of β-Si_3N_4

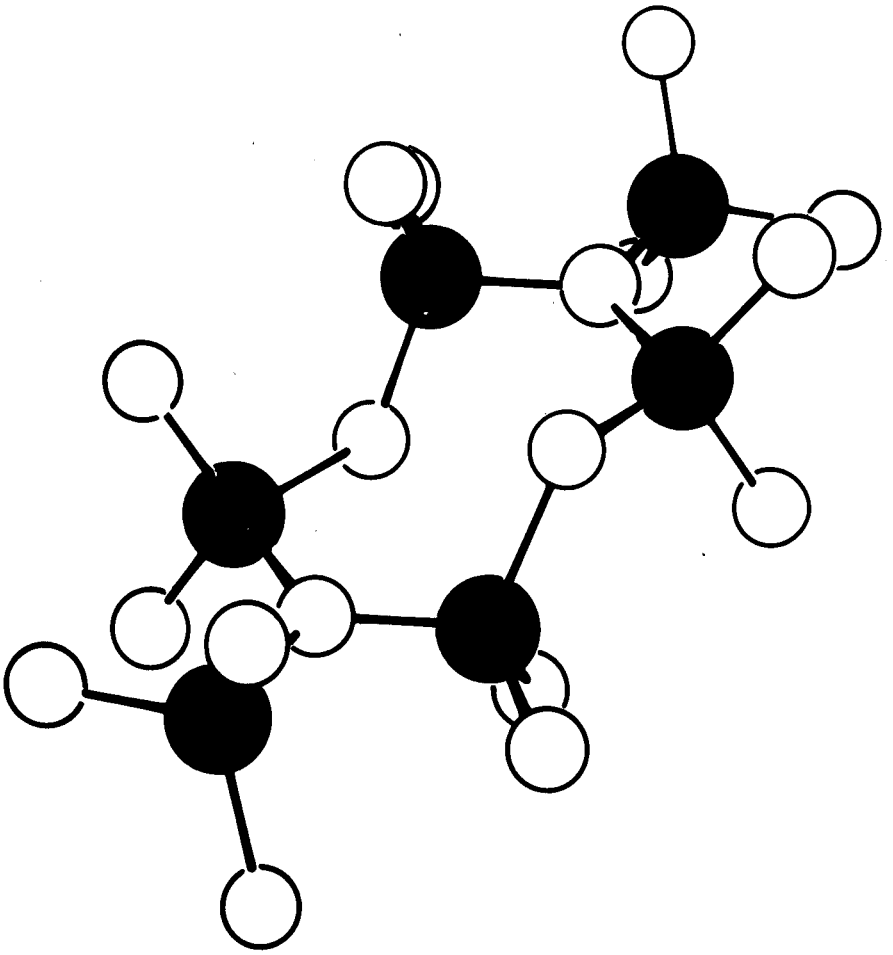

BOND LENGTHS

Si - N1 1·730

Si - N1 1·739

Si - N2 1·745

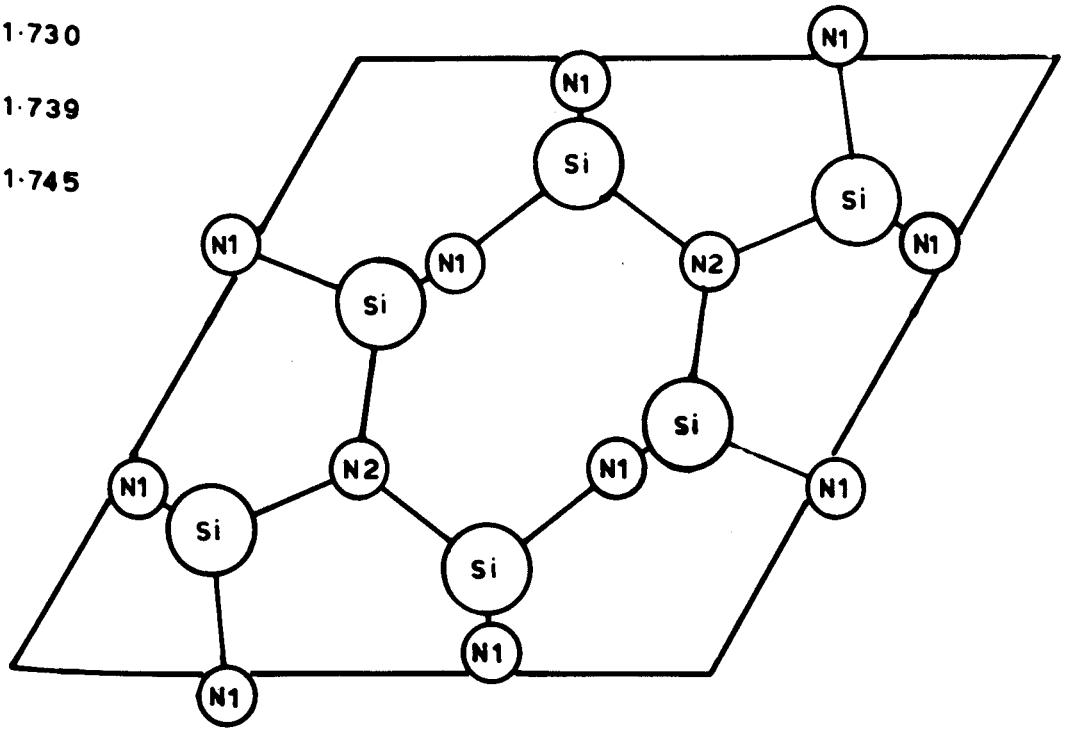

PROJECTION ALONG c AXIS

Figure II.2

The crystal structure of α-Si_3N_4

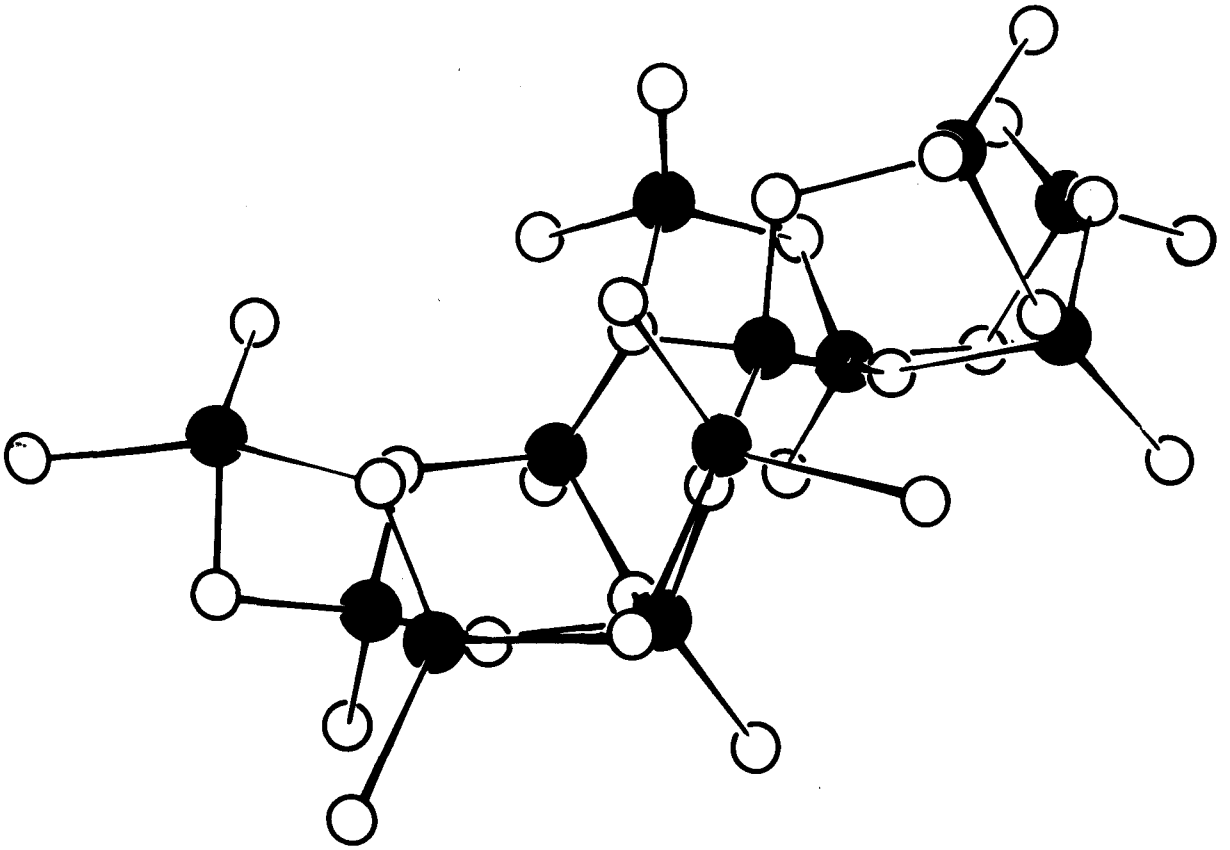

BOND LENGTHS

N1 - Si1	1·566
N1 - Si1	1·687
N1 - Si2	1·896
N2 - Si2	1·893
N2 - Si2	1·562
N2 - Si1	1·795
N3 - Si1	1·781
N4 - Si2	1·782

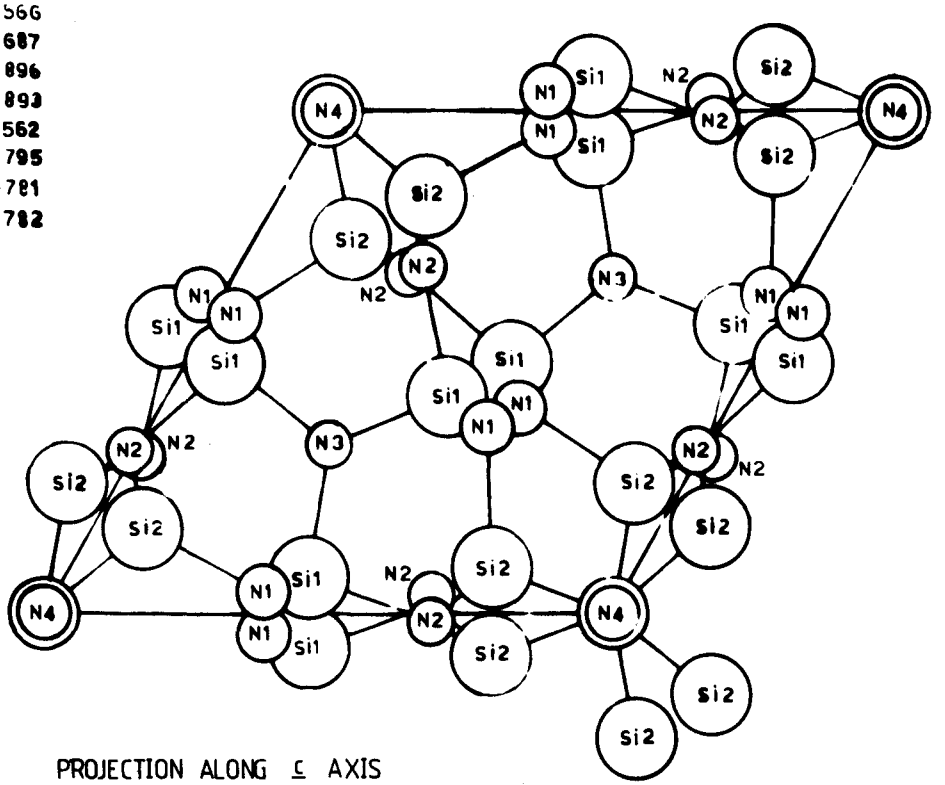

PROJECTION ALONG c AXIS

oxygen (Kijima et al., 1975), whereas α made by nitriding silicon invariably contains a small amount of oxygen (Feldet al., 1974; Amato et al., 1975). Recent work at Newcastle on α'-sialons (Hampshire et al., 1978) suggests that the most satisfactory explanation for the structure of α involves atoms of reduced silicon (Si^{2+}) occupying large holes in the structure.

II.2 The sialons

II.2.1 Si-Al-O-N System

Concurrent work in the Si_3N_4-Al_2O_3 system by Jack & Wilson (1972) and by Oyama & Kamigaito (1971) produced new compounds isostructural with β-Si_3N_4 but with expanded unit cell dimensions and containing up to 70 w/o Al_2O_3. Subsequently Lumby et al. (1975), Gauckler et al. (1975) and Jack (1976) showed that β'-sialon has a compositional range corresponding to $Si_{6-z}Al_zO_zN_{8-z}$ where $0 < Z < 4.2$. Figure II.3 shows the Si-Al-O-N behaviour diagram established at Newcastle (Roebuck & Thompson, 1977) by hot-pressing mixtures of Si_3N_4, AlN, Al_2O_3 and SiO_2 at 1700°C.

The six phases occurring at the AlN-rich corner of the diagram, were first prepared by Gauckler et al. (1975) and occur along lines of constant metal:non-metal ratio (M:X) along which (Si + N) is replaced by (Al + O). These phases were characterized by Thompson (1977) as polytypoids based on the AlN structure and are similar in some respects to the polytypes of SiC but differing from the latter in that their structures are directly related to their compositions, M_mX_{m+1}, where $4 \leqslant m \leqslant 10$. The structures are either hexagonal or rhombohedral and

Figure II.3

The Si-Al-O-N behaviour diagram

at 1700^{o}C

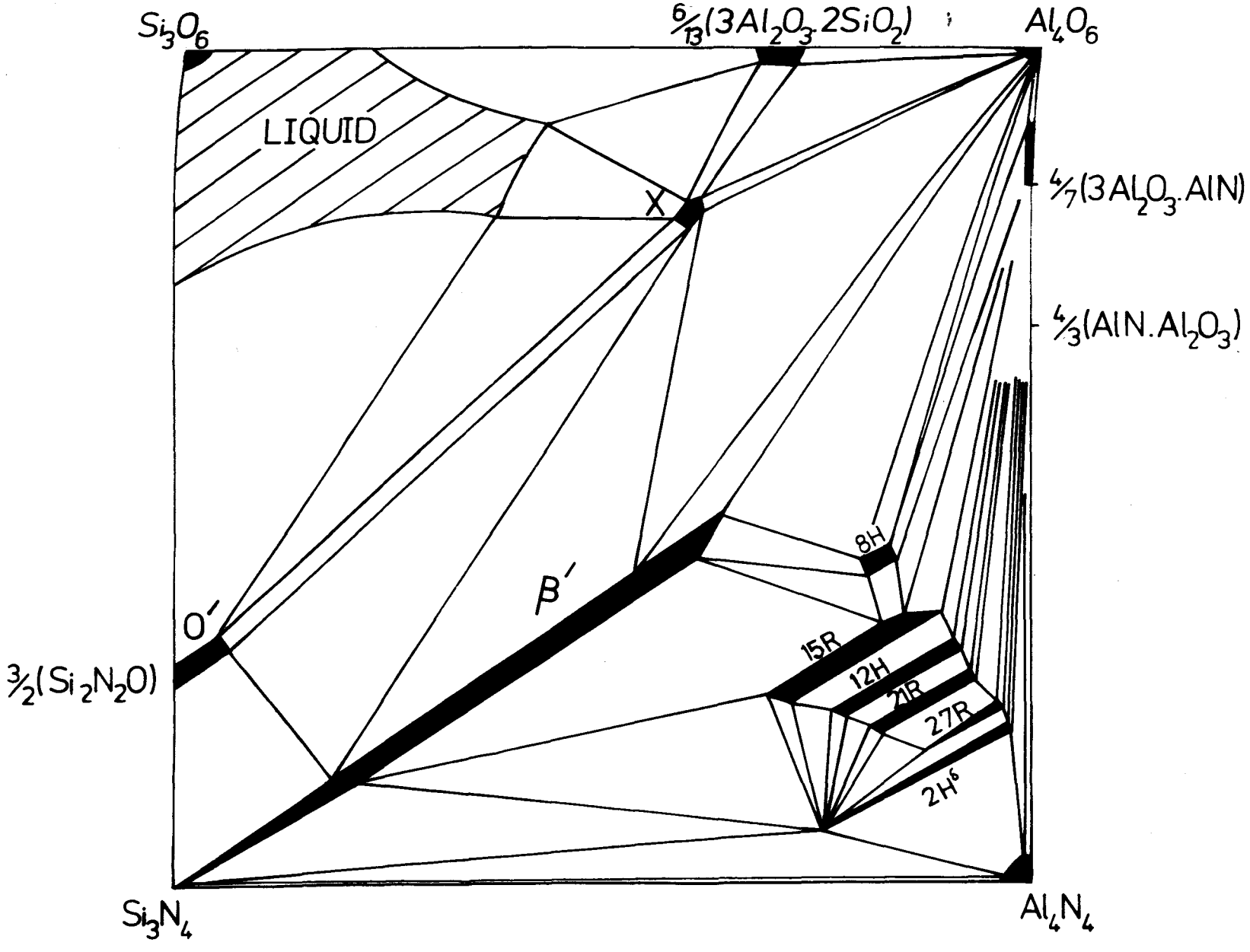
Si_3O_6
$\frac{6}{13}(3Al_2O_3.2SiO_2)$
Al_4O_6
LIQUID
X
$\frac{4}{7}(3Al_2O_3.AlN)$
$\frac{4}{3}(AlN.Al_2O_3)$
8H
B'
O'
15R
12H
21R
27R
2H^6
$\frac{3}{2}(Si_2N_2O)$
Si_3N_4
Al_4N_4

are designated by the Ramsdell* symbols 8H, 15R, 12H, 21R, 27R and 2H. They occur along the constant M:X lines 4M:5X, 5M:6X, 6M:7X, 7M:8X, 9M:10X and ~11M:12X respectively.

The O'-phase has the same structure as silicon oxynitride, Si_2N_2O, and has a limited range of composition extending along the 2M:3X line towards Al_2O_3.

Sialon X-phase was first reported independently by Oyama & Kamigaito (1971) and by Jack & Wilson (1972) as a minor phase formed together with β' by reacting α-Si_3N_4 and Al_2O_3 at 1700°C. Several compositions and erroneous interpretations of its X-ray diffraction pattern have been proposed but recent work at Newcastle has shown that it occurs in two forms, "high" and "low". Both forms are triclinic with identical compositions close to $Si_3Al_{5.7}O_{11}N_2$ and a detailed single crystal X-ray study combined with high resolution electron microscopy has determined the structure and resolved many of the complexities of this phase (Korgul & Thompson, 1982).

II.2.2 M-Si-Al-O-N Systems

The addition of another metal (M) to the Si-Al-O-N system produces a 5 component system, compositions in which are represented by Jänecke's triangular prism (Jänecke, 1907) where all the sides are of

*Ramsdell (1947) devised this notation to describe the silicon carbide polytypes but the nomenclature is applicable to all layered structures. The number of layers in the unit cell is followed by a letter designating the crystal symmetry: C, cubic; H, hexagonal; R, rhombohedral. For example a compound with a hexagonal unit cell and a two-layer repeat in the c direction is designated 2H.

equal length. Figure II.4 shows a general M-Si-Al-O-N system represented in this manner, the left hand and right hand triangular faces being pure oxides and pure nitrides respectively.

In many M-Si-Al-O-N systems the phases in the basic sialon square extend into the prism along planes of constant M:X ratio. For example, small ranges of solid solution exist between β-Si_3N_4 and $LiAl_5O_8$ (Jama et al., 1975), and Hendry et al. (1975) showed the existence of a β'-sialon phase containing Mg with compositions along the Si_3N_4-$MgAl_2O_4$ join. Also, each of the sialon polytypoids extend into the Mg-Si-Al-O-N system (Perera, 1976; Buang, 1979). The range of composition of β'-sialon follows a plane of constant metal:non-metal ratio 3M:4X (see Figure II.4).

Whereas β'-sialons have crystal structures based on β-silicon nitride another group of sialons have structures based on α-silicon nitride. These "α'-sialons" have a range of homogeneity extending along a plane of composition $M_x(Si,Al)_{12}(O,N)_{16}$ where $X \neq 2$ and M is Li, Ca, Y and all the rare earth elements except La and Ce (see Figure II.4).

II.2.3 α'-sialons

α'-sialons were first observed by Jack & Wilson (1972) who reported that α-silicon nitride structures were formed by the reaction of lithium-silicon nitride, $LiSi_2N_3$, with alumina. α'-sialons were also observed as minor phases by Jama et al. (1975), Masaki et al. (1975), Jack (1976), Mitomo (1977) and Goeuriot et al. (1977). Hampshire (1977) successfully prepared pure α'-phases by adding Y_2O_3 or CaO to mixtures of Si_3N_4 and AlN and concluded that a liquid phase was necessary for reaction. He suggested that the α'- structure was derived from α-Si_3N_4 by partial

Figure II.4

Representation of the M-Si-Al-O-N system

with β' and α' regions outlined

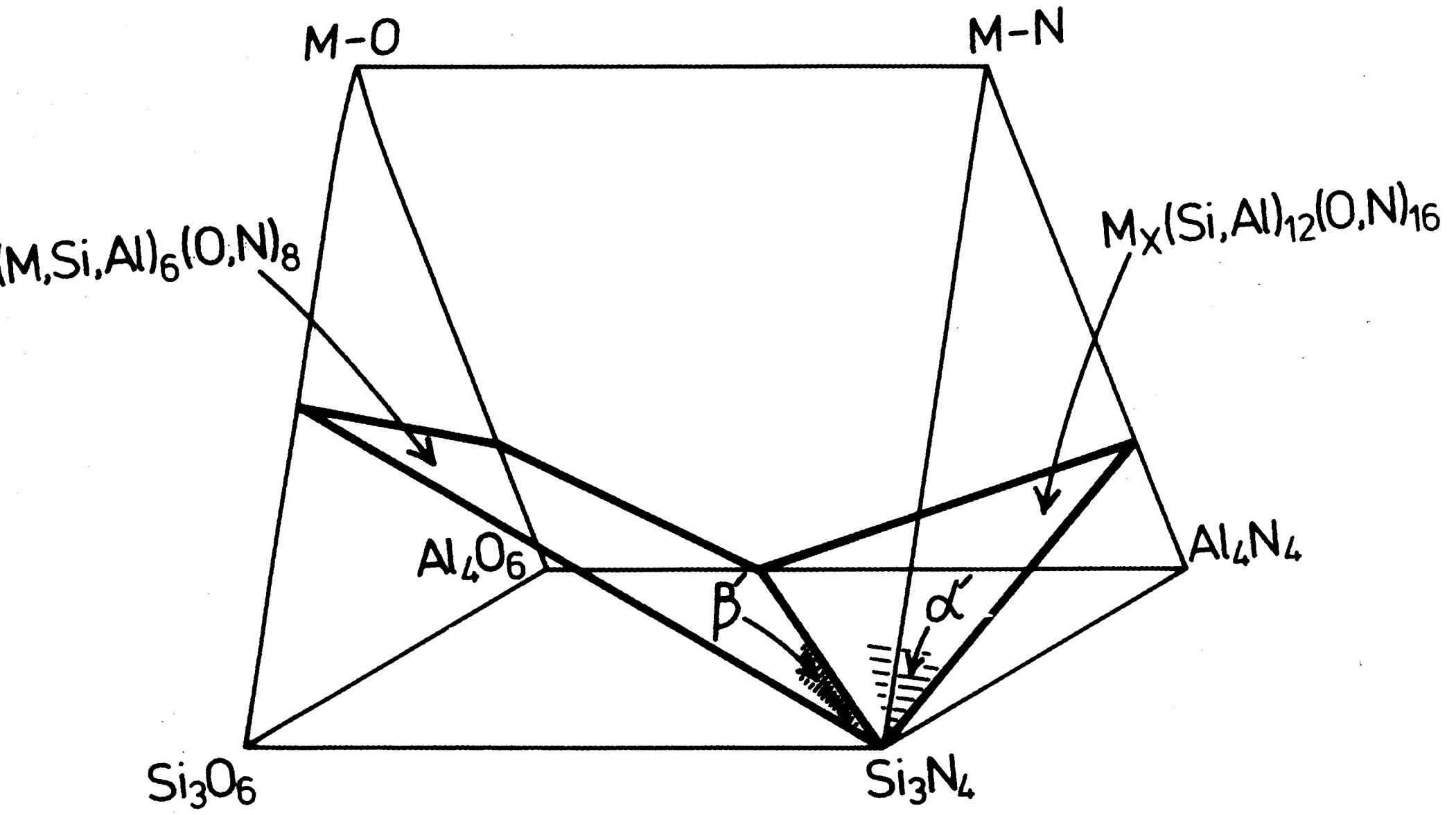
M-O
M-N
$(M,Si,Al)_6(O,N)_8$
$M_x(Si,Al)_{12}(O,N)_{16}$
Al_4O_6
Al_4N_4
β
α
Si_3O_6
Si_3N_4

replacement of Si by Al and was therefore of composition $Si_9Al_3N_{15}$ with a limited range of homogeneity. However, direct microprobe-analysis gave a composition which included the Y_2O_3 or CaO in the final product (Park, 1977& 1978). Further work at Newcastle (Hampshire et al., 1978) suggested that α'-sialons were derived from α-silicon nitride by partial replacement of silicon by aluminium valency compensation being achieved by the modifying cations Y or Ca partially occupying the two interstices in the unit cell of the α-structure. Thus, the materials are similar to the feldspars or zeolites in which Al^{3+} replaces Si^{4+} and positive valency deficiencies are compensated by Na^+, K^+ or Ca^{2+} occupying structural interstices.

II.3 Silicon carbide-aluminium nitride alloys

An investigation at Newcastle on the stability of α'-$CaSi_9Al_3ON_{15}$ in a reducing (carbon) environment produced a single phase product with a wurtzite type structure formed according to the reaction:

$$CaSi_9Al_3ON_{15} \rightarrow 9SiC.3AlN + 6N_2\uparrow + CO\uparrow + Ca\uparrow \quad \ldots II.1$$

The product had unit-cell dimensions intermediate between AlN and 2H-SiC and since the X-ray diffraction photograph showed no calcium-containing phases it was assumed that all calcium had vaporized during the course of the reaction.

In subsequent experiments, instead of using preformed α'-sialon, mixtures of Si_3N_4, AlN, C and CaO were reacted at 1800°C and produced the same series of solid-solutions, the unit-cell dimensions of which varied smoothly between the two end members(see Figure II.5). The addition of CaO provides a transient oxynitride liquid in which the reactants are soluble thus allowing the product to precipitate from solution.

Figure II.5

Cell dimension variations in

SiC-AlN alloys after

Cutler et al.(1978)

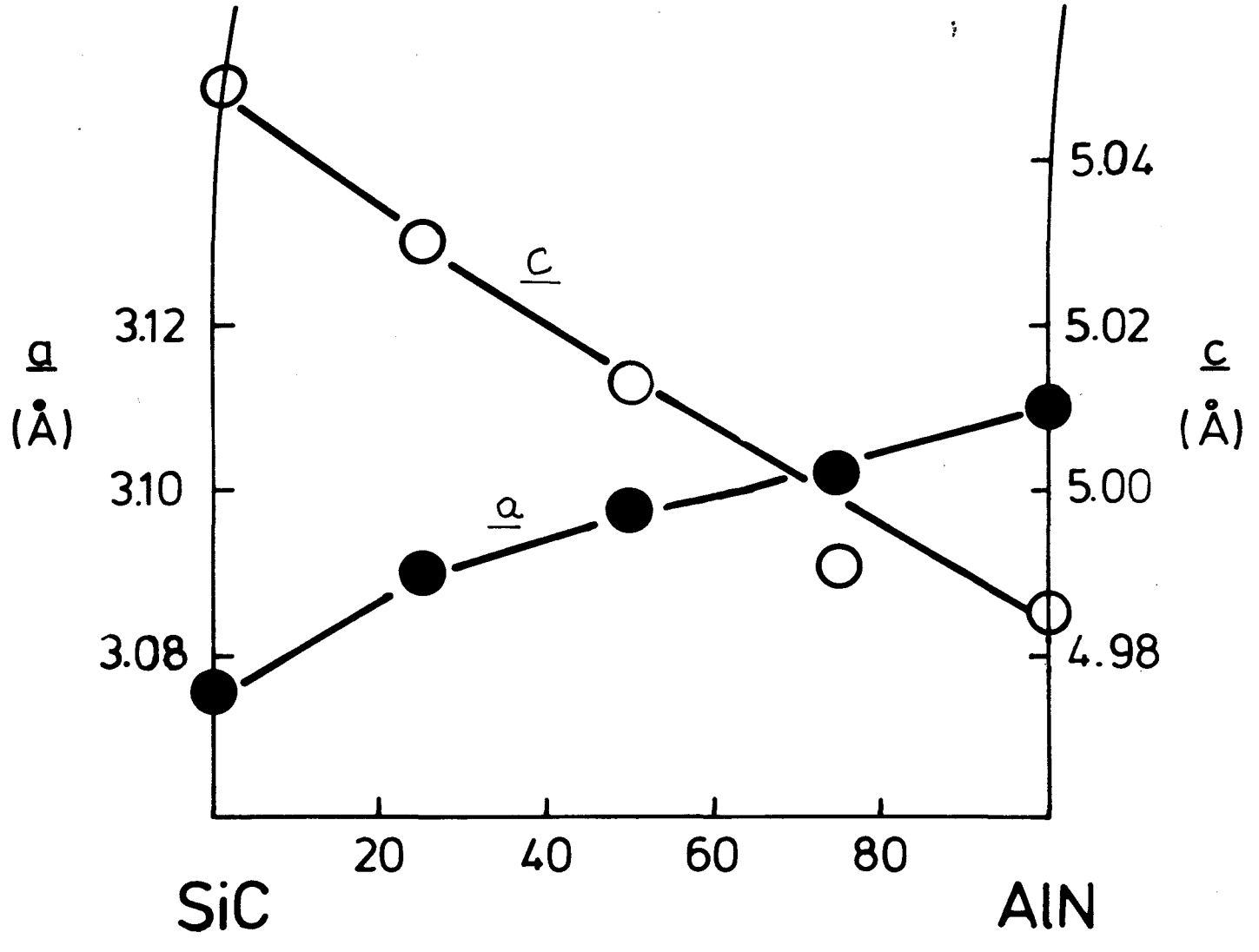

(Cutler et al., 1978)

Concurrent work at Utah showed that intimate mixtures of amorphous silica, carbon and aluminium hydroxide when heated in argon or nitrogen to 1600°C also formed a series of wurtzite-type compounds. Results of the work at Newcastle and Utah were published jointly (Cutler et al., 1978) and showed that a complete series of solid solutions existed between SiC and AlN and also between SiC and aluminium oxycarbide (Al_2OC) which also has a wurtzite-type structure (Foster et al., 1956).

SiC-AlN solid solutions have since been prepared by Rafaniello et al. (1981) and by Tsukuma et al. (1982). The former prepared the alloys by carbothermal reduction of alumina-silica mixtures derived from mixed silica, aluminium chloride and starch, and resulting single phase powders were hot-pressed without additives to maximum density providing that the AlN content exceeded about 10 w/o. However, further work (Rafaniello et al., 1983) has shown that a hot-pressing temperature of 2300°C is necessary to produce homogeneous materials, otherwise in the compositional range ∿15-75 w/o AlN, two phase products result. Recent work by Ruh & Zangvil (1982) claims that dense SiC-AlN solid solutions of up to 65 m/o AlN can be formed in the absence of a liquid phase when mixtures of β-SiC and AlN are hot-pressed in vacuum at temperatures >2100°C.

The stabilization of the 2H form of SiC by additions of AlN suggests that the polytype modifications are strongly influenced by small amounts of impurity elements or by isostructural compounds. Indeed, an extensive literature exists on the role of impurity elements in the semiconductor applications of SiC. The remainder of this Chapter is therefore devoted to a discussion of the preparation, formation, structure and stability of silicon carbide with particular reference to the 2H polytype.

II.4 Silicon carbide

II.4.1 Introduction

Silicon carbide was observed by a number of investigators (Berzeluis, 1824; Schutzenberger & Colson, 1881) in laboratory experiments before its industrial and commercial importance was realized. Naturally occurring silicon carbide was first discovered by Moissan (1905) in a meterorite and subsequently several small deposits have been found (Regis & Sand, 1958; Bobrievich et al., 1957; Bauer et al., 1963).

The technical importance of silicon carbide was first realized by Cowless & Cowless (1885) and Acheson (1892). Indeed the present day large scale manufacturing process still follows Acheson's method. The silicon carbide produced by this process is normally a mass of tiny crystals best suited for manufacture into abrasive powders, but to exploit the high temperature semiconducting properties of SiC, large-sized single crystals are required. A detailed description of the methods for growing such crystals is given by Verma & Krishna (1966), but briefly the three main methods are as follows:

(i) Crystallization from solution

Because carbon has an appreciable solubility in silicon at $1700^{\circ}C$ it is possible to grow SiC crystals from a C-rich Si melt, the solution being supersaturated with respect to SiC. Only the cubic polytype 3C is produced by this method.

(ii) Sublimation and condensation

Using technical grade SiC, pure single crystals are grown by this process at 2500°C. Impurities are incorporated deliberately into the crystals by adding substances into the inert gas atmosphere. Since the sublimation is carried out above 2500°C, the resulting crystals are always of the high-temperature hexagonal modifications.

(iii) Chemical vapour deposition

Silicon carbide is prepared by heating a tungsten wire in a hydrogen atmosphere containing either $SiCl_4$-toluene mixtures or CH_3SiCl_3. Crystals of various modifications are deposited on the filament depending on the temperature.

Currently the production of dense polycrystalline SiC ceramics by hot-pressing, pressureless sintering and reaction-bonding (see Chapter I) is opening up a wider field of applications for SiC as engineering materials.

II.4.2 The structure of silicon carbide

The crystal structure was first described by Hull (1919 & 1920) for β-SiC and by Ott (1925a,b) for α-SiC*. Ott realized that all silicon carbide polytypes are composed of coordinating tetrahedra (either SiC_4 or CSi_4) which are arranged in such a way as to share corners thereby satisfying the 4-fold coordination requirements of the carbon and silicon atoms. The tetrahedra occupy positions analogous to those occupied by spheres in close-packed structures and are stacked in such a way that one corner lies out of the layer plane; see Figure II.6 . The stacking sequence of the silicon-carbon double layers can be described by an ABC notation. Cubic (ABCABC...) and hexagonal (ABAB...) stacking sequences are found and in this respect SiC is analogous to zinc sulphide (ZnS). However, a large number of ordered and disordered structures or a complex mixture of both cubic and hexagonal stacking arrangements are also found.

Over the years several notations have been employed to distinguish the large number of structurally similar polytypic modifications. The simplest notation due to Ramsdell (1947) has already been described (see section II.2). The nomenclatures of Wyckoff (1948) and Jagodzinski (1949) describe the close packings in which each layer is specified by the orientation of the layers on either side. Thus if the preceding and succeeding layers have the same orientation (hexagonal packing) the layer in question is denoted h. Alternatively if the layers on either

---

*The term α-SiC is applied collectively to include all hexagonal modifications of SiC, whereas β-SiC is reserved solely for the cubic form.

Figure II.6

Arrangement of SiC_4 tetrahedra

in the 3C, 2H, 4H and 6H polytypes.

The zig-zag sequence of tetrahedral

faces is outlined.

3C

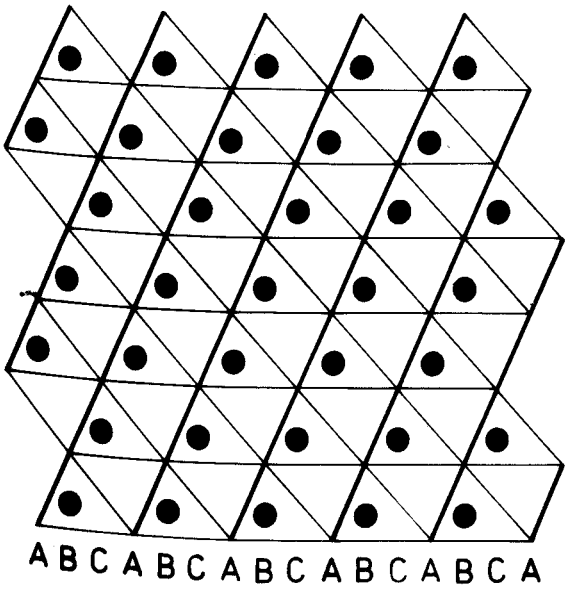
A B C A B C A B C A B C A B C A

2H

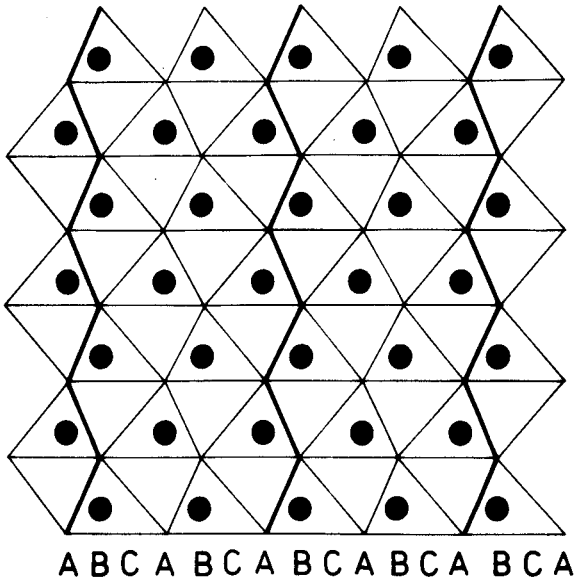
A B C A B C A B C A B C A B C A

4H

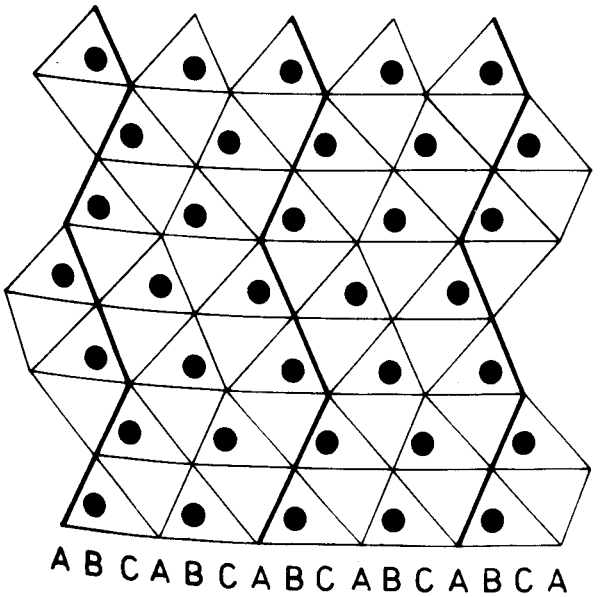
A B C A B C A B C A B C A B C A

6H

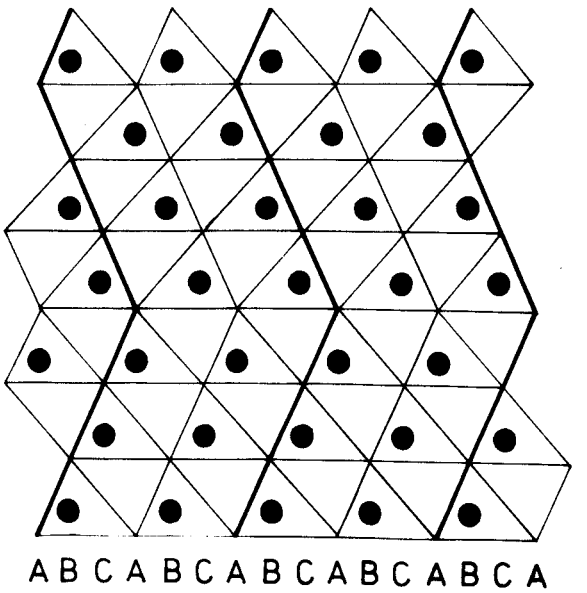
A B C A B C A B C A B C A B C A

side have dissimilar orientations (cubic packing) the symbol c is used. Thus 6H (ABCACB...) is denoted hcchcc... Ramsdell (1945) also noted that the zig-zag sequence of non-basal plane faces could be used to describe the stacking sequence of the tetrahedral layers (see Figure II.6,). This notation groups together the number of consecutive layers which occur without rotation. Thus 6H (ABCACB...) becomes (33) in the Zhdanov-Ramsdell nomenclature. Here, the wurtzite type 2H is (11), (each layer being rotated by π with respect to the preceding layer) and the cubic modification is indicated by (∞). The basic polytypes of SiC as described by the various notations are listed in Table II.1. Table II.2 lists all the known polytypes of SiC, together with the Zhdanov symbols for those structures where the stacking sequence has been determined (see Jepps, 1979).

Until recently the stacking sequences of SiC polytypes were determined by X-ray diffraction and although much has been deduced about polytypic structures, detailed information about fine-scale structural variations was unobtainable. Individual defects can, however, be resolved using transmission electron microscopy (TEM) as van Landuyt & Amelinckx (1971) showed when they observed and characterized stacking faults in the 6H polytype from one dimensional fringes. Measurement of the fringe spacing has also been used to help in the structure determination of long-period (Sato et al., 1974; Dubey & Singh, 1977; Dubey & Singh, 1978; Singh & Singh, 1980; Kuo et al., 1982) and disordered polytypes (Sato & Shinozaki, 1975; Shinozaki & Kinsman, 1978; Singh & Singh, 1981). However one dimensional lattice fringes enable only the number of layers in any region or the whole of the unit cell to be determined. The exact stacking sequence cannot be deduced by this method

Table II.1

The basic polytypes of SiC as described by the various notations

Ramsdell notation	ABC sequence	Zhdanov symbol	h-c notation
2H	AB...	11	hh
3C	ABC...	∞	ccc
4H	ABCB...	22	$(hc)_2$
6H	ABCACB...	33	$(hcc)_2$
15R	ABCBACABACBCACB	$(23)_3$	$(hchcc)_3$

Table II.2

SiC polytypes and stacking sequence where known

Ramsdell notation	Zhdanov symbol	Ramsdell notation	Zhdanov symbol
2H	11	$36H_1$	$(33)_4 34\ 32$
3C	∞	$36H_2$	$(33)_2 32 (33)_2 34$
4H	22	39H	$(33)_2 32 (33)_2 (32)_2$
6H	33	39R	$(33\ 34)_2$
8H	44	42H	
9H	63	45R	$[(32)_2 23]_3$
10H	32 23	48R	$[(32)_2 22]_3$
14H	$(22)_2 33$	48H	
15R	$(32)_3$	$51R_1$	$[33_2 32]_3$
16H	$(33)_2 22$	$51R_2$	$[(22)_3 23]_3$
18H	$(22)_3 33$	54H	$(33)_6 32\ 33\ 34$
19H	$(32)_3 22$	57R	
$20H_1$	$(22)_3 44$	58H	
$20H_2$	$(32)_2 (23)_2$	60H	
21R	$(34)_3$	60R	
24R		64H	
26H		66H	
$27H_1$	$(32)_3 (33)_2$	$69R_1$	$[(33)_3 32]_3$
$27H_2$	$(32)_{33} (33)$	$69R_2$	$[43\ 33\ 22\ 33]_3$
27R	$(22\ 23)_3$	72H	
$33H_1$	$(33)_2 35\ 33\ 34$	72R	
$33H_2$	$(33)_3 (23)_3$	75R	$[(32)_3 (23)_2]_3$
33R	$(33\ 23)_3$	78H	

Cont'd.

Table II.2 (Cont'd.)

78R		135R	$[((32)_2(23)_2)_2 32]_3$
80H		141H	
81H	$(33)_5 35 (33)_6 (34)$	141R	$[(33)_7 32]_3$
81R		144R	
84R	$[(33)_3(32)_2]_3$	$147R_1$	$[(33)_7 34]_3$
87R	$(33)_4 32_3$	$147R_2$	$[(33\ 32)_4 32]_3$
90R	$[(23)_4 33\ 22]_3$	150R	
93R		153R	
96H		159R	
$96R_1$	$[(33)_3(34)_2]_3$	165H	
$96R_2$	$[(33)_2 22\ 32\ 33\ 32]_3$	168R	$[(23)_{10} 33]_3$
97H		171R	$[(33)_8 32\ 22]_3$
99R	$[(33)_4\ 32\ 22]_3$	174R	$[(33)_3 6 (33)_5 4]_3$
102R	$[(34)_4 33]_3$	180R	$[(23)_{11} 32]_3$
105R	$[(33)_5 32]_3$	189R	$[(43)_8 34]_3$
106H		192R	
108R		201R	
111R	$[(33)_5 34]_3$	207R	$[(33)_{10} 32\ 22]_3$
117R		210H	
120R	$[(22)_5 32\ 22\ 33\ 32]_3$	210R	
123R	$[(33)_6\ 32]_3$	213R	
126R	$[(33)_3 34\ 34\ 33\ 32]_3$	216H	
130H		222R	$[(33)_6 34 (33)_4 34]_2$
$132R_1$	$(33)_3(32)_3(33)_2 22$	231R	
$132R_2$	$(33)_2 32 (33)_2 22\ 33\ 32$	237R	

Cont'd.

Table II.2 (Cont'd.)

243R		513R
249R	$\left[(33)_{13}(32)\right]_3$	522R
253R		595R
264R		636R
267R		654R
270R		676R
279R		831R
282R		937R
288R		1041R
303R	$\left[(33)_{16}32\right]_3$	1080R
318R		1200R
321R		1560H
333R		2400R
339R		4680R
354R		
384R		
393R	$\left[(33)_{21}32\right]_3$	
400H		
408H		
417R		
420R		
453R		
459R		
498R		

alone and the final structure has to be selected so as to best fit the calculated and observed intensity distribution of the diffraction patterns. Using TEM the basic polytypes are easily recognizable by their electron diffraction patterns and the Ramsdell symbols (nH or nR) can be deduced from the distribution of diffracted intensity along the $10\bar{1}\ell$ reciprocal lattice rows which are visible in a $[2\bar{1}\bar{1}0]$ beam direction (cubic $(1\bar{1}0)$ direction). All SiC polytypes give a reflexion corresponding to the fundamental layer spacing (0.25 nm) and the occurrence of other reflexions from the origin to the fundamental layer are governed by the lattice-type and space group. Thus, in hexagonal polytypes double diffraction can cause all normally absent reflexions to appear while in the cubic or rhombohedral structures only every third reflexion can occur because of lattice type absences (Smith et al., 1978). Figures 11.7(a) & (b) are diagrammatic representations of mixed diffraction patterns for (3C + 6H) and (3C + 2H) polytypes respectively and by considering the number of reflexions along $10\bar{1}\ell$ lattice rows it is possible to determine which structures are present in any one diffraction pattern.

Stacking sequences can only be observed by careful choice of lattice imaging conditions. For example, in thin specimens, tilted-beam lattice imaging using reflexions corresponding to the individual tetrahedral layers (e.g. $(111)_{3C}$, $(0006)_{6H}$) simply shows fringes of 2.5 Å spacing and no information regarding the stacking sequence is obtained. In thicker specimens double diffraction effects enable reflexions corresponding to the $\underline{c}$ repeat distance of the polytype to be used for imaging e.g. $(0001)_{4H}$, (0001_{6H}) either alone or superimposed on the fundamental layer fringes (Jepps et al., 1979). However, the particular stacking sequence and the exact nature of stacking faults cannot be elucidated by imaging these

Figure II.7

Superimposed electron diffraction patterns for:

(a) 3C + 6H

(b) 3C + 2H

zone axes $\left[1\bar{1}0\right]_{3C}//\left[2\bar{1}\bar{1}0\right]_{6H}//\left[2\bar{1}\bar{1}0\right]_{2H}$

(a)

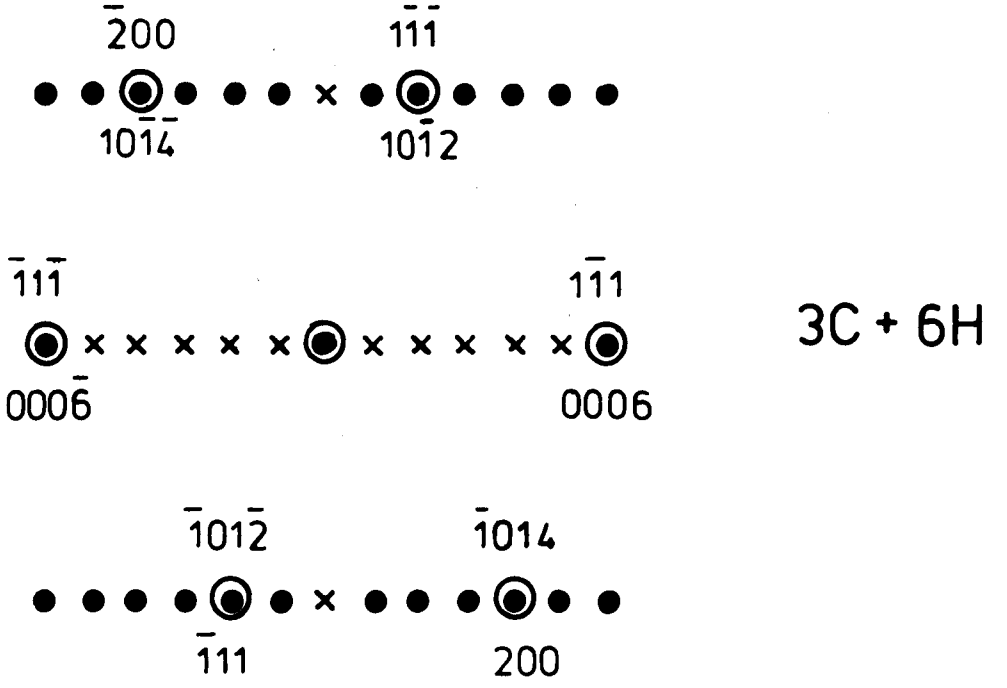

3C + 6H

(b)

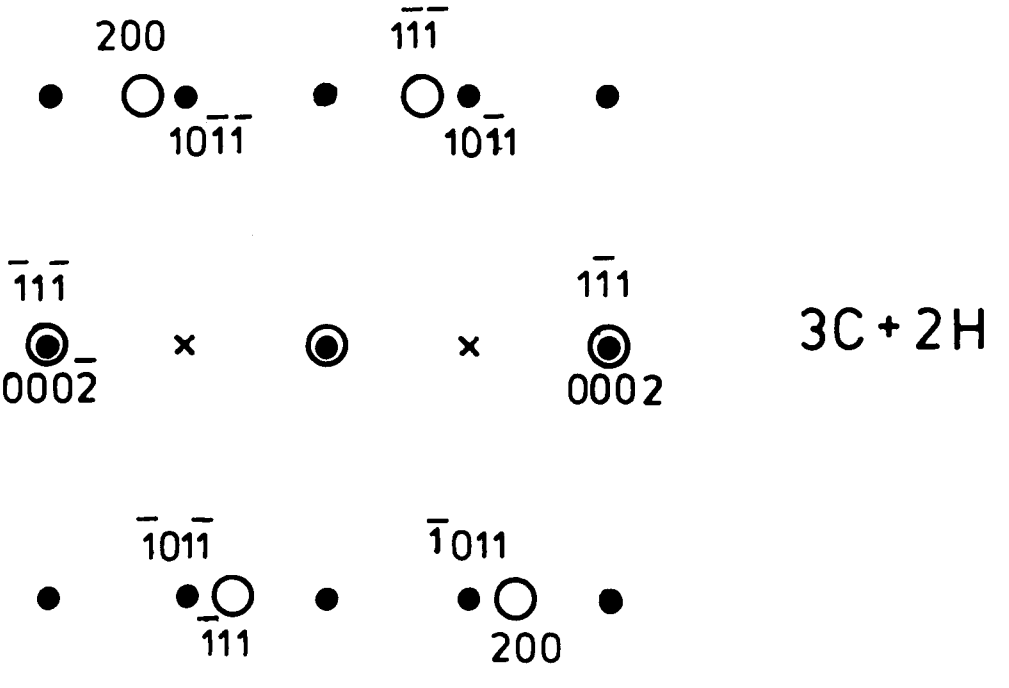

3C + 2H

× Double diffraction

reflexions alone (Jepps et al., 1979). As explained in section II.5 the stacking sequence of SiC_4/CSi_4 tetrahedra can be described in terms of the zig-zag sequence of non-basal plane faces. Thus, by imaging these planes the ABC sequence is uniquely identified.

Jepps (1979) has explained that the reticular density of these planes varies according to the stacking sequence. In 6H, the tetrahedral plane $(10\bar{1}2)$ has a high reticular density in one half of the unit cell whilst $(10\bar{\bar{1}}\bar{2})$ has a similar appearance in the other half. Other similar planes occur in structures where stacking operations occur in units of three(e.g. 6H and 3C) but are systematically absent in other polytypes(e.g. 2H, 4H, 15R). Nevertheless, in these structures alternative planes which potentially contain similar information about the stacking sequence can be imaged. For example the $(10\bar{1}1)$ and $(10\bar{\bar{1}}\bar{1})$ planes are suitable in 2H.

II.4.3 Mechanisms of crystal growth

Several different theories of polytypism (reviewed by Trigunayat & Chadha, 1971) have been put forward to account for polytypism in crystals and particularly in SiC; these are briefly outlined in the following section.

The first reasonable explanation (Frank, 1951) proposed a screw-dislocation theory of polytypic growth in which material was deposited from the vapour phase around screw dislocations emerging on the (0001) faces of initial crystal nuclei. This theory was supported by the observation of spiral markings on the surface of silicon carbide crystals (see Verma & Krishna, 1966) but Verma (1951a,b) was the first to measure 15.1 and 15.2 Å step heights on the surface of 6H crystals ($\underline{c}$ = 15.079Å).

Mitchell (1957), later calculated that nearly all the known structures of SiC could be derived on the basis of screw-dislocations exposed on 4H, 6H and 15R nuclei. However, the discovery of 2H (Adamsky & Merz, 1959) and the anomaly of the known 8H polytype, both of which were not predicted by the theory, cast doubt on the basic assumptions. Verma & Krishna (1966) subsequently modified the theory to explain all the known polytypes including rhombohedral structures. Pandey & Krishna (1975 & 1976) have further deduced the SiC polytypes that can result from the spiral growth round a single screw dislocation created in faulted 6H, 4H and 15R matrices by calculating the relative probabilities of different fault configurations from their stacking fault energies. Excellent agreement is found between experimentally-observed structures and those theoretically predicted without resorting to complicated configurations of cooperating screw dislocations.

Nevertheless, many crystals exhibit no growth spirals on their surfaces and it is difficult to explain the commonly observed feature of syntactic coalescence of two or more polytypes within the same crystal. Furthermore the screw-dislocation theory fails to account for the thermal stability of the polytype structures or the existence of the one-dimensional disorder which is found in a large number of SiC crystals. In an attempt to account for these observations Jagodzinski (1954) developed a theory which considered that because the internal energies may be assumed equal, the minimum free energy was determined by a maximum entropy. The total entropy of a structure consists of two parts - configurational and vibrational. The configurational entropy increases with increasing disorder, being highest when the structure is completely disordered, whereas the vibrational entropy increases as the

stacking faults are ordered. Thus disorder can be stabilized through the agency of the vibrational entropy. Jagodzinski also assumed that the only truely stable modification was 3C and that all other polytypes were derived by suitable insertion of stacking faults which are preferentially ordered because of their vibrational entropy contribution.

Other theories based on entropy considerations have been proposed by Schneer (1955) and Peibst (1963). The former treats polytypism in a similar manner to the cooperative phenomenon of order-disorder in alloys and polytypes represent intermediate states in the phase transition from cubic to hexagonal close-packed over a given temperature range. Accordingly, it should be possible to associate definite polytypes with specific temperatures but, except for a few simple structures, this is not observed. The temperature-structure relationship which seems to exist for the small-period SiC polytypes is by no means exact and temperature dependencies are often masked by impurities which are known to play a role in polytype stabilization (see section II.4.5).

The approach favoured by Peibst (1963) considers that during growth, the order in a crystal is determined by the mutual action of lattice vibrations which can eventually bring about a periodic distribution of stacking faults. However, by its very nature, it is not possible to accummulate experimental evidence to support or refute this theory.

At present the general consensus of opinion is that no single theory is in itself sufficient to explain satisfactorily all the available experimental data but that a number of contributing factors i.e. occurrence of dislocations, temperature, conditions of growth, impurities and entropy considerations, all to varying degrees play contributory parts in determining the final polytypic structure.

II.4.4 Polytype stability

Of the many polytypic structures which occur in SiC all have structures based on one or more of the five basic phases 2H, 3C, 4H, 15R and 6H. These are short-period polytypes and are considered to be thermodynamically stable since they occur most frequently (Verma & Krishna, 1966). Long-period polytypes are much less common and consist of blocks of short-period polytypes which are broken by regularly occurring stacking faults.

As outlined in section II.4.3, many factors influence the polytypism of SiC. Knippenberg (1963) observed the formation of the cubic polytype under conditions of high supersaturation(i.e. non-equilibrium conditions) at 1000°-2750°C in preference to the other basic structures which led him to conclude that 3C is a metastable phase growing only in non-equilibrium conditions over the entire temperature range. Shaffer (1969a) has also established that 3C-SiC is formed under conditions of rapid growth from the vapour phase in the presence of excess silicon irrespective of the temperature; excess carbon favours the formation of the hexagonal modifications. Inomata et al. (1969b,c) also claimed that high supersaturation at 2500°C produced 3C initially although this subsequently recrystallized to give hexagonal polytypes. Subsequently Tairov & Tsvetkov (1981) calculated the free energy of crystallization of 3C and 6H polytypes and showed that the cubic structure was more stable at the nucleation stage although it was metastable in the bulk. They concluded that the lower energy barrier to 3C nucleation is responsible for its smaller value of critical supersaturation and accordingly results in its higher rate of formation as observed by Knippenberg (1963) and Inomata et al. (1969b,c).

Knippenberg (1963) has defined the stability regions for the basic structures shown in Figure II.8, but slightly different results were determined by Inomata & Inoue (1970) from sublimation and growth experiments. They propose that stability regions for 2H, 3C, 4H and 6H are respectively below 1400°, 1400°-1600°, 1600°-2100° and above 2100°C. The 15R polytype was considered metastable over the whole temperature range (but least unstable around 2500°C) and is formed only coalesced with 6H from which it probably grows (Inomata et al., 1969a).

Of the polytypes considered by Knippenberg (1963) and Inomata & Inoue (1970), 2H is considerably rarer than any of the others. The wurtzite or 2H modification of SiC does not occur in commercial SiC and has only been synthesised by the thermal decomposition of methyl-trichlorosilane (CH_3SiCl_3) or silicon tetrachloride ($SiCl_4$)-toluene (C_7H_8) mixtures at 1400-1500°C in a hydrogen atmosphere (Adamsky & Merz, 1959). Crystals of 2H-SiC have been grown from silica-carbon mixtures in a hydrogen atmosphere at 1380°C by doping with lanthanum, or at 1320°C if aluminium is also added, or at 1450°C if nitrogen is included in the gas mixture (Knippenberg & Verspui, 1968). Interestingly, little attention has been paid to a report by Sokhov & Glukhov (1965) who described the formation of 2H-SiC (and 3C) when trying to synthesize silicon nitride from silica and starch at 1400°C in an atmosphere of nitrogen. Prior to the discovery of 2H, Mitchell (1957) reasoned on the basis of the screw-dislocation theory of polytypism that such a modification should not exist and indeed no other polytype of SiC with the number 1 in its Zhdanov symbol has ever been found (see Table II.1).

The discovery of the 2H modification, which in some cases has been co-deposited with 3C, casts doubt on the low temperature stability of

Figure II.8

Stability diagram for silicon carbide polytypes according to Knippenberg, 1963

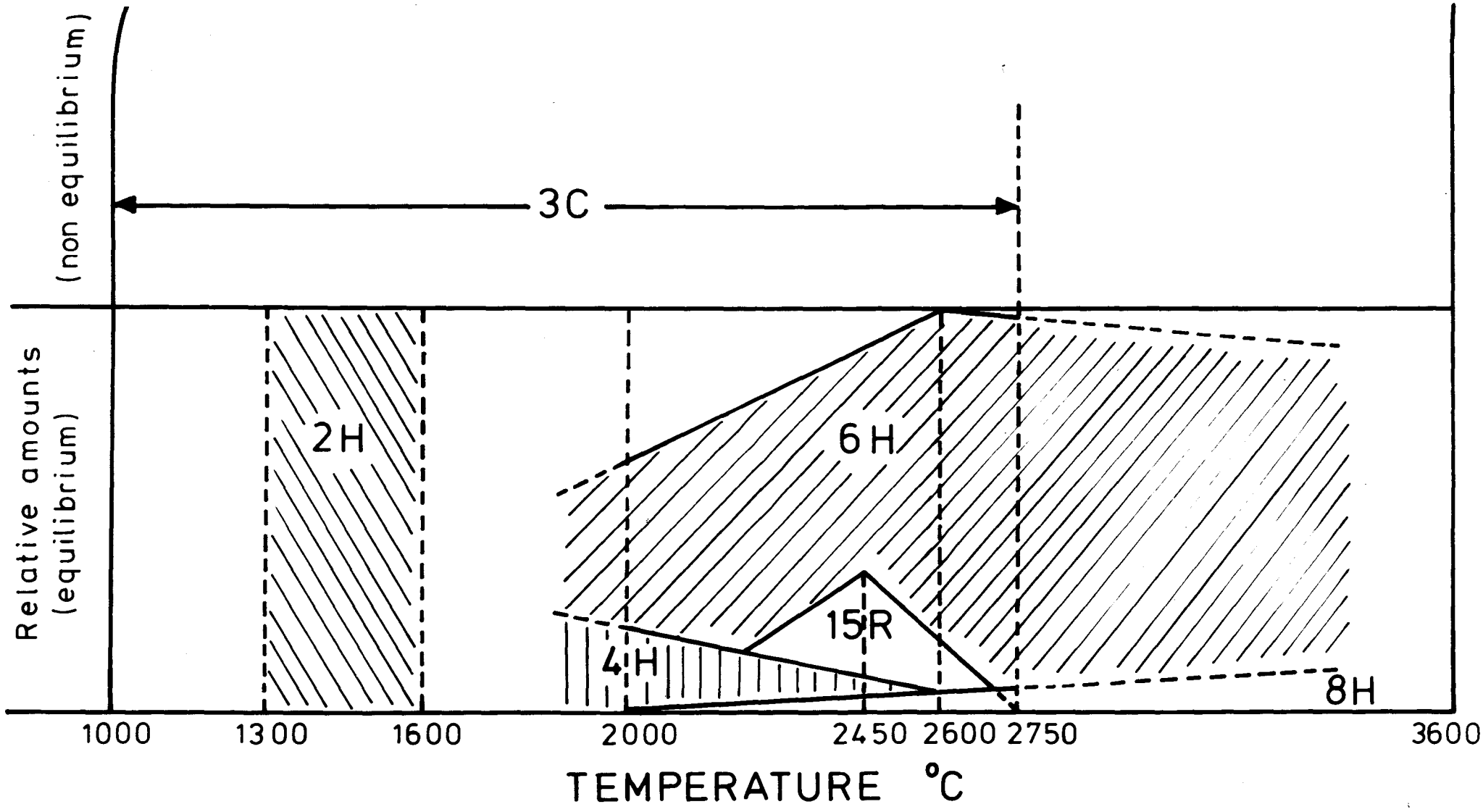

(After Knippenberg, 1963)

3C. Although Knippenberg (1963) has concluded that the cubic modification is metastable at all temperatures, observations that 2H transforms to 3C above 1400°C indicate that 3C is probably thermodynamically stable around 1400°C, eventually transforming above 1600°C to hexagonal polytypes. This apparent stability of the cubic polytype is a problem in the otherwise gradual progression with increasing temperature from 2H through to the 4H and 6H polytypes, this being accompanied by an increase in the degree of cubic packing (Jepps, 1979). The progression corresponds to a decrease in band gap with increasing percentage of cubic packing (Knippenberg, 1963); see Table II.3. The differences in band gap can be correlated with the lattice energy of the polytype and consequently leads to the conclusion that cubic SiC is an unstable modification whereas 2H is the most stable form. Indeed the systematic variation of band-gap has led Knippenberg (1963) to suggest that the energy of electrons may have an important influence on the choice of structure by placing a demand on the arrangement of stacking faults.

II.4.5 Polytype transformations

Polytype transformations in SiC are well documented, particularly the $\beta \rightarrow \alpha$ transformation observed during postfabrication isothermal annealing of dense SiC polycrystalline compacts (Heuer et al., 1978; Jepps, 1979; Ogbuji et al., 1981a,b) and in undensified powder specimens (Kieffer et al., 1969). Similar transformations have been observed in REFEL-SiC (Smith et al., 1978; Jepps & Page, 1979, 1980) by using lattice imaging which allows changes in stacking sequence to be observed directly; see section II.4.2. Using this technique Jepps & Page (1979) suggested that 3C→6H takes place through the initial formation

Table II.3

Relationship between the structure and the band-gap of SiC polytypes (Knippenberg, 1963)

polytype	percentage cubic packing	band gap (eV)
2H	0	>3
4H	50	3.1
15R	60	2.9
6H	67	2.86
21R	71	2.77
24R	75	2.72
8H	75	2.56
3C	100	2.2

of fine 3C twins which provide 6H nuclei and give intermediate transformation structures (Jepps & Page, 1980) before the formation of the final 6H.

The $\beta \rightarrow \alpha$ transformation observed by Kieffer et al. (1969) and later by Jepps (1979) at 2500°C in argon was also found to be reversed by subsequent annealing in 30 atmospheres of nitrogen at the same temperature.

In addition to the $\beta \rightarrow \alpha$ transformation other transformations have been reported: 4H→6H, 15R→6H (Bootsma et al., 1971); 6H→4H (Martin, 1979); 2H→6H (Krishna & Marshall, 1971a,b; Bootsma et al., 1971; Powell & Will, 1972).

The transformations in 2H observed by Krishna & Marshall (1971a,b) were initiated above 1400°C and resulted in the formation of 3C which itself underwent a transformation to 6H. However, if annealed at 2400°C the 2H single crystals transformed directly to 6H. Using X-ray diffraction methods the transformation, either 2H→3C or 2H→6H, proceeded by the insertion of random stacking faults before giving the new ordered arrangement. 2H single crystals of Tagai et al. (1971) behaved somewhat differently in that although X-ray reflexions corresponding to 3C, 4H and 6H appeared at 1600°, 1900° and 2000°C respectively the 2H reflexions did not disappear completely, suggesting that some microscopic regions of the crystals remained unchanged because nucleation of a second phase could occur only in particular regions.

Powell & Will (1972) reported transformations in 2H single crystals at temperatures as low as 400°C but the resulting structure had a disordered arrangement of layers although at higher temperatures a faulted 3C-6H structure formed.

Solid state transformations in SiC were initially considered to

occur by three possible mechanisms (Pandey & Krishna, 1973). Firstly, the periodic-slip mechanism envisages that changes in the layer sequence take place by the movement of partial dislocations round a screw dislocation. Alternatively, changes in the stacking sequence could occur by randomly introduced stacking faults which eventually order and result in the new structure - a layer-displacement mechanism. Thirdly, a vapour or surface flow mechanism based on observations of changes in crystal morphologies and transformation rates has been proposed by Bootsma et al. (1971) where the important consideration is the detachment of molecules into a "liquid" surface layer which is then followed by redeposition onto a nucleus provided either by a disordered region or by solid-state transformation.

Pandey et al. (1980) have recently calculated the changes expected in a 2H diffraction pattern when these crystals undergo solid state transformation to 6H by either the layer displacement mechanism or the periodic-slip mechanism. They concluded that the 2H→6H transformation occurring by layer displacements has the following characteristics: (1) insertion of a large number of random stacking faults causes intensification of streaks along 0001 reciprocal lattice rows; (2) intensity maxima characteristic of the new structure appear on the streak; and (3) the resulting structure will invariably contain a large concentration of random stacking faults. In contrast, when periodic-slip occurs the resulting structure contains few or no stacking faults, and diffraction spots from the new structure appear at an early stage of transformation. The available experimental evidence strongly indicates that transformations from the 2H structure take place by layer displacements. Indeed, Jagodzinski (1971) has independently concluded from theoretical

calculations and from experimental data that the 3C→6H transformation occurs by displacement of layers in the solid state.

II.4.6 Impurities

Impurities play an important part in determining the polytypic form of SiC. They also affect the colour (Baumhauer, 1912; Thibault, 1944) and have important consequences in determining physical properties; e.g. the low resistance of SiC heating elements is due to nitrogen impurities. Cutler (1978) has remarked that in the absence of impurities α-SiC is always formed in preference to 3C. Moreover, all the transition elements of the first long period except Ti promote 3C formation whilst Al, Ti, Zr, Nb promote α-SiC formation with Al being a particularly strong α promoter. A wide range of impurities can be incorporated into SiC (B, N, Al, P, Ge, Be, Ga, Se, La, Sc, In, Cr) mainly to produce p-n junctions. The donors N, P and O, and the acceptors B, Al, Ga, In, Be, Sc and Cr significantly affect the semi-conducting properties of SiC and, for example, Ga and Be are used as luminescence activators.

II.4.6.1 Aluminium

Lundquist (1948) first showed quantitatively that in the absence of impurities 6H is the stable form of SiC but when aluminium is added 4H is preferentially stabilized: Figure II.9(a). Mitomo et al. (1970 & 1971) reported similar findings at 2000°-2400°C; see Figure II.9(b). Bind (1978) and Tajima & Kingery (1982) also agree that 4H is stabilized by aluminium, although Knippenberg (1963) found that aluminium in the range 0.01-0.1% did not stabilize any particular polytype.

Figure II.9

Correlation between aluminium content and the relative amount of silicon carbide polytypes as observed by:

(a) Lundquist (1948)

(b) Mitomo et al.(1970)

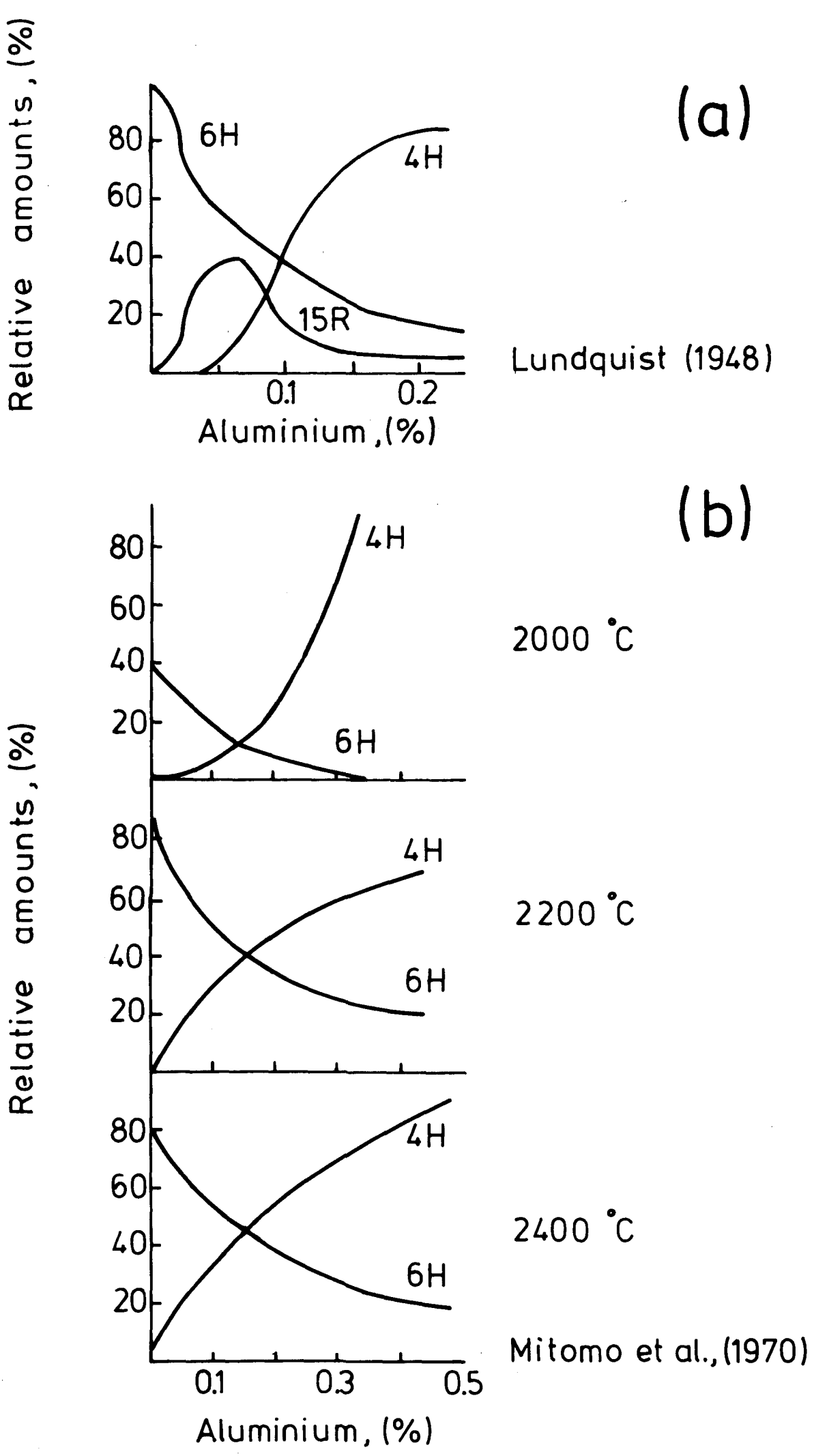
(a)
Relative amounts, (%)
80
60
40
20
6H
4H
15R
0.1
0.2
Aluminium, (%)
Lundquist (1948)
(b)
Relative amounts, (%)
80
60
40
20
4H
6H
2000 °C
4H
6H
2200 °C
4H
6H
2400 °C
0.1
0.3
0.5
Aluminium, (%)
Mitomo et al., (1970)

Mitomo et al. (1970) and more recently Tajima & Kingery (1982) agree that Al stabilizes 4H and that this occurs with an increase in unit cell dimensions as Si-C bonds (1.88 Å) are replaced by Al-C bonds (2.01 Å); see Figure II.10. Mitomo et al.determined a solubility limit of ∿0.38 w/o whereas Tajima & Kingery obtained a higher value of ∿0.9 w/o Al. Differences in the c dimensions of 4H at zero Al addition probably arise because of other impurities. Experiments carried out in the present work agree that Al stabilizes 4H with an increase in lattice parameters, the maximum value of c = 10.079 Å corresponding to an Al addition of ≲1.8 w/o at 2000°C. Tajima & Kingery (1982) assumed that the amount of Al dissolved in the lattice was equal to the initial addition but since their experiments were carried out at 2200°C i.e.above the boiling point of Al (2057°C) this assumption is invalid. On the other hand Mitomo et al. (1971) determined Al contents spectrophotometically and so their results may be more reliable. In contrast to these findings Batha & Hardy (1973) report little change in the a and c unit-cell parameters as a function of aluminium concentration but since their experiments were carried out at 2500°C, i.e. 450°C above the boiling point of aluminium,their conclusion is not really surprising. The present evidence indicates that aluminium stabilizes 4H by entering into the lattice and inducing a rearrangement 6H→4H.

II.4.6.2 Boron

Boron does not stabilize a particular polytype but has been used with carbon as an additive (typically 0.4 and 0.6 w/o respectively) to pressureless sinter submicron β-SiC powder to high densities at ∿2000°C (Prochazka, 1973). Martin (1979) used boron to hot-press 6H

Figure II.10

The variation in c dimension of 4H

with aluminium content, according

to Mitomo et al. (1971) and Tajima & Kingery (1982)

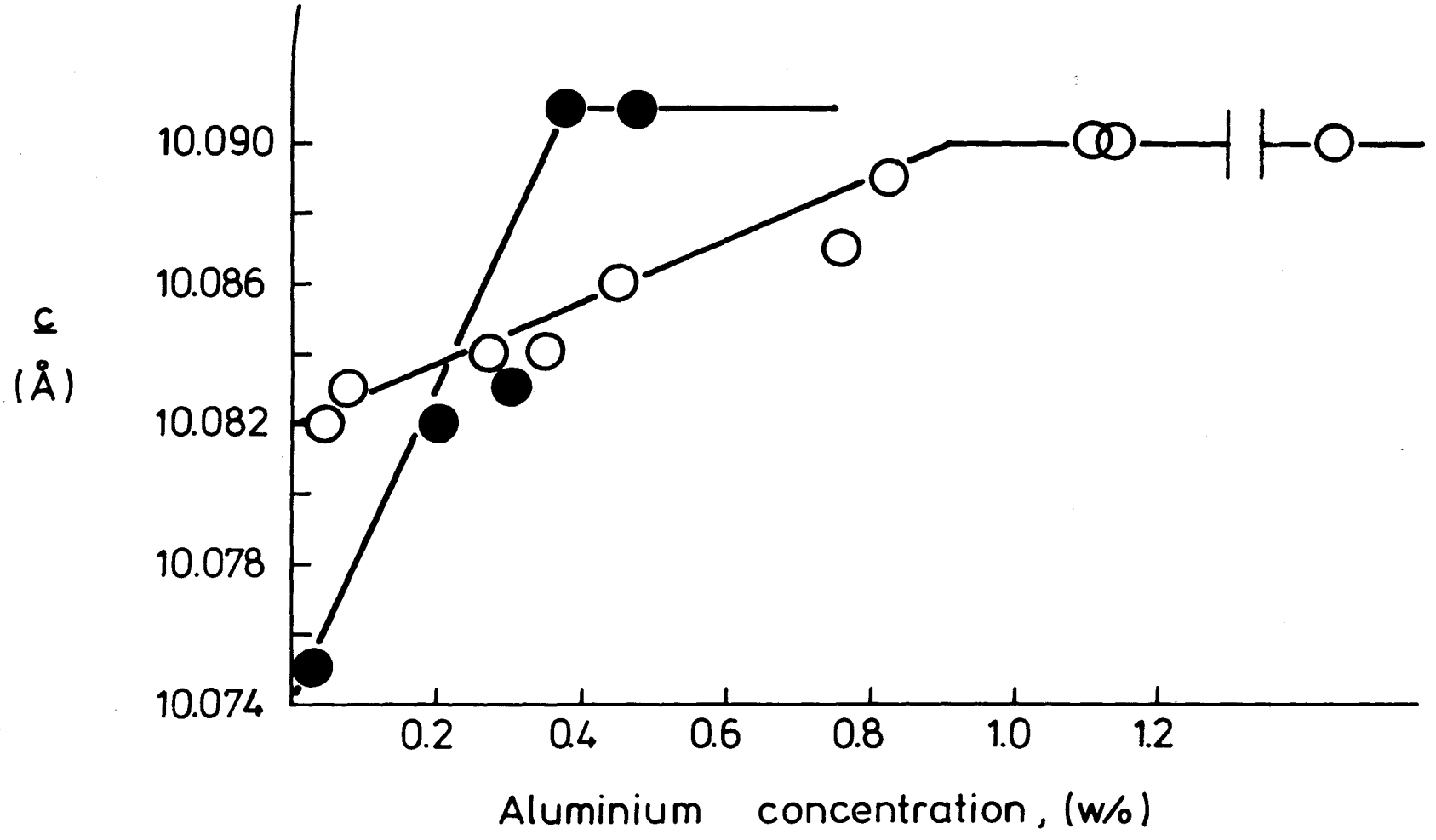
c
(Å)
10.090
10.086
10.082
10.078
10.074
0.2
0.4
0.6
0.8
1.0
1.2
Aluminium concentration, (w/o)
Mitomo et al., (1970)
Tajima & Kingery, (1982)

SiC to give dense 4H polytype. In contrast Batha & Hardy (1973) and Shaffer (1969b) observed 6H in the presence of boron at temperatures above 2000°C and both have determined the solid solubility of boron in SiC as ∿0.1 w/o. Vodakov & Mokhov (1973) report a similar value. A slightly higher solubility limit is given by Murata & Smoak (1978) (0.4 w/oB as B_4C at 2200°C). Lattice parameters (Shaffer, 1969b; Batha & Hardy, 1973; Murata & Smoak, 1978) are reduced suggesting that B substitutes for Si, but electron spin resonance (Woodbury & Ludwig, 1961) indicates that B substitutes for C. Tajima & Kingery (1982) reconsidered all the available data and are of the opinion that to minimize the free energy of the system B replaces both Si and C but the situation is still not entirely clear.

II.4.6.3 Nitrogen

It is well known that nitrogen can be accommodated in the SiC lattice and in so doing stabilizes 3C, especially at high temperatures and high pressures of nitrogen (Addamiano & Staikoff, 1965; Slack & Scace, 1965; Kieffer et al., 1969; Jepps, 1979). Slack & Scace (1965) determined by vacuum fusion the nitrogen content of 3C prepared from 6H at 2720°C under 35 atmospheres of nitrogen and found 0.3 a/o; the unit-cell dimension 4.357 Å is less than 4.3598 Å for material prepared at low temperatures in a nitrogen-free atmosphere. Using powders, Kieffer et al. (1969) and Jepps (1979) for dense polycrystalline materials determined that 30 atmospheres of nitrogen is sufficient to stabilize 3C at 2500°C and exchanging nitrogen for argon reverses the transformation. The nitrogen content of both the 3C and α materials was extremely low and no changes in lattice parameters were observed.

Prochazka et al. (1978) obtained 0.8 w/o N by inert gas fusion in 3C sintered at 2300°C with boron under one atmosphere of nitrogen. Shaffer (1969b) has also observed that at 2500°C and high nitrogen pressures 3C is stabilized and adding boron and aluminium stabilizes 6H and 4H respectively; see Figure II.11(a) and (b). However, Figure II.11(b) is somewhat ambiguous as the meaning of "100% addition of Al" is not clear and therefore these claims should be considered cautiously.

The diffusion of nitrogen from the gas phase into SiC single crystals has been determined from conductivity measurements (Carrol, 1960; Kroko & Milnes, 1966; Lilov et al., 1976) and concentrations of $\sim$0.1 a/o have been obtained. Lilov et al. also observed that the nitrogen partial pressure dictates the relative amounts of 3C, 6H and 15R formed in growth experiments at 2300°C with 3C increasing as the nitrogen pressure increases.

Figure II.11

SiC polytype stability at 2,500°C as a function of N_2 pressure and (a) boron and (b) aluminium additions (Shaffer, 1969)

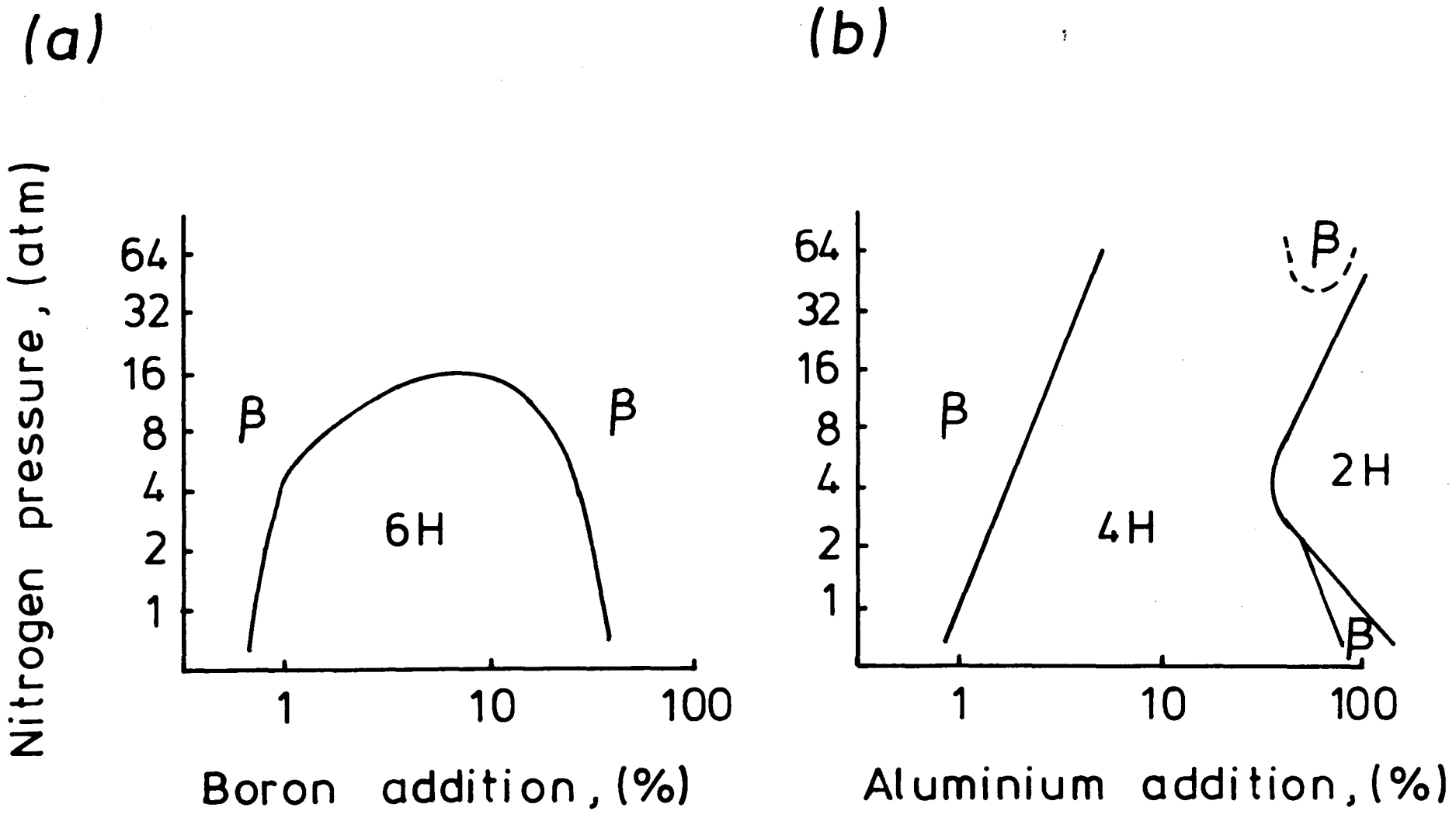

Shaffer, (1969)

III SCOPE OF THE PRESENT INVESTIGATION

The present study was undertaken initially to confirm that the large metal ions present in α'-sialon were incorporated into the interstitial sites of the structure. For this purpose a series of calcium α'-compositions of increasing calcium content was prepared and a complete structure determination carried out on the most calcium-rich single-phase α'-composition. The formation of α'-sialons is assisted by the presence of a transient calcium aluminium-silicon oxynitride liquid which allows solution of the starting oxides and nitrides followed by precipitation of α'. This liquid also plays an important role when α'-sialons are reduced by carbon to form silicon carbide-aluminium nitride solid solutions with the wurtzite (2H) structure. A more direct method for producing the potentially interesting silicon carbide-aluminium nitride alloys from silicon nitride, aluminium nitride, carbon and calcium oxide has been investigated and using this method phase relationships in the silicon carbide-aluminium nitride system have been determined. The investigation was extended to low aluminium nitride contents to establish whether small amounts of aluminium and nitrogen influence the formation of different silicon carbide polytypes.

The thermal stability of (Si,Al)(N,C) alloys was determined over the temperature range 800-2100°C. In addition, a complementary microstructural study using scanning and transmission electron microscopy coupled with chemical analysis by energy dispersive X-ray techniques was used to determine specimen homogeneity and to observe structural and morphological changes.

A review of silicon nitride ceramics and relevant areas of silicon carbide technology has been described in Chapter II and the experimental methods used in the present study are given in Chapter IV. The structure determination of a calcium-rich α'-sialon is presented in Chapter V and the formation of silicon carbide from silicon nitride and carbon is discussed in Chapter VI. The alloying of silicon carbide with aluminium nitride is described in Chapter VII and Chapter VIII contains a description of the structure of a variety of prepared silicon carbide materials using transmission electron microscopy and lattice imaging techniques.

IV EXPERIMENTAL METHODS

IV.1 Powder preparation

The analyses of the starting powders are given in Table IV.1. Three types of silicon nitride were used; each contained different levels of impurities and about 4 w/o silica as an amorphous surface layer. Aluminium nitride (H.C. Starck-Berlin) was nominally 99 w/o pure but contained approximately 4 w/o alumina as a surface layer. Boron nitride (New Metals and Chemicals Ltd.), in which the pellets were usually embedded during firing, had a particle size of <10 μm. The particle size distribution of the starting materials was established by scanning electron microscopy; see Figures IV.1 and IV.2. The Starck and Toshiba silicon nitrides, IV.1(a) and (b) respectively, both have similar average particle sizes, although the size distribution in the Toshiba powder is more uniform. The G.T.E. powder is less homogeneous with two distinct crystal morphologies, needles and smaller equiaxed particles; see Figure IV.1(c). The aluminium nitride powder has a range of larger particle sizes (3-8 μm) (see Figure IV.2(a)) and the calcium oxide crystallizes as cubes with size range 7-20 μm, (Figure IV.2(b)) but since it is very reactive this wide range of large particle sizes does not cause problems.

The calcium oxide was prepared by calcining calcium carbonate (Analar) at 920°C to constant weight. Silicon nitride and aluminium nitride powders were vacuum dried at 120°C for several hours before use.

Silica and carbon mixtures were prepared by sol-gel processing described by Szweda (1980), and were also vacuum dried at 120°C before

Table IV.1

Characterization of starting materials

powder	particle size (μm)	impurities (w/o)	X-ray analysis (w/o)
Si_3N_4 Starck-Berlin	0.8-2.5	C, 0.2 Ca, 0.2 Fe, 0.3	95 α-Si_3N_4 5 β-Si_3N_4
Si_3N_4 Toshiba	0.8-1.2	C, 0.88 Fe, 0.004 Ca, 0.007	80 α-Si_3N_4 20 β-Si_3N_4
Si_3N_4 G.T.E. Small particles needles (	0.8-1.2 8->20 long 0.4-3.5 wide	Unknown	70 α-Si_3N_4 30 β-Si_3N_4
AlN Starck	3-8	Fe, 0.15 C, 0.08	100 AlN
$CaCO_3$ Analar	7-20 (CaO)	Sr, 0.06 Ba,Na, 0.03 Mg, 0.02 K, 0.005 Cu,Fe,Pb, 0.001	100 CaO (after calcining)
Carbon Monarch 1300	13 nm	-	amorphous
Cabosil M-5 fumed SiO_2	14 nm	no impurities > 0.0003	amorphous

Figure IV.1

S.E.M.'s of starting powders

(a) Starck-Berlin Si_3N_4

(b) Toshiba Si_3N_4

(c) G.T.E. Si_3N_4

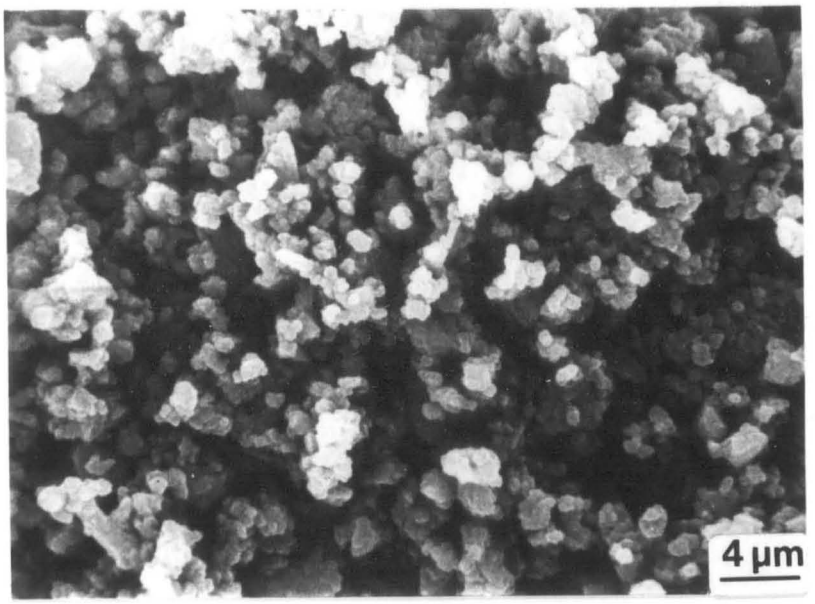

(a)

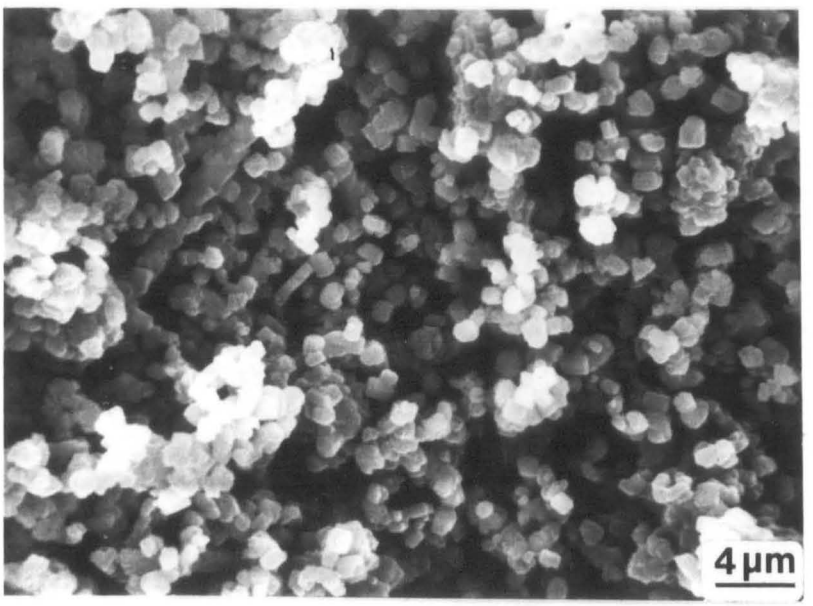

(b)

(c)

Figure IV.2

S.E.M.'s of starting powders

(a) Starck-Berlin AlN (b) CaO

(c) Monarch-1300C (d) Cabosil M-5 fumed SiO_2

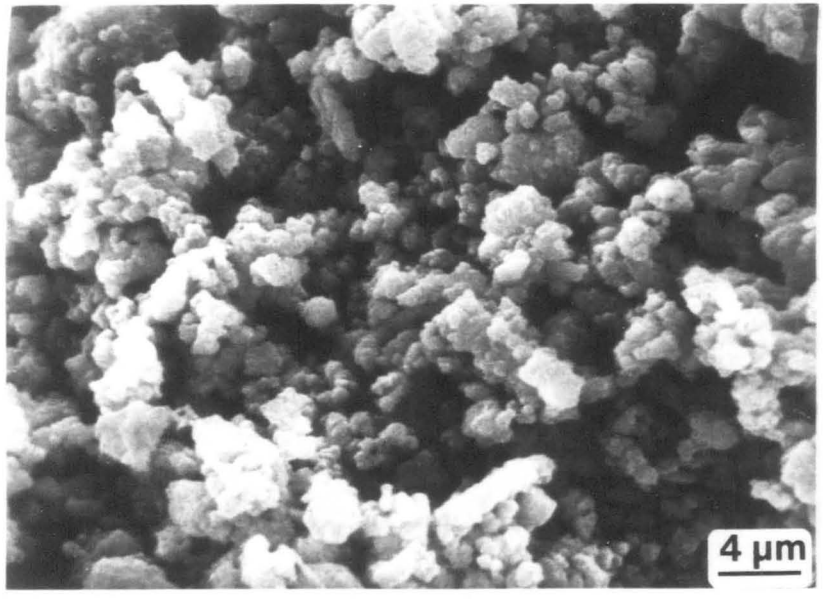

(a)

(b)

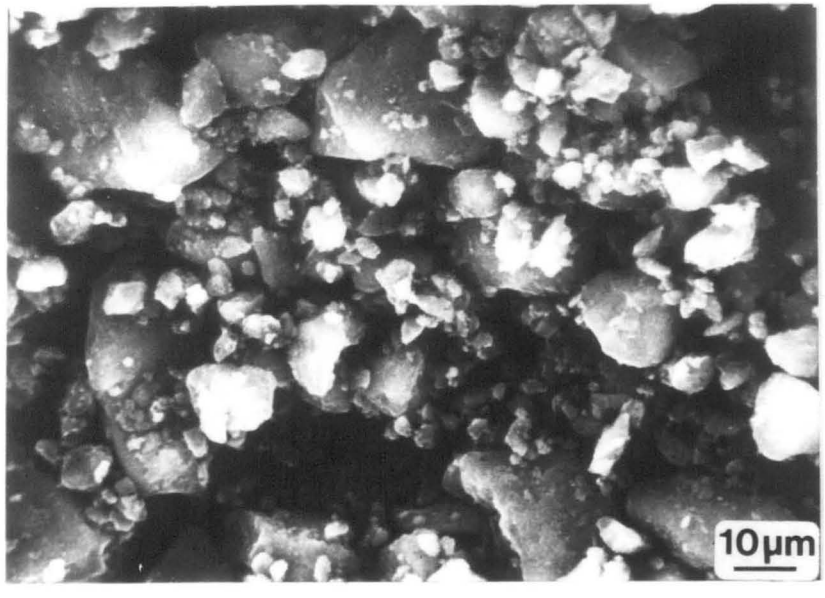

(c)

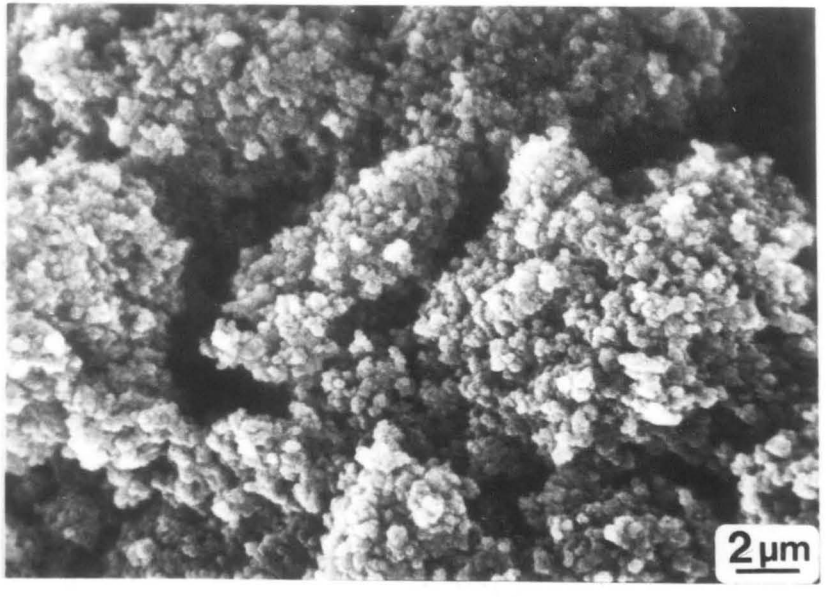

(d)

use.

Other weighed powders were dry-milled, for 20 minutes, in a 5 cm diameter steel cylinder with one steel-ball using a Glen-Creston M280 mixer-mill.

IV.2 Pressure-forming of compacts

Cylindrical "green" pellets were formed by uniaxially pressing powder mixtures in a 1 cm steel die using a hydraulic press and a pressure of 42 MPa (, OO psi). The effect of wall friction gives rise to pressure differences throughout the compact (Kamm et al., 1949) which results in non-uniform density and laminations or cracking when using fine powders. These effects were minimized by keeping the length: diameter ratio less than unity.

Silica-carbon mixtures could not be uniaxially pressed because of their extremely small particle size and so they were isostatically pressed in thin-walled rubber containers using a Stansted laboratory isostatic press. Laminations still occurred but it was possible to produce discs 1-3 mm thick.

IV.3 Furnace methods

(a) Graphite resistance heating

A graphite resistance furnace was used for heat-treatments at 1600°-2200°C; see Figure IV.3. The pellet (<2 g), frequently embedded in boron nitride powder, was placed in a graphite crucible supported on a graphite plinth at the centre of the cylindrical element. A graphite cover was placed over the crucible and the element was surrounded by four molybdenum heat shields. After evacuation the furnace

Figure IV.3

Graphite resistance furnace

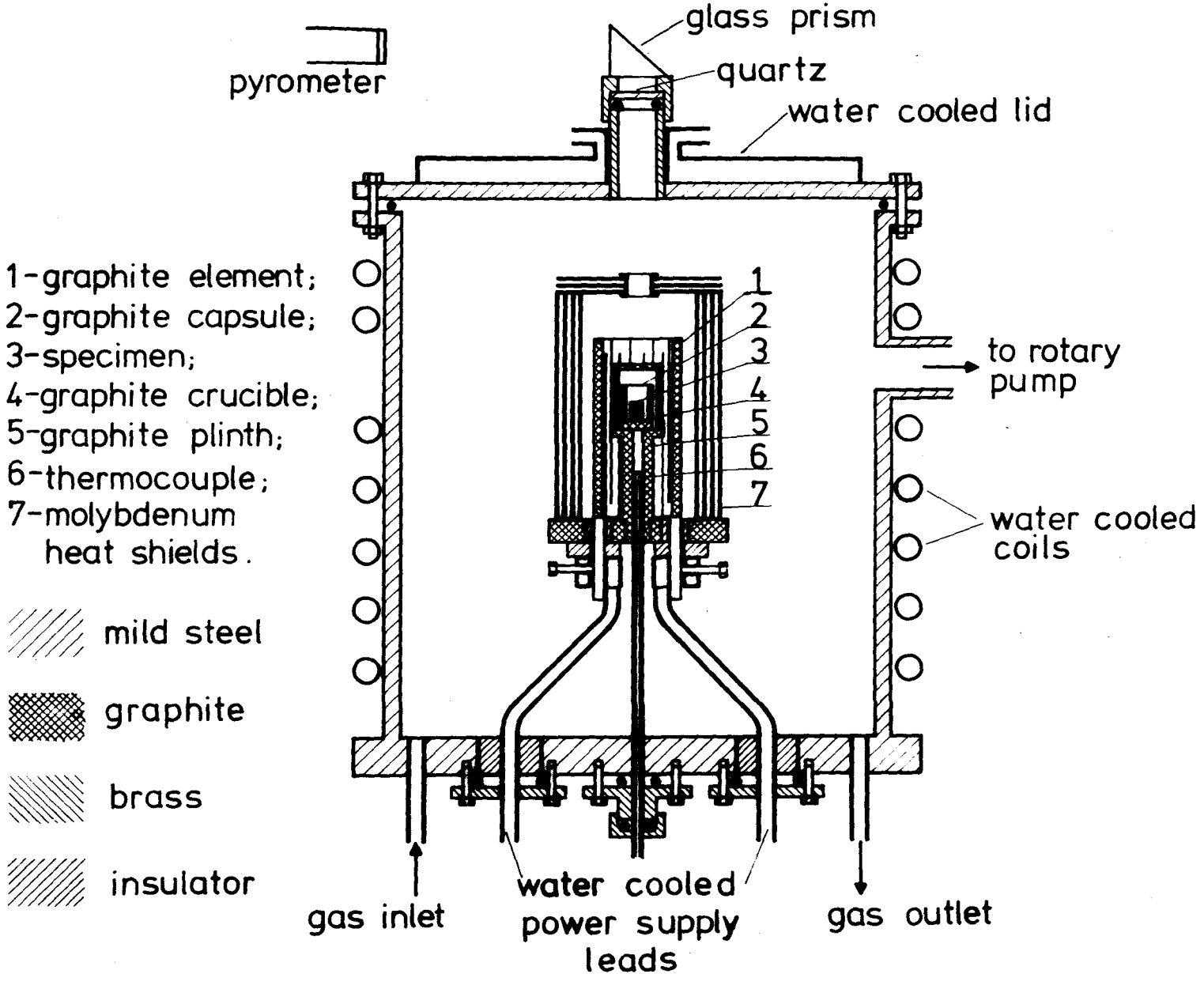
pyrometer
glass prism
quartz
water cooled lid
1-graphite element;
2-graphite capsule;
3-specimen;
4-graphite crucible;
5-graphite plinth;
6-thermocouple;
7-molybdenum heat shields.
1
2
3
4
5
6
7
to rotary pump
water cooled coils
mild steel
graphite
brass
insulator
gas inlet
water cooled power supply leads
gas outlet

chamber was filled with nitrogen or argon, purified from oxygen and moisture by passing over a zirconium getter at 920°C. Power was supplied from a 30 kW DC welding generator via water cooled buzz-bars; the outside wall and lid of the furnace were also water cooled. The temperature was measured by an optical pyrometer focused onto the graphite cover over the specimen and this temperature was calibrated against an Ir/Ir:40 w/o Rh thermocouple that was periodically raised into the hot-zone of the furnace. Rapid cooling at ∿500°C per minute was obtained by switching off the power supply.

(b) Tungsten resistance heating

A tungsten resistance element furnace (see Figure IV.4) was used to carry out heat treatments on∿1g samples up to 1750°C in an inert atmosphere. The sample was usually embedded in boron nitride powder and placed inside an alumina or graphite crucible on a plinth at the centre of a spiral element wound from 4 mm diameter tungsten rod. The element was surrounded by tungsten radiation shields and the steel furnace chamber was water cooled. After evacuation, purified nitrogen or argon was passed into the chamber. Power was supplied via a transformer and rectifier at 150 amps DC and 10V and controlled by a hand-operated voltage regulator. Specimens were normally heated to the firing temperature at ∿200°C per minute. The temperature was recorded with an Ir/Ir:40 w/o Rh thermocouple which was outside the hot-zone and was calibrated against a Pt:6 w/o Rh/Pt:30 w/o Rh thermocouple placed intermittently in the hot-zone.

Figure IV.4

Tungsten resistance element furnace

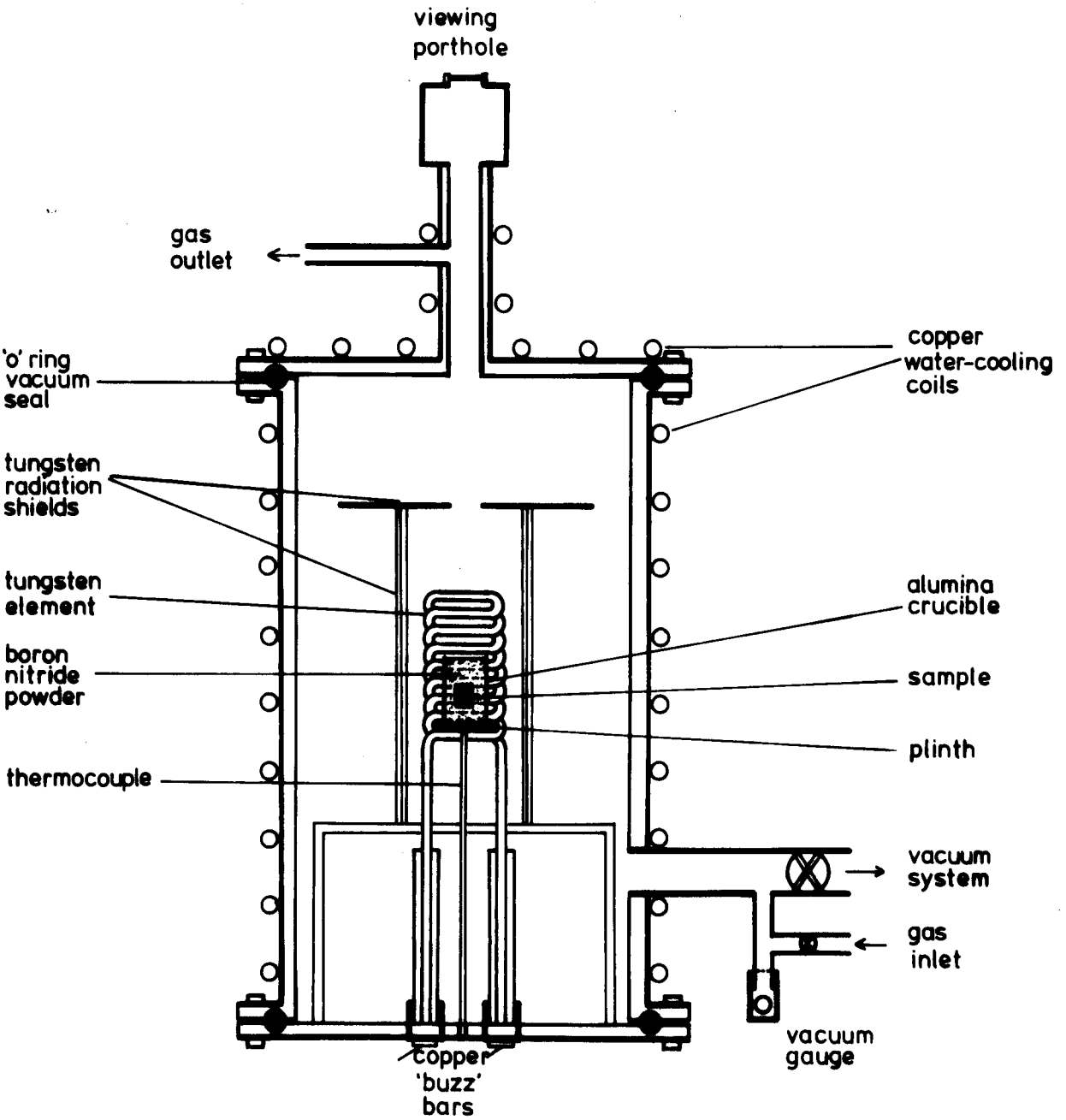
viewing porthole
gas outlet
'o' ring vacuum seal
copper water-cooling coils
tungsten radiation shields
tungsten element
alumina crucible
boron nitride powder
sample
plinth
thermocouple
vacuum system
gas inlet
vacuum gauge
copper 'buzz' bars

(c) Hot-pressing

The experimental arrangement for hot-pressing is shown in Figure IV.5. The graphite die is surrounded by a copper work coil in a "Sindanyo" box supported by refractory bricks. Thermal and electrical insulation between the work coil is provided by fused stabilised zirconia and a vitreous silica cylinder which also protect the die from excessive oxidation.

Preformed pellets are then placed between the two graphite plungers inside the liner and surrounded by a layer of boron nitride which acts as a pressure transmitting medium. Pressures of up to 30 MPa (4.0 psi) are transmitted to the die from the hydraulic press via a reaction-bonded silicon nitride plunger.

A 500 kHz Radyne RI50E high frequency generator with a maximum output of 15 kW supplied the power for induction heating through the water-cooled copper work coil. The temperature was measured with a disappearing filament pyrometer sighted through a 12.5 mm diameter alumina tube onto the wall of the graphite liner through a hole drilled in the die. No temperature correction was made since radiation emitted by the graphite was assumed to be black-body. A constant hot-pressing temperature was usually maintained to within $\pm$ 20°C.

IV.4 Density determination

(a) Density measurements were made with a mercury displacement balance (Ashworth, 1969; Figure IV.6). The sample is introduced into the holder and weights are added to sink the balance until the brass pointers touch the mercury surface. The volume of mercury displaced is equal to the bulk volume of the sample and therefore:

Figure IV.5

The hot-pressing equipment

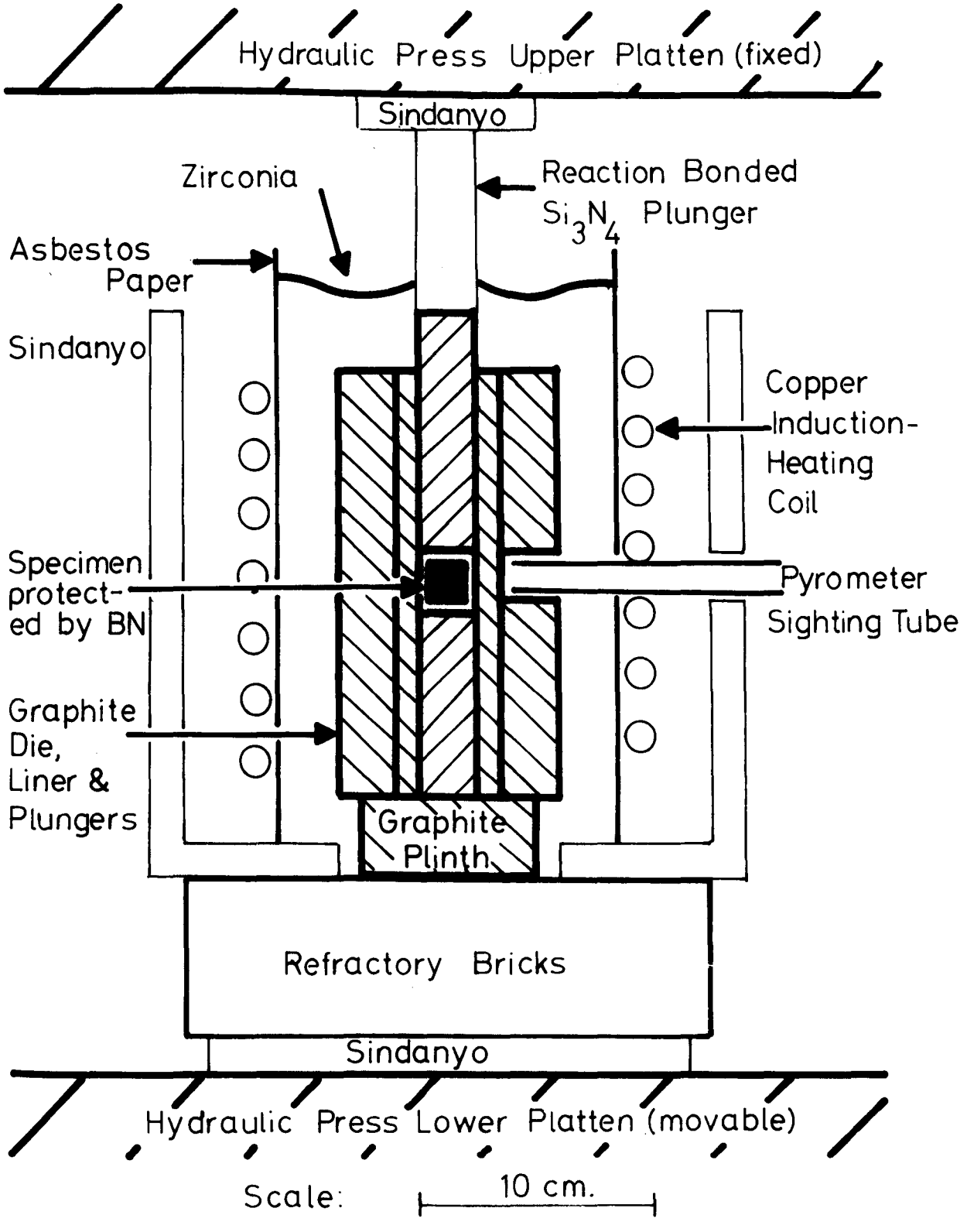
Hydraulic Press Upper Platten (fixed)
Sindanyo
Zirconia
Reaction Bonded
Si_3N_4 Plunger
Asbestos
Paper
Sindanyo
Copper
Induction-
Heating
Coil
Specimen
protect-
ed by BN
Pyrometer
Sighting Tube
Graphite
Die,
Liner &
Plungers
Graphite
Plinth
Refractory Bricks
Sindanyo
Hydraulic Press Lower Platten (movable)
Scale:
10 cm.

Figure IV.6

Mercury displacement balance

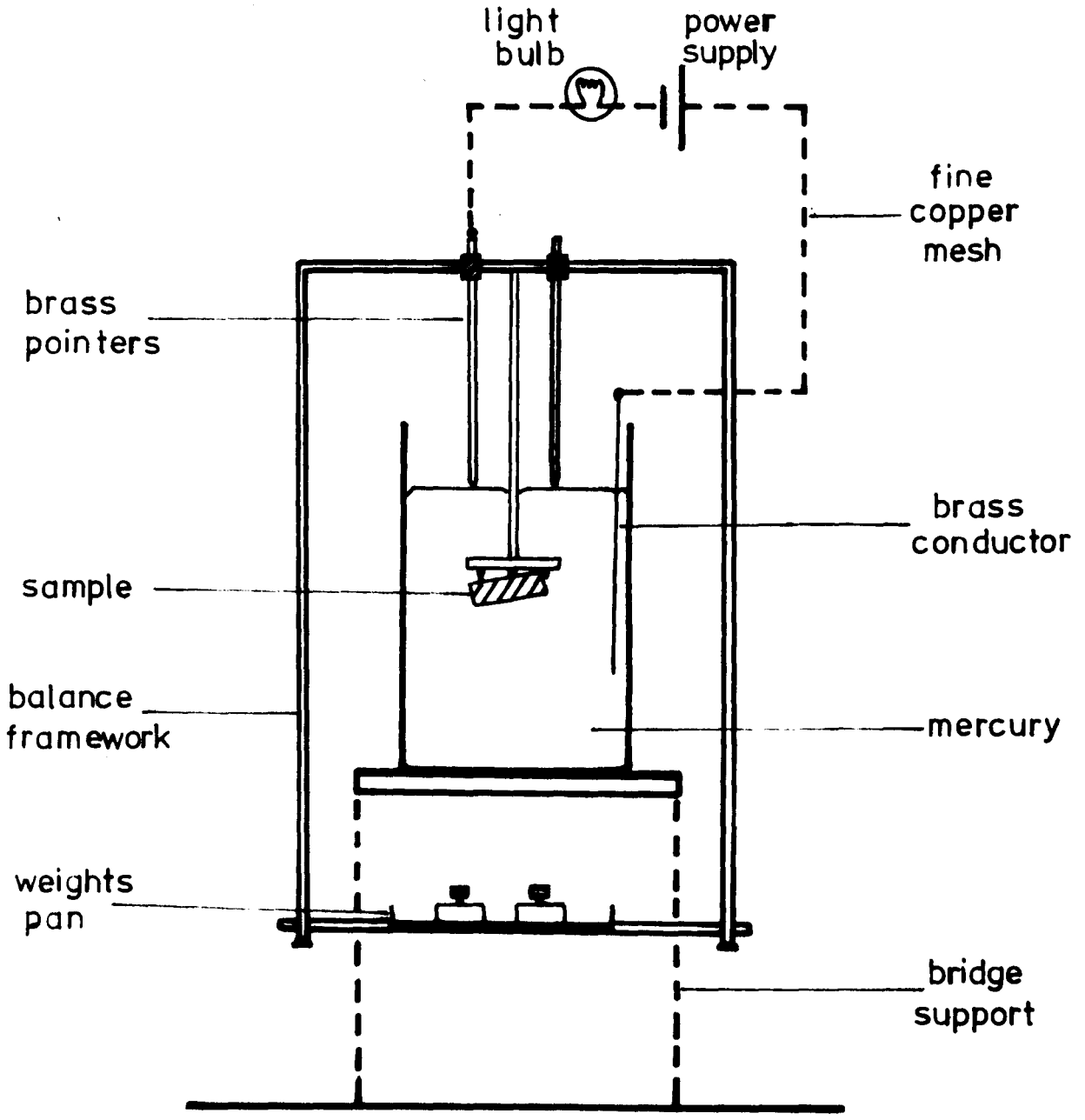
light bulb
power supply
fine copper mesh
brass pointers
brass conductor
sample
balance framework
mercury
weights pan
bridge support

$$\text{Bulk density of sample} = \frac{\text{weight of sample} \times \text{density of mercury}}{\text{weight of sample} + \text{weight required to immerse sample}} \ (\text{gcm}^{-3}) \quad \ldots\text{IV.1}$$

where the density of mercury is taken as 13.56 gcm^{-3}.

IV.5 X-ray diffraction methods

Phase identification and routine unit-cell dimension determinations were carried out with Hägg-Guiner focusing cameras (type XDC-700) using $CuK\alpha_1$ radiation and potassium chloride as an internal standard. The geometry of the system is shown in Figure IV.7.

Weight percentages of the phases identified were estimated by visually comparing the most intense diffraction lines of each phase relative to others in the same photograph. Unit-cell dimensions were obtained using a least-squares computer program (LS) written for the Newcastle University IBM360/370 computer.

Accurate unit-cell dimensions of REFEL SiC were obtained from X-ray powder patterns taken in a Unicam 19 cm Debye-Scherrer camera with monochromated Fe $K\alpha$ radiation (if 3C was present $K\beta$ was also used) and using a Nelson-Riley extrapolation computer program (NR).

Intensity data for the α' structure analysis were collected from suitable Hägg-Guiner X-ray films using a Dobson-type microdensitometer (Taylor, 1951; Figure IV.8). This instrument compares the intensity of a narrow light beam passing through the film with a similar beam from the same source passed through a linear optical wedge.

IV.6 Optical microscopy

Specimens were mounted in thermosetting bakelite and polished using first 220 and 800 grades of silicon carbide paper and then 8, 3

Figure IV.7

Geometrical representation of the Hägg-Guiner

focusing camera system

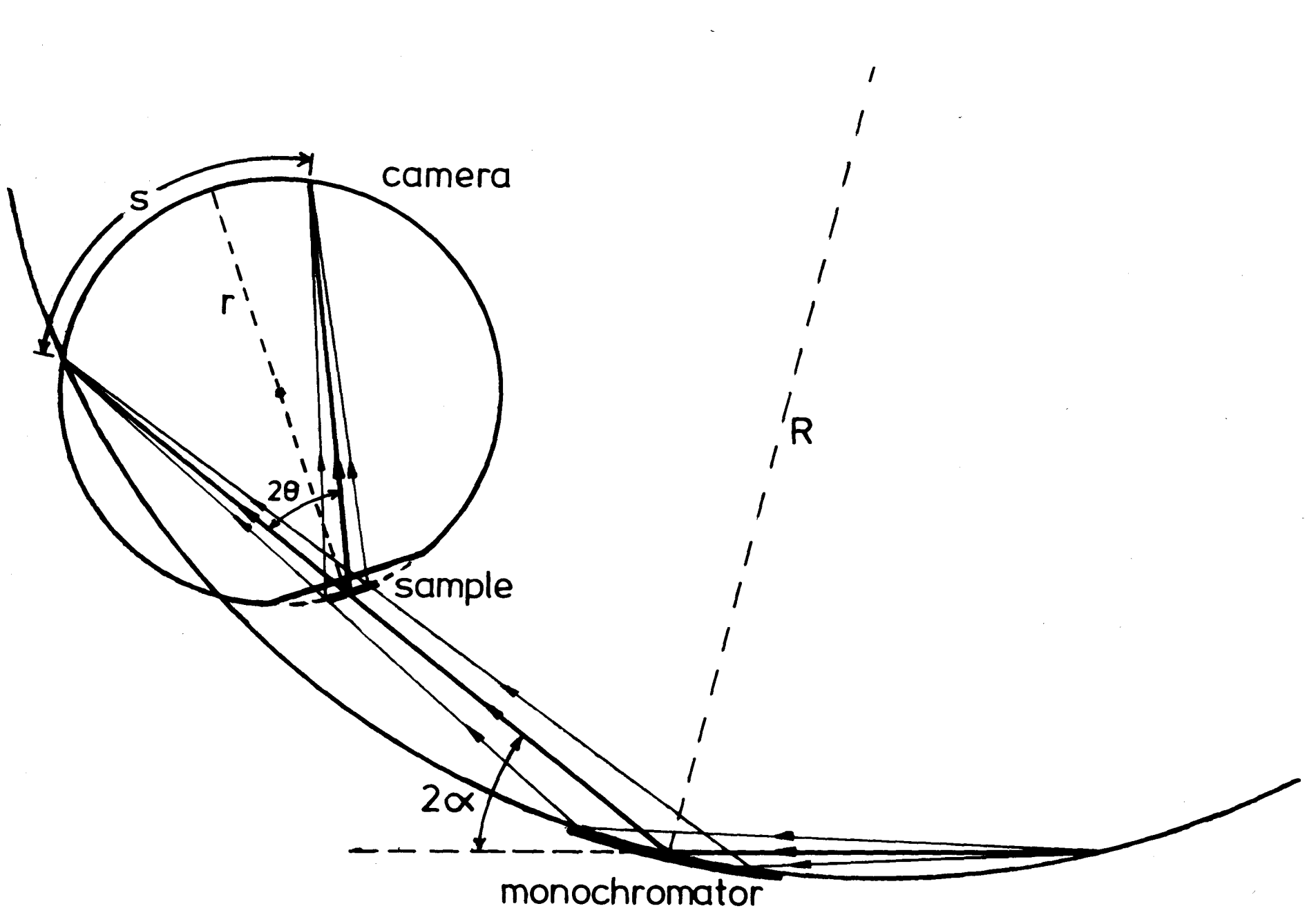
camera
s
r
R
2θ
sample
2α
monochromator

Figure IV.8

Taylor's microdensitometer

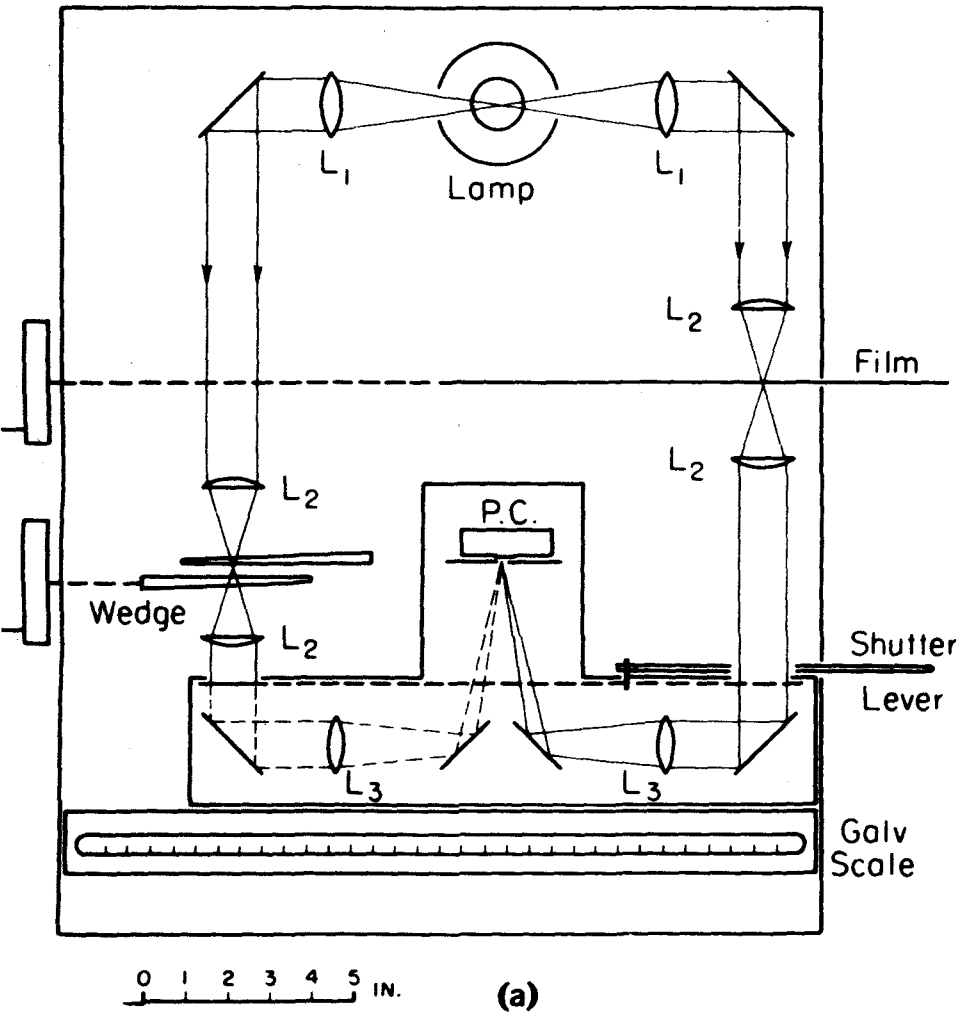

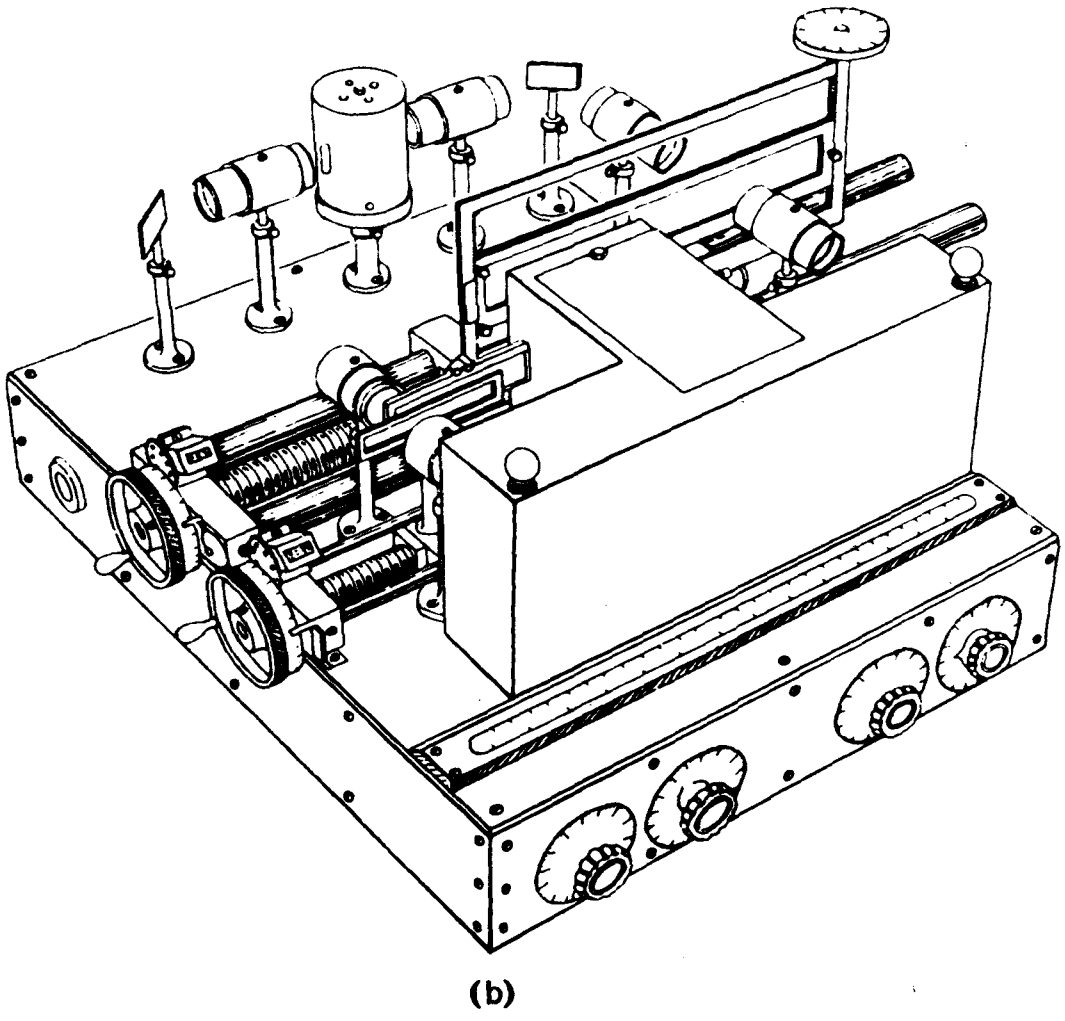

(*a*) Plan of microdensitometer. (*b*) General view of instrument.

and 1 μm diamond paste. Where necessary, the polished specimens were etched with 10% HF for ∿10 seconds to reveal grain boundaries and then examined using either a Vickers or Reichert MeF2 optical microscope.

IV.7 Scanning electron microscopy

Confirmation of powder particle sizes and examination of fracture surfaces of prepared specimens were carried out with a Jeol JSM-T20 scanning electron microscope.

Specimens were mounted on aluminium or graphite studs with "Aquadag" high conductivity silver paint or graphite paste, and then covered with either a carbon or gold coating.

IV.8 Transmission electron microscopy

Specimen preparation for examination by high resolution electron microscopy was identical for all samples. A small piece of the sintered product was crushed in an agate mortar and the crystal fragments made into a suspension with ethanol. A drop of the suspension was then deposited on a holey carbon support film and the solvent allowed to evaporate. Carbon support grids were made following the method outlined by Gannon & Tilley (1976). Examinations were carried out on a Jeol JEM-100CX transmission electron microscope with a high-resolution goniometer stage capable of tilting up to $\pm 10^{\circ}$ in 2 mutually perpendicular directions. The maximum magnification of the microscope was 820,000x with a limit of line resolution 1.4 Å, and point to point, 3.0 Å. Suitable fragments having approximately the correct orientation and with thin edges projecting over holes in the carbon support film were located by searching the specimen grid. Optimum image contrast

was achieved by careful photographic processing of the negative.

IV.9 Chemical analysis

Microanalysis of polished specimens was made with a Cameca "Camebax" electron probe at the Material Development Division, A.E.R.E., Harwell. Fracture surfaces of other specimens were examined using a Jeol JSM-35 scanning electron microscope with an analytical attachment.

The general schematic layout in both instruments is shown in Figure IV.9(a). The main difference between the two instruments is that the JSM-35 has a non energy-dispersive detector whereas the Camebax instrument is fitted with a crystal spectrometer. This means that in the former case the complete spectrum of X-rays is recorded simultaneously but in the latter case only one X-ray wavelength, corresponding to a single element, is detected at any one time. The specimen must therefore be scanned separately for each individual element.

The JSM-35 was operated at 15 kV and the electron beam was focused to $\sim$0.01 μm diameter on the specimen surface.

The identification and concentration of any particular element in the specimen depends on the detection of X-rays which are emitted from the specimen as it is bombarded by the electron beam. Characteristic X-rays are emitted from a depth of approximately 0.5-5 μm depending on the specimen composition and incident electron energy; see Figure IV.9(b). Generally, the larger the energy of the incident electrons and the smaller the average atomic number of the specimen, the more deeply electrons penetrate the specimen which results in X-rays being emitted from a larger volume.

Figure IV.9

(a) General layout of electron probe instrument

(b) Schematic diagram of signal emission area

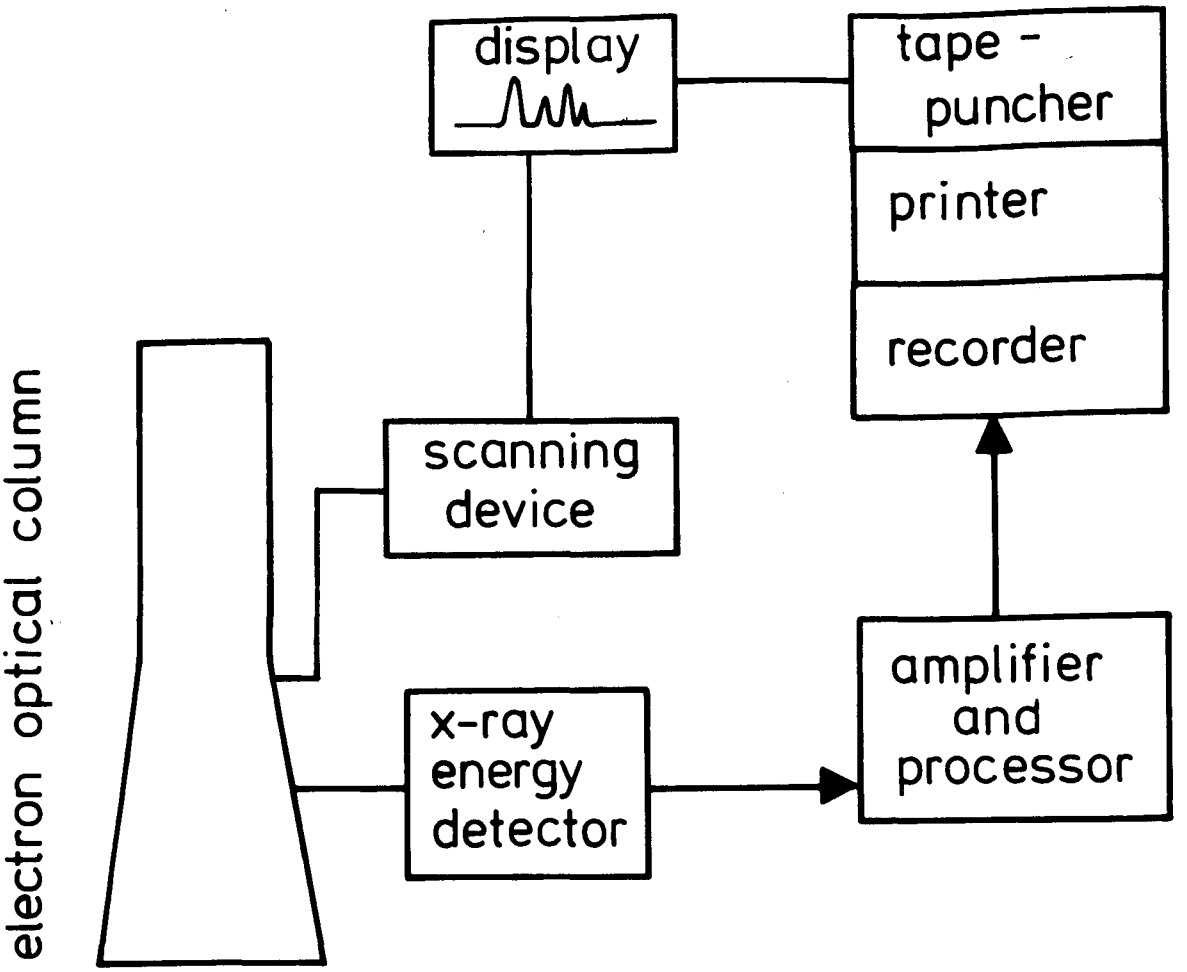
display
tape - puncher
printer
recorder
scanning device
electron optical column
x-ray energy detector
amplifier and processor

(a)

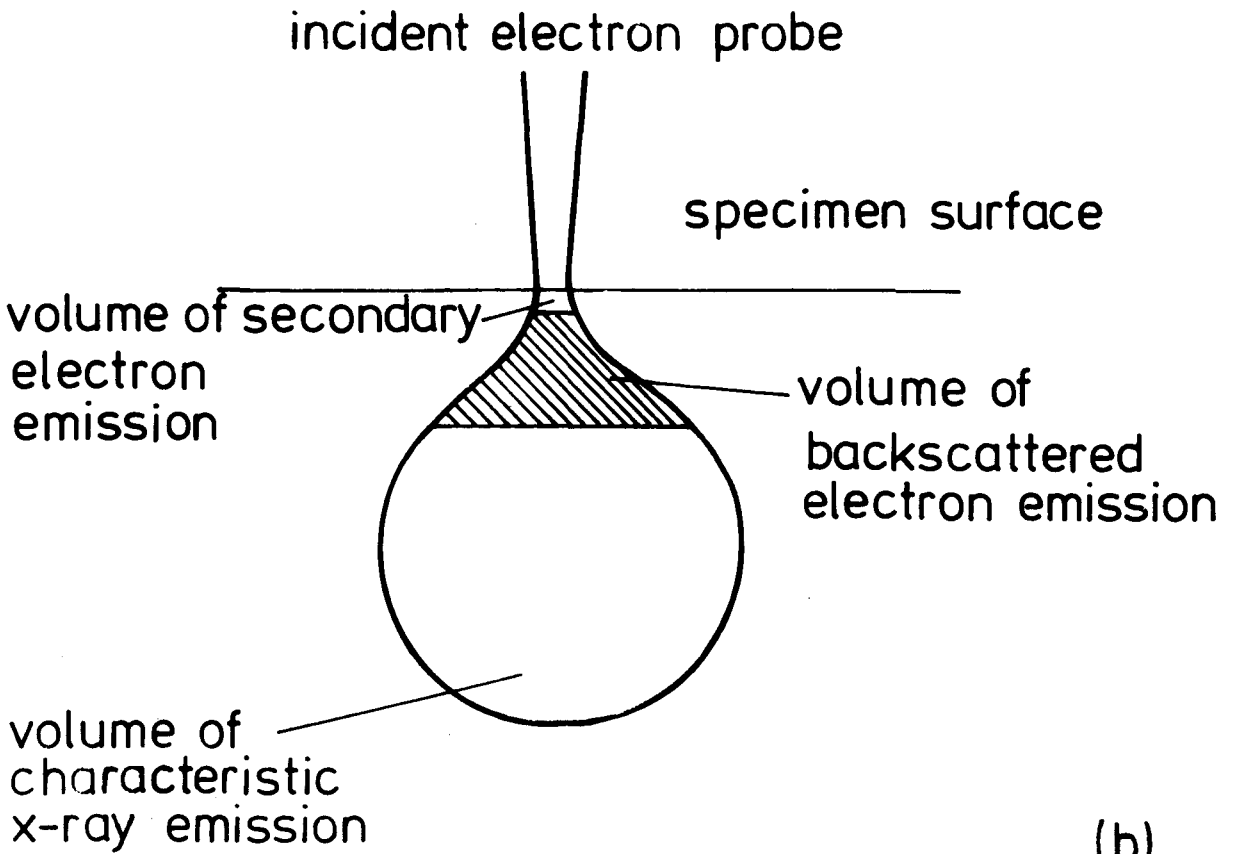
incident electron probe
specimen surface
volume of secondary electron emission
volume of backscattered electron emission
volume of characteristic x-ray emission

(b)

Contributions from areas other than that of interest were generally quite large because of the small crystal size (∿0.1 μm) and low atomic numbers of specimens. In order to restrict spurious contributions as much as possible, specimens for analysis were prepared by gently crushing a small sample under ethanol in an agate mortar and applying a drop of the resulting suspension to a holey carbon support film. The grid was then stuck on a graphite stub with graphite paste. Using this method it was possible to analyse individual crystals free from background contributions.

Results of all chemical analyses were corrected for atomic number, absorption and fluorescence (ZAF corrections) by on-line computers linked directly to both the JSM-35 and Camebax systems.

IV.10 Nitrogen determination

Nitrogen analysis was carried out by inert gas fusion using the A.E.R.E. Harwell Leco TC-136 instrument. Fusion is carried out at 3000^{o}C in a resistance-heated graphite cup. Helium is passed through the equipment as the temperature of the graphite cup is raised and at temperature, the specimen, contained in a nickel basket, is dropped into the crucible. When the sample drops, the flow of helium is interrupted by a valve and the sample is fused. In the case of silicon carbide the nickel basket acts as the flux. After fusion, the gas valve opens and helium flushes out the combustion products, i.e. carbon monoxide and nitrogen or nitrogen oxides. The carbon monoxide is passed over copper oxide and converted to carbon dioxide which is then detected by an infra-red cell. The nitrogen is measured directly in a katharometer using a standard nitrogen-hydrogen mixture in one of the

katharometer cells. A micro-computer in the instrument gives an automatic read-out of nitrogen in weight percent. The total time for analysis is approximately 40 seconds.

V CALCIUM α'-SIALONS

V.1 Introduction

Although it is known that Ca α'-sialons have a structure similar to α-Si_3N_4 it was necessary to confirm the exact locations of the Ca atoms, the number of which is ≤ 2 per unit cell. The structure of α and β-silicon nitride can be described in terms of the stacking sequence of Si-N atom layers i.e. ABAB... in β and ABCD... in α (Hampshire et al., 1978). In β the ABAB... sequence creates long continuous channels parallel to the hexagonal [0001] direction (see Figure V.1) whereas in α the c-glide plane relating the CD and AB layers replaces the channels of β with large closed interstices at 1/3, 2/3, 3/8 and 2/3, 1/3, 7/8 (see Figure V.1). Thus in α-silicon nitride two sites per unit cell exist which are large enough to accommodate additional metal atoms or ions.

It was realised that the difference in position of the X-ray reflexions in the diffraction patterns from α' compositions and α-Si_3N_4 could be explained by the substitution of aluminium for silicon and oxygen for nitrogen in the lattice. However there were also slight variations in the intensities of the reflexions which could not be explained merely by a composition corresponding to

$$(Si,Al)_{12}(O,N)_{16}$$

or a vacancy structure having a formula

$$Si_{12-x}Al_xN_{16-x/3}$$

The possibility that electroneutrality could be maintained by metal ions occupying the two interstices in the structure was considered since this could also explain the observed intensity differences between

Figure V.1

"Idealised" atom configuration in

α and β silicon nitrides

Idealised Si-N layers

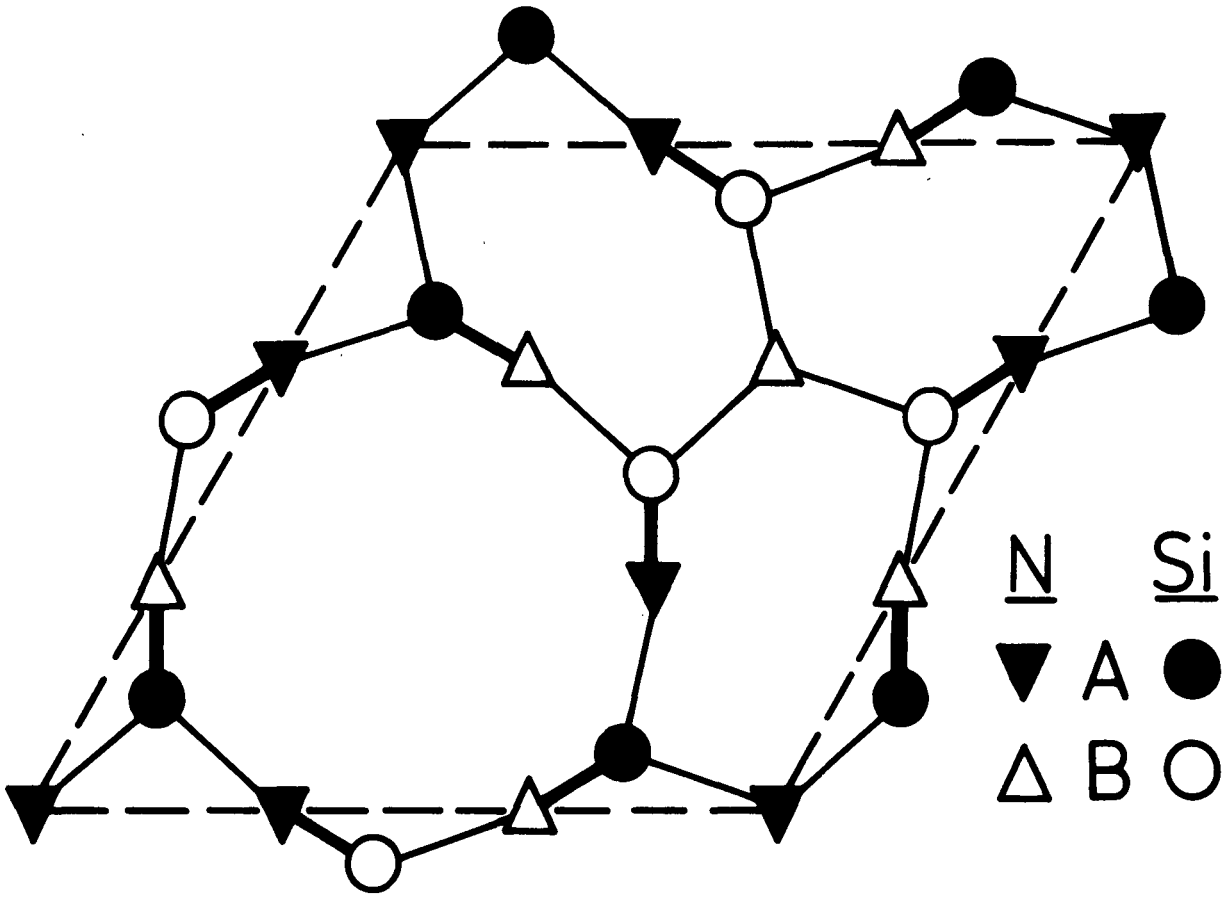

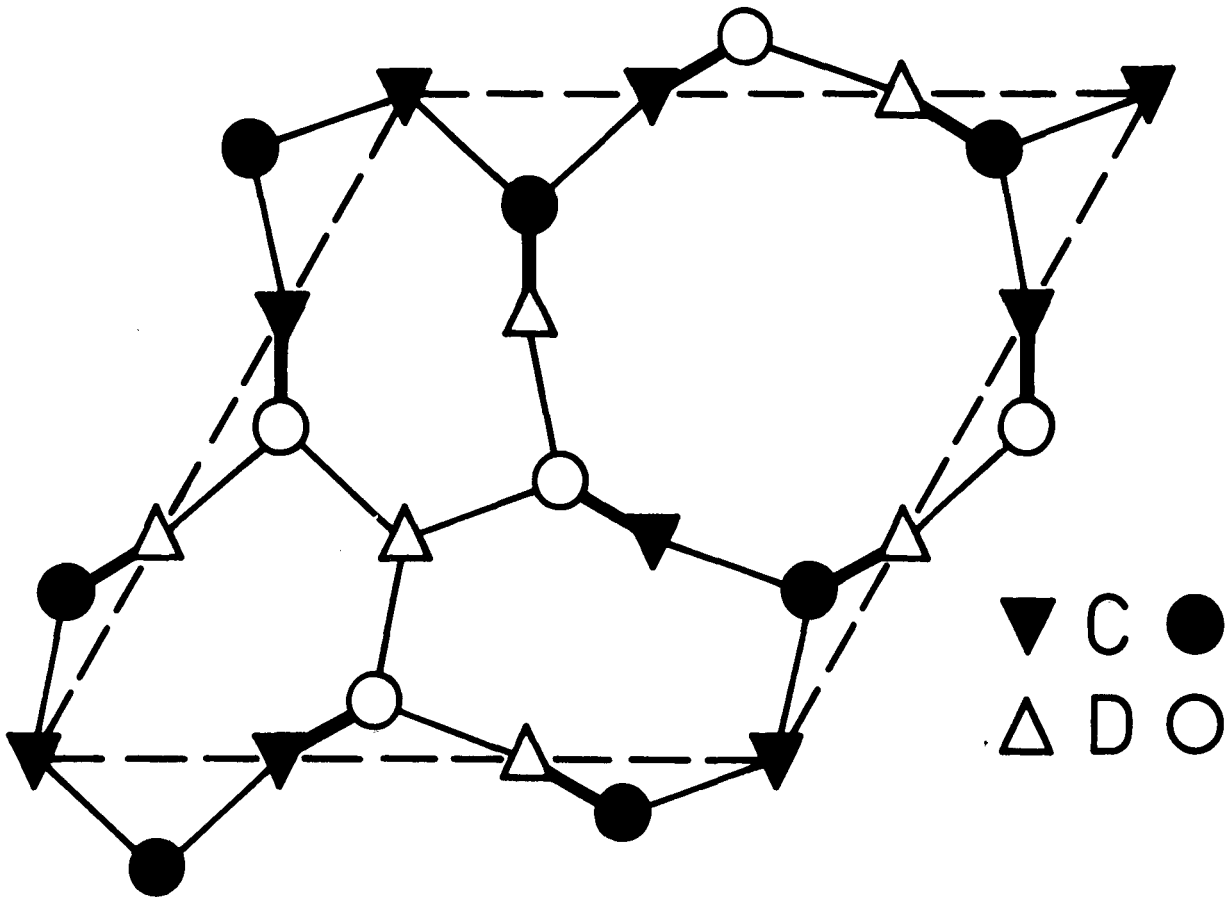

α : ABCD

β : ABAB

the α and α' X-ray diffraction patterns.

Thompson (1978) carried out a structure determination for an α' composition Ca $Si_9Al_3ON_{15}$ which on refinement showed that on average 0.5 Ca occupied each of the holes but, because this corresponded only to an additional 20 electrons, the intensity data were not significantly different from those of α-Si_3N_4. Further evidence was required to demonstrate convincingly that in the α' structure cations occupy the two interstitial sites per cell giving a general composition:

$M_x(Si,Al)_{12}(O,N)_{16}$, where $x \leqslant 2$.

A range of α' compositions containing increasing amounts of calcium was prepared and examined for intensity variations. In addition, a structure determination of the α'composition containing as close to 2Ca per unit cell as possible was carried out.

V.2 Calcium α'-sialon series

Four α'-sialons were prepared by firing appropriate amounts of Si_3N_4, AlN and CaO in the tungsten furnace at 1750°C for 15 minutes; see Table V.1. The compositions were chosen in approximately equal successive increments of calcium to show corresponding progressive changes in X-ray reflexion intensities. The expected compositions were estimated from the position and intensity of the X-ray reflexions. One X-ray diffraction pattern for each calcium α'-sialon and for a chemically vapour deposited (CVD) α-Si_3N_4 was taken using a Hägg-Guiner focusing camera with $CuK\alpha_1$ radiation. The emulsion was removed from the outside of each film and intensity data from the first thirteen reflexions were obtained using

Table V.1

Calcium α'-sialons prepared at 1750°C

starting composition (moles)			expected formula	X-ray analysis (w/o)			
				α'	AlN	α Si_3N_4	β Si_3N_4
CaO	Si_3N_4	AlN					
0.67	3.33	2.0	$Ca_{0.67}Si_{10}Al_2O_{0.67}Al_{15.33}$	93	1	5	1
1.0	3.0	3.0	$CaSi_9Al_3ON_{15}$	98	2	-	-
2.0	2.5	3.0	$Ca_{1.5}Si_{8.5}Al_{3.5}O_{0.5}N_{15.5}$ + glass	95	5	-	-
3.0	2.0	3.0	$Ca_2Si_8Al_4N_{16}$* + glass	95	5	-	-

*E.P.M.A. gives a composition $Ca_{1.6}Si_{8.4}Al_{3.6}N_{16}$ although a structure determination (see V.3) gives $Ca_{1.8}Si_{8.3}Al_{3.7}N_{16}$.

a microdensitomer as explained in section IV.5. In the case of $CaSi_9Al_3ON_{15}$ intensity data obtained by Thompson (1978) were used. The data were corrected for background radiation before scaling each film so that the 102 peaks, i.e. the most intense reflexions, had the same values in each film. No absorption correction was applied but in any case this varied in a similar way for each film and hence made little difference in the θ range of interest.

The shift in X-ray line positions associated with the changing composition of the α'-sialon is shown very clearly in Figure V.2 , and results from the replacement of Si-N bonds (1.75 Å) by Al-N bonds (1.87 Å). As expected, both the a and c cell dimensions increase (see Table V.2).

The variations in the X-ray reflexion intensities can also be seen in Figure V.2. The measured intensities of these films are plotted as a function of θ in Figure V.3. The most obvious variation in intensity occurs in the 100 reflexion, being relatively strong in α-Si_3N_4 and gradually decreasing to zero at a composition $Ca_{1.5}Si_{8.5}Al_{3.5}O_{0.5}N_{15.5}$. This reflexion reappears faintly at a value of 1.8 calciums per unit cell. The 101 and 110 reflexions also become progressively weaker as the calcium content increases. A less obvious trend of decreasing intensities with increasing calcium content can be observed for the 200 and 201 reflexions whilst the 211 peak shows a general increase.

Although silicon and nitrogen are partly substituted for aluminium and oxygen these changes do not greatly alter the intensities of the X-ray reflexions, because the atomic numbers of Al(13) and O(8) are similar to those of Si(14) and N(7) and so too are the corresponding

Figure V.2

X-ray powder patterns showing the

variation in d-spacing for α'compositions

containing (b) 0.67 Ca

(c) 1.0 Ca

(d) 1.5 Ca

(e) 1.8 Ca

compared with CVD α-Si_3N_4 (a)

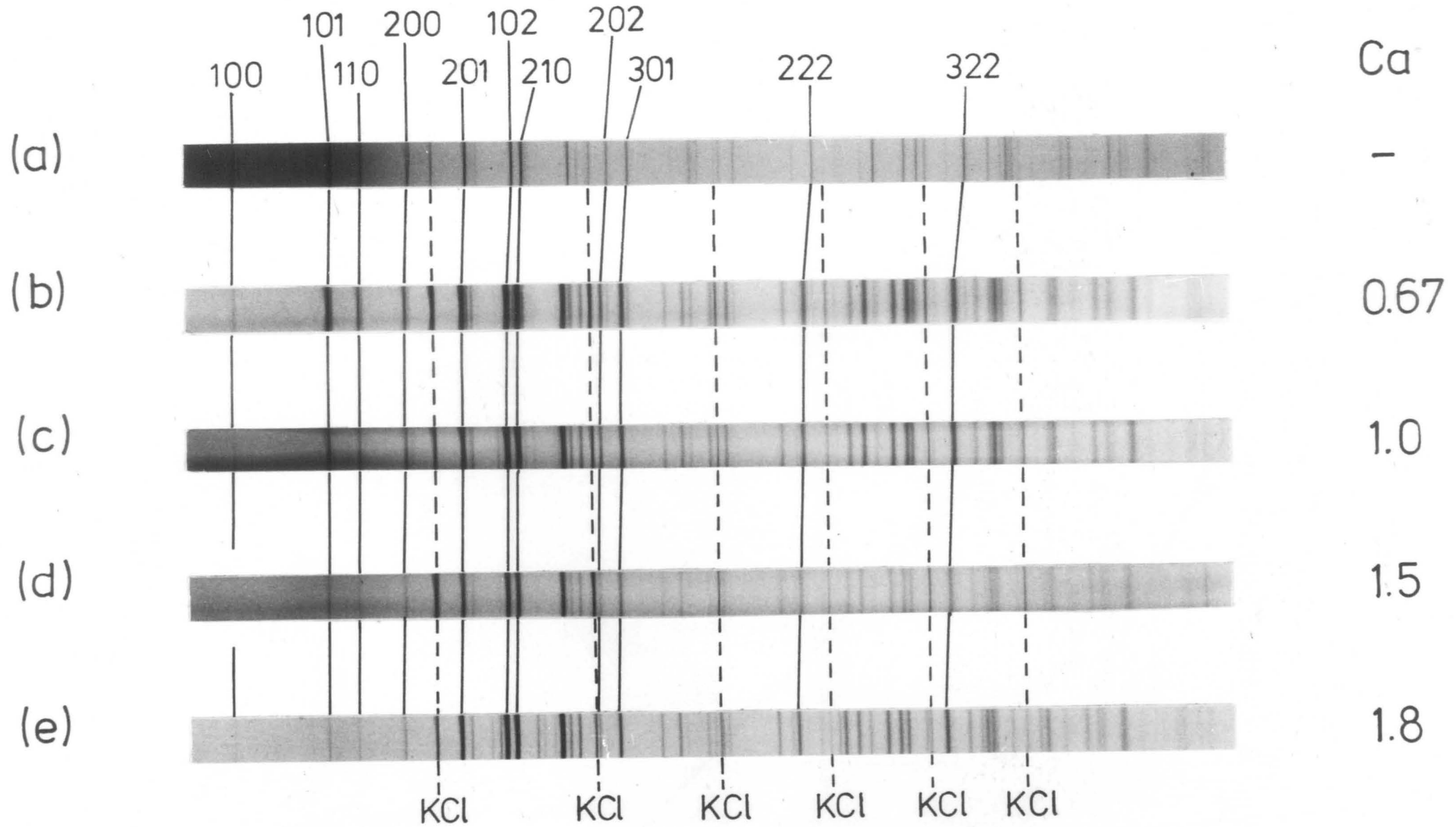
100
101
110
200
201
102
210
202
301
222
322
Ca
(a)
–
(b)
0.67
(c)
1.0
(d)
1.5
(e)
1.8
KCl
KCl
KCl
KCl
KCl
KCl

Table V.2

Cell dimensions and cell volumes of Ca α'-sialons compared with α-Si_3N_4

	a (Å)	c (Å)	% increase in cell volume relative to α-Si_3N_4
α-Si_3N_4	7.752	5.619	-
0.67 Ca	7.823	5.692	3
1.0 Ca	7.871	5.724	5
1.5 Ca	7.905	5.739	6
1.8 Ca	7.948	5.770	8

Figure V.3

The variation in X-ray reflexion

intensity for a series of calcium α'compositions

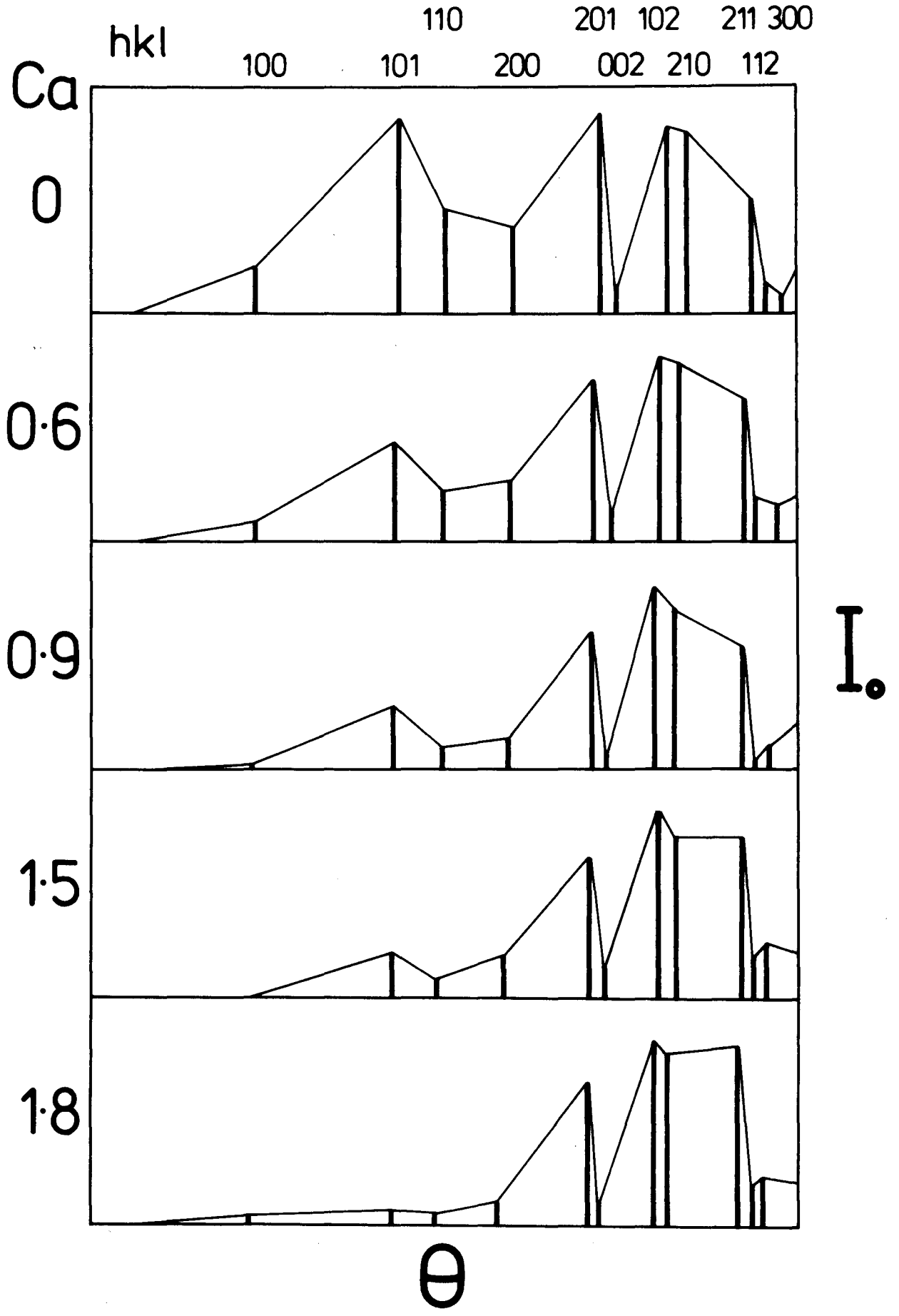
hkl
100
101
110
200
201
002
102
210
211
112
300
Ca
0
0·6
0·9
1·5
1·8
I₀
θ

atomic scattering factors.

Optical micrographs of polished samples of each calcium α'-sialon are shown in Figure V.4. The X-ray analyses of these samples show mainly single phase α'-sialons but all specimens contain some glassy phase (darkest regions). In (e) the dark areas are due to grain-boundary effects and not glass but otherwise the amount of glassy phase decreases as the calcium content of the α'-sialon decreases. This trend is reflected in the starting compositions (see Table V.1) where an excess of lime, and hence more liquid phase, is required to produce the α'-sialons of highest calcium content. A hot-pressed material (a) of the most calcium-rich composition is more crystalline than the pressureless sintered sample (b) of the same composition.

V.3 The crystal structure of calcium α'-sialon

V.3.1 Crystal data

To finalize unequivocally the crystal structure of α'-sialon, a complete structure determination was carried out on the composition containing the most calcium, i.e. having an X-ray diffraction pattern showing the greatest difference from that of α-Si_3N_4; compare Figures V.2 (e) & (a).

The calcium α'-sialon was prepared by hot-pressing the mixture 3CaO, $2Si_3N_4$, 3AlN at 1850°C for 1 h using a small holding pressure. A second sample was prepared from the same mixture by firing at 1750°C for 15 minutes in the tungsten furnace. The X-ray diffraction patterns from both samples showed 95% purity with AlN and "E-phase" as the impurities. E-phase is thought to be orthorhombic with composition $CaAlSiN_3$; see section VII.2.2. Results of electron probe microanalyses

Figure V.4

Optical micrographs for the

calcium α'compositions containing:

(a) 1.8 Ca (hot-pressed)

(b) 1.8 Ca (sintered)

(c) 1.5 Ca (sintered)

(d) 1.0 Ca (sintered)

(e) 0.67 Ca (sintered)

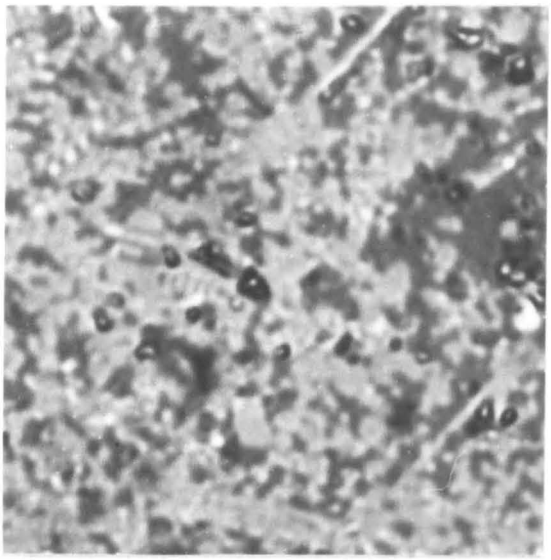

(a)

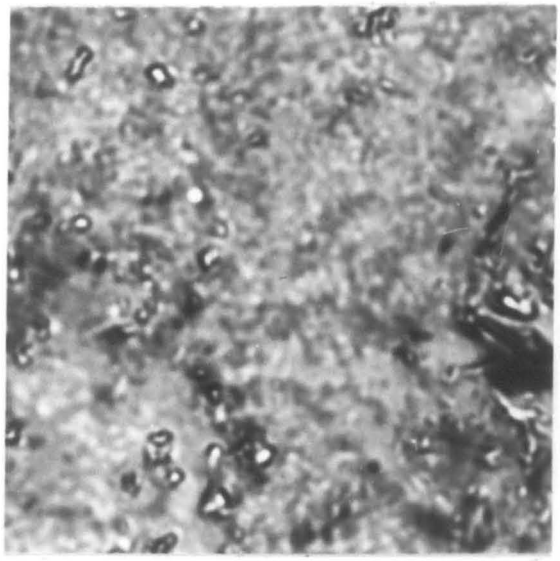

(b)

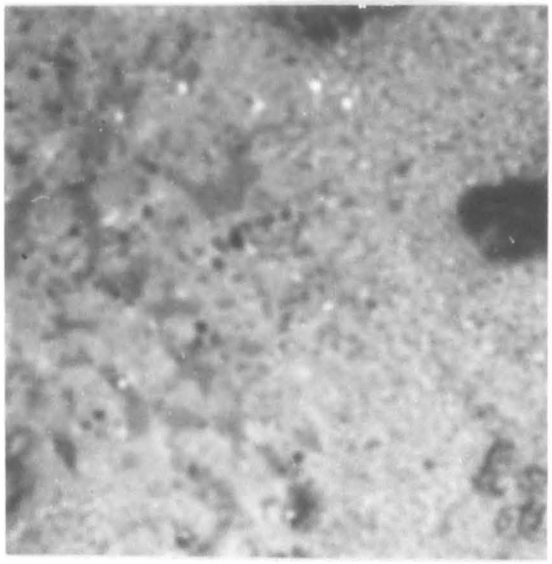

(c)

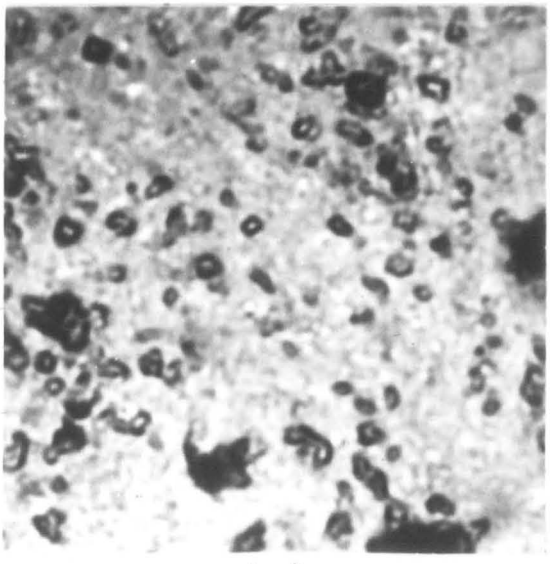

(d)

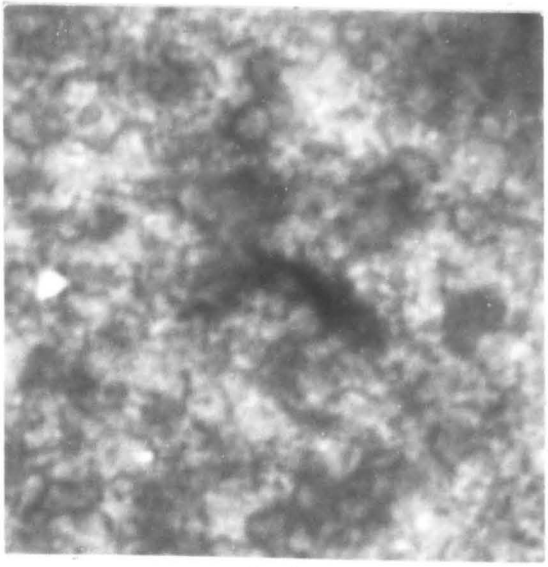

(e)

are given in Table V.3 and show that the α'-phase and glassy matrix have essentially the same composition in both specimens. The α' composition corresponds to $Ca_{1.6}Si_{8.4}Al_{3.6}N_{16}$.

The reflexions on X-ray powder photographs were indexed on the basis of a hexagonal unit cell with dimensions:

$\underline{a}$, 7.948 ± .002Å; $\underline{c}$, 5.770 ± .003Å; $\underline{c}/\underline{a}$, 0.726Å.

The only absences were of the type hhl with l odd, indicating space groups P31c, $P\bar{3}1c$, $P6_3mc$ or $P\bar{6}2c$ but because the α'-sialon structure was assumed to have the same symmetry as α'-Si_3N_4 space group, P31c was used in the refinement.

Due to the large amount of glassy phase there was a poor peak to background ratio on 19 cm Unicam X-ray photographs but a better resolution was obtained using a Hägg-Guiner X-ray camera. Four photographs were taken using $CuK\alpha_1$ radiation; three from the hot-pressed material and one from the pressureless sintered sample. Intensity data from each film were measured as explained in section IV.5 and readings taken at intervals of 0.1 mm on the film were plotted on graph paper and the peak areas measured with a planimeter to give the peak intensity. Fifty-one intensities were measured on each film corresponding to eighty-two hkl values. The intensities of similar reflexions on the four films were scaled together and the contributions from AlN and E-phase were subtracted from eleven reflexions before applying corrections for Lorentz and polarization effects. Absorption corrections (N) were applied empirically on the basis of the curves of Sas & de Wolff (1966) using the equation:

$$N = 7.55 - 6.3 \cos x \qquad \text{where } x = (2\theta - \psi)$$

and ψ is the angle between the specimen normal and crystal primary beam,

Table V.3

Electron probe micro-analysis of hot-pressed and pressureless sintered calcium α'-sialon; (unit cell contents)

sample	phase	element Ca	Si	Al	O	N	(a/o)
hot-pressed	α'	1.62	8.46	3.66	0.0	16.0	
	glass matrix	5.56	5.35	1.60	10.80	5.20	
sintered	α'	1.41	8.35	3.92	0.0	16.0	
	glass matrix	5.29	5.82	1.44	9.88	6.12	

in this case 30°. Finally, the observed intensities were corrected for multiplicity.

V.3 Refinement

The structure refinement was carried out using the Shel-X computer program (Sheldrick, 1975) which gives least squares refinement of positional parameters, temperature factors and occupation numbers for each atom in the structure. R-factors, bond lengths and bond angles were listed after each cycle of the refinement. A special feature of the program is the facility to use 'free variables'. These can be used to tie together related parameters so that constraints can be included in the refinement.

Using the α'-sialon parameters determined by Thompson (1978) and a composition corresponding to the maximum amount of calcium possible in the structure i.e. $Ca_2Si_8Al_4N_{16}$, the initial R-factor was 23%. This was reduced to 9.34% by allowing the x, y and z coordinates to vary with the exception of special positions and the (Si,Al)Z z position (see Table V.4, underlined values). To improve this value the observed chemical composition was substituted but surprisingly after refinement R had increased to 10.52% and even after allowing the x, y and z coordinates and isotropic temperature factors to vary, R was still 10.32%. The best R value was obtained by allowing the calcium occupation number, x, y and z coordinates and temperature factors to vary which gave a final value of 5.90% and composition of $Ca_{1.8}Si_{8.3}Al_{3.7}N_{16}$.

It is surprising that the α' composition from E.P.M.A. did not give a lower R value since this method of analysis is generally considered accurate. However, since the intensities are particularly

sensitive to the calcium content, a small error in measurement will greatly affect the R value and hence it is reasonable that the best composition is slightly more calcium-rich than indicated by the analysis.

Final atomic parameters, together with those obtained for $CaSi_9Al_3ON_{15}$ and α-Si_3N_4 by Thompson (1978 & 1974), are listed in Table V.4. Bond lengths are given in Table V.5 and observed and calculated structure amplitudes are listed in Table V.6.

V.4 Discussion

The structure is topologically identical to α-Si_3N_4 except that on average 0.9 calcium atoms occupy each of the two interstial sites. The structure is therefore 90% fully "stuffed" with calcium atoms. These atoms are 7 coordinated to 3 N1 atoms, 3 N2 atoms and 1 N3 atom and as a result of the high coordination number the shift observed for any one nitrogen atom is relatively small. The N1 atoms move very slightly inwards towards the calcium (see Figure V.5) and the N2 atoms are also shifted although not obviously towards the calcium. However, the greatest shift occurs in the N3 z-coordinate as it is pushed away by the calcium atom in an effort to achieve a realistic Ca-N bond length. Nevertheless it is still short at 2.37Å compared with the Ca-N1 and Ca-N2 bond lengths of 2.47 and 2.66Å respectively; see Table V.5. A large shift also occurs in the N4 z-coordinate which moves upwards to 0.05. This is apparently caused by the decrease in the x and y coordinates of the N1 atom when it is pulled towards the calcium atom. Figure V.5 shows the positions of the nitrogen atoms as determined for the composition $Ca_{1.8}Si_{8.3}Al_{4.7}N_{15}$ as well as the positions of the nitrogens in α-Si_3N_4 (Thompson, 1974) when viewed along [001].

Table V.4

Final atomic parameters for $Ca_{1.8}Si_{8.3}Al_{3.7}N_{16}$, $CaSi_9Al_3ON_{15}$ (Thompson, 1978) and α-Si_3N_4 (Thompson, 1974) space group $P31c$-C_3^4; No.159

compound	atom	site	x	y	z
	Ca	2(b)	1/3	2/3	0.1348
	(Si,Al)1	6(c)	0.0839	0.5087	0.6206
	(Si,Al)2	6(c)	0.2528	0.1727	0.4059
$Ca_{1.8}Si_{8.3}Al_{3.7}N_{16}$	N1	6(c)	0.6522	0.5923	0.4160
	N2	6(c)	0.3304	0.3271	0.6707
	N3	2(b)	1/3	2/3	0.5464
	N4	2(a)	0	0	0.4315
	Ca	2(b)	1/3	2/3	0.1261
	(Si,Al)1	6(c)	0.0823	0.5096	0.6213
	(Si,Al)2	6(c)	0.2523	0.1708	0.4059
$CaSi_9Al_3ON_{15}$	N1	6(c)	0.6607	0.6037	0.4149
	N2	6(c)	0.3177	0.3248	0.6659
	N3	2(b)	1/3	2/3	0.5721
	N4	2(a)	0	0	0.4115
	Si,1	6(c)	0.0820	0.5111	0.6144
	Si,2	6(c)	0.2538	0.1672	0.4059
α-Si_3N_4	N1	6(c)	0.6563	0.6075	0.3884
	N2	2(c)	0.3176	0.3203	0.6474
	N3	2(b)	1/3	2/3	0.5544
	N4	2(a)	0	0	0.4028

Table V.5

Bond lengths in $Ca_{1.8}Si_{8.3}Al_{3.7}N_{16}$, $CaSi_9Al_3ON_{15}$ (Thompson, 1978), α-Si_3N_4 (Thompson, 1974)

from	to	no. of bonds	bond lengths (Å)		
			$Ca_{1.8}Si_{8.3}Al_{3.7}N_{16}$	$CaSi_9Al_3ON_{15}$	α-Si_3N_4
Ca	N1	3	2.47	2.47	-
	N2	3	2.66	2.72	-
	N3	1	2.37	2.54	-
(Si,Al)1	N1	2	1.70,1.85	1.71,1.86	1.73 1.75
	N2	1	1.76	1.75	1.74
	N3	1	1.79	1.75	1.74
(Si,Al)2	N1	1	1.85	1.76	1.73
	N2	2	1.86,1.74	1.82,1.69	1.81 1.68
	N4	1	1.78	1.75	1.73

Table V.6

Observed and calculated X-ray data for

$Ca_{1.8}Si_{8.2}Al_{3.7}N_{16}$

P31c, $\underline{a}$ = 7.948Å, $\underline{c}$ = 5.770Å

hkl	d_{obs}	d_{calc}	F_{obs}	F_{calc}
100	6.915	6.883	4	8
101	4.422	4.422	6	7
110	3.977	3.974	13	9
200	3.486	3.441	16	21
201	2.959	2.956	43	46
002	2.887	2.885	41	43
102	2.662	2.661	62	60
210	2.605	2.601	56	60
211	2.376	2.372	52	52
112	2.334	2.335	36	36
300	2.297	2.294	42	41
202	2.217	2.211	24	26
301	2.135	2.132	43	42
220	1.989	1.987	38	37
212	1.933	1.932	30	39
310	1.911	1.909	15	12
103	1.854	1.852	22	20
311	1.812	1.812	22	22
302	1.797	1.796	21	20
400	1.720	1.721	6	8
203	1.680	1.679	33	32
401	1.648	1.649	22	19
222	1.638	1.636	29	28
312	1.594	1.592	10	9
320	1.580	1.579	12	8
213	1.547	1.547	29	25
321	1.525	1.523	43	45
410	1.503	1.502	29	31
402)	1.475	1.478	6	6
303)		1.474	48	47
411	1.455	1.454	14	14
004	1.442	1.442	108	105
104	1.414	1.412	26	17
322)	1.387	1.385	46	47
500)		1.382	15	19
114)	1.355	1.356	12	12
313)		1.355	14	14
501	1.340	1.339	31	29
412)	1.333	1.332	41	43
204)		1.330	17	18
330	1.325	1.325	54	58
420	1.302	1.301	23	25
403	1.286	1.282	11	15
421	1.270	1.269	22	23
214	1.261	1.262	21	23
502	1.243	1.242	20	23
510	-	1.236	11	11
304)	1.221	1.221	16	15
323)		1.220	25	24
422)	1.185	1.186	18	18
413)		1.184	33	33
224	-	1.167	12	14
314	-	1.151	10	10
600	-	1.147	6	6
105	1.139	1.138	7	7
512)	1.133	1.136	15	15
430)		1.132	23	22
601)	1.122	1.125	11	11
503)		1.119	20	20
431	1.113	1.110	14	13

Figure V.5

Atomic arrangement of $Ca_{1.8}Si_{8.3}Al_{3.7}N_{16}$

projected on (0001)

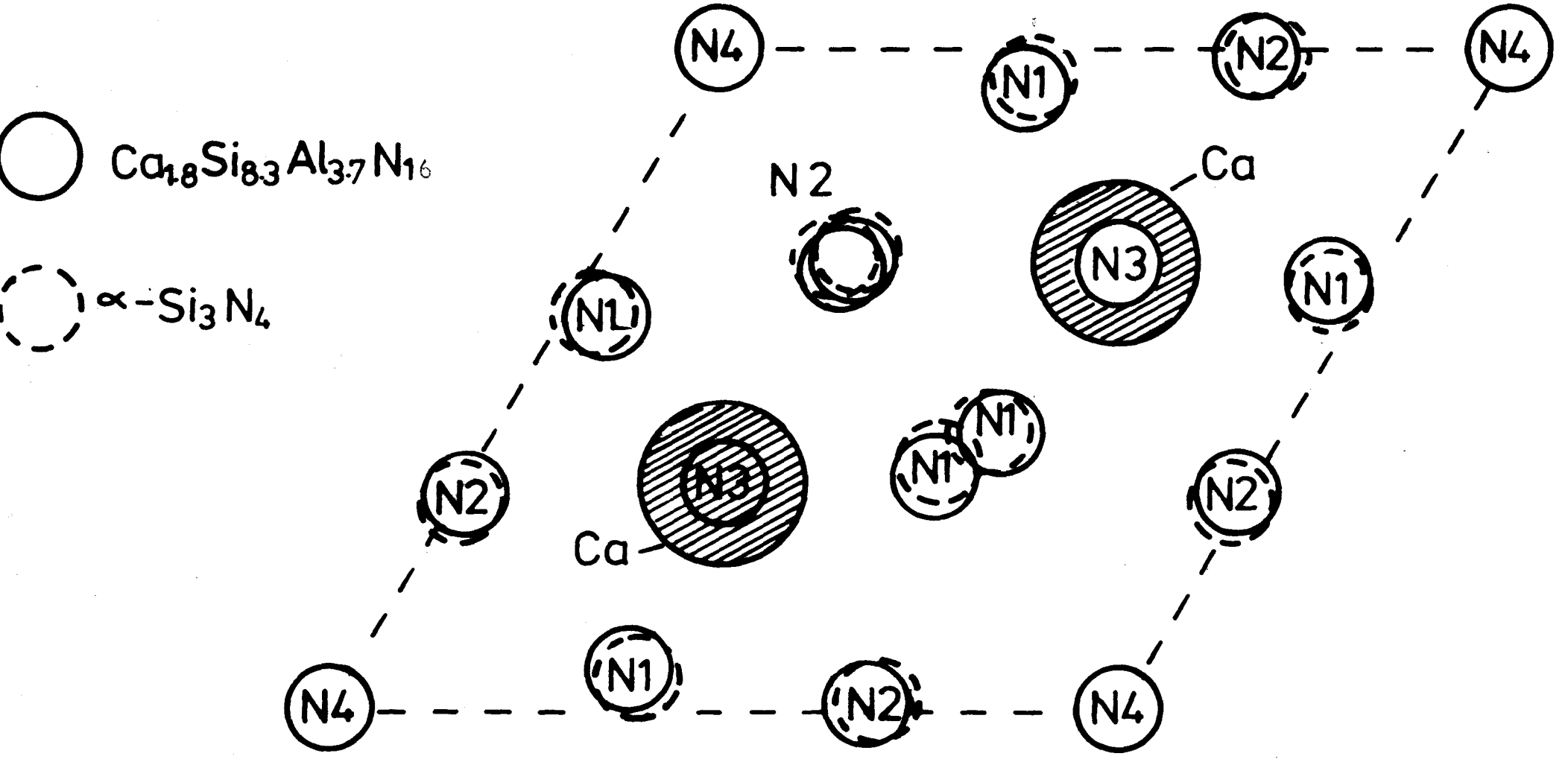

projection along c-axis

Comparing the bond lengths with those obtained by Thompson (1978) for $CaSi_9Al_3ON_{15}$ and for α-Si_3N_4 (Thompson, 1974) (see Table V.5), a general expansion of the (Si,Al)(O,N) network is observed as the calcium content increases rather than any large changes in selected atomic positions. There is a significant decrease in the calcium to nitrogen bond length as the calcium content of the α'-sialon increases, presumably because the effective concentration of positive charge in the "calcium" site increases.

V.5 Conclusions

Variations in X-ray reflexion intensities of calcium α'-sialons clearly indicate that calcium atoms occupy the large closed interstices in the (Si,Al)(O,N) framework. Final confirmation was obtained from the structure determination of a Ca α'-sialon containing 90% of the maximum theoretical value of 2Ca per unit cell. The variations in d-spacings of the reflexions are a result of the increasing degree of aluminium substitution which accompanies higher calcium levels. Nevertheless the aluminium content does not significantly distort the (Si,Al)(O,N) framework compared to that in α-Si_3N_4.

VI THE PREPARATION OF SILICON CARBIDE FROM SILICON NITRIDE-CARBON MIXTURES

VI.1 Introduction

Polytypism in SiC has not been satisfactorily explained although several plausible theories have been developed during the last thirty years, as discussed in section II.4.3. Although each theory is capable of accounting for some observations, no single one is all-embracing and it is apparent that polytypism is a result of several cooperating factors. In particular, impurities stabilise certain polytypes, for example, aluminium stabilises 4H and nitrogen 3C. Some polytype transformations are induced by doping with impurities and/or annealing at temperatures from 1500° - 2500°C (see Chapter II). In this way various stability regions for the basic polytypes have been suggested.

Impurities are frequently introduced via the gas phase during the growth of SiC by sublimation or by applying a diffusant to the surface before annealing. Nitrogen can be diffused into SiC at ∿2000°C up to ∿0.1a/o(Vodakov & Mokhov, 1973). To achieve higher nitrogen levels several atmospheres of nitrogen and high temperatures have been used (Slack & Scace, 1965) but these nitrogen levels (∿0.3 a/o) are still comparatively low. It was thought that silicon carbide crystals with higher nitrogen contents might be prepared from silicon nitride.

VI.2 The silicon nitride-carbon reaction

The reduction of silicon nitride with carbon over the temperature range 1600° - 2000°C and the effect of heating rate and gas atmosphere were studied in experiments carried out in the carbon furnace using a starting mixture of Starck Si_3N_4 plus 10 m/o excess C above that required for complete conversion to SiC.

In a nitrogen atmosphere no reaction occurred below 1650°C but at this temperature and above, 3C and, surprisingly, the 2H modifications of SiC were formed in approximately equal amounts. Accurate estimation of the relative proportions of the two polytypes is difficult because the strong cubic reflexions overlap with hexagonal ones as shown in Figure VI.1. The 2H : 3C ratio was estimated visually from the X-ray diffraction pattern by assuming that the weak (200) cubic non-overlapping reflexion was approximately ten times weaker than the cubic (111) reflexion (Adamsky and Merz, 1959; Ruska et al., 1979). Also taken into account was the relative intensity of the $(002)_{hexagonal}/(111)_{cubic}$ overlap compared with the $(100)_{hexagonal}$ and $(101)_{hexagonal}$ reflexions. Since these were the only SiC polytypes observed, this method was adequate for the determination of 2H : 3C ratios.

With increasing temperature the 2H : 3C ratio decreased and was also independent of time (see Table VI.1). After only five minutes at 2000°C the final product was almost pure 3C and contained only a trace of the 2H. The maximum amount of the rare 2H polytype (∿60%) in the final product was obtained by reacting the Si_3N_4 - C mixture at 1650°C for 1 hour in nitrogen.

Frequently after firing, a black layer ∿0.1 mm thick formed on the surface of pellets. A similar observation has been reported by Kroko & Milnes (1966) when heating SiC at temperatures above about 1800°C and

Figure VI.1

X-ray powder diffraction patterns of

2H and 3C silicon carbide

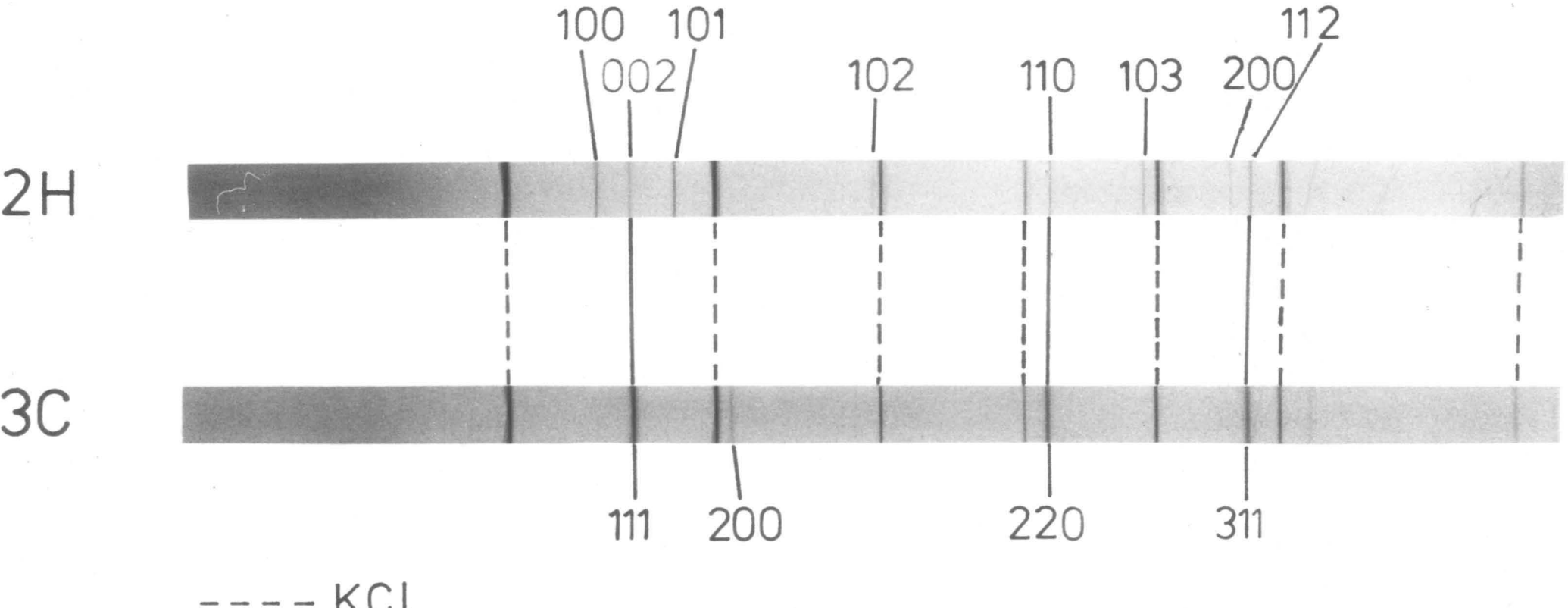
100
101
002
102
110
103
200
112
2H
3C
111
200
220
311
---- KCl

TABLE VI.1

Reaction products of 33 Si_3N_4 + 11OC mixtures heated in a nitrogen atmosphere for various temperatures and times

heat treatment	X-ray analysis (w/o)		
°C/minute	2H	3C	α - Si_3N_4
1650/60	60	40	tr
1750/30	50	50	-
1800/5	40	60	-
1800/15	40	60	-
1800/30	40	60	-
1900/5	10	90	-
2000/5	tr	100	-

they suggest that if there is little SiO and CO vapour more silicon than carbon will leave the lattice during crystal growth and produce a graphite-like surface layer on the specimen. The surface skin, observed once the Si_3N_4 - C pellets had been fired, contained unreacted Si_3N_4 (and hence also unreacted carbon) but the amount of carbon appeared larger than could be explained merely by incomplete reaction.

Substituting nitrogen by argon produced less 2H (cf. Tables VI.2 and VI.1). Argon promoted the formation of 3C-SiC especially at 1650°C where virtually pure 3C was obtained after 60 minutes. In attempts to prepare a pure 2H-SiC, four different heating rates from 1000°C to the final temperature (see Figure VI.2) were explored, e.g. a firing temperature of 1800°C could be achieved in 12, 18, 33 and 48 minutes, i.e. rates 1, 2, 3 and 4 respectively. However, the 2H : 3C ratio was independent of the heating rate and, as before, increasing temperature produced less 2H, although this could be partially compensated by a slower heating rate because of the longer time spent in the 2H forming region at ∿1650°C.

Pure 2H was obtained by adding 7 m/o CaO to a mixture of Si_3N_4 and C and firing at 1650°C for 30 minutes in a nitrogen atmosphere. The addition of CaO provides a liquid phase in which efficient homogenization of the reactants takes place and in so doing facilitates the formation of 2H and eliminates vapour phase side reactions which give 3C.

Several groups have reported that 2H transforms to 3C at temperatures above 1400°C (Bootsma et al.,1971; Krishna et al.,1971; Krishna & Marshall, 1971a,b). Considering that 2H-SiC has poor thermal stability and strong tendency towards transformation to 3C, it is most unusual to observe 2H in the present work and to find that over a wide

TABLE VI.2

Reaction products of 33 Si_3N_4 + 11OC mixtures heated in an argon atmosphere for various temperatures and times

heat treatment	X-ray analysis (w/o)	
^{o}C/minute	2H	3C
1650/60	tr	100
1800/5	20	80
1800/15	5	95
1900/5	-	100

Figure VI.2

Heating rates used in preparing

SiC from Si_3N_4/C mixtures

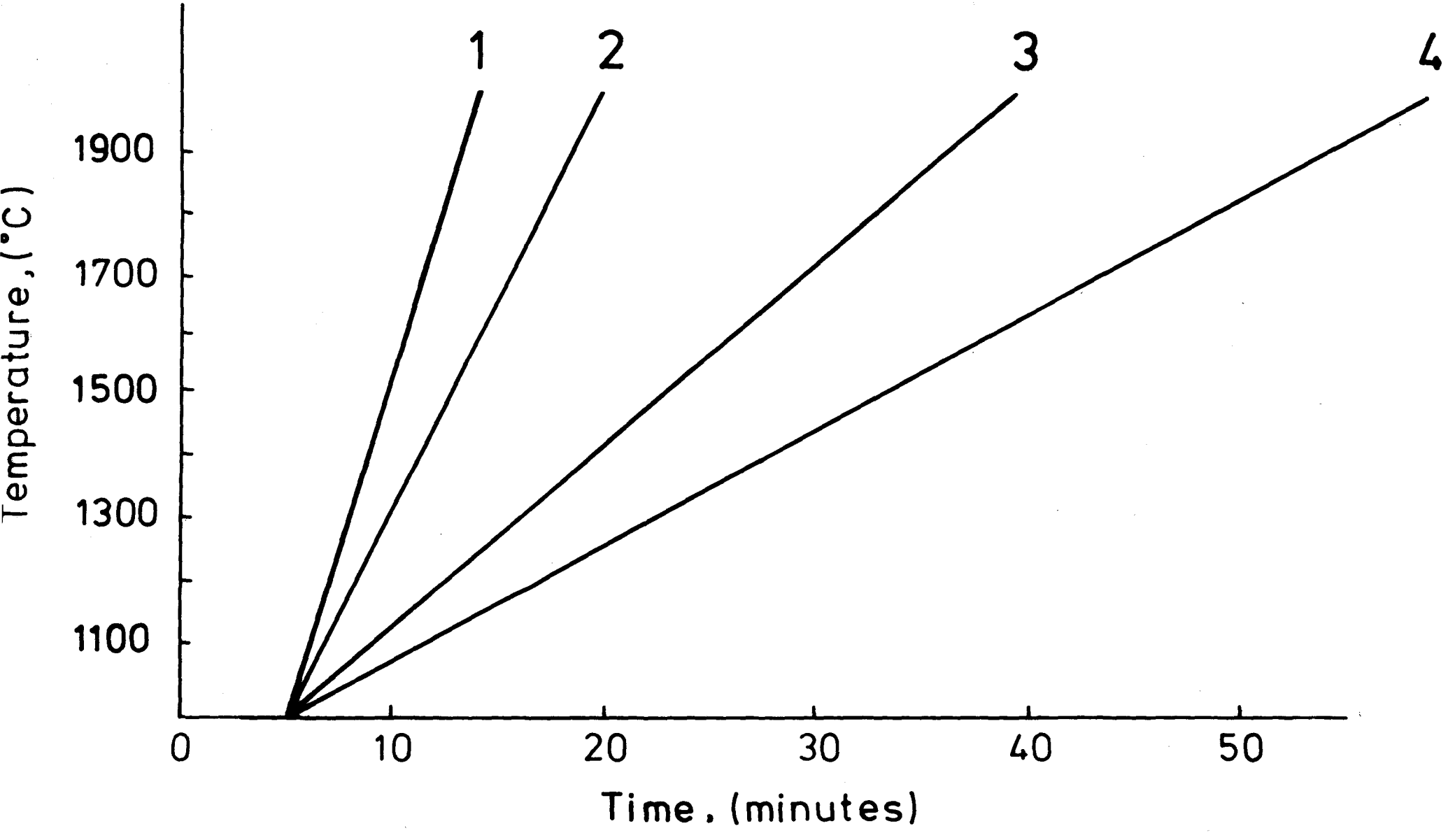
1
2
3
4
1900
1700
1500
1300
1100
Temperature, (°C)
0
10
20
30
40
50
Time, (minutes)

range of temperatures it is stable with respect to the 3C polytype.

Close observation of the X-ray diffraction patterns from the materials listed in Table VI.1 showed small shifts in the positions of X-ray reflexions giving smaller unit cell dimensions of both 2H and 3C phases than those of the pure polytypes (see Table VI.3). Also, there is a gradual increase in the cell dimensions of both the hexagonal and cubic phases towards previous literature values with increasing formation temperature. Those of 2H made from 7m/o CaO added to Si_3N_4 + C were:

$$\underline{a} = 3.060 \pm .002\text{Å}, \qquad \underline{c} = 5.013 \pm .005\ \text{Å}$$

and are $\sim$ 0.6% lower than pure 2H - SiC. This lattice contraction in the SiC is clearly due to solid solution of an element which also stabilizes 2H relative to 3C.

VI.3 Formation of SiC by carbothermal reduction of silica

To understand more completely the conditions for 2H - SiC formation, silica-carbon mixtures were reacted at 1500° - 1800°C in both the carbon and tungsten furnaces using argon and nitrogen atmospheres.

It has been shown that a transition temperature of around 1400°-1550°C exists between the formation of SiC and Si_3N_4 in the SiO_2-C-N_2 system (Komeya & Inoue, 1975; Lee & Cutler, 1975 & 1977; Hendry, 1975). Above this temperature SiC forms and below it Si_3N_4 forms. From 1300°-1600°C four phases occur, SiC, Si_3N_4, Si_2N_2O and SiO according to the reactions:

$$SiO_2 + 3C \rightarrow SiC + 2CO \qquad \ldots \text{VI.1}$$

$$3SiO_2 + 6C + 2N_2 \rightarrow Si_3N_4 + 6CO \qquad \ldots \text{VI.2}$$

$$2SiO_2 + N_2 + 3C \rightarrow Si_2N_2O + 3CO \qquad \ldots \text{VI.3}$$

TABLE VI.3

Cell dimensions of 2H and 3C products listed in Table VI.1

formation temperature °C	2H		3C
	a(Å)	c(Å)	a(Å)
1650	3.070±.002	5.026±.005	4.351±.003
1800	3.074±.002	5.038±.005	4.354±.003
1900		-	4.359±.002
2100		-	4.359±.002
literature values			
Adamsky & Merz, (1959)	3.076	5.048	-
Taylor & Laidler, (1950)		-	4.3590±.0001

$$SiO_2 + C \rightarrow SiO + CO \quad \ldots \text{VI.4}$$

The SiC formed as a result of reaction VI.1 is always the 3C modification (Lee & Cutler, 1975; Szweda, 1980) but since the main interest in reducing SiO_2 with C is usually the formation of Si_3N_4, SiC is avoided by careful temperature control.

Thus experiments were carried out at 1500° - 1800°C to observe SiC formation. In argon, only the 3C polytype was formed although weak X-ray reflexions corresponding to 2.67 and 2.38 Å interplanar spacings and considerable background scatter indicated a small amount of disordered material. With a nitrogen atmosphere silicon oxynitride (Si_2N_2O) was formed at 1450° - 1500°C (see Table VI.4) and, apart from a greater tendency to form α-Si_3N_4 at < 1500°C in the tungsten furnace, there was no other difference between the results obtained in the two environments. Significantly, when 5w/o CaO was added to the SiO_2 + 15C mixture and fired at 1650°C in nitrogen, between 10-20% of the 2H-SiC polytype formed although the major phase was 3C-SiC with some glass and free silicon. This again indicates that the presence of a liquid phase favours the formation of 2H.

Visual comparison of the X-ray powder diffraction patterns of 3C-SiC showed a shift of X-ray reflexions to slightly higher d-spacings in samples prepared in argon, compared with preparations in nitrogen. Also, d-spacings of 3C prepared from SiO_2 and C were higher than those of 3C made by the reduction of Si_3N_4. The fact that the SiO_2 and C reaction carried out in argon gave the highest unit-cell dimensions, i.e.

$$\underline{a} = 4.361 \pm .002 \text{ Å}$$

strongly suggests that in the Si_3N_4 - C and SiO_2 - C - N_2 specimens

TABLE VI.4

Reaction products of SiO_2 + 15C mixtures heated in nitrogen or argon atmospheres at various temperatures

formation temperature		X-ray analysis		
°C/minute	atmosphere	3C	Si_2N_2O	disorder
1450/60	N_2	-	√	-
1500/60	N_2	-	√	-
1500/60	Ar	√	-	√
1650/60	N_2	√	-	√
1650/60	Ar	√	-	√
1800/60	N_2	√	-	√
1800/60	Ar	√	-	√

nitrogen is incorporated into the lattice. This is consistent with the Si-N bond length (1.75 Å) being 7% smaller than the Si-C bond length (1.88 Å). Figure VI.3 compares X-ray diffraction photographs of a crushed single crystal of 2H-SiC (prepared by the thermal decomposition of CH_3SiCl_3 at ~1400°C) and a pure well-crystallised commercial 3C specimen with those of the "nitrogen-2H" and nitrogen-free 3C. The nitrogen-2H has a unit-cell volume of 40.65Å^3, i.e. 1.7% smaller than that of pure 2H-SiC (V, 41.36Å^3) The nitrogen-2H X-ray reflexions which overlap with 3C reflexions show the large shift in d-spacing that accompanies dissolution of nitrogen.

A possible alternative explanation for the small cell dimensions of the 2H and 3C polytypes is the incorporation of boron or boron nitride from the protective packing surrounding the pellets during reaction. Boron is known to have a limited solubility of ~1.5 a/o in SiC at 1600°C and has been observed to cause a contraction of the lattice (Shaffer, 1969a; Batha & Hardy, 1973; Vodakov & Mokhov, 1973; Murata & Smoak, 1978). This possibility was eliminated by omitting the BN packing in later experiments. The initial results were confirmed and so the conclusion that nitrogen is incorporated into the SiC lattice causing a lattice contraction, is fully substantiated.

VI.4 The nitrogen content of 2H and 3C silicon carbides

The experiments described in section VI.3 show that 2H and 3C silicon carbide are formed when Si_3N_4 - C mixtures are reacted at 1650° - 2100°C and unit-cell dimensions are consistent with nitrogen replacing carbon in both structures. Rough estimation of the nitrogen contents from the deviation from 'normal' lattice parameters indicated that the

Figure VI.3

X-ray powder diffraction photographs

of: (a) 2H-SiC (b) "nitrogen-2H"

(c) 3C from SiO_2 + C (d) 3C-SiC

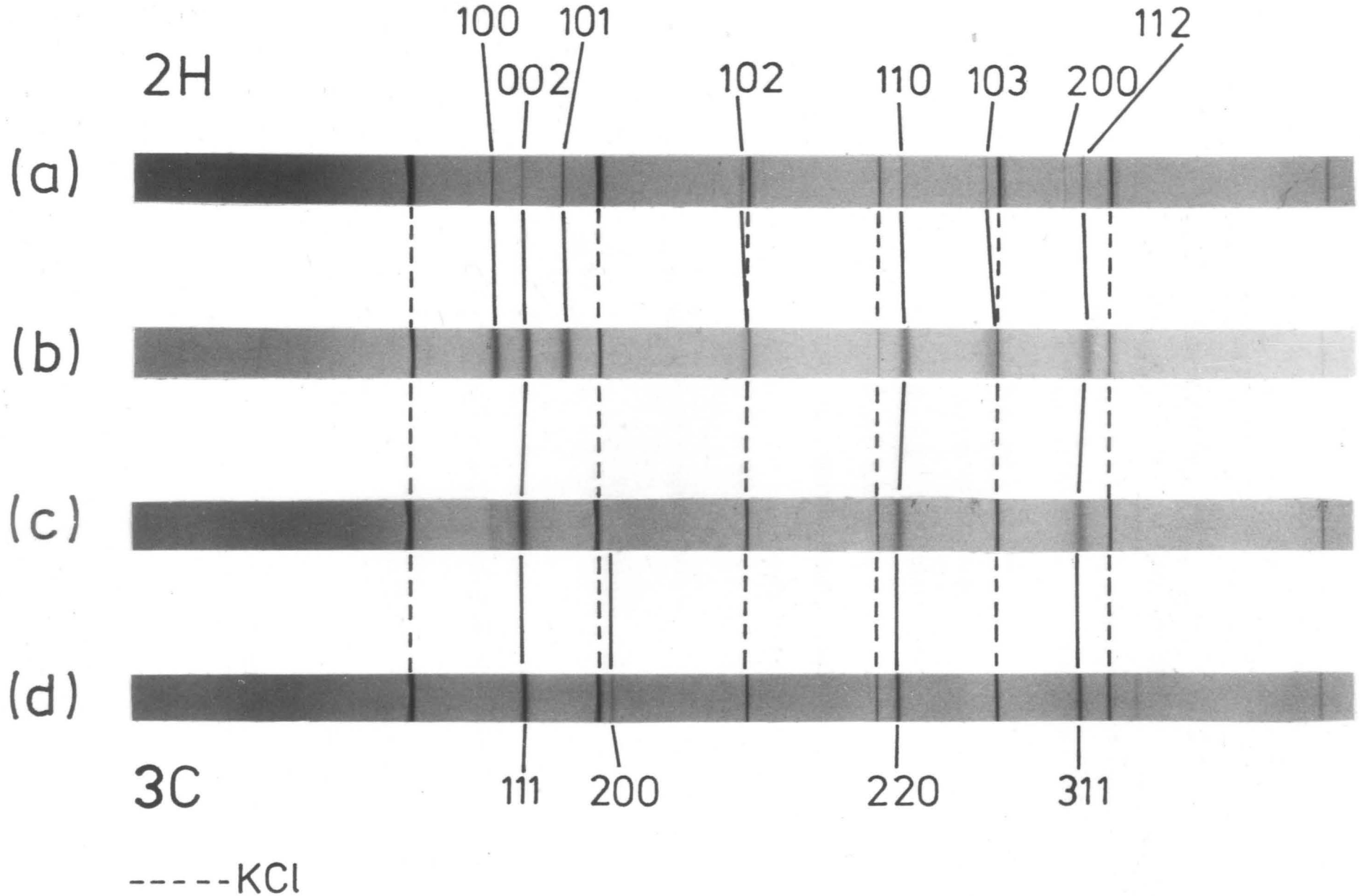
100
101
112
2H
002
102
110
103
200
(a)
(b)
(c)
(d)
3C
111
200
220
311
-----KCl

nitrogen was of the order of a few percent, i.e. an order of magnitude greater than any previously observed. Direct chemical analyses were therefore carried out on selected specimens, usually in quadruplicate, at U.K.A.E.A. Harwell, by inert gas fusion (see section IV.10).

The results given in Table VI.5 for each specimen are completely self-consistent and, as anticipated from the unit-cell dimensions, show appreciable solubilities of nitrogen. The difference between specimens A and B is partly due to the effect of temperature but also partly because 1m/o AlN was added to the Si_3N_4 - C - CaO starting mixture of specimen A. Nevertheless, even taking into account this difference (0.5 a/o N), the solubility of nitrogen in 2H - SiC ($\sim$ 10a/o) under the present conditions is ten times greater than previously reported (see section II.4.5).

Substituting xN atoms for C atoms in SiC, the chemical formula becomes:

$$Si_{1-x/4}\ C_{1-x}\ N_x$$

creating 1 - x/4 silicon vacancies. Assuming this formula, the pure 2H specimens containing~8 a/o and~12 a/o respectively correspond to the compositions:

$$Si_{48.95}\ C_{42.62}\ N_{8.43}$$

and $$Si_{48.53}\ C_{39.73}\ N_{11.73}$$

The formation of the 2H polytype, which normally is unstable at 1650°C in pure SiC, is favoured by the substitution of a significant quantity of nitrogen for carbon below $\sim$1900°C.

Annealing the $\sim$60% 2H + $\sim$40% 3C - SiC mixture, prepared by reacting Si_3N_4 + C at 1650°C (see section VI.2), transformed 2H to 3C at above

TABLE VI.5

Nitrogen content of some silicon carbide specimens

	starting composition (m/o)				heat treatment	unit cell dimensions (Å)		nitrogen content
	Si_3N_4	C	AlN	CaO	°C/minute	2H	3C	(a/o)
Specimen A	21.3	71.0	0.6	7.1	1650/30	$\underline{a}$ = 3.060±.002 $\underline{c}$ = 5.013±.005	-	11.8
Specimen B	21.5	71.4	-	7.1	1650/30	$\underline{a}$ = 3.063±.002 $\underline{c}$ = 5.017±.003	-	8.4
Specimen C	∿60%2H + ∿40%3C		SiC		1800/30	$\underline{a}$ = 3.072±.003 $\underline{c}$ = 5.092±.005	$\underline{a}$ = 4.352±.003	2.5
Specimen D	"				1800/30	$\underline{a}$ = 3.076±.002 $\underline{c}$ = 5.038±.005	$\underline{a}$ = 4.356±.002	1.2
Specimen E	"				2100/15	-	$\underline{a}$ = 4.359±.002	0.3
Specimen F	"				2100/15	-	$\underline{a}$ = 4.359±.002	0.7

1650°C (see section VI.6). Analyses on specimens containing 40% 2H + 60% 3C and 100% 3C prepared by annealing the 60% 2H + 40% 3C mixture at 1800° and 2100°C respectively (see Table VI.5, specimens C-F) show that the 2H structure progressively transforms to 3C at successively higher temperatures by loss of nitrogen.

The cell dimensions of the analysed materials show a direct correlation with the nitrogen content. Figure VI.4(a) and (b) give values of a and c respectively for pure 2H specimens (A and B in Table VI.5) and the 2H component of the 2H-3C mixtures (C and D in Table VI.5). Although reasonably large errors are associated with each measurement as shown by the breadth of the X-ray reflexions, there is no doubt that a decrease in lattice parameter accompanies the increase in nitrogen content of 2H. A similar relationship is also apparent in the 3C-phase as shown in Figure VI.4(c), where closed circles represent analyses from pure 3C specimens (E and F in Table VI.5 and the 3C component of specimens C and D (see Table VI.5). The hexagonal a and c parameters plotted on the previous two graphs, (a) & (b), are recalculated in terms of an a 'cubic' parameter and are also plotted on Figure VI.4(c), as dashed open circles. For calculation details, see Appendix 1. These calculated values are in good agreement with the others in Figure VI.4(c) and justify the assumptions made in their evaluation.

Slack and Scace, (1965) also observed a decrease in lattice parameter with nitrogen substitution for a 3C specimen produced by annealing 6H-SiC at 2720°C in 35 atmospheres of nitrogen but the nitrogen solubility was much lower (∿0.3a/o); see Figure VI.4(c). The current work indicates that less nitrogen can be accommodated in 3C compared with 2H but the relative change in cell dimensions with degree of nitrogen substitution is the same for both polytypes.

Figure VI.4

Variation in lattice parameters of 2H

and 3C-SiC with nitrogen content

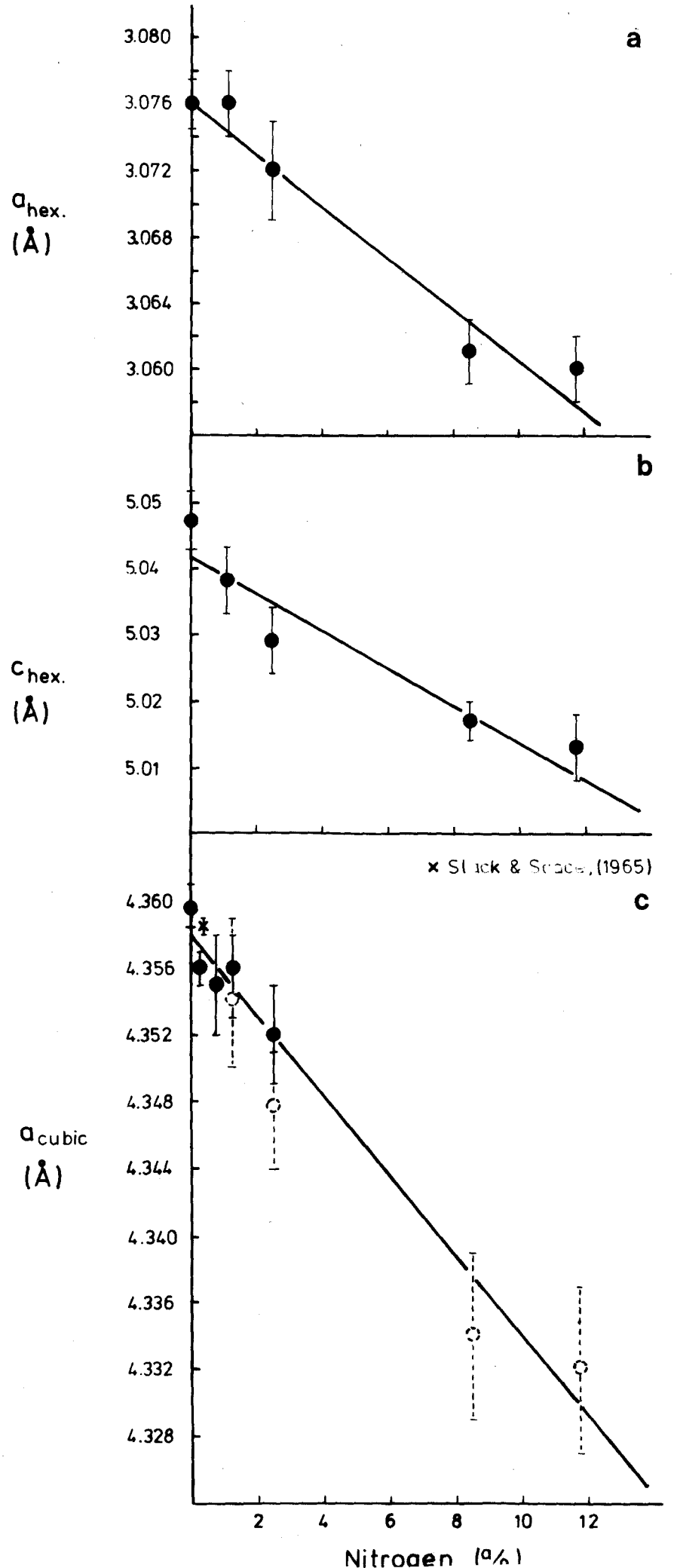
a
3.080
3.076
3.072
3.068
3.064
3.060
$a_{hex.}$ (Å)
b
5.05
5.04
5.03
5.02
5.01
$c_{hex.}$ (Å)
× Stuck & Seraca, (1965)
c
4.360
4.356
4.352
4.348
4.344
4.340
4.336
4.332
4.328
a_{cubic} (Å)
2
4
6
8
10
12
Nitrogen (a%)

It should be pointed out that if, say, 10% of a calcium sialon glass was produced, the maximum nitrogen content of this phase would be of the order of 10 a/o (Hampshire, 1980). Any glassy phase present in the specimen could therefore account only for a maximum of 1 a/o N which would not significantly alter the nitrogen contents of 2H and 3C SiC found in the present work.

Such large amounts of nitrogen have been incorporated into the SiC because of the preparative route employed. When pure 2H-SiC was prepared from Si_3N_4 - C mixtures in an argon atmosphere, the cell dimensions were very similar to those of materials prepared in nitrogen and similarly all other results (see section VI.2 and VI.3) show that it is the nitrogen in the silicon nitride which is responsible for the change in cell dimensions.

VI.5 The effect of high nitrogen pressure

High pressures of atmospheric nitrogen stabilise the 3C-SiC polytype at temperatures around 2250°C in preference to 6H which is the stable polytype in the absence of deliberately added impurities. The results of Slack & Scace (1965) have already been mentioned and Kieffer et al. (1969) has noted that the $\alpha \rightarrow \beta$ transformation is reversible by substituting nitrogen for argon as the controlling atmosphere. Jepps (1979) observed the $\alpha \rightarrow \beta$ transformation in α-REFEL material under 30 atmospheres of nitrogen and has also established that it is prevented in argon. There is therefore ample evidence to indicate that 3C is stabilized by nitrogen in preference to 6H but, apart from the work of Slack & Scace (1965), there have been no determinations of lattice parameter as a function of nitrogen content in any SiC. In order to investigate this, Dr Jepps

kindly supplied samples of his high pressure α-REFEL materials. Unit-cell dimensions of these materials were determined as described in section IV.5 : the results, given in Table VI.6, show that the cell dimensions of the 3C formed by annealing in nitrogen are significantly smaller than those of β-REFEL which has dimensions normally quoted for pure 3C (Taylor & Laidler, 1950). This is evidence for the incorporation of nitrogen which, in lowering the cell dimensions, induces the transformation to 3C.

VI.6 The 2H → 3C transformation

The 2H → 3C transformation in nitrogen-free SiC has been observed on a number of occasions (Bootsma et al., 1971; Powell & Will, 1971; Krisha & Marshall, 1971a,b) generally within a temperature range of 1500°- 1700°C. In the current work a similar transformation has been observed in two specimens:

(a) pure nitrogen-2H, prepared as described previously in section VI.2 and (b) consisting of ∿60% 2H and ∿40% 3C prepared in a similar way but in the absence of lime. Both specimens were subjected to post-preparative heat treatment over the temperature range 800° - 2100°C.

Specimen (b) was initially annealed at 800°C for 7 days but the X-ray diffraction pattern showed that no change had occurred and even after heating for 3h at 1600°C the relative amounts of 2H and 3C were unchanged (see Table VI.7). Although 1h at 1800°C still produced no significant changes, at 2000°C 90% of the specimen had transformed to 3C and at 2100°C the 2H → 3C transformation was complete. The nitrogen-saturated 2H specimen (a), also showed no tendency to transform to 3C at temperatures of < 1800°C but at 2000°C 75% transformation

TABLE VI.6

Cell dimensions of REFEL silicon carbide materials

	6H (Å)	4H (Å)	3C (Å)
α-REFEL	a = 3.0810±.001 c = 15.1202	-	-
α-REFEL annealed in Ar at 2250°C	-	a = 3.0790±.0002 c = 10.0836	a = 4.3570±.001
α-REFEL annealed in N_2 at 2250°C	-	-	a = 4.3583±.0001
β-REFEL	-	-	a = 4.3596±.0002
pure 3C-SiC (Taylor & Laidler, 1950)			a = 4.3590±.0001

TABLE VI.7

Annealing of 2H-3C mixture and nitrogen-2H SiC; X-ray data

post-preparative heat-treatment (°C/minute)	X-ray analysis (w/o) 2H	3C	Si_3N_4
starting composition	60	40	tr
800/7 days	60	40	tr
1600/120	50	50	-
1800/60	40	60	-
2000/15	10	90	-
2000/30	10	90	-
2100/15	-	100	-
starting composition (A in Table VI.5)	100	-	-
1600/240	100	-	-
1800/60	100	-	-
2000/15	25	75	-
2100/15	tr	100	-

occurred after only 15 minutes and almost pure 3C was produced by annealing at 2100°C for 15 minutes in nitrogen; X-ray analyses are given in Table V.7.

The 2H → 3C transformation in polycrystalline SiC observed by Bootsma et al. (1971) proceeded very slowly at 1500°C and took 70h to complete. At 1600° and 1700°C the rate of transformation became increasingly fast and conversion to 3C was achieved after 7h and 1.5h respectively. Krishna & Marshall (1971a) observed that 2H single crystals transform slowly to 3C by annealing between 1400° and 1800°C; at higher temperatures (2000° - 2200°C) a 6H structure forms. In the present work the rate of conversion from 2H → 3C observed with nitrogen-2H and the 2H-3C mixture is much slower than described above for nitrogen-free 2H, and it is also notable that the 6H polytype never occurs. From previous experiments (see section VI.3) it is known that specimen A contains ∿12 a/o nitrogen which stabilizes it relative to 3C at 1650°C and this strongly suggests that the nitrogen content retards the transformation to 3C during post-preparative heat-treatment. In this specimen the 2H → 3C transformation is initiated at about 1900°C compared with 1600°C in the 95% 2H : 5% 3C specimen of Bootsma et al. (1971). The 2H-3C specimen (b) also showed a similar reluctance to transform to 3C below ∿1800°C, thus again indicating that nitrogen stabilizes 2H relative to 3C at temperatures up to ∿1900°C.

The X-ray diffraction patterns of the 2H-3C mixture, taken after annealing, not only showed the changes in 2H : 3C ratio but also small shifts in the positions of the reflexions to larger d-spacings; see Figure VI.5. Inert gas fusion analysis (see section VI.4) shows that loss of nitrogen occurs during annealing and this is the cause of the

Figure VI.5

X-ray powder diffraction patterns

showing the 2H-3C transformation in SiC

(a) initial 2H/3C mixture

(b) annealed at 800°C/7 days

(c) annealed at 1650°C/120 minutes

(d) annealed at 1800°C/60 minutes

(e) annealed at 2000°C/15 minutes

(f) annealed at 2100°C/15 minutes

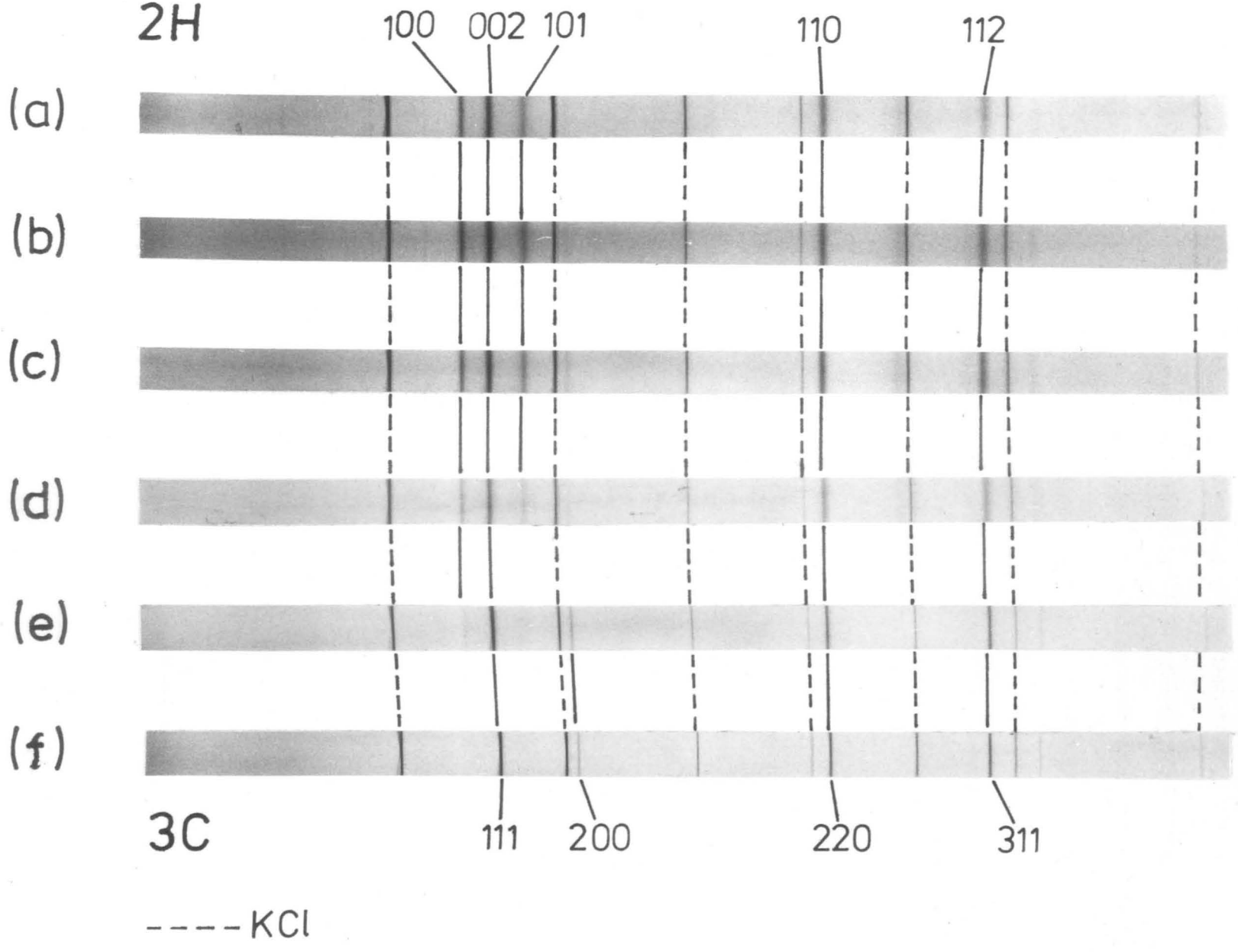
2H
100
002
101
110
112
(a)
(b)
(c)
(d)
(e)
(f)
3C
111
200
220
311
----KCl

shifts in the X-ray reflexions. The 2H polytype loses nitrogen more rapidly than the 3C polytype thus becoming thermodynamically less stable at the higher temperatures when only 3C is formed. Annealing nitrogen-2H also causes the release of nitrogen as indicated by the shift in the X-ray reflexions to larger d-spacings giving an increase in the unit-cell dimensions, as shown in Figure VI.6 and Table VI.8. Moreover, in both specimens the loss of nitrogen is accompanied by a sharpening of the reflexions indicating a more crystalline product.

VI.7 Microstructure

Microstructural changes during post-preparative heat-treatment in nitrogen-2H and a SiC specimen fabricated at 1650°C and estimated to contain ∿60% 2H plus ∿40% 3C (with a trace of unreacted Si_3N_4) were observed by scanning electron microscopy. Initially the latter material was composed of equiaxed crystals ∿0.6 μm diameter and a smaller amount of needle-like crystals 0.1 - 0.4 μm thick and several microns long, as shown in the scanning electron micrographs of Figure VI.7(a) and (b). The needles are in clusters restricted by the size of the pores into which they grow. No change in the microstructure is observed after annealing at 830°C for 7 days (Figure VI.7(c)) but at 1800°C only the small crystals are visible (Figure VI.7(d) although there is no change in the X-ray diffraction pattern. Consistent with X-ray analysis the most obvious change occurs after heat-treatment at 2000°C and 2100°C, as illustrated in micrographs (a) - (d) of Figure VI.8. The growth of anomalously large crystals 10 - 15 μm in size occurs although the majority of the specimen is still composed of small crystals of the same size as in the starting

Figure VI.6

X-ray powder diffraction pattern

showing the 2H → 3C transformation in

(a) nitrogen - 2H

(b) annealed at 1600°C/240 minutes

(c) annealed at 2000°C/60 minutes

(d) annealed at 2000°C/15 minutes

(e) annealed at 2100°C/15 minutes

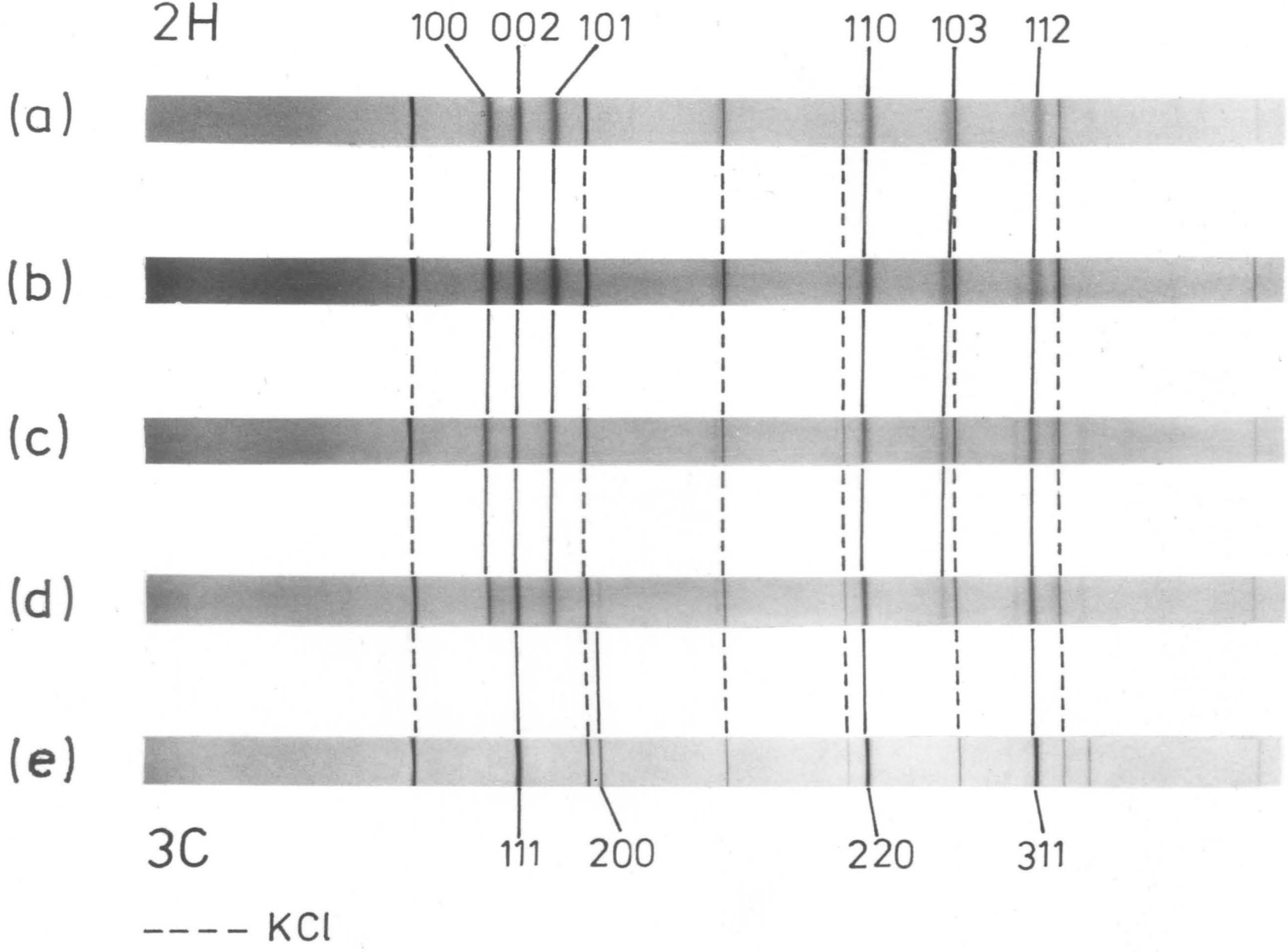
2H
100
002
101
110
103
112
(a)
(b)
(c)
(d)
(e)
3C
111
200
220
311
---- KCl

TABLE VI.8

Cell dimensions of nitrogen-2H after annealing

annealing conditions	2H		3C
	a (Å)	c (Å)	a (Å)
Starting material	3.060±.002	5.013±.005	-
1600/4 h	3.062±.002	5.025±.005	-
1800/1 h	3.072±.002	5.044±.005	-
2000/15 minutes	3.078±.002	5.045±.005	4.357±.002
2100/15 minutes	-		4.356±.002

Figure VI.7

Microstructures of initial 2H/3C mixture (a), (b)

and after annealing at 830°C (c)

and 1800°C (d)

(a)

(b)

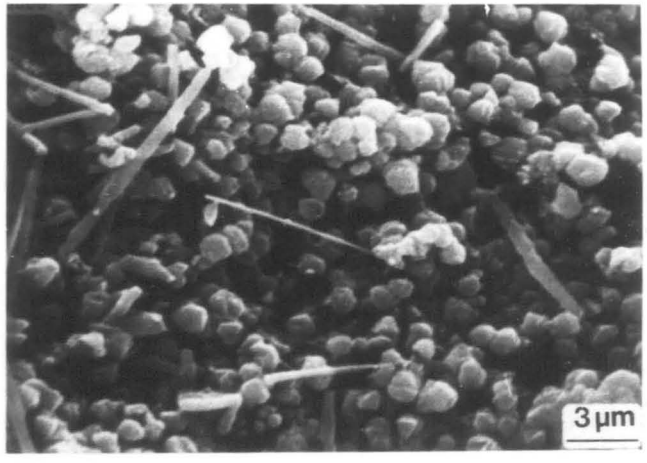

(c)

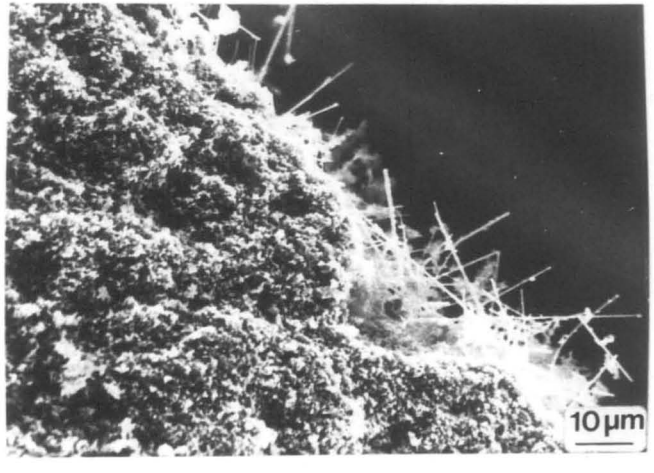

(d)

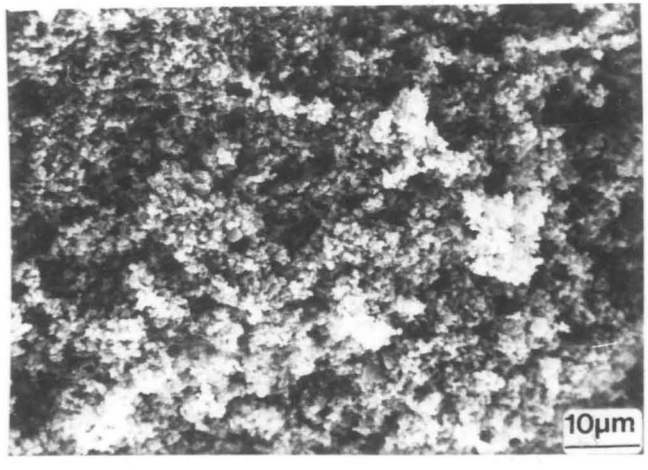

Figure VI.8

Microstructures of 2H/3C mixture after annealing at 2000°C (a), (b) and 2100°C (c), (d)

(a)

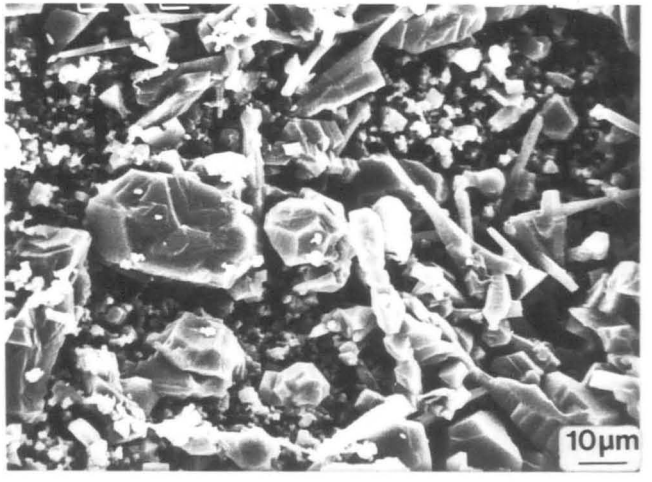

(b)

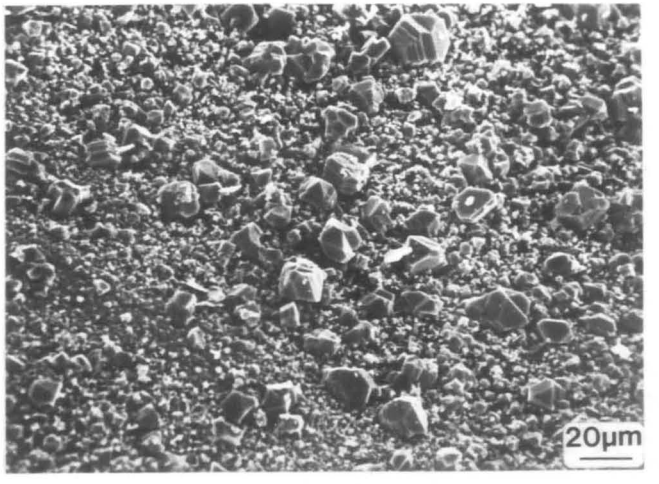

(c)

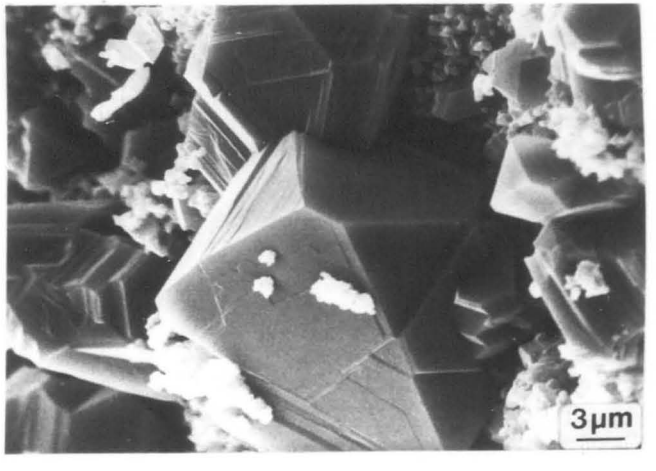

(d)

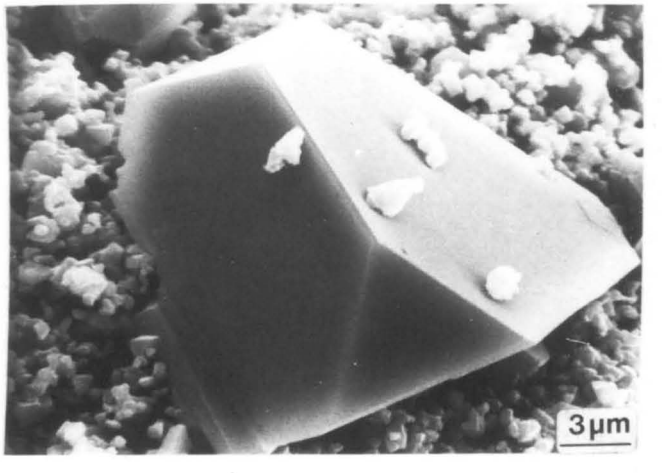

material. The new crystals are less well defined at 2000°C than at 2100°C (Figure VI.8 (a) and (b)) and although they have many growth steps on their surfaces, there is no evidence of spiral markings and so the crystals probably grow by vapour deposition onto a suitable mucleus. Figures VI.8(c) and (d) show that some crystal faces predominate, particularly the {111} type.

The nitrogen-2H material is in many respects very similar, in that the starting material also consists of equiaxed crystals (∿ 0.5 μm diameter) and needles (see Figure VI.9 (a) and (b)). In this specimen the elongated crystals are more numerous and also have globular terminations indicative of growth by a liquid phase mechanism. Since this specimen was fabricated by deliberately adding CaO to provide a liquid phase, the beads on the end of these crystals are most probably a calcium aluminium silicon-oxynitride liquid.

The disappearance of the needles during post-preparative heat-treatment at 1800°C is the first morphological change (see Figure VI.9 (c) and (d)) and, as in the case of the previous specimen, this is accomplished with apparently little or no change in the X-ray diffraction pattern. At 2000°C the 2H → 3C transformation proceeds rapidly and this is again accompanied by growth of crystals 5 - 10 μm in size as shown in Figure VI.10(a). The remainder of the specimen is composed of the small equiaxed crystals ∿ 0.5 μm diameter although some have grown by vapour deposition to 2 - 3 μm diameter; see Figure VI.10(b). X-ray analysis shows that at 2100°C the transformation to 3C is almost complete after 15 minutes and the final microstructure is shown in Figure VI.10(c) and (d). It contains no anomalously large crystals and appears homogeneous with an average crystal size of 2-6 μm.

Figure VI.9

Microstructure of nitrogen - 2H (a), (b)

and after annealing at 1800^{o}C (c), (d)

(a)

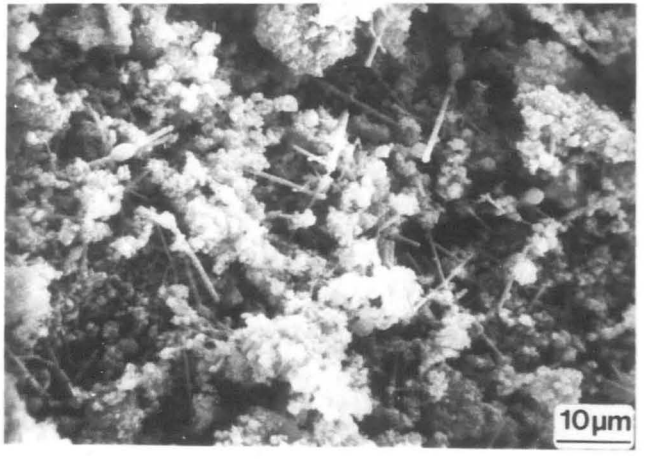

(b)

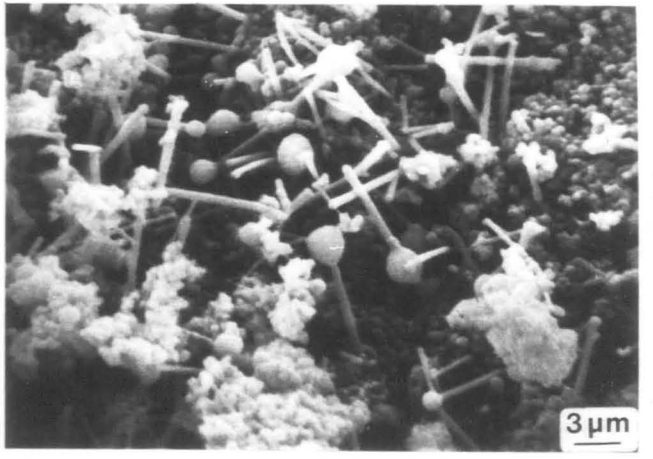

(c)

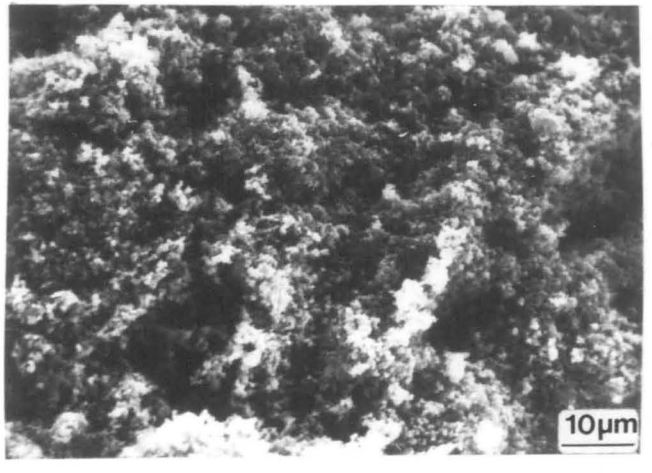

(d)

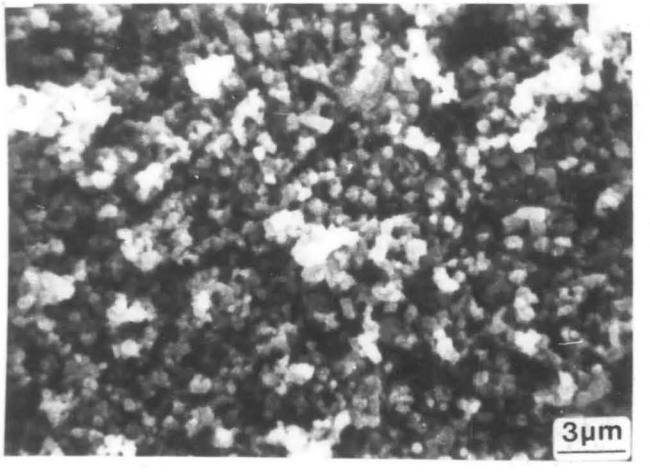

Figure VI.30

Microstructure of nitrogen - 2H

after annealing at 2000°C (a), (b)

and 2100°C (c), (d)

(a)

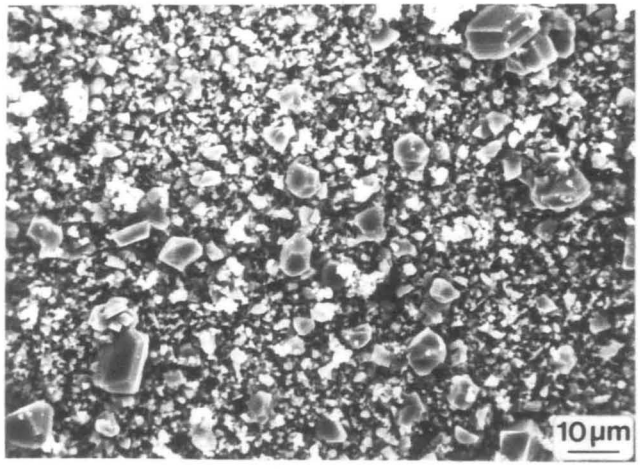

(b)

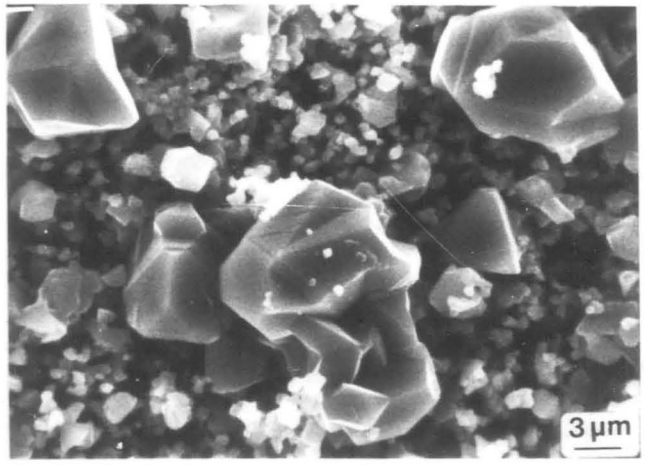

(c)

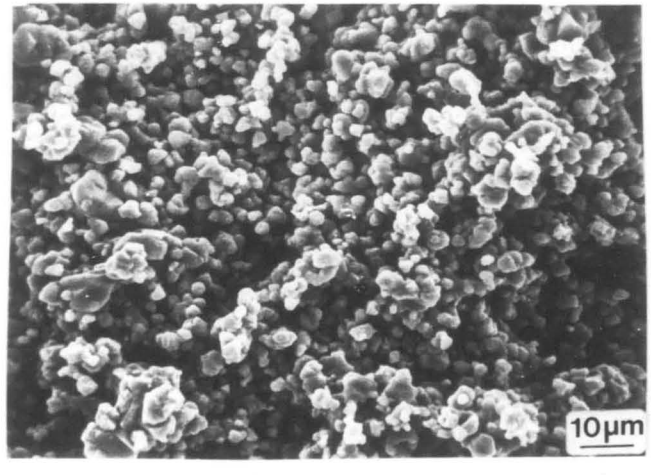

(d)

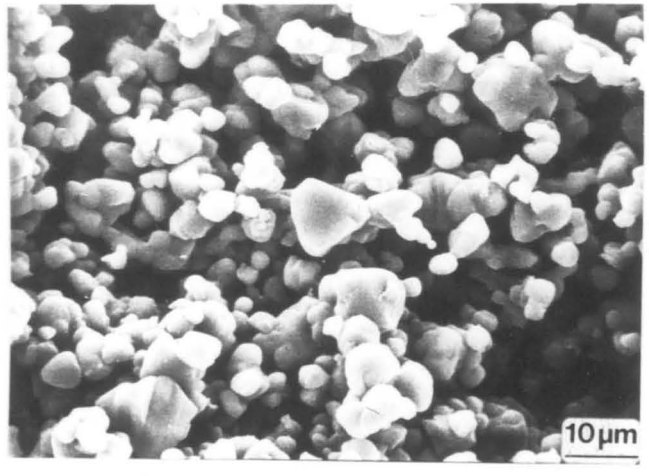

These morphological changes observed during post-preparative heat-treatment are similar to those reported by Bootsma et al. (1971) when annealing a polycrystalline 2H-SiC specimen. Their starting material consisted of filamentous crystals, which, concurrent with transformation to 3C became shorter and thinner as equiaxed crystals grew (∿ 1.5 - 4 μm diameter). Although both the nitrogen-2H and the 2H-3C mixture contain filamentous crystals, the majority of each specimen are smaller crystals but, like Bootsma et al., the disappearance of the needles and coarsening of the equiaxed crystals accompanies transformation to 3C.

VI.8 Conclusions

By preparing silicon carbide from silicon nitride and carbon, nitrogen is incorporated into the lattice and in so doing stabilizes the 2H and 3C polytypes. 2H is stabilized to about 1900°C by ∿ 12 a/o nitrogen which causes an appreciable reduction in the cell dimensions. The solubility of nitrogen in 3C is less (∿ 3 a/o at 1800°C) and loss of nitrogen from 2H at temperatures above ∿ 1900°C accompanies the transformation to 3C. Experiments using high nitrogen pressures show that very small quantities of nitrogen are required to stabilize 3C in preference to 6H at high temperatures. The 2H → 3C transformation is also accompanied by a change in crystal morphology giving a much higher proportion of large equiaxed particles.

VII SILICON CARBIDE-ALUMINIUM NITRIDE ALLOYS

VII.1 Introduction

The original paper describing the formation of SiC-AlN solid solutions (Cutler et al., 1978) mentioned three fabrication routes. These were:

(a) At Newcastle, the carbon reduction of α'-sialons at 1800°C i.e.

$$CaSi_9Al_3ON_{15} + 10C \rightarrow 9SiC{:}3AlN + Ca\uparrow + CO\uparrow + 6N_2\uparrow \quad ...VII.1$$

(b) At Newcastle, reaction of silicon nitride, aluminium nitride, carbon and lime at a similar temperature, i.e.

$$Si_3N_4 + AlN + 4C + CaO \rightarrow 3SiC{:}AlN + Ca\uparrow + CO\uparrow + N_2\uparrow \quad ...VII.2$$

(c) At Utah, reaction of intimate mixtures of silica, carbon and aluminium hydroxide at 1600°C in a nitrogen atmosphere i.e.

$$3SiO_2 + Al(OH)_3 + 9/2C + N_2 \rightarrow 3SiC{:}AlN + 3/2H_2O\uparrow + 3/2CO\uparrow + 1/2N_2\uparrow \quad ...VII.3$$

All three methods established the existence of a complete series of solid solutions between SiC and AlN and route (c) when carried out in argon apparently showed that another series of solid solutions occurred between SiC and Al_2OC. Route (b) was originally thought to involve the formation of a calcium oxynitride liquid which was reduced by carbon to volatile species after the formation of the final product. The present investigation was concerned with this method for the preparation of SiC-AlN solid solutions.

VII.2 High temperature preparative studies in the silicon nitride-aluminium nitride-calcium oxide-carbon system

VII.2.1 Sample preparation

Samples were prepared by firing powder mixtures of Si_3N_4, AlN, C and CaO in the graphite resistance and tungsten resistance furnaces at temperatures from 1700° to 2100°C, as described in section IV.3. It was necessary to use the graphite furnace for the majority of the experiments as the maximum operating temperature of the tungsten furnace at 1750°C was the minimum temperature at which reaction occurred. In all experiments, the inert gas atmosphere was nitrogen and the time at the reaction temperature was kept constant at 30 minutes. No densification occurred in the final product and typical densities were less than $2gcm^{-3}$ but this is not surprising since a number of vapour species are evolved during the reaction (see equation VII.2).

VII.2.2 E-phase

During the fabrication of SiC-AlN alloys additional reflexions were observed on X-ray photographs which could not be identified as due to any known compound. This phase (termed "E") had also been observed during the preparation of calcium α'-sialons (see Chapter V) and therefore attempts were made to obtain a pure sample from compositions in the $CaO-Si_3N_4$-AlN system. The purest specimen (∿90 w/o E) was obtained by firing 60m/o CaO, 20m/o Si_3N_4 and 20m/o AlN at 1700° for 30 minutes in the tungsten furnace and although further attempts at hot-pressing and varying the starting composition did not produce a purer product (the main impurity being AlN), the results indicated that the phase had a small range of homogeneity extending towards AlN.

Its X-ray diffraction pattern was indexed on the basis of an orthorhombic unit cell with dimensions;

$$a = 5.640\ \text{Å}, \quad b = 9.532\ \text{Å}, \quad c = 4.989\ \text{Å}.$$

The relative intensities, d-spacings and indices of the X-ray reflexions given in Table VII.1 are very similar to those of the quaternary nitrides $MnAlSiN_3$ (Siddiqui, 1980) and $MgAlSiN_3$ (Perera, 1976) (see Table VII.2) which have similar unit-cell dimensions (see Table VII.3). This strongly suggests that E-phase has the formula $CaAlSiN_3$. However, results of electron probe microanalysis (E.P.M.A.) of hot-pressed and pressureless sintered samples containing ∿90% E-phase gave an approximate composition $CaSi_2AlN_{4.3}$ (see Table VII.4) for both specimens and (consistent with X-ray analysis) areas of unreacted AlN were found. SE micrographs of the pressureless sintered material showed lath-like crystals of E-phase embedded in a glassy matrix (Figure VII.1(a)) whereas specimens prepared by hot-pressing gave a more intertwined structure where the glassy matrix was not easily distinguishable; see Figure VII.1(b). E.P.M.A. of the glassy phase showed it to be oxygen rich with an approximate composition $Ca_{6.06}Si_{4.74}Al\ O_{9.28}N_{5.17}$ (see Table VII.4).

Since the X-ray diffraction evidence, combined with the existence of the similar compounds $MgAlSiN_3$ and $MnAlSiN_3$ strongly suggests the composition $CaAlSiN_3$ it seems unreacted Si_3N_4 was included in the regions of E.P.M.A, i.e.

$$CaSiAlN_3 + 1/3Si_3N_4 \rightarrow CaSi_2AlN_{4.3} \qquad \ldots VII.4$$

The systematically absent reflexions in the X-ray diffraction pattern are:

hkl with h + k odd

0kl with l odd

Table VII.1

X-ray diffraction data for E-phase

hkl	d_{obs}	d_{calc}	I_{obs}
110	4.854	4.854	vw
020	4.765	4.766	w
111	3.481	3.479	w
200	2.819	2.820	m
130	2.767	2.768	s
002	2.495	2.495	s
201	2.455	2.455	s
220	2.420	2.427	s
131	2.418	2.421	w
040	2.370	2.383	w
112	2.224	2.219	w
022	-	2.210	vw
221	2.183	2.182	vw
202	1.869	1.869	vw
132	1.853	1.853	w
310	-	1.844	-
240	1.816	1.820	-
150	-	1.806	-
222	-	1.740	
311	-	1.730	-
042	1.723	1.723	-
241	-	1.710	-
151	-	1.698	-
330	1.618	1.618	m
060	1.589	1.589	w
113	-	1.573	-
331	1.538	1.539	w
312	-	1.483	-
242	-	1.470	-
152	-	1.463	-

Cont'd.

Table VII.1 (Cont'd.)

203	1.432	1.433	m
133	1.426	1.426	m
400	1.404	1.410	vvw
260	-	1.384	-
223	1.371	1.372	vw
332)		1.358	-
401)	1.358	1.357	m
420)		1.352	
062	1.333	1.340	m

Table VII.2

Comparison of observed d-spacings of E-phase with $MnAlSiN_3$ (Siddiqui, 1980) and $MgAlSiN_3$ (Perera, 1976)

hkl	E-phase	$MnAlSiN_3$	$MgAlSiN_3$
110	4.853	(	
		(4.718	4.704
020	4.765	(	
111	3.481	3.428	3.391
200	2.819	2.739	(
			(2.707
130	2.767	2.729	(
002	2.495	2.474	2.454
201	2.455	2.398	2.374
220	2.420	(	-
		(2.388	
131	2.418	(	2.374
040	2.370	2.360	-

Table VII.3

Orthorhombic unit-cell dimensions of some nitrides

	a(Å)	b(Å)	c(Å)	b/a	cell volume (Å^3)
AlN	5.394	9.342	4.986	1.732	251.2
Si_2N_2O	5.498	8.877	4.853	1.615	236.9
$LiSi_2N_3$	5.303	9.196	4.780	1.734	233.1
$MgAlSiN_3$	5.439	9.399	4.923	1.728	251.7
$MnAlSiN_3$	5.480	9.432	4.949	1.721	255.8
E-phase	5.640	9.532	4.989	1.690	268.2

Table VII.4

Electron probe microanalysis results for E-phase

	Ca	Si	Al	O	N	(a/o)
starting composition	20.00	20.00	6.67	20.00	33.33	
hot-pressed 1600°C/60 mins., 30 bars	12.11	24.19	11.69	-	52.01	
pressureless sintered 1700°C/30 mins.	11.47	22.28	14.45	-	51.80	
	23.08	18.06	3.81	35.35	19.71	(glass)

Figure VII.1

Micrographs of E-phase

(a) pressureless sintered

(b) hot-pressed

(a)

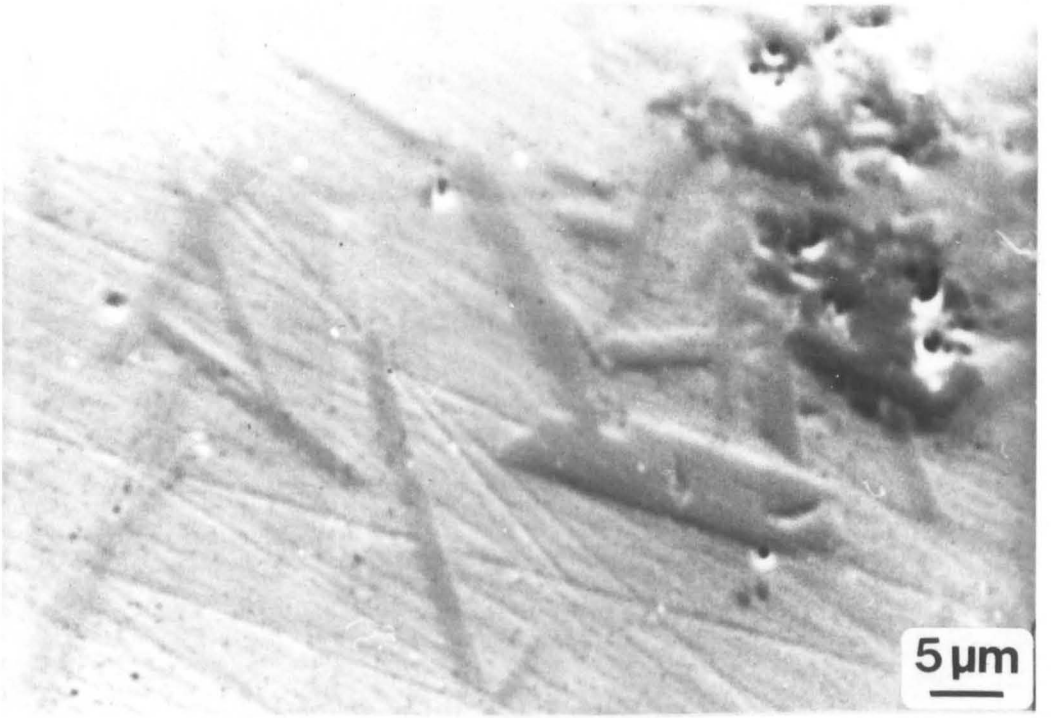

(b)

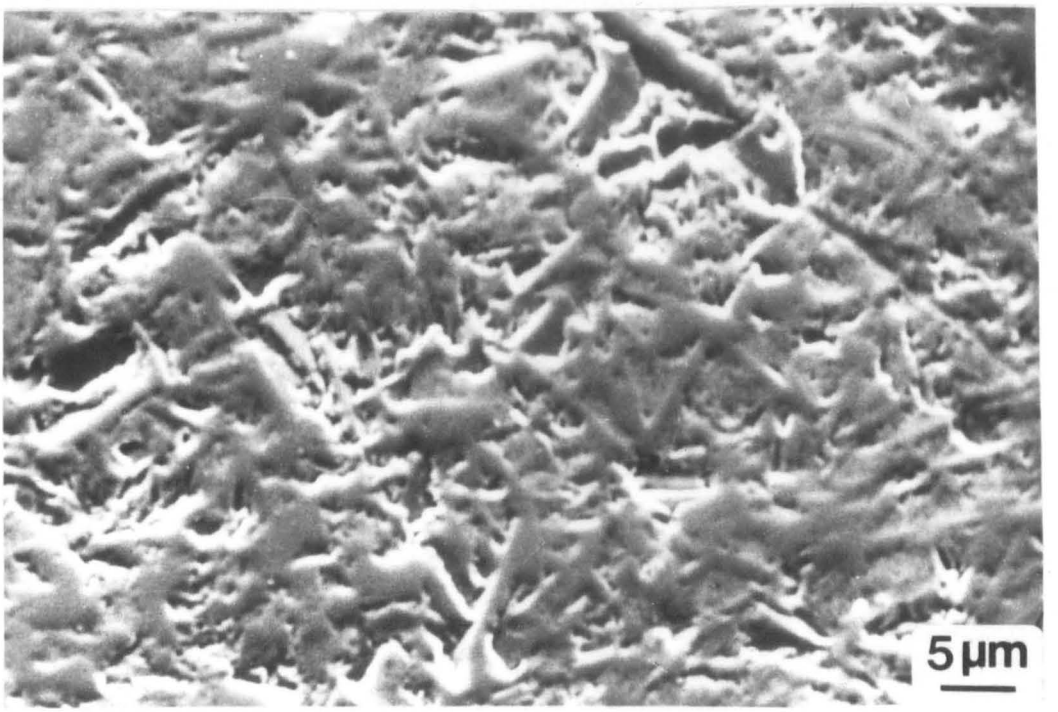

which are identical to those of other compounds in Table VII.3 that all belong to the space group $Ccm2_1$.

The compounds $MnAlSiN_3$, $MgAlSiN_3$ and $LiSi_2N_3$ are isostructural, with a structure based on AlN but with the Mn, Mg or Li atoms respectively ordered in 4(a) sites and the Al and Si atoms (in the case of $MnAlSiN_3$ and $MgAlSiN_3$) disordered over 8(b) sites giving a cell volume six times that of AlN. The atomic arrangement in $MgAlSiN_3$ projected down <001> (Perara, 1976) is shown in Figure VII.2. A similar structure is envisaged for E-phase with Ca 4-fold coordinated by nitrogen. This is rather unusual since Ca normally prefers higher coordination (6 or 8) but has been observed in 4-fold coordination in α-Ca_3N_2 (Laurent et al., 1968).

The reflexions in the X-ray diffraction pattern fall into two groups: strong reflexions corresponding to the basic wurtzite-type lattice, and weak superlattice reflexions. This distinction has also been made for $MgAlSiN_3$ (Perara, 1976) and $MnAlSiN_3$ (Siddiqui, 1980).

VII.2.3 Silicon carbide-aluminium nitride system

By simply varying the proportions of Si_3N_4, AlN and C in the starting mixtures, SiC-AlN alloys of compositions between pure 2H-SiC and pure AlN can be prepared e.g.

$$Si_3N_4 + AlN + 4C + CaO \rightarrow 3SiC.AlN + 2N_2\uparrow + CO\uparrow + Ca\uparrow \quad ...VII.5$$

$$Si_3N_4 + 3AlN + 4C + CaO \rightarrow 3(SiC.AlN) + 2N_2\uparrow + CO\uparrow + Ca\uparrow \quad ...VII.6$$

$$Si_3N_4 + 9AlN + 4C + CaO \rightarrow 3(SiC.3AlN) + 2N_2\uparrow + CO\uparrow + Ca\uparrow \quad ...VII.7$$

provided CaO is present in the starting mix.

The X-ray diffraction patterns of the three solid solutions given by equations VII.5, 6 and 7 are shown in Figure VII.3, together with

Figure VII.2

Atomic arrangement in $MgAlSiN_3$

projected on (001)

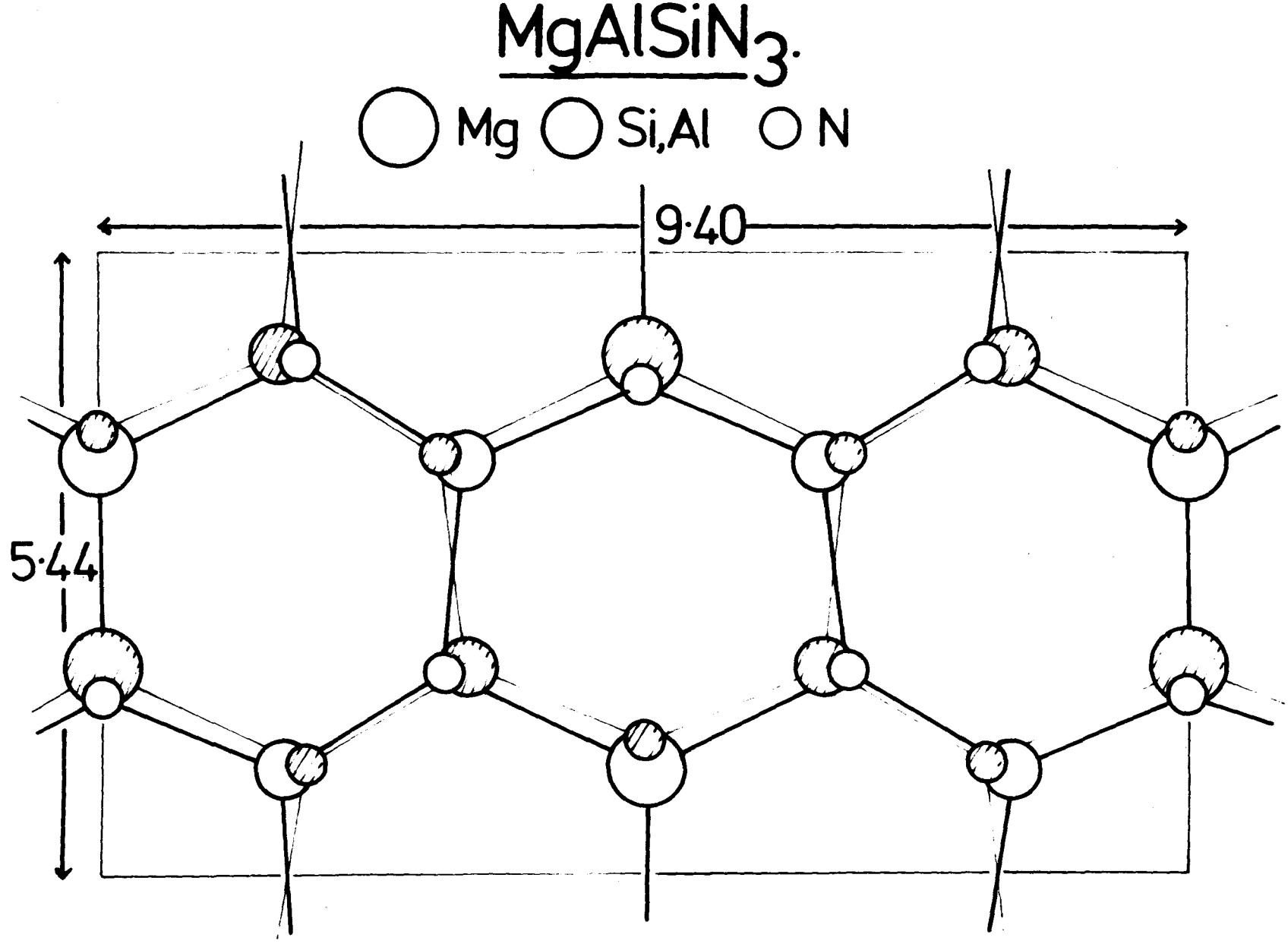
MgAlSiN3.
Mg
Si,Al
N
9·40
5·44

Figure VII.3

X-ray powder diffraction patterns of SiC-AlN alloys showing the variation in d-spacing with AlN content

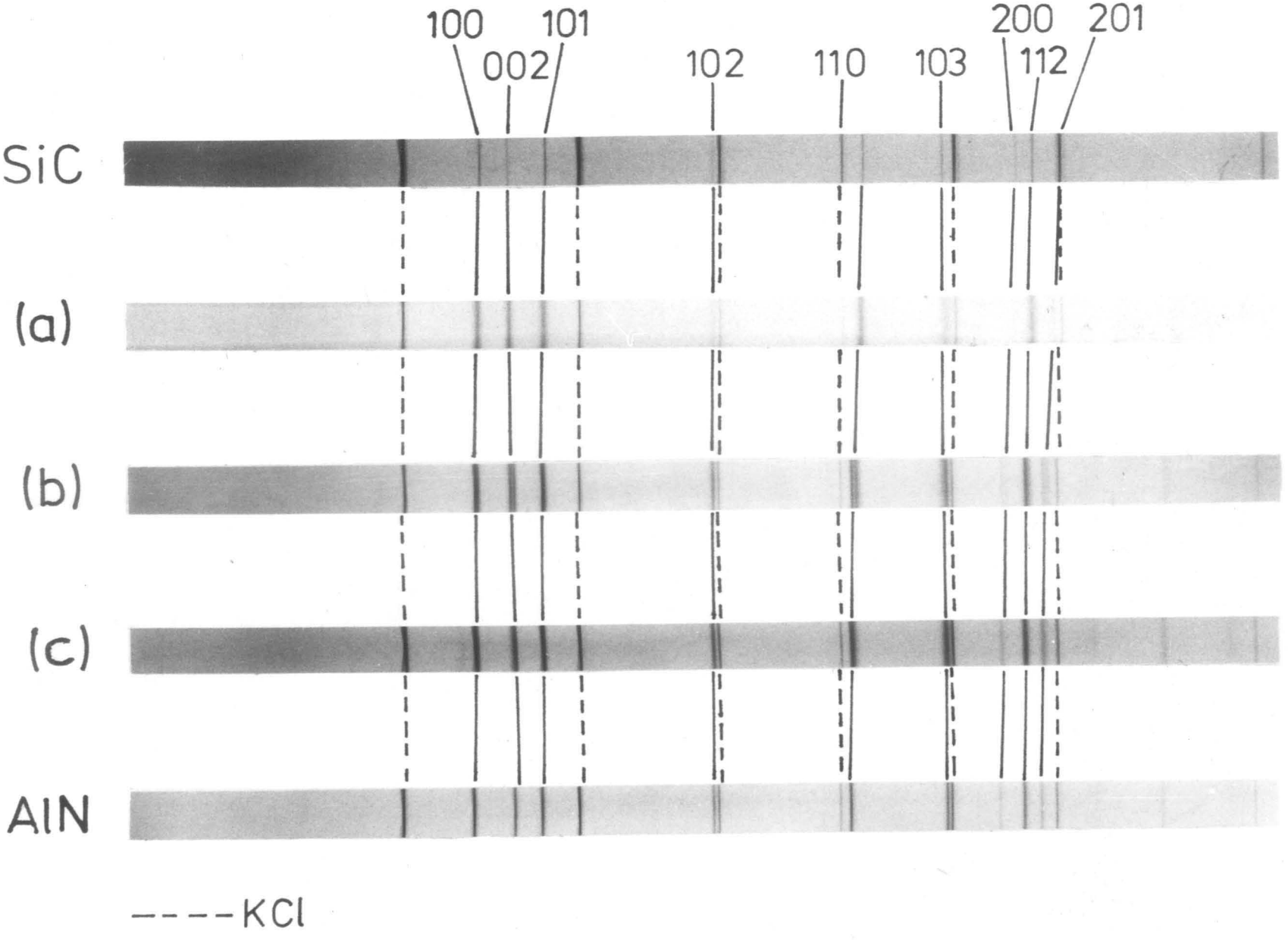
100
002
101
102
110
103
200
112
201
SiC
(a)
(b)
(c)
AlN
----KCl

photographs of pure 2H-SiC and pure AlN. The cell dimensions of the end members are:

2H-SiC $\underline{a}$ = 3.076 Å, $\underline{c}$ = 5.048 Å;

AlN $\underline{a}$ = 3.114 Å, $\underline{c}$ = 4.986 Å.

Consequently, as Al and N are progressively substituted for Si and C the X-ray reflexions shift as $\underline{a}$ increases and $\underline{c}$ decreases. More detailed examination of X-ray VII.3(b) shows not one but two 2H phases are present.

The miscibility gap near the centre of the SiC-AlN join was not recognised in the original publication announcing the formation of SiC-AlN solid solutions, and it was stated that there was a smooth variation in cell dimensions between the two end members (Cutler et al., 1978).

In the current work the region of inhomogeneity was first noticed in a starting composition corresponding to 50 m/o AlN fired at 1800°C. Two 2H solid solutions of cell dimensions:

$\underline{a}$ = 3.106 Å, $\underline{c}$ = 4.990 Å;

and $\underline{a}$ = 3.092 Å, $\underline{c}$ = 5.027 Å

were obtained. Firing the same mixture at higher temperatures produced little changes in the $\underline{a}$ and $\underline{c}$ parameters. Further runs corresponding to the compositions 33, 40, 60 and 66 m/o, each at four different temperatures, showed the full extent of the two-phase region in the system.

The separate phase compositions were determined by calculating cell dimensions from Hägg-Guiner X-ray diffraction patterns and assuming a continuous variation in both the $\underline{a}$ and $\underline{c}$ dimensions from pure 2H-SiC to pure AlN but because the X-ray reflexions were not sharp, errors are

not insignificant. However, the two compositions calculated from a and c for each specimen are usually in good agreement.

Figure VII.4 shows the calculated compositions as a function of temperature. Below 1900°C, a single phase 2H-SiC-rich alloy (designated $2H_{SiC'}$)exists up to ∿38 m/o AlN; from ∿84 m/o AlN to pure AlN there is also a single phase 2H region ($2H_{AlN'}$). The miscibility gap extends over the range 38-84 m/o AlN at 1750°C and contracts only slightly to 40-80 m/o AlN at 2050°C.

Ruh & Zangvil (1982) have prepared apparently single-phase SiC-AlN alloys for AlN contents greater than ~35 m/o by hot-pressing SiC-AlN mixtures at >2100°C in vacuum, and lattice parameter measurements of the products show a uniform linear variation with AlN content (see Figure VII.5). Materials that were single phase by X-ray diffraction were also analysed by scanning transmission electron microscopy (STEM) which showed that they were inhomogeneous with compositions of individual crystals varying from 35 to 65 m/o AlN for a material nominally 50 m/o AlN. These limits are not very different from those of the miscibility gap observed in the present work and it is suggested that Ruh & Zangvil's diffractometer method was not sufficiently sensitive to resolve the two phases. Also very recently Rafaniello et al. (1983), on the basis of optical and chemical analysis, found that SiC-AlN materials hot-pressed at <2100°C were uniform only in the compositional range ⟨ 20-⟩80 m/o AlN. Moreover a 50 m/o AlN composition gave a two phase mixture with compositions of 30 and 85 m/o AlN; again in very good agreement with the limits of the miscibility gap proposed in the present work. However, they too were unable to obtain satisfactory X-ray diffraction evidence.

Figure VII.4

Proposed SiC-AlN phase diagram

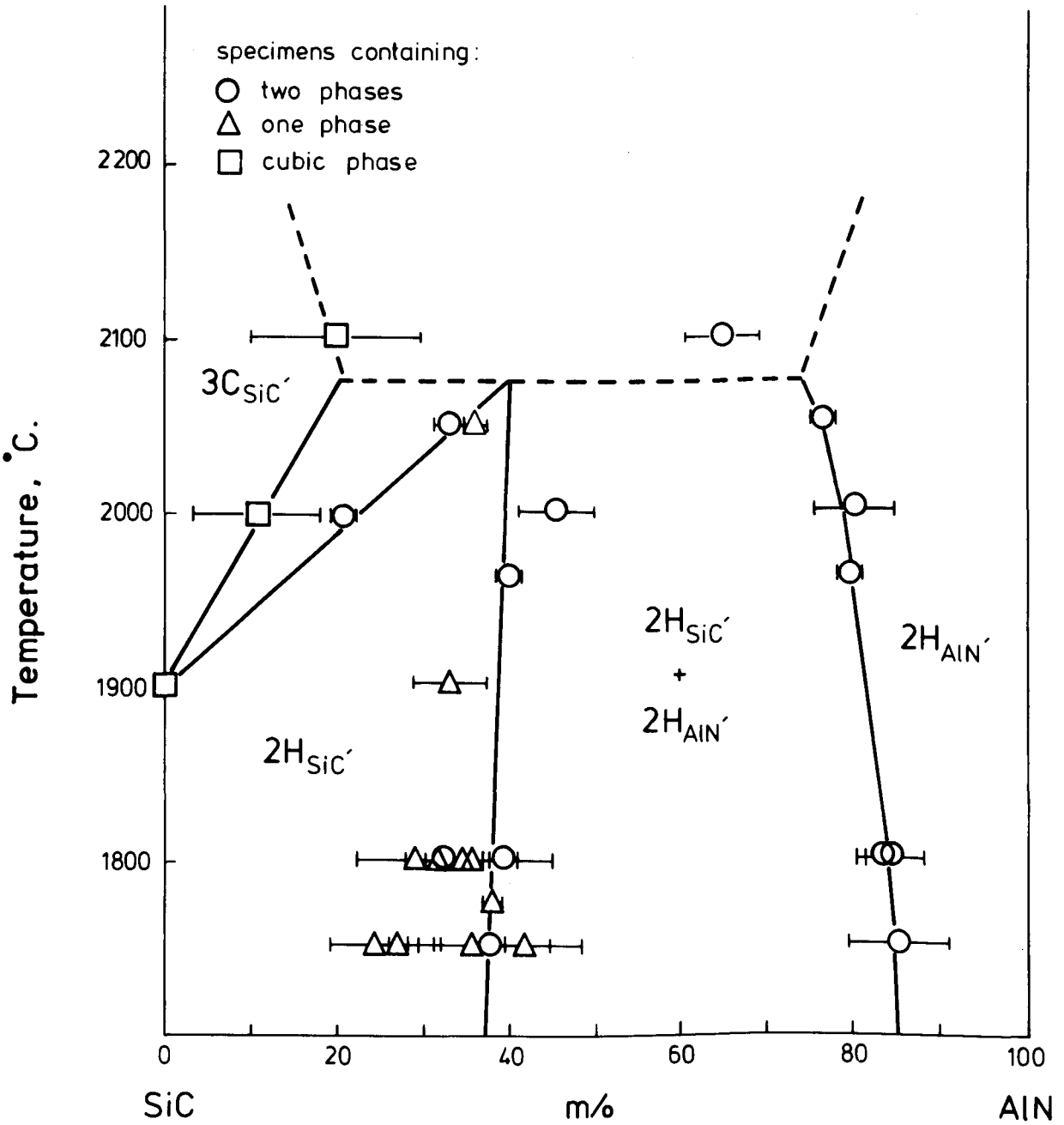
specimens containing:
two phases
one phase
cubic phase
2200
2100
2000
1900
1800
Temperature, °C.
3C SiC´
2H SiC´
2H SiC´
+
2H AlN´
2H AlN´
0
20
40
60
80
100
SiC
m/o
AlN

Figure VII.5

Lattice parameter variations of

SiC-AlN alloys (Ruh & Zangvil, 1982)

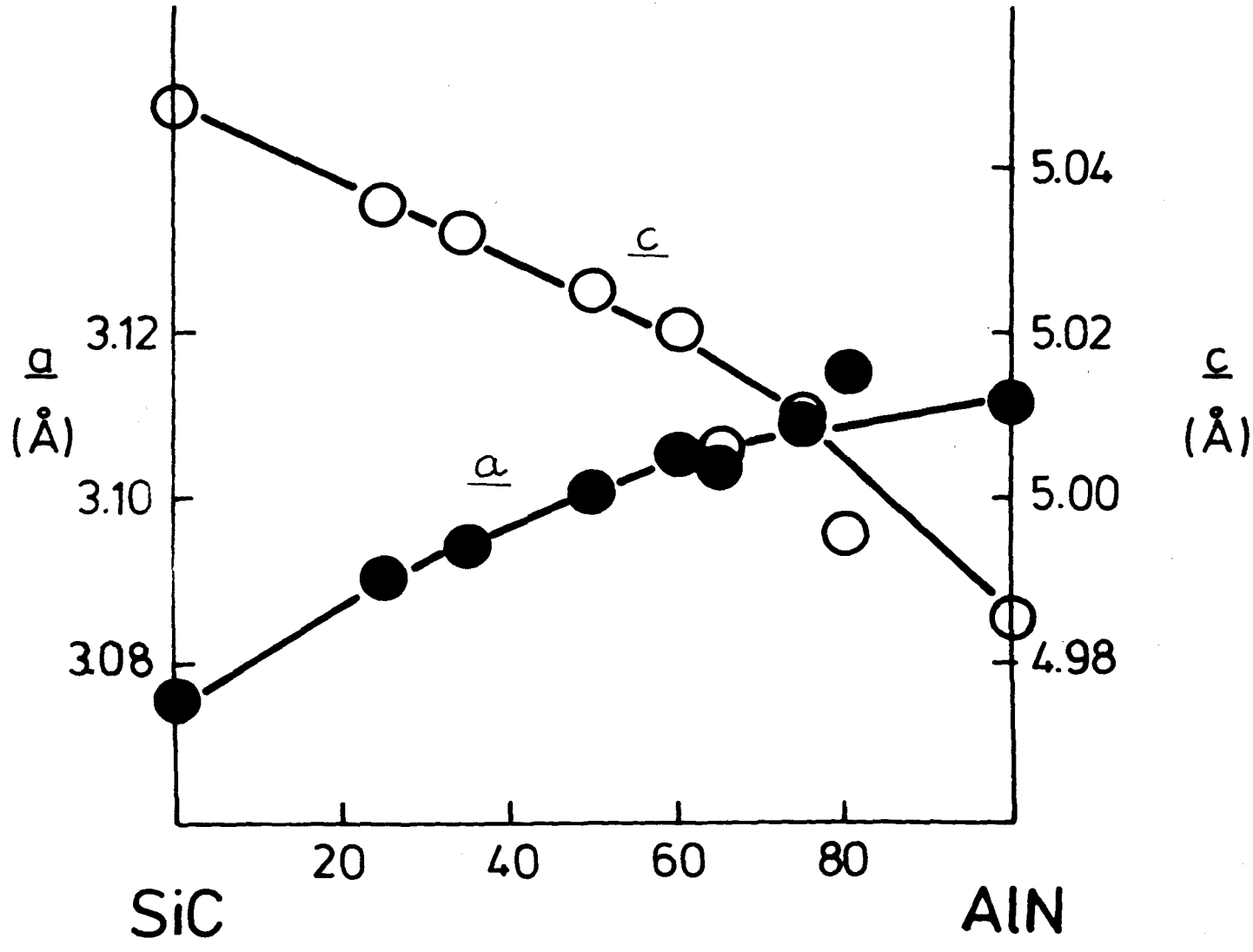

(Ruh and Zangvil, 1982)

The existence of a two-phase region is somewhat surprising because both the a and c cell dimensions in 2H-SiC and AlN differ only by 1.2%. Moreover, Si and Al are adjacent in the periodic table as are C and N and therefore there are little differences in the atomic radii of the substituting atoms. It is possible that differences in bond lengths i.e. Si-C 1.88, Si-N 1.75, Al-C 2.01, Al-N 1.88 Å's, produce too much lattice strain, so making it energetically more favourable for intermediate compositions to occur as two phases, one rich in SiC and the other rich in AlN.

The present work shows that low AlN content solid solutions although single phase below ~1900°C transform to 2H-3C mixtures above this temperature (see Figure VII.4). Note that the 2H→3C SiC transformation temperature of 1900°C applies to nitrogen-saturated 2H as discussed in Chapter VI. The compositions of the cubic phases were calculated from the cell dimensions assuming pure 3C-SiC has a = 4.3596 Å and "3C-AlN" has a = 4.376 Å. The lattice parameter of "3C-AlN" was calculated in the same way as outlined in Appendix 1, assuming that an average value for a can be obtained from the two relationships:

$$a_{cubic} = a_{hex} \times \sqrt{2} \qquad \ldots VII.8$$

$$a_{cubic} = \left[\left(\frac{a_{hex}}{\sqrt{2}}\right)^2 + \left(\frac{c_{hex}}{2}\right)^2\right]^{1/2} \times \sqrt{2} \qquad \ldots VII.9$$

Results show that the maximum s of AlN in 3C-Si is ~20% at 2050°C but because the complete range of 3C cell dimensions is small, this may be in considerable error. At 2100°C only the AlN-rich 2H phase is observed because the 2H-SiC-rich phase transforms to 3C.

The transformation 2H→3C is well known in pure SiC (see Chapter II) but occurs at much lower temperatures (typically 1600°C) than in SiC-AlN solid solutions. The presence of nitrogen alone increases the 2H→3C transformation temperature to ∿1900°C (see Chapter VI) but with aluminium also incorporated into the SiC structure a further increase to between 2000° and 2100°C is achieved. Above 2000°C, the 3C-SiC polytype transforms to 6H according to Bootsma et al. (1971), Kieffer et al., (1969) and Jepps (1979) but in all experiments forming SiC or SiC-AlN alloys in a nitrogen atmosphere the 6H structure was never observed. It seems possible that the non-occurrence of 6H is either because nitrogen cannot be accommodated in the structure, thus making it unstable relative to 3C, or because in the presence of nitrogen 6H has a stability region above 2100°C.

VII.3 The role of calcium oxide

The necessity of a liquid phase to form SiC-AlN solid solutions from powder mixtures of Si_3N_4, AlN, C and CaO by pressureless sintering was established by excluding CaO from the reaction mixtures of a solid solution; instead of a solid solution, the end product was 3C-SiC and AlN in amounts determined by the starting composition. However, in some cases when the AlN content was <15 m/o, a 2H phase was formed even in the absence of CaO. The most likely explanation is that metal oxide impurities in the Starck silicon nitride form a relatively low viscosity liquid with surface oxides on the AlN and Si_3N_4 powders. When different Si_3N_4 powders (Toshiba and G.T.E.), containing very few metal oxide impurities, were substituted, less solid solution was observed (∿20% compared with ∿50%). Moreover, when CaO was added to mixtures composed

of either Starck, Toshiba or G.T.E. silicon nitrides and containing 6 or 12% AlN, almost pure solid solutions were formed.

Having established that a liquid phase promotes the formation of SiC-AlN solid solutions, three compositions were chosen (25, 50 and 75 m/o AlN) and in each case the minimum amount of lime required to form pure 2H solid solution at 1800°C was determined. If insufficient CaO was added, 3C-SiC was formed and thus prevented further reaction; alternatively if too much was added a small quantity of E-phase occurred as an impurity in compositions up to ∿50 m/o AlN. At higher AlN contents, excess lime remained unreacted. In all runs, 3 m/o CaO in the starting mix generated sufficient liquid to promote the formation of pure 2H solid solution.

The addition of CaO to mixtures of 3C-SiC and AlN does not produce SiC-AlN solid solutions even though a liquid phase is present. Indeed, if 3C-SiC forms during the course of a reaction, complete conversion to the alloy is impossible below 2000°C. The recent work of Ruh & Zangvil (1982) indicates that 3C-SiC and AlN can be made to react at temperatures >2100°C if external pressure is applied. However, the 3C powder which was used in these experiments contained relatively large amounts of impurities which might also facilitate the reaction.

In all experiments involving the preparation of SiC-AlN alloys from mixtures Si_3N_4, AlN, CaO and C, 10 w/o excess of C was used, but some experiments with a reduced excess showed that with less than the stoichiometic amount of C the only crystalline phase in the product after firing was AlN. A residual glassy phase was also formed, presumbably because the deficiency of C prevents the evolution of CO in the final

breakdown of the Ca-Si-Al-O-N liquid.

VII.4 Post-preparative heat treatment

To determine the thermal stability of pre-prepared 2H-SiC-AlN alloys, three compositions, corresponding to 75, 50 and 25 m/o AlN, were annealed for different times in nitrogen at 800°-2100°C.

The three specimens were stable up to 1800°C and gave no additional phases. However, at 2000°C a polytypic transformation from the 2H (hexagonal) structure to a 3C (cubic) structure was observed in the SiC-rich alloy. The rate of transformation was reasonably slow at 2000°C and only 10-15% of the specimen had transformed after 15 minutes, a similar result being obtained after 30 minutes. There was a marked increase in the transformation rate at 2100°C with 75% conversion after only 15 minutes. Figure VII.6 shows the X-ray diffraction photographs after post-preparative heat treatment at progressively higher temperatures. All the cubic reflexions overlap with hexagonal lines (except the weak 200 reflexion) thus making it difficult to determine the exact quantities of each phase present, but the gradual strengthening of the lines in the cubic positions and the weakening of hexagonal lines accompanying the transformation is clearly visible. The overlap of the cubic and hexagonal reflexions implies that AlN is dissolved in the cubic phase, indeed cell dimensions show that the solubility limit is between 10 and 20 m/o; see section VII.2.3.

The alloy mid-way between SiC and AlN, consisting of two 2H phases, showed no tendency to transform to a cubic structure at 2000°C but at 2100°C the SiC-rich phase started to transform slowly with ∿5 m/o of the material now 3C. No transformation was observed in the 75 m/o AlN alloy

Figure VII.6

X-ray powder diffraction patterns of (a) 3SiC:AlN alloy after annealing at:

(b) 1800°C/60 minutes, (c) 2000°C/15 minutes

(d) 2100°C/15 minutes, (e) 2100°C/15 minutes

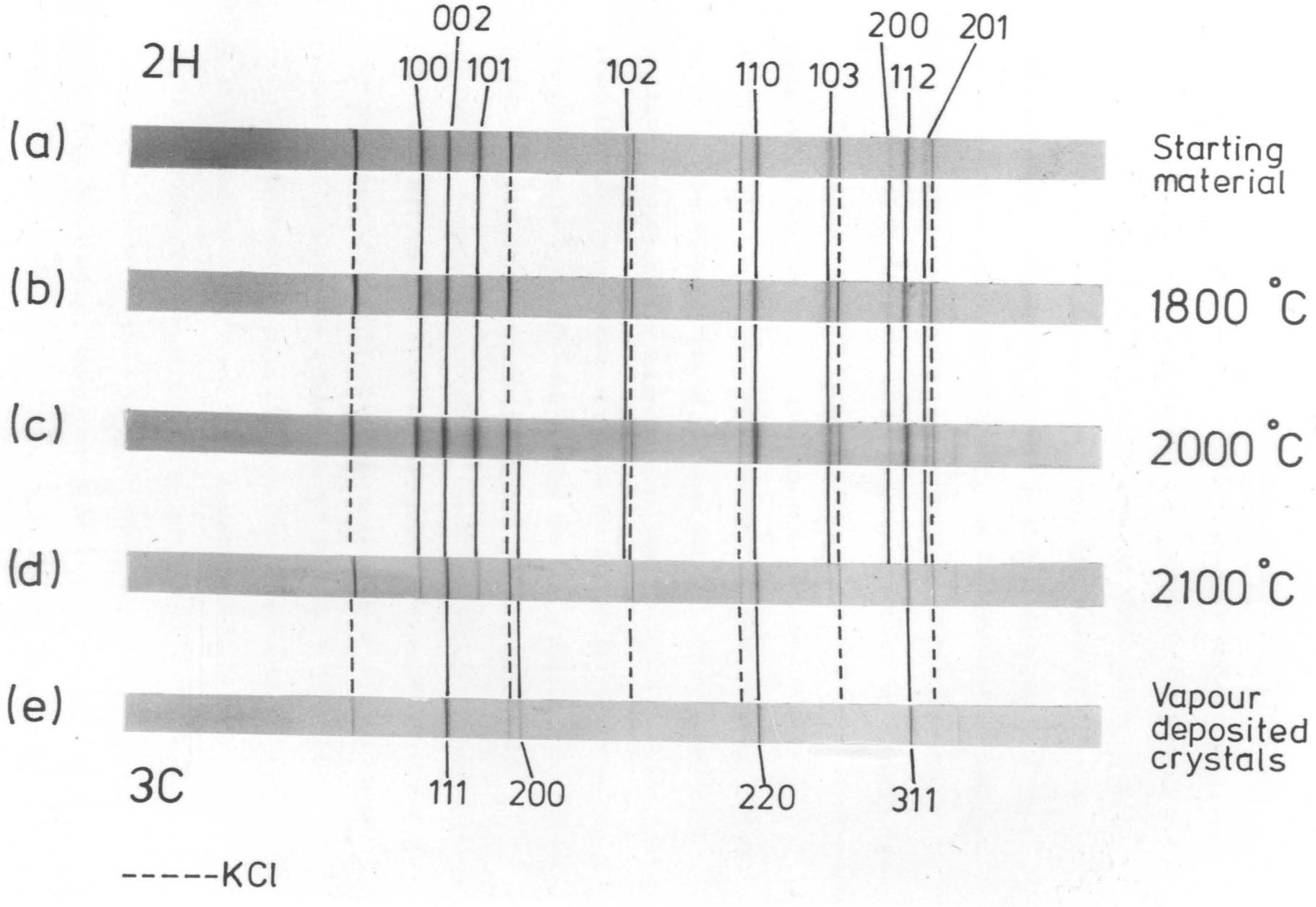
2H
002
100
101
102
110
103
200
112
201
(a)
Starting material
(b)
1800 °C
(c)
2000 °C
(d)
2100 °C
(e)
Vapour deposited crystals
3C
111
200
220
311
-----KCl

at 2100°C although X-ray reflexions from silicon appeared in the diffraction pattern at 2000° and 2100°C indicating some decomposition.

No weight losses were registered for either of the three alloys after annealing at 800°, 1200°or 1600°C but at 1800°, 2000°and 2100°C losses were high (see Figure VII.7). The most AlN-rich alloy had a greatest overall weight loss (40 w/o at 2100°C) as a result of its decomposition at temperatures ≥2000°C. In all specimens the decrease in weight is partially due to loss of Ca (or calcium-containing phases) but it is difficult to satisfactorily explain the complete loss.

In pure SiC the 2H→3C transformation occurs quickly at temperatures above 1600°C (Bootsma et al., 1971; Krishna & Marshall, 1971a,b), although Powell & Will (1972) have observed the transformation as low as 400°C. The incorporation of nitrogen into SiC significantly raises the transformation temperature to ∿1900°C (see Chapter VI) but by simultaneously substituting aluminium for silicon the region of 2H stability can be raised 400°-500°C above the temperature stability limit of 2H. In the case of SiC-AlN alloys the stability varies with composition, becoming more stable as the AlN content is increased. Unlike SiC, AlN does not exist in different polytypic modifications and therefore transformation to other structures at high temperatures becomes more unlikely the greater the AlN content of the alloy.

The stable modification of SiC in the absence of impurities is 6H at temperatures >2000°C but it is claimed that Al (acceptor) added to SiC stabilizes the 4H polytype above 2000°C (Lundquist, 1948; Mitomo et al., 1971; Tajima & Kingery, 1982), and it has also been established that N(donor) stabilizes 3C at similar temperatures (Slack & Scace, 1965; Kieffer et al., 1969; Jepps, 1979). The current work

Figure VII.7

Weight losses of SiC-AlN alloys during post-preparative heat-treatment

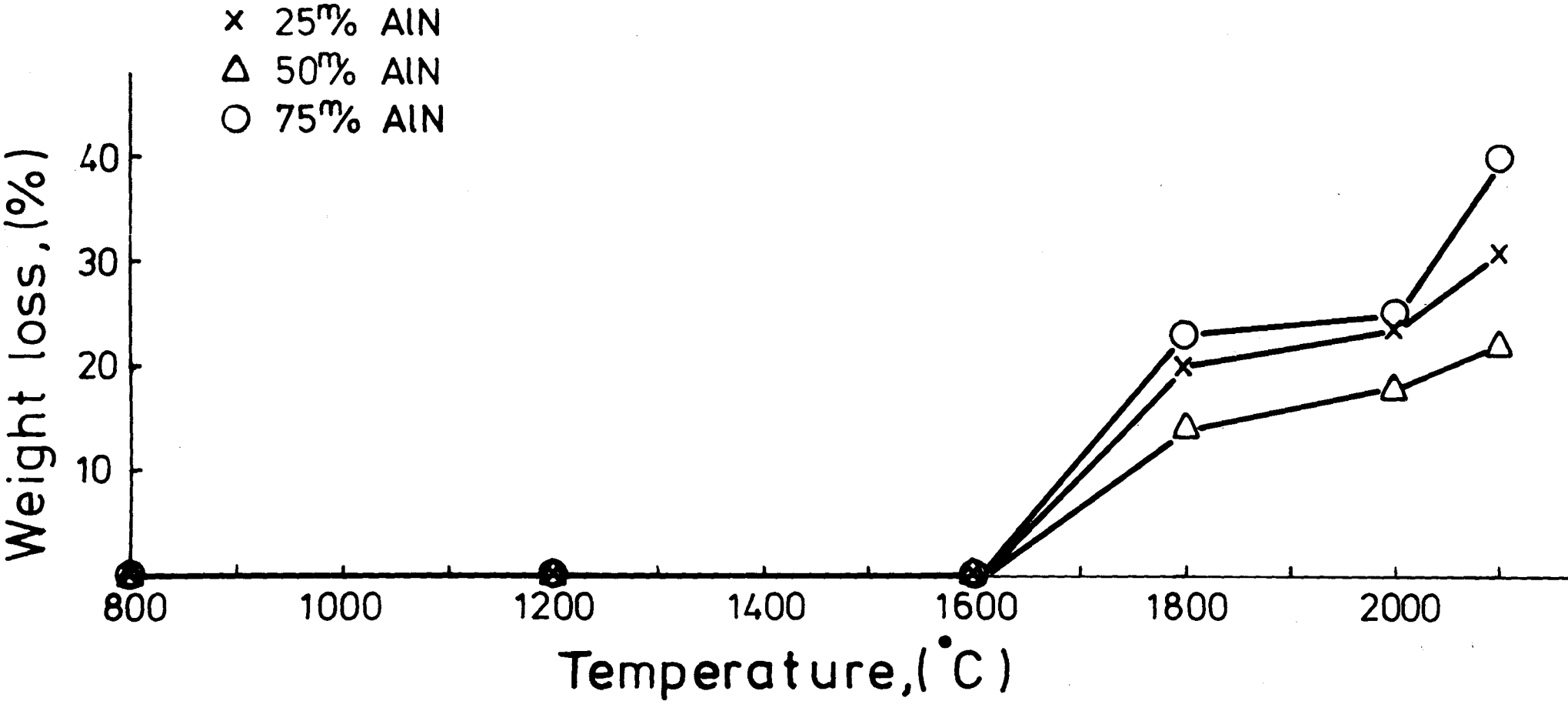
× 25m% AlN
Δ 50m% AlN
○ 75m% AlN
Weight loss,(%)
40
30
20
10
800
1000
1200
1400
1600
1800
2000
Temperature,(°C)

establishes that the combination of Al and N stabilizes the normally very unstable 2H modification up to ∿2000°C and thereafter the 3C polytype is favoured relative to 4H and 6H.

VII.5 Scanning electron microscopy

Fracture-surfaces of pure SiC-AlN solid solutions have been examined by scanning electron microscopy using a Jeol T20 electron microscope, as described in Chapter IV.

Figure VII.8(a) shows a typical low magnification micrograph of an alloy containing 25 m/o AlN and distinguishes two crystal morphologies: needles up to 40 μm long, 0.6 μm wide and small equiaxed particles, ∿0.4 μm diameter. The structure of the needle shaped crystals is shown in greater detail in Figure VII.8(b) and globular terminations can now be seen on the end of each crystal. Gribkov et al. (1972) first observed this type of morphology in α-silicon nitride whiskers and proposed that growth occurred by a vapour-liquid-solid (VLS) mechanism. SiO condenses onto the bead of liquid silicon that is kept fluid by virtue of iron impurities lowering the melting point by as much as 200°C. Molecular nitrogen then reacts with the silicon at the solid-liquid interface and silicon nitride is precipitated onto the surface. Jennings & Richman (1976) have observed similar crystals of silicon nitride as well as others without terminal beads attached to larger grains. They suggest that these larger grains grow out of a 'puddle' of liquid on the surface and therefore can serve the same purpose as a drop in VLS growth. In the case of the SiC-AlN crystals in Figure VII.8(b) a Ca-Si-Al-O-N liquid acts similarly. Merz (1959) and Krishna & Marshall (1971b) also noticed ball-like terminations on 2H-SiC whiskers

Figure VII.8

(a) Microstructure of 25 m/o AlN alloy

(b) Crystals grown by V.L.S. mechanism

(a)

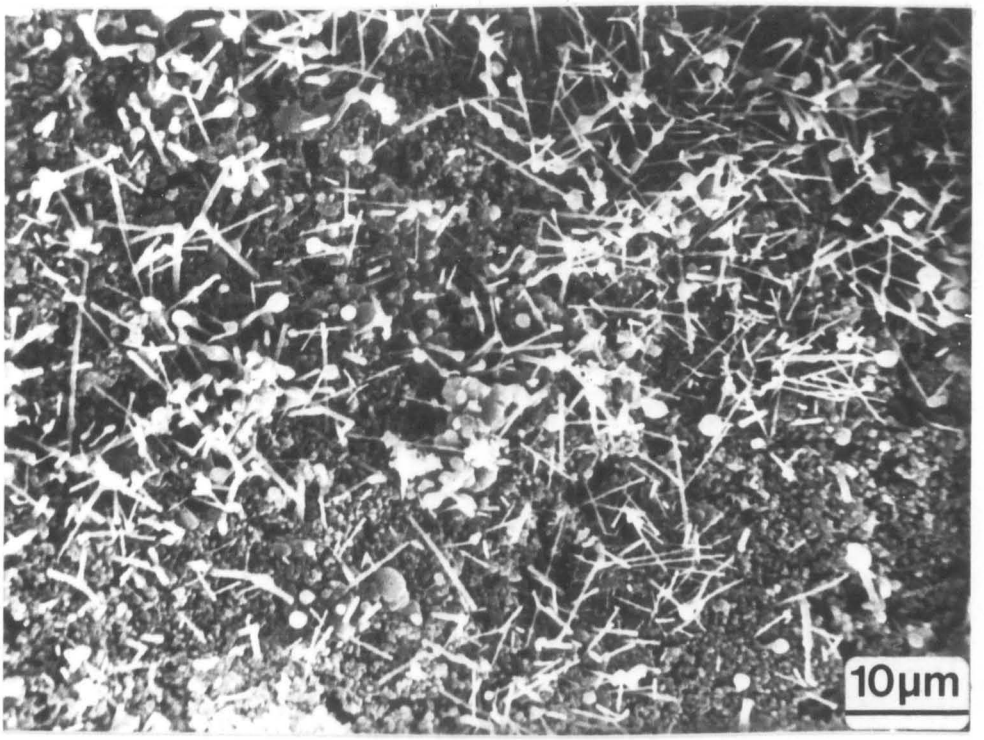

(b)

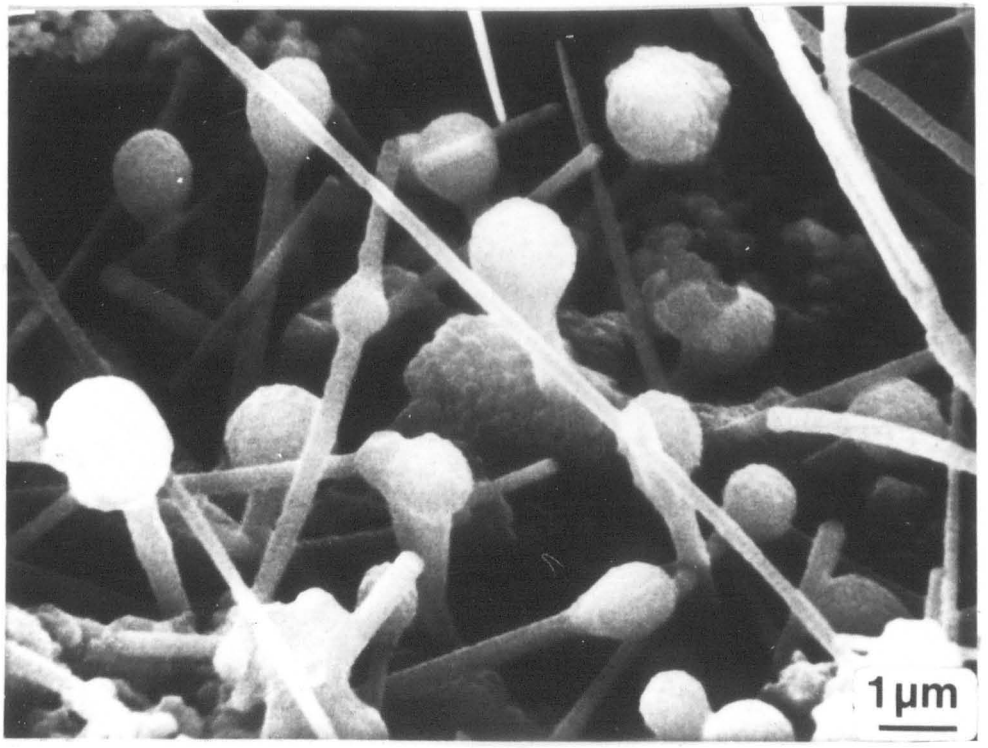

grown by the thermal decomposition of methyltrichlorosilane (CH_3SiCl_3) at 1400°C.

Figure VII.9(a) is the fracture surface of an alloy made from a 50 m/o AlN composition. It is similar to the alloy previously described except that most of the needles do not have terminal beads, indicating growth by a 'puddle' mechanism rather than by a liquid droplet. No densification occurs during fabrication and so needles can grow unimpeded into the pore network. In both these specimens (25 and 50 m/o AlN) the majority of the crystals are small equiaxed particles and it is only because, when fractured, cracks occur along the pore paths that a large number of the elongated crystals are exposed.

The AlN-rich material shown in Figure VII.9(b) appears the most homogeneous of the three and is essentially composed of equiaxed particles 1-3 μm diameter.

The post-preparative heat-treatment of the three alloys shown in Figures VII.8(a) and VII.9(a) & (b) has been discussed in section VII.4; microstructural changes in these specimens have also been observed by SEM. X-ray diffraction patterns of the SiC-rich alloy indicated that transformation to a cubic phase occurred only at >2000°C. Indeed, the SEM observations show little morphological change in the specimen until 2000°C when large crystals ∿15 μm in size are detected. These crystal are also present after heating at 2100°C, and therefore accompany the transformation 2H→3C previously observed by X-ray methods. Figure VII.10(a) shows a typical area after annealing at 2100°C; a cluster of large 3C crystals has grown and the needles have disappeared. At higher magnifications these crystals appear as cuboids or octahedra and are highly faceted, exhibiting many growth steps on their surfaces; see

Figure VII.9

Microstructures of SiC-AlN alloys

containing nominally:

(a) 50 m/o AlN

(b) 75 m/o AlN

(a)

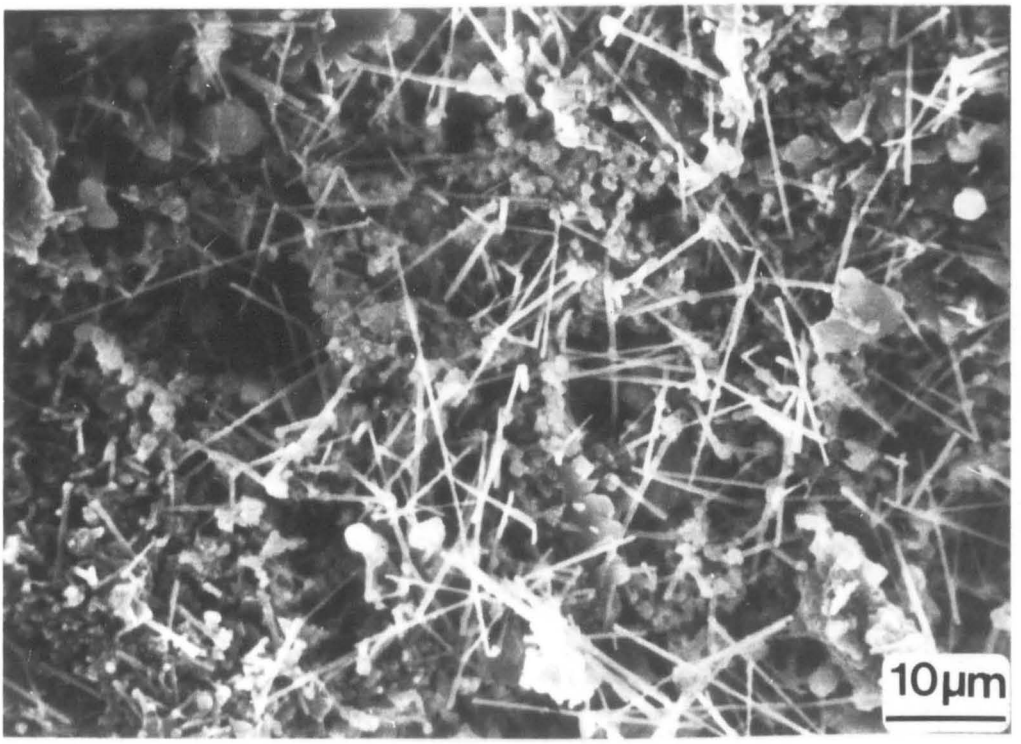

(b)

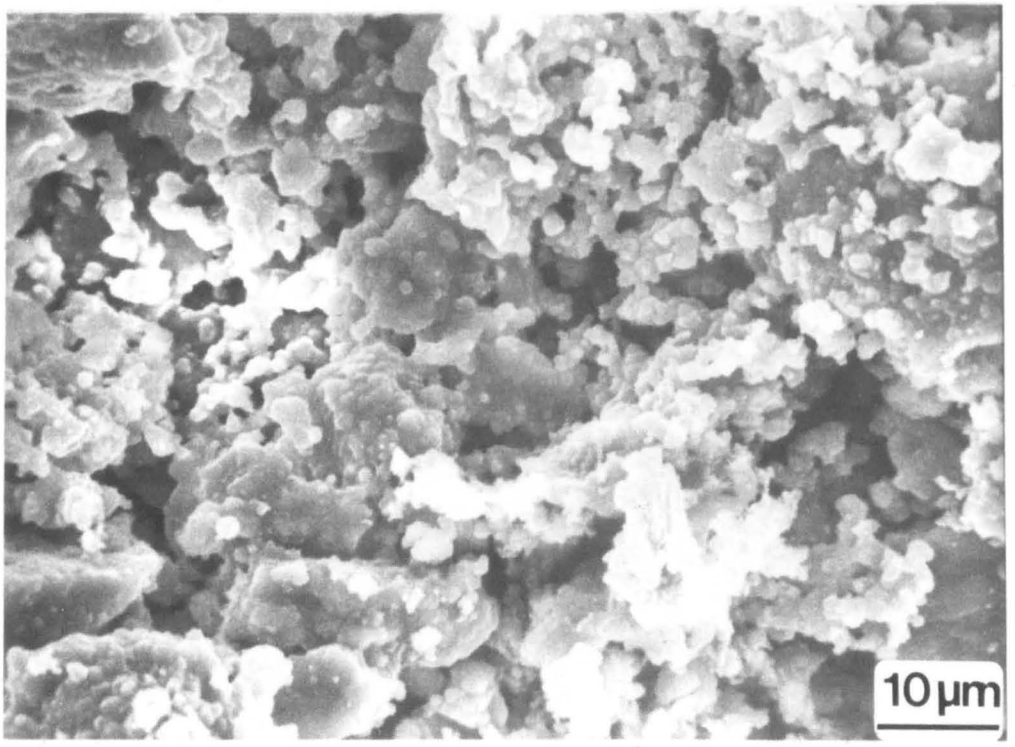

Figure VII.10

(a) Microstructure of 25 m/o AlN alloy after annealing at 2100°C for 15 minutes

(b)-(d) enlargement of 3C crystals grown by vapour deposition mechanism

(a)

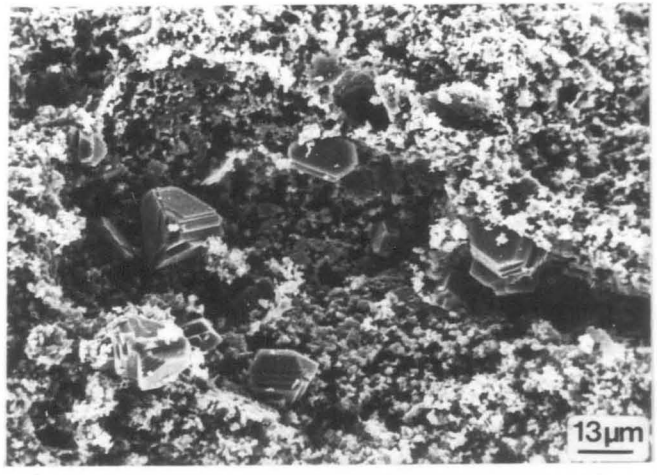

(b)

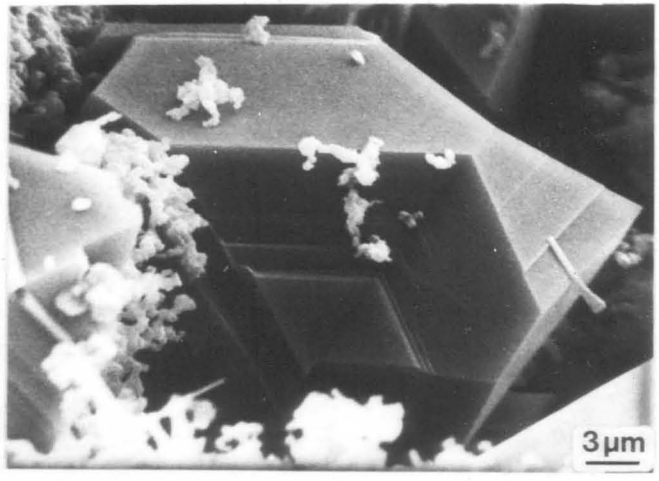

(c)

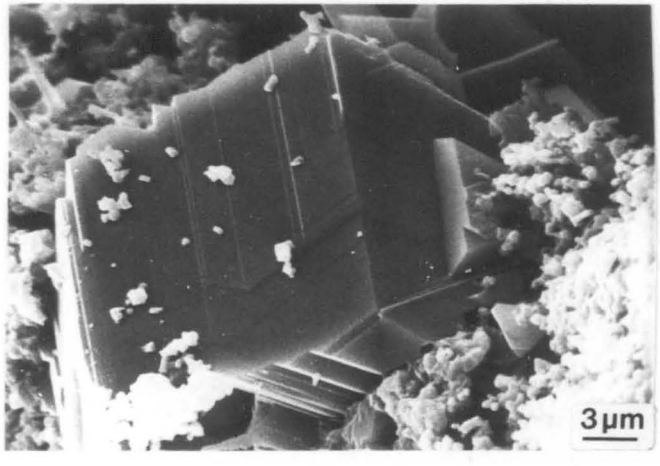

(d)

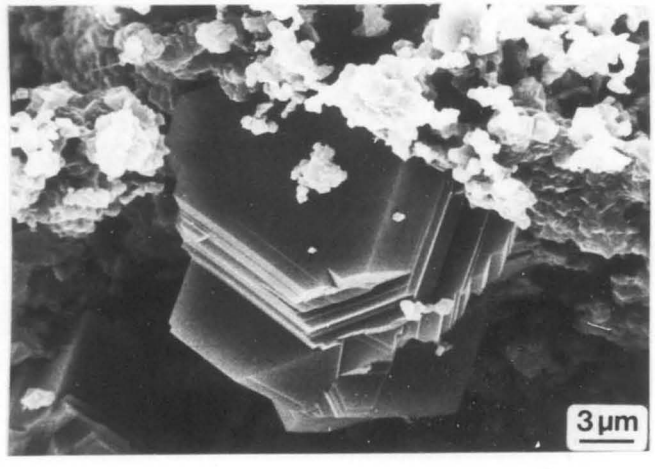

Figure VII.10(b) & (c). Their morphologies are typical of growth from the vapour phase and are similar to the 3C-SiC grown by vapour phase deposition by Knippenberg & Verspui (1973).

X-ray diffraction showed that the 50 m/o AlN alloy transformed slowly to 3C at 2100°C. SEM has confirmed that this is also accompanied by the growth of large crystals (∿15 μm) although they are by no means as numerous as in the SiC-rich alloy (see Figure VII.11). It is also noticeable that the needle-shaped crystals are fewer and shorter whereas in the previous specimen they have almost completely disppeared. It therefore seems that these crystals are not very stable and are the first to decompose during annealing.

There were no observable changes in the microstructure of the AlN-rich alloy at any stage of post-preparative heat treatment, in good agreement with the X-ray analysis.

VII.6 Chemical anlysis

The role of lime was originally envisaged as allowing the reaction between Si_3N_4, AlN and C to proceed via a liquid phase which eventually evaporated once the solid solution had crystallized, leaving the final product free of calcium. In the present work, energy dispersive analysis (EDX) has been used to test this, and also to establish the homogeneity of SiC-AlN solid solutions.

The basic crystal morphologies of several alloys have been described in section VII.5; EDX analysis has also been carried out on these specimens. The solid solutions prepared from powder mixtures containing Si and Al in the ratio 3:1 and 1:1 are composed of two types of crystals: needles up to 40 μm long and 0.6 μm wide, and equiaxed

Figure VII.11

Growth of 3C-SiC crystals in a 50 m/o AlN after annealing at 2100°C for 15 minutes

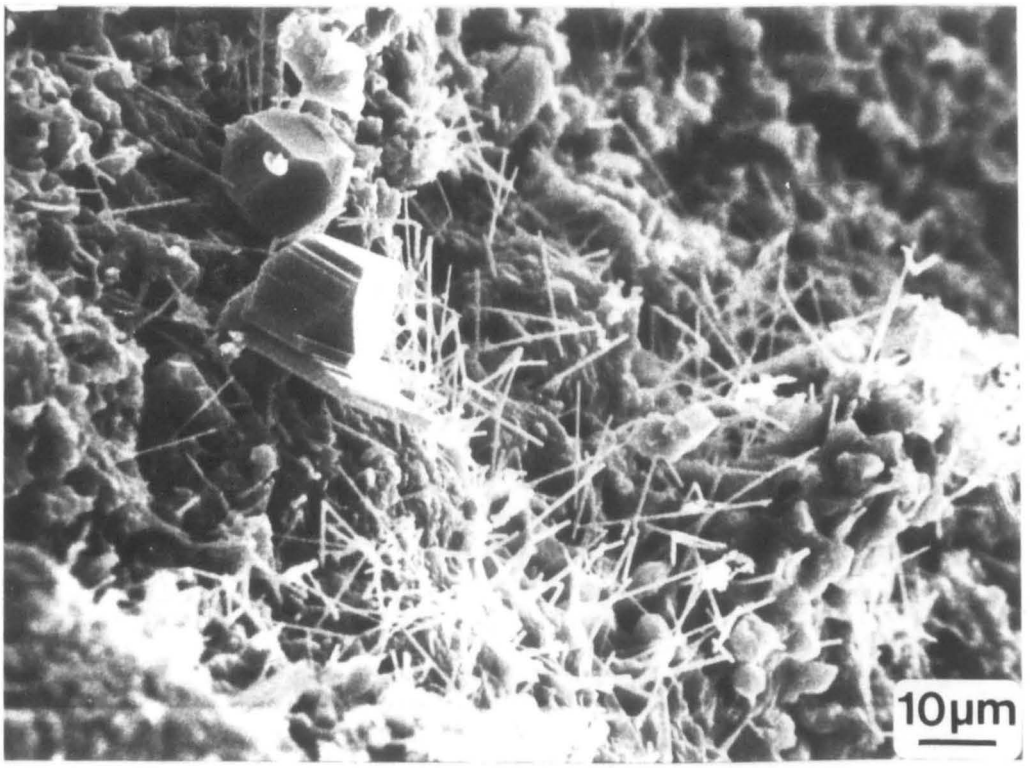
10µm

particles ∿0.4 μm in diameter. To obtain individual chemical analysis of these crystals, samples were applied to holey carbon grids which were then stuck on graphite stubs as described in section IV.9. Analyses for a specimen containing nominally 25 m/o AlN are given in Table VII.5 (Specimen X) and show that although 90% of the calcium volatilizes during the reaction the remainder is still associated with the new crystals. There is no significant difference in composition between needles and equiaxed crystals, and the individual results are in good agreement except for a few isolated exceptions.

SEM has shown that needles in this specimen have globular shaped tips similar to those in silicon nitride whiskers grown by a VLS mechanism. It is assumed that an analogous mechanism operates in SiC-AlN alloys because of the similar crystal morphologies but although a concentration of calcium was detected in the needle tips, it was not significantly different from the rest of the crystal (see Table VII.5). Since the Ca-Si-Al-O-N liquid is fluid at the reaction temperature, a concentration of calcium in the tip is not required to lower the melting point still further. The analysis also indicates that calcium can somehow be accommodated either in the growing crystal or on its surface.

X-ray analysis showed that a SiC-AlN alloy fabricated from a starting composition of 50 m/o AlN is composed of two phases of ∿38 and 80 m/o AlN. Since SEM showed two crystal morphologies (needles and equiaxed particles) EDX analysis was used to determine if the dissimilar crystal shapes were related to different compositions. Initially, an X-ray map for aluminium distribution over an area of the grid was obtained and areas of high and low concentration were distinguished. Point analysis of crystals identified in this manner

Table VII.5

Chemical analyses for SiC-AlN samples

	Al	Si	Ca	
specimen X				
initial composition	21.2	66.2	12.6	w/o
expected final composition	24.3	75.7	0	
actual final composition:				
(1) needles				
A needle	15.9	83.1	1.0	
A tip	16.2	82.6	1.6	
B needle	17.1	82.0	0.9	
B tip	16.9	82.2	0.9	
C needle	19.1	79.9	1.0	
C tip	19.0	79.0	2.0	
D needle	18.2	80.7	1.1	
D tip	18.0	81.1	0.9	
E needle	19.3	77.5	3.2	
E tip	22.8	75.8	1.4	
(2) equiaxed crystals				
average value	19.4	79.2	1.3	

Cont'd.

Table VII.5 (Cont'd.)

	Al	Si	Ca	
specimen Y				
initial composition	39.4	41.1	19.5	w/o
expected final composition	49.1	50.9	0.0	
actual final composition:				
(1) needles (average value)	34.0	58.1	7.9	
(2) equiaxed crystals (average value)				
Type 'A'	38.3	51.1	10.6	
Type 'B'	62.1	28.9	9.0	
specimen Z				
initial composition	54.3	18.8	26.9	w/o
expected final composition	74.3	25.7	0.0	
actual final composition (average value)	64.0	26.8	9.2	

Table VII.6

Chemical analysis of a SiC-AlN alloy after annealing

	Al	Si	Ca	
initial composition	Specimen X in Table VII.5			
composition after annealing at 2100°C/15 minutes:				
large crystals (average value)	6.2	93.8	0.0	w/o
equiaxed crystals (average value)	10.2	92.8	0.0	
initial composition	Specimen Y in Table VII.5			
composition after annealing at 2100°C/15 minutes:				
large crystals (average value)	9.9	90.5	0.0	
equiaxed crystals (average value)	19.2	80.6	0.2	

showed that although all the needles had compositions rich in silicon, the smaller crystals could be separated into two groups; one with a composition similar to the needles (type 'A') and the other with an aluminium-rich composition (type 'B'; see Table VII.5, Specimen Y). The compositions found by X-ray methods are in good agreement with the two phases found using EDX.

It is of interest that in the two-phase alloy, the needles have a composition rich in silicon as do the needles observed in the SiC-rich alloy (specimen X). In contrast, the AlN-rich alloy has crystals of only one morphology, the composition of which is in reasonable agreement with the expected final composition although 9 w/o of the calcium remains in the specimen after firing (specimen Z).

When alloys X and Y (see Table VII.5) containing nominally 25 and 50 m/o AlN were annealed at 2100°C, transformation to a cubic structure occurred (see section VII.4) and large crystals were observed in the specimens by SEM (see section VII.5). X-ray diffraction indicated that AlN had a solubility of between 10 and 20 m/o in the cubic phase (see section VI.2) and this has been substantially confirmed by EDX analysis (see Table VII.6).

VII.7 Conclusions

Silicon carbide can be alloyed with aluminium nitride to stabilize the 2H modification but along the SiC-AlN join a two-phase immiscibility gap occurs between ∿38 and 84 m/o AlN at 1800°C, and this does not significantly contract at higher temperatures. The 2H→3C transformation occurs at 2100°C in silicon carbide-rich alloys and the 3C formed can accommodate up to 20 m/o AlN. A Ca-Si-Al-O-N liquid is necessary for

solid solution formation and not all the Ca is volatilized in the final stages of the reaction. The microstructure of SiC-AlN alloys is homogenised by post-preparative heat-treatment below the 2H→3C transformation temperature.

VIII HIGH RESOLUTION ELECTRON MICROSCOPY OF SILICON CARBIDE ALLOYS

VIII.1 Introduction

Transmission electron microscopy is an invaluable tool in the study of materials and one of the most exciting recent developments is the use of lattice imaging techniques as a means of studying the structure of crystals directly.

The conditions for obtaining lattice images are very stringent, i.e. thin specimens are required and to minimize the effect of spherical aberration the microscope must be operated slightly out of focus. This condition is called the Scherzer focus (Δf_s), as given by the following equation:

$$\Delta f_s = 2.5\left(\frac{C_s\lambda}{2\pi}\right)^{\frac{1}{2}} \qquad \ldots\text{VIII.1}$$

where C_s is the coefficient of spherical aberration

and λ is the wavelength of the electron beam.

The seven basic steps involved in obtaining and recording a lattice image are summarized in Figure VIII.1. Initially a suitable crystal is oriented such that the electron beam is parallel to a principal crystallographic direction in the crystal and the electron diffraction pattern is symmetrically aligned. To obtain a lattice image with a resolution of $\sim$5 Å at 100 kV, which can be interpreted in terms of the projected charge density of the object, the specimen must be no thicker than $\sim$50 Å.

If necessary, the illumination is then tilted so that the transmitted beam and diffracted beams are equidistant from the optical axis. The optimum objective aperture size is chosen to transmit only the

Figure VIII.1

Lattice imaging procedures

LATTICE IMAGING

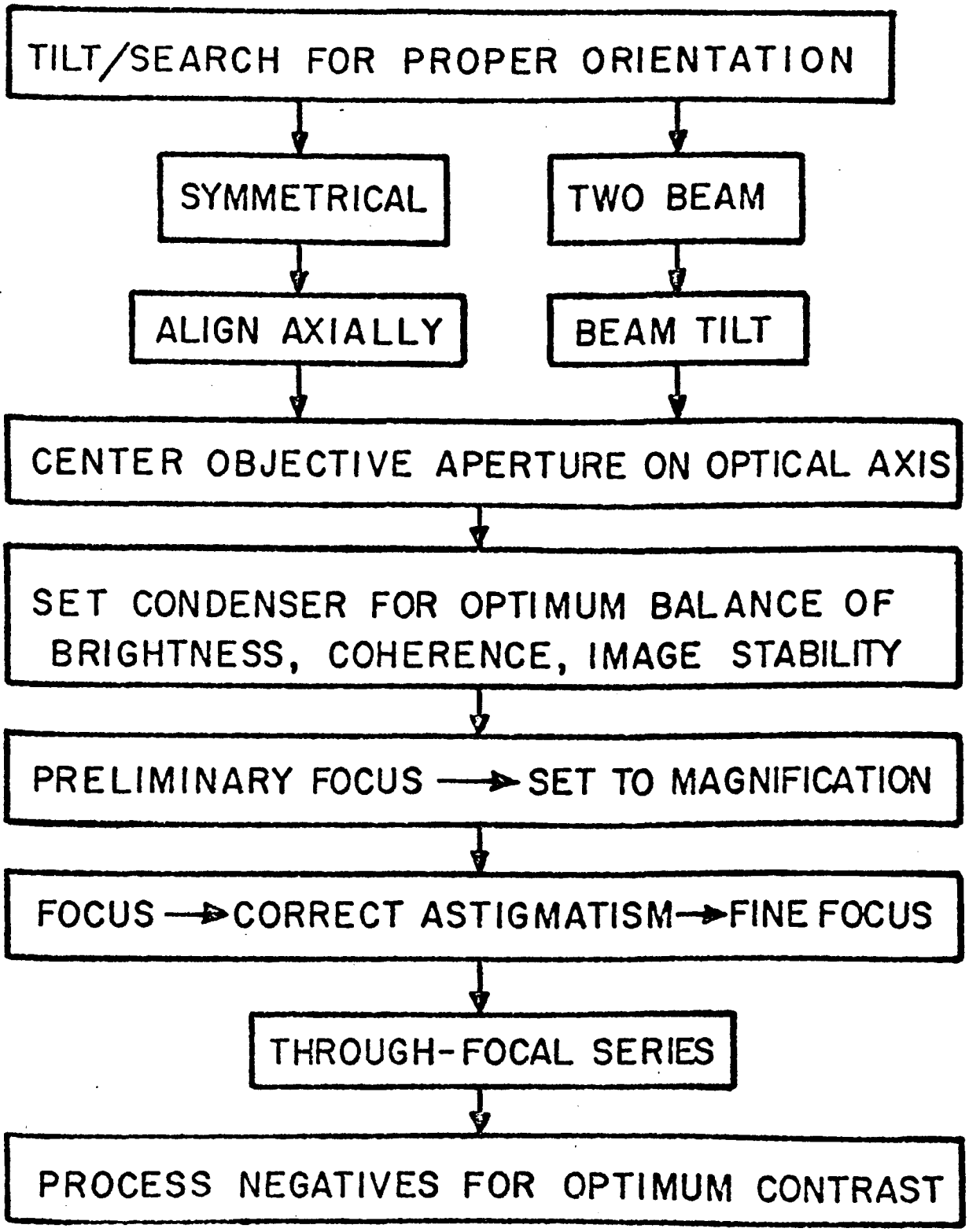

diffracted beams corresponding to the image resolution required, since 'higher' order reflexions only add to the background and reduce the overall contrast of the image. In the image mode, after the magnification is increased and the approximate focus is found, the astigmatism is corrected on the area to be imaged. Finally, a through focal series of images is recorded and the negatives are processed for optimum contrast. In general, the recorded image cannot be intuitively interpreted in terms of the crystal structure because of the effects of microscope aberrations. This has resulted in the development of computational methods to simulate the observed image and hence provide additional confirmation of structural features.

VIII.2 Calculated images

VIII.2.1 Introduction

Although modern high resolution electron microscopes have the capability of ∿1.5 Å line resolution and ∿3 Å point-to-point resolution, it is only by the careful choice of imaging conditions that it is possible to image directly the crystal lattice. Considerable effort has been devoted to establishing the conditions under which observed lattice images can be satisfactorily and readily interpreted in terms of the real lattice.

Various computer programs have been written which use the n-beam dynamical methods developed by Cowley & Moodie (1957a-d) to calculate the contrast expected for a particular crystal structure for various values of thickness, defocus, objective aperture size and spherical aberration coefficient. The computation involves multi-slice approximations (Grinton & Cowley, 1971) to obtain the amplitudes and

phases of a large number of diffracted beams as a function of the crystal thickness. In the present case, computed images were matched with observed images in order to confirm the validity of image interpretation. The programs used were written by Skarnulis (1976).

Initially, program FCOEFF gave Fourier coefficients for 2H-SiC projected down the [100] direction and subsequently program DEFECT calculated the lattice images at different crystal thicknesses and values of defocus. A full description of the programs and underlying principles can be found in Skarnulis (1976).

FCOEFF generates all the atomic coordinates from a specified set of symmetry operators and the original atomic coordinates. Reflexions are then tested against the stipulated zone using the zone law, before structure factors are calculated for allowed hkl's. New $\underline{x}$ and $\underline{y}$ axes are chosen such that the shortest vector becomes $\underline{x}$, and $\underline{y}$ is either the other one-dimensional vector or the vector which most closely makes an angle of 90° with the new $\underline{x}$ axis. Finally, the three-dimensional indices are converted to two-dimensional indices, which are then outputted along with the Fourier coefficients, intensities of reflexions and the plane angle of projection (the angle between the new $\underline{x}$ and $\underline{y}$ axes).

The input data required for program DEFECT, apart from the Fourier coefficients, new $\underline{x}$ and $\underline{y}$ axes and the plane angle of projection, are the number of beams to be used in the image calculation (in the present case 50), the slice thickness (3 Å), and the number of slices in the crystal (thickness, Å/3 Å). The experimental parameters which must also be specified include the accelerating voltage (100 kV), the spherical constant (0.70 mm), depth of focus (170 Å), aperture radius (0.550 $Å^{-1}$) and contrast scaling factor (0.65-0.75). The multislice calculation to

obtain images differing by 200 Å was carried out using tilted illumination, the axis of which was 0.00, 0.60, for several crystal thicknesses. The calculated images were printed using a 6-line overprint routine and a 32-point greyness scale.

VIII.2.2 Comparison of observed and calculated images

Computed images were calculated to ascertain if the image interpretation of chevron-type fringes in 2H-SiC corresponded to the ABAB... stacking sequence in the real lattice, and also to determine the maximum thickness and optimum defocus at which such fringes could be observed. A series of images at defocuses ranging from +80 to -140 nm, at crystal thickness of 2.1 to 7.7 nm, were computed. These calculations showed that chevron-type fringes in 2H-SiC could be obtained in the narrow range of focus +40 to +20 nm and -20 to -40 nm for specimens ∿2 nm thick, but when the specimen thickness was increased to ∿4.5 nm a zig-zag pattern of fringes was observed only at +30 and -30 nm. For specimens thicker than 4.5 nm, chevron-type fringes were unobtainable in 2H-SiC. For longer period polytypes e.g. 4H and 6H, it is possible to use thicker specimens because the zig-zag sequence is enlarged by a factor of 2 and 3 respectively. Chevron-type fringes are unobtainable in 3C because the stacking operation involves no rotation of the tetrahedra and therefore only parallel lines of spacing 0.25 nm are observed.

Figure VIII.2(a)-(d) shows a series of micrographs matched successfully with computed images. The first image (a) is matched with the image calculated for a specimen 2.1 nm (i.e. 7 slices) thick and an overfocus of +20 nm. The next image is from a specimen 3.0 nm thick and overfocus +10 nm. It is apparent, that as the specimen thickness increases

Figure VIII.2

Observed lattice images of 2H-SiC

matched with calculated images:

	thickness	focus
(a)	2.1 nm	+20 nm
(b)	3.0 nm	+10 nm
(c)	7.5 nm	-20 nm
(d)	7.5 nm	0.0 nm

(a)

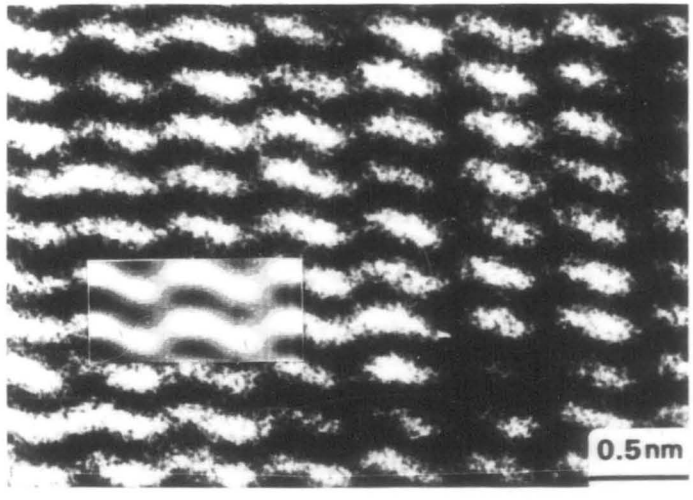

(b)

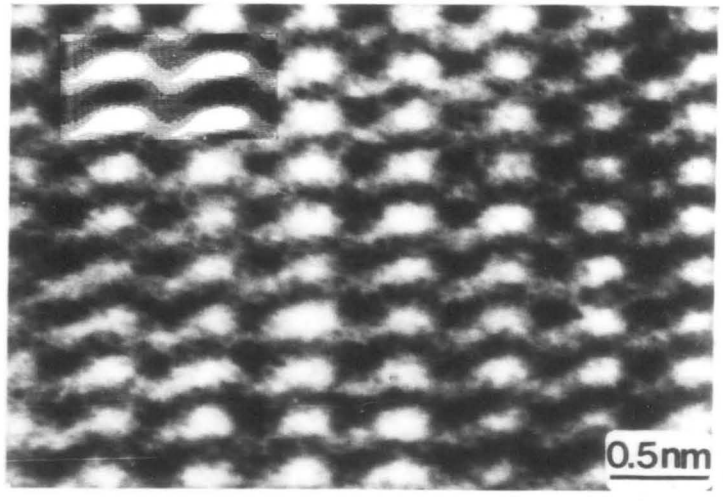

(c)

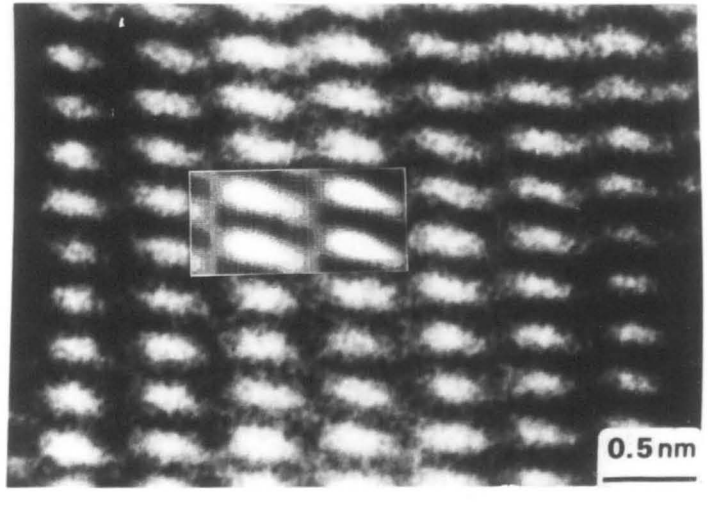

(d)

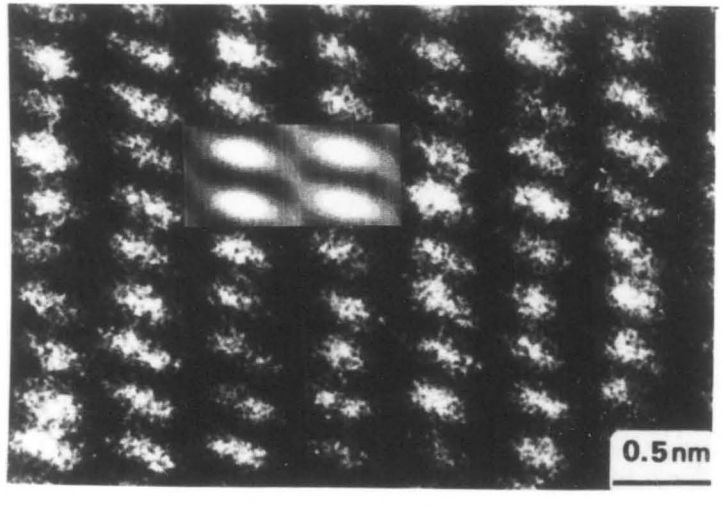

(a)-(d), the zig-zag pattern of the $(10\bar{1}1)$ and $(10\bar{1}\bar{1})$ planes in 2H becomes less obvious, as shown in Figures VIII.2(c) and (d) where observed images are matched with calculated images for a crystal thickness of 75 Å and two defocus conditions; -200 Å (c) and 0.0 Å (d).

Computed images for 2H-SiC, as expected, agreed equally well with images obtained from SiC-AlN alloys, because of the small differences in scattering factors (and hence Fourier coefficients) for the (Si,Al) and (C,N) atoms. Excellent agreement between observed and calculated lattice images both for SiC and SiC-AlN alloys, justifies the direct interpretation of chevron-type fringes in terms of the stacking sequence of tetrahedra and therefore enables detailed structural variations to be deduced.

VIII.3 2H and 3C silicon carbide

VIII.3.1 2H single crystals

Pure 2H-SiC single crystals were examined by high resolution electron microscopy (HREM), so that a comparison could be made with 2H-SiC-AlN alloys and other 2H structures prepared during the course of this work. The 2H crystals were grown in the usual way by the thermal decomposition of methyltrichlorosilane (CH_3SiCl_3) at 1400°C and were kindly provided by Dr J.A. Powell, Lewis Research Centre, N.A.S.A., Cleveland, Ohio, U.S.A.

When examined under reflected light, using a Vickers optical microscope, the crystals were 0.5-1.5 mm long x 0.5 mm wide with faults visible in most crystals.

To observe changes in the ABAB... stacking sequence, it is necessary

to obtain diffraction patterns containing c*; a suitable orientation is $[10\bar{1}0]$. Diffraction patterns from suitably aligned fragments showed varying degrees of faulting within each. The inset diffraction patterns in the micrographs shown in Figure VIII.3(a),(b) & (c) were taken using a $[10\bar{1}0]$ beam direction and hence contain both the a* and c* reciprocal lattice directions. In addition to strong spots corresponding to a 2H unit cell, small amounts of streaking in (b) and (c), parallel to the $[0001]$ direction, reflect the degree of faulting in the basal planes. Only a few $[10\bar{1}0]$ zone diffraction patterns from perfect 2H fragments were observed and usually some degree of faulting occurred in each fragment.

One-dimensional lattice images taken, using the 0001, $000\bar{1}$ and the undiffracted beam, show irregularities in the stacking sequence in good correlation with the degree of streaking in the diffraction pattern, as shown in increasing amounts in Figures VIII.3(a),(b) & (c). The distance between fringes corresponds to the unit cell c dimension, i.e. 0.50 nm. Faults are clearly revealed by changes in contrast and correspond to a disruption in the ABAB... continuous sequence by the occasional insertion of a C layer, giving local regions of cubic stacking. From these images it is clear that the 2H polytype of SiC has a strong tendency to fault during growth.

VIII.3.2 3C from silicon-carbon mixtures

The preparation of 3C-SiC from silica and carbon in argon, i.e. nitrogen free atmospheres, is described in Chapter VI.3. X-ray analysis indicated that the specimens also contained some α-SiC (probably disordered

Figure VIII.3

(0001) lattice fringes from

a single crystal of 2H-SiC

revealing varying degrees of faulting

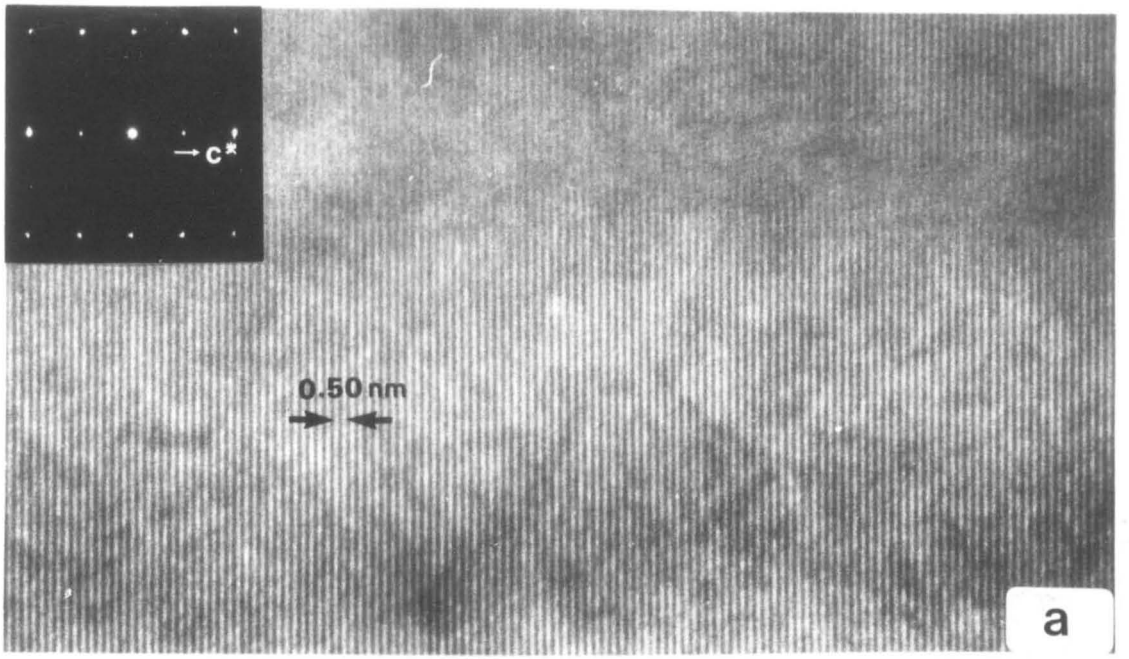
c*
0.50 nm
a

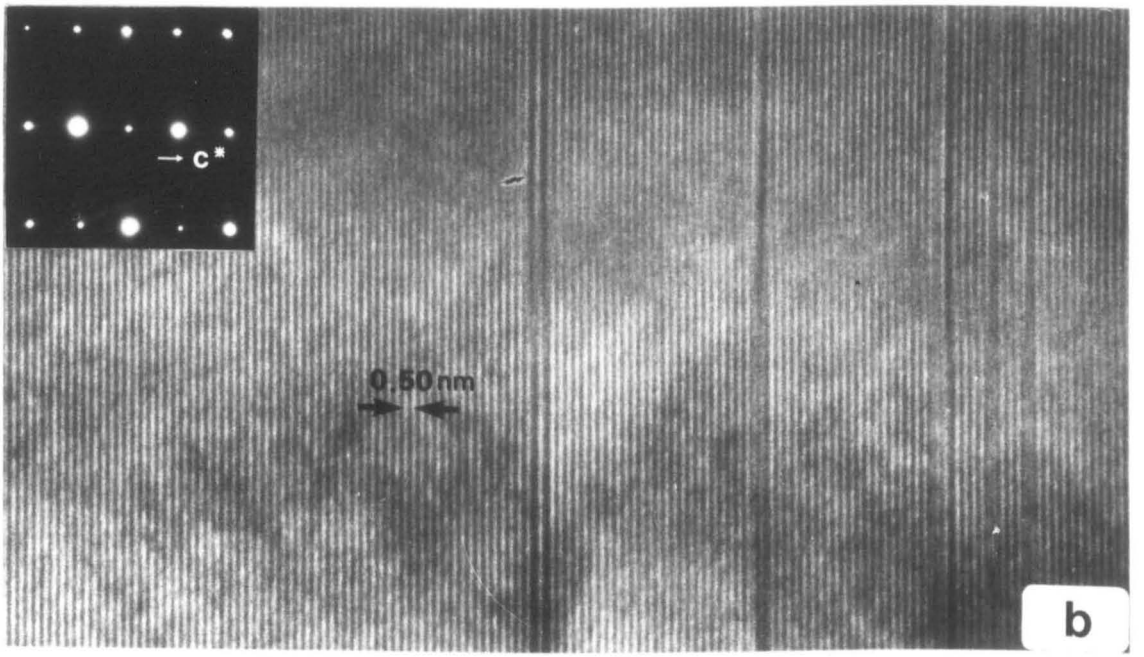
c*
0.50 nm
b

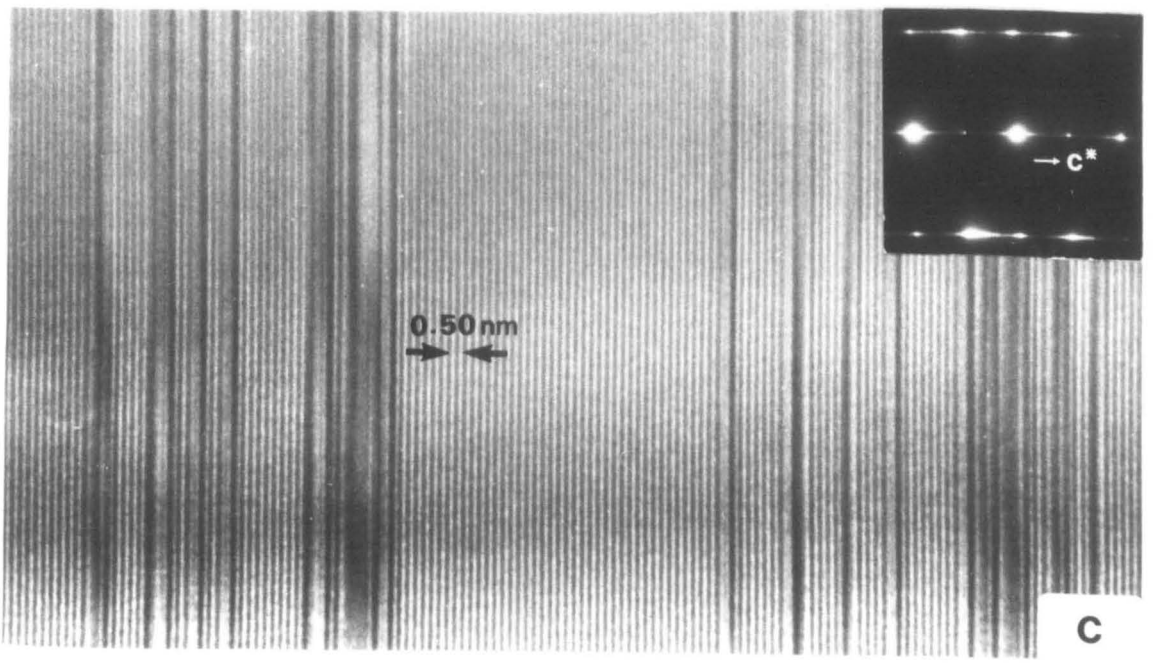
c*
0.50 nm
c

or 2H). With transmission electron microscopy, the specimen consisted mainly of agglomerates of small equiaxed crystals, 45 nm in size as shown in Figure VIII.4(a) which were usually faulted; see Figure VIII.4(b). Electron diffraction data were limited to ring patterns from which it was not possible to establish conclusively whether they were 2H or 3C. Since this crystal morphology comprised ~80% of the specimen, it is probable that they are cubic. The remainder of the specimens were thin needles, 60-100 nm wide and up to 10 times as long; see Figure VIII.5(a). $[10\bar{1}0]$ zone diffraction patterns show extremely heavy streaking parallel to the [0001] direction, due to the high concentration of stacking faults perpendicular to the long axis of the needle; see Figure VIII.5(c) & (d). The degree of faulting varies between crystals and, in some cases, there is increased diffracted intensity at points corresponding to 2H reflexions (see Figure VIII.5(c)), whilst other diffraction patterns are from essentially disordered α-SiC material, as shown in Figure VIII.5(d). The density of faults within the needles is sufficiently high that, in one dimensional lattice images, perfect regions extend only to lengths of 2.5 nm along the c-axis; see Figure VIII.5(b).

VIII.3.3 2H and 3C from silicon nitride-carbon mixtures

HREM of SiC produced by the reaction of silicon nitride and carbon at 1800°C, and which by X-ray diffraction consisted of approximately equal amounts of the 2H and 3C, showed only equiaxed crystals 0.25-1.0 μm in diameter. Some crystals were mainly 2H, although heavily faulted (see Figure VIII.6(a)), whereas others contained both 2H and 3C polytypes (Figure VIII.6(b) & (c)) and some consisted of 3C heavily faulted on the {111} planes. For example, one cubic crystal was faulted in such a

Figure VIII.4

Faulted equiaxed 3C-SiC crystals

prepared from SiO_2-C mixtures

at 1650°C

(a)

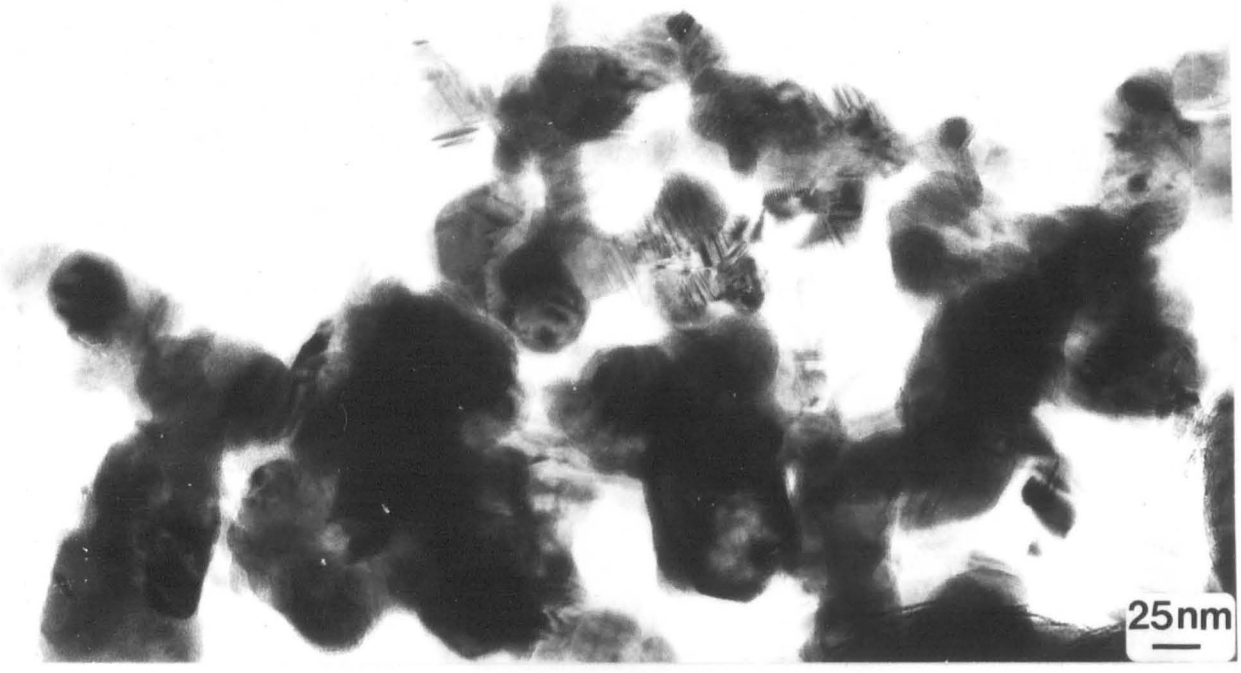

(b)

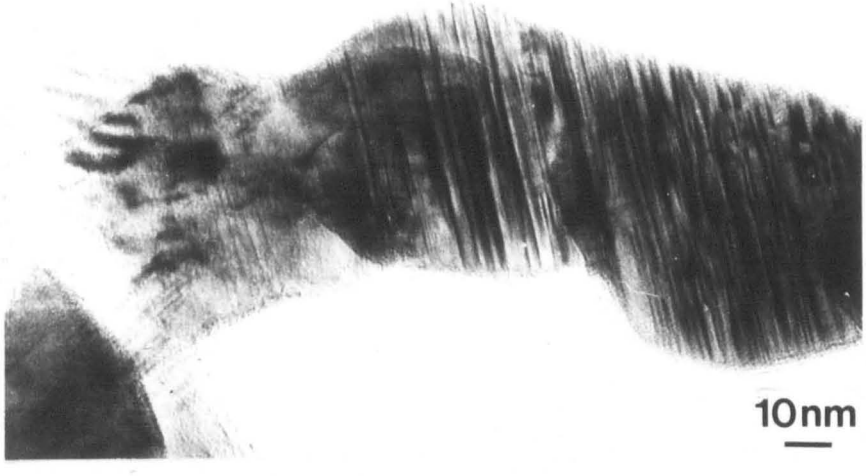

Figure VIII.5

(a)-(b) Heavily faulted needles found in SiC prepared from SiO_2-C mixtures at 1650°C

(c)-(d) $[10\bar{1}0]$ zone electron diffraction patterns from needles showing heavy streaking parallel to c*

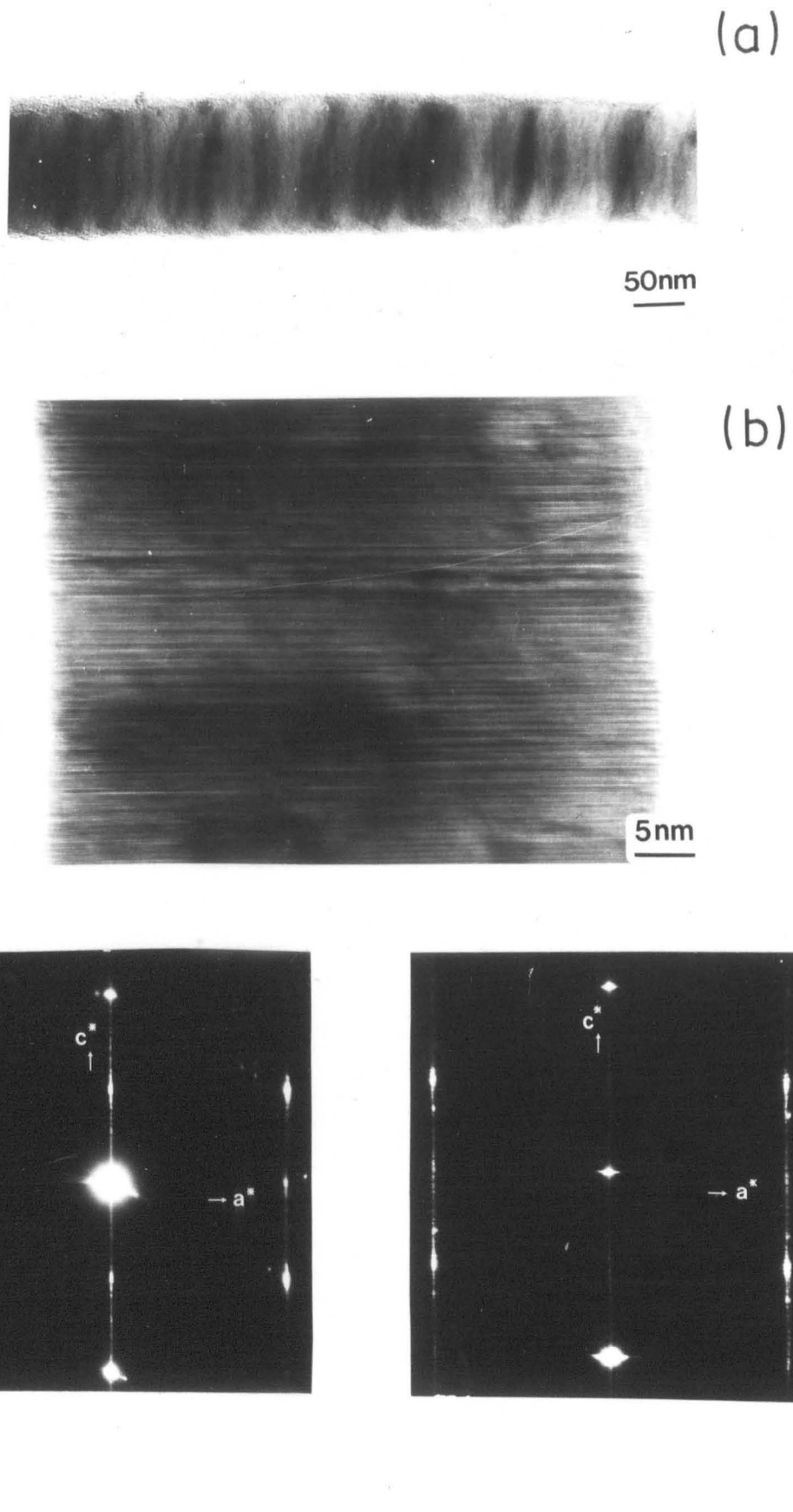
(a)
50nm
(b)
5nm
(c)
c*
a*
(d)
c*
a*

Figure VIII.6

(a) - (d) $[1\bar{1}0]_{2H}$// $[1\bar{1}0]_{3C}$ zone

electron diffraction patterns

showing varying amounts of

2H and 3C found in crystals

from a specimen prepared

by the reaction of Si_3N_4 + C at 1800°C

(a)

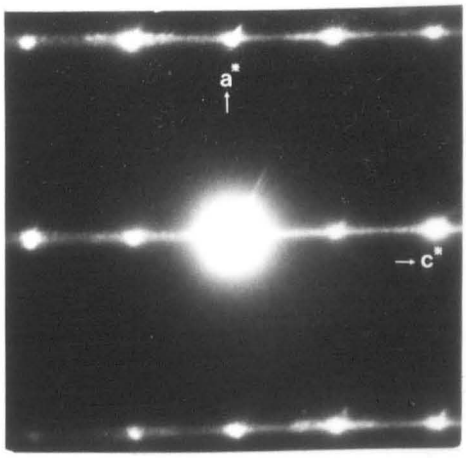
a*
c*

(b)

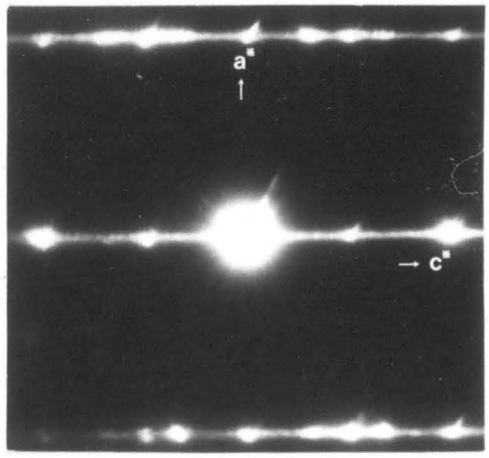
a*
c*

(c)

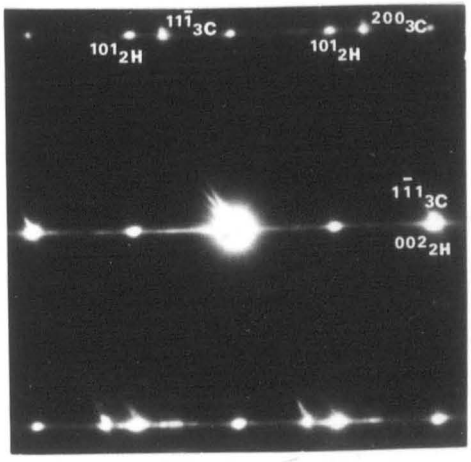
$10\bar{1}_{2H}$
$11\bar{1}_{3C}$
$10\bar{1}_{2H}$
200_{3C}
$1\bar{1}\bar{1}_{3C}$
002_{2H}

(d)

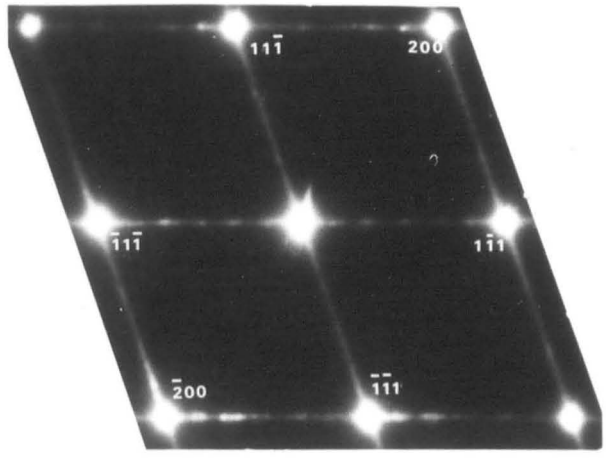
$11\bar{1}$
200
$\bar{1}1\bar{1}$
$1\bar{1}1$
$\bar{2}00$
$\bar{1}\bar{1}1$

way that weak spots corresponding to 6H were present; Figure VIII.6(d). This regular faulting can also be considered as a series of 3C micro-twins, since the stacking sequence of 6H, ABCACB..., is that of 3C, twinned after every unit cell. Lattice images from several crystals showed regions of perfect 2H, 5-10 nm wide, further areas 7-20 nm wide, of unfaulted 3C, and randomly faulted regions, sometimes extending to 15 nm in width. Two such areas are shown in the micrographs of Figure VIII.7(a) & (b) where the regions of 2H and 3C are indicated. The two competing factors, namely the transformation to 3C at temperatures >1600°C and the stabilizing of 2H by nitrogen, result in coalesced regions of 2H and 3C and the amount of each is probably dependent on local fluctuations in nitrogen concentration.

VIII.4 Silicon carbide-aluminium nitride alloys

VIII.4.1 Silicon carbide-rich alloys

Scanning electron microscopy shows that a SiC-AlN alloy, nominally containing 25 a/o AlN, is mainly composed of small equiaxed crystals, 0.4 μm in diameter, but also contains needles, most of which have globular tips (see section VII.5). However the X-ray diffraction pattern shows single phase material, although the reflexions were reasonably diffuse, indicating a small particle size and/or faulting within the crystals.

Selected area $[10\bar{1}0]$ zone diffraction patterns from suitably oriented needles revealed that the growth axis was parallel to [0001] and in addition, continuous streaking occurred perpendicular to the (0001) planes, as shown in Figure VIII.8(a). Superimposed on the streaking, intensity maxima, corresponding to the 2H polytype, were usually observed

Figure VIII.7

Lattice fringes showing isolated regions of 2H and 3C stacking

zone axis $[10\bar{1}0]_{2H} \;//\; [1\bar{1}0]_{3C}$

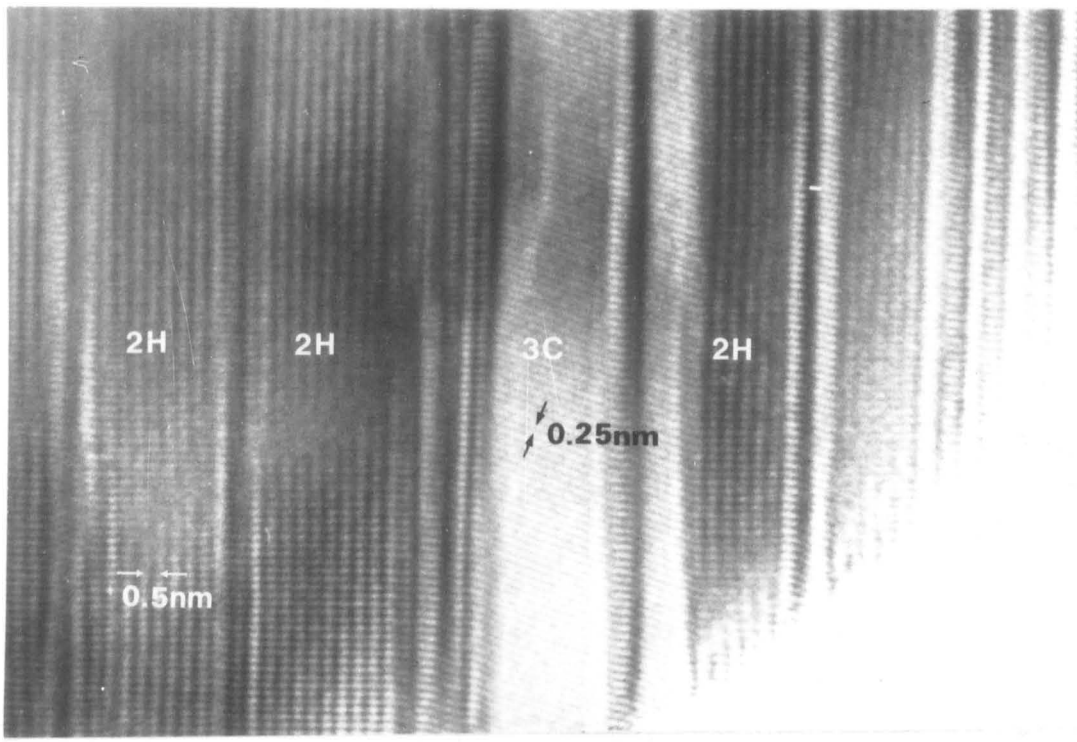

(a)

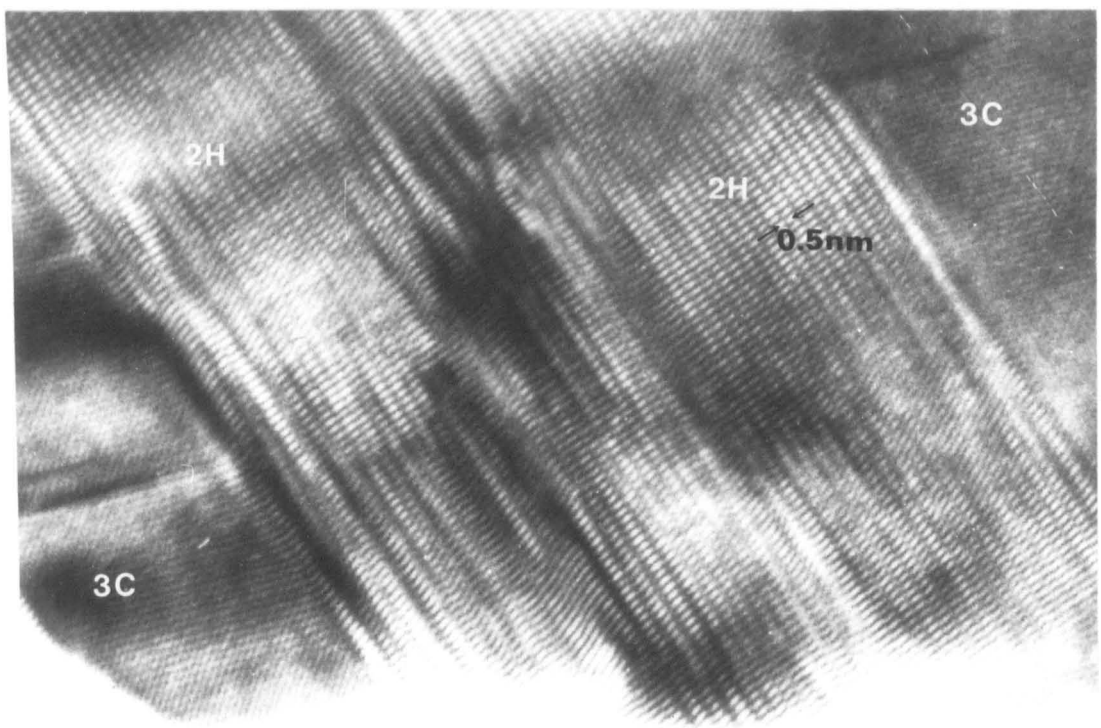

(b)

Figure VIII.8

$[10\bar{1}0]$ zone selected area electron diffraction patterns showing (a) a 2H structure and (b)-(d) progressive amounts of disorder

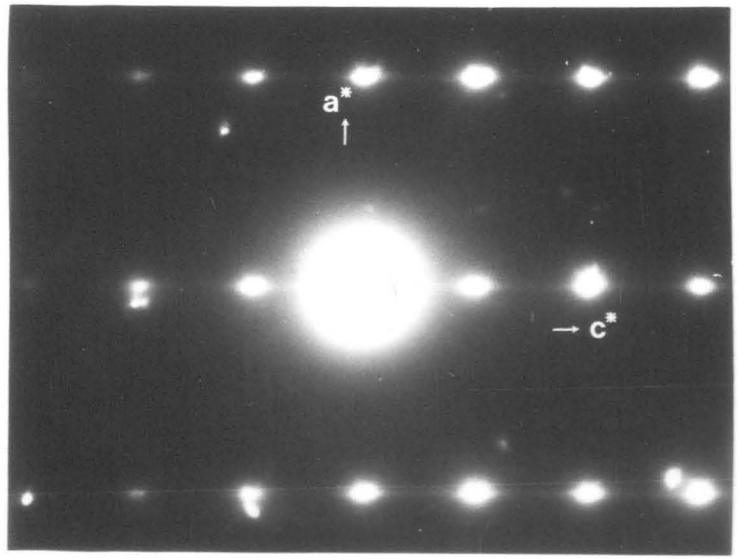

(a)

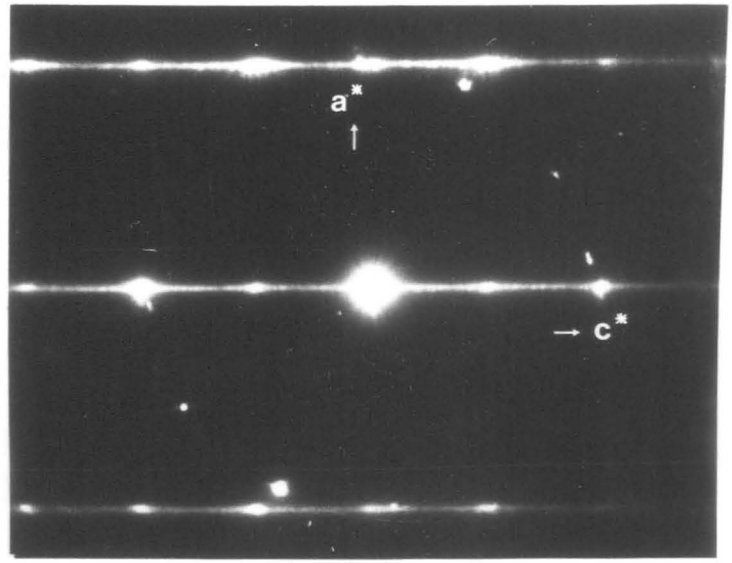

(b)

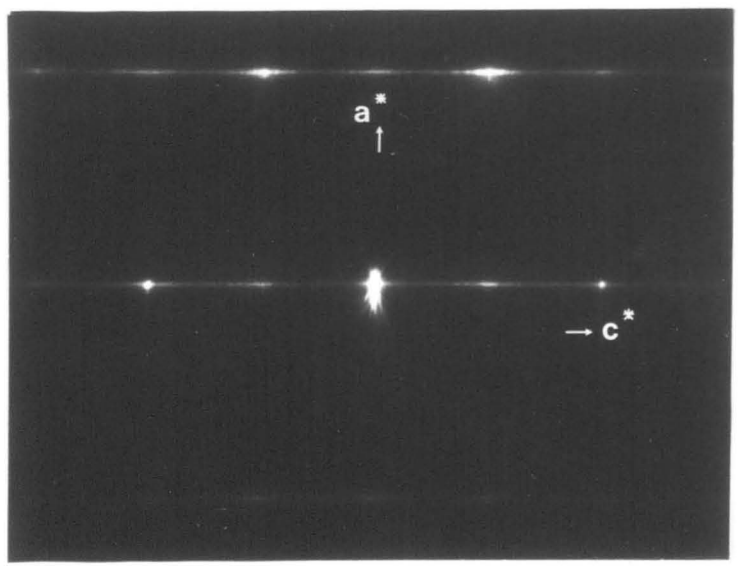

(c)

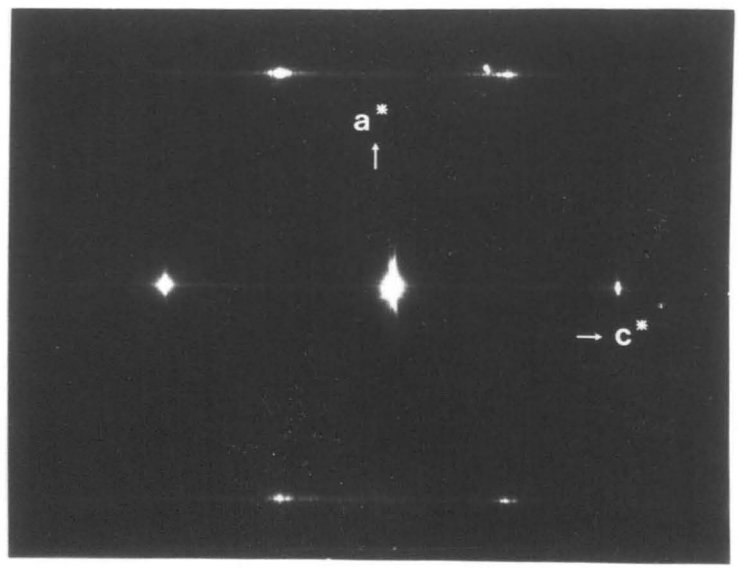

(d)

for all needles examined, although the degree of random faulting varied between crystals. Figure VIII.8(a)-(d) shows a selection of typical diffraction patterns from the needle-like crystals, where the various degrees of faulting in the (0001) planes are apparent.

Although SEM shows that each needle has a globular termination characteristic of VLS growth, this was observed by TEM in only a few crystals because specimen preparation necessitated crushing and most of the fragile tips were broken off. Of the intact crystals, the tips were polycrystalline and the ring diffraction pattern showed the presence of some 3C polytype; a bright-field micrograph of a typical tip is shown in Figure VIII.9(b). Figure VIII.9(a) shows the growing point of a needle where the tip has been broken off, revealing unevenly tapered sides. This morphology is presumably a consequence of the gradual precipitation of solid from the liquid droplet (which surrounds the terminal part of the crystal) as more vapour condenses. It is also noteworthy that spotty defects, which are visible along the length of the crystal, appear to originate at its growing surface. These defects are always present and are distributed centrally about the long axis of the crystal, as shown clearly in Figure VIII.10; note also their heavily faulted nature. One-dimensional lattice fringes from this crystal, taken by centering the optical aperture between the undiffracted beam and the (0001) reflexion show thin lamellae of perfect 2H (arrowed), about 5 nm wide, with the remainder of the needle randomly faulted; the diffraction pattern contains no spots from any other polytype (see Figure VIII.11).

In diffraction studies of SiC crystals, prepared in several ways, (Verma & Krisna, 1966; Shinozaki & Kinsman, 1978; Sato & Shinozaki, 1975)

Figure VIII.9

Bright field electron micrographs showing the growing tip of a needle (a) and a needle with globular tip intact (b)

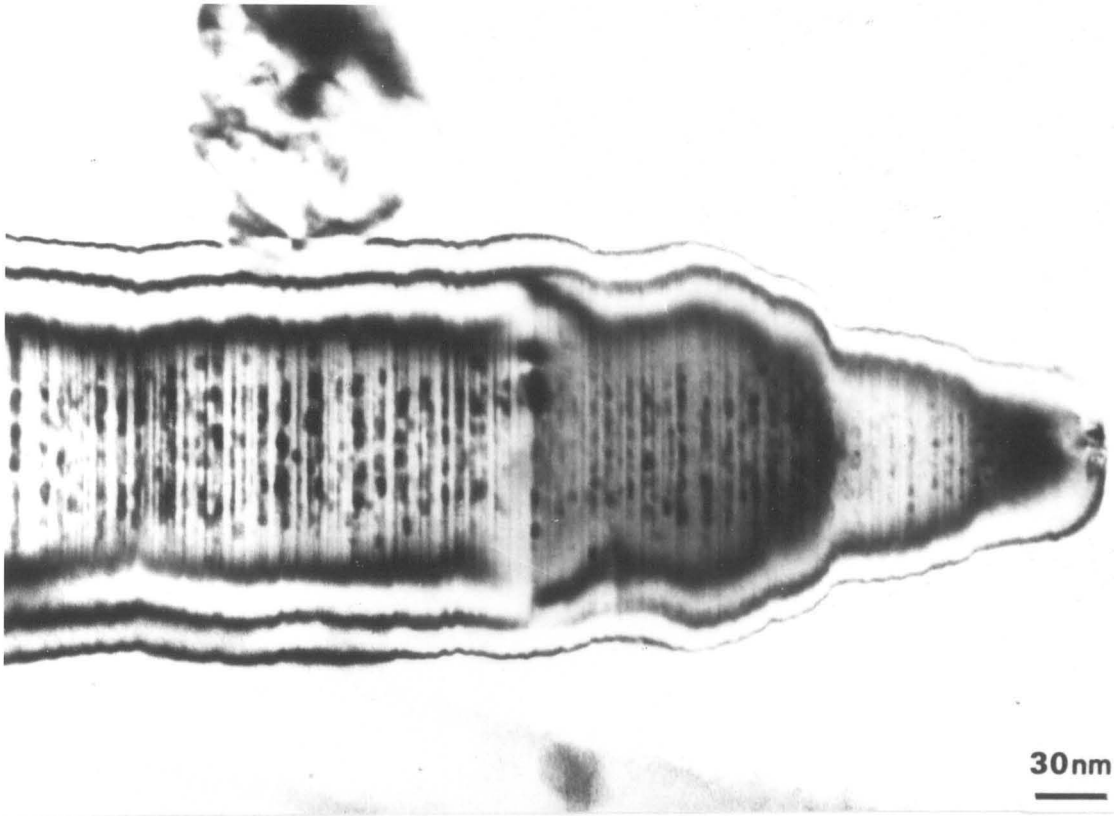

(a)

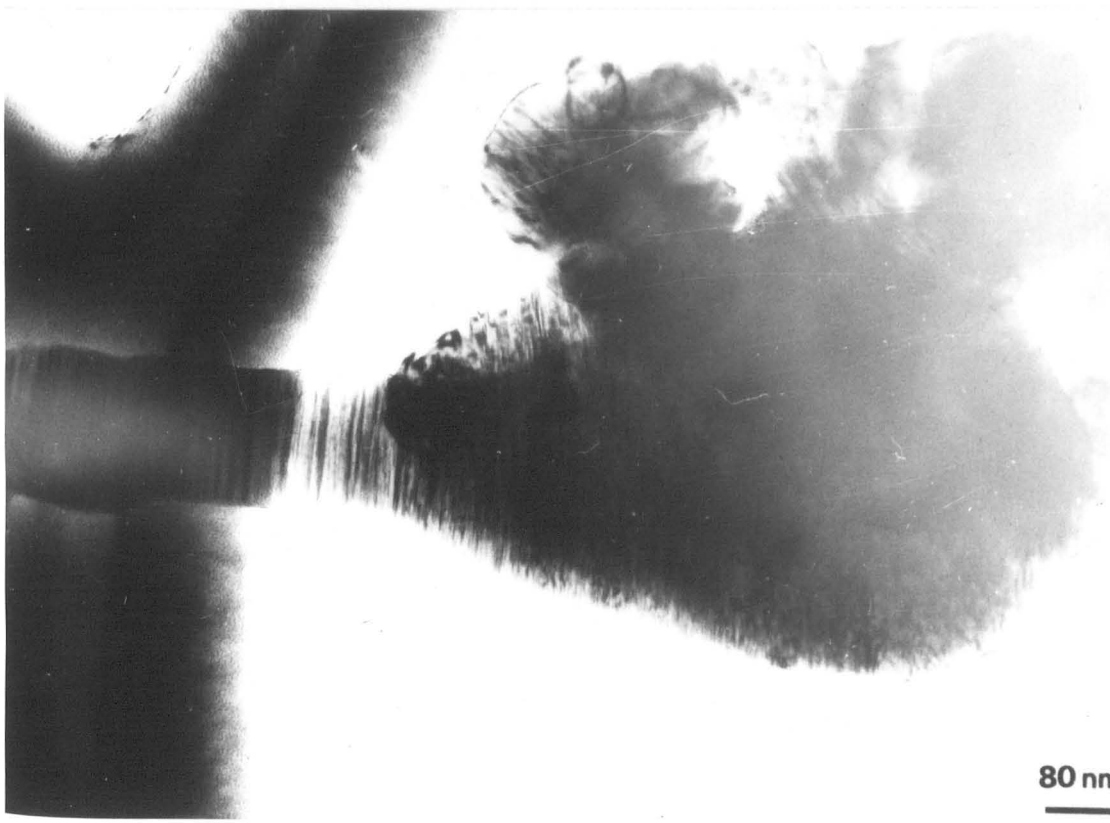

(b)

Figure VIII.10

Dark field electron micrograph of a needle revealing faults on (0001) planes and spotty defects distributed centrally about the long axis

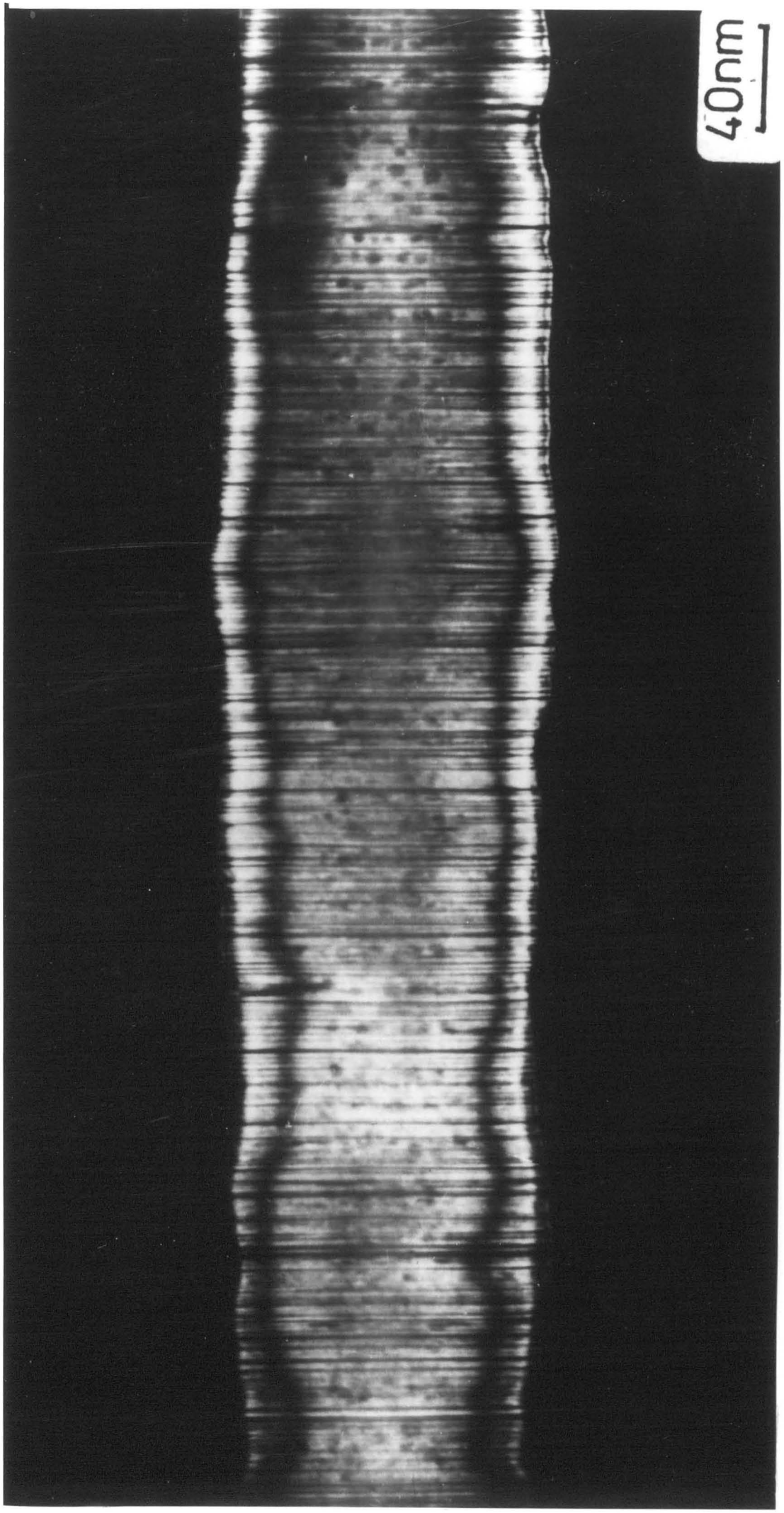
40nm

Figure VIII.11

Lattice fringes from a heavily faulted needle

showing small areas of 2H (arrowed)

zone axis [$10\bar{1}0$]

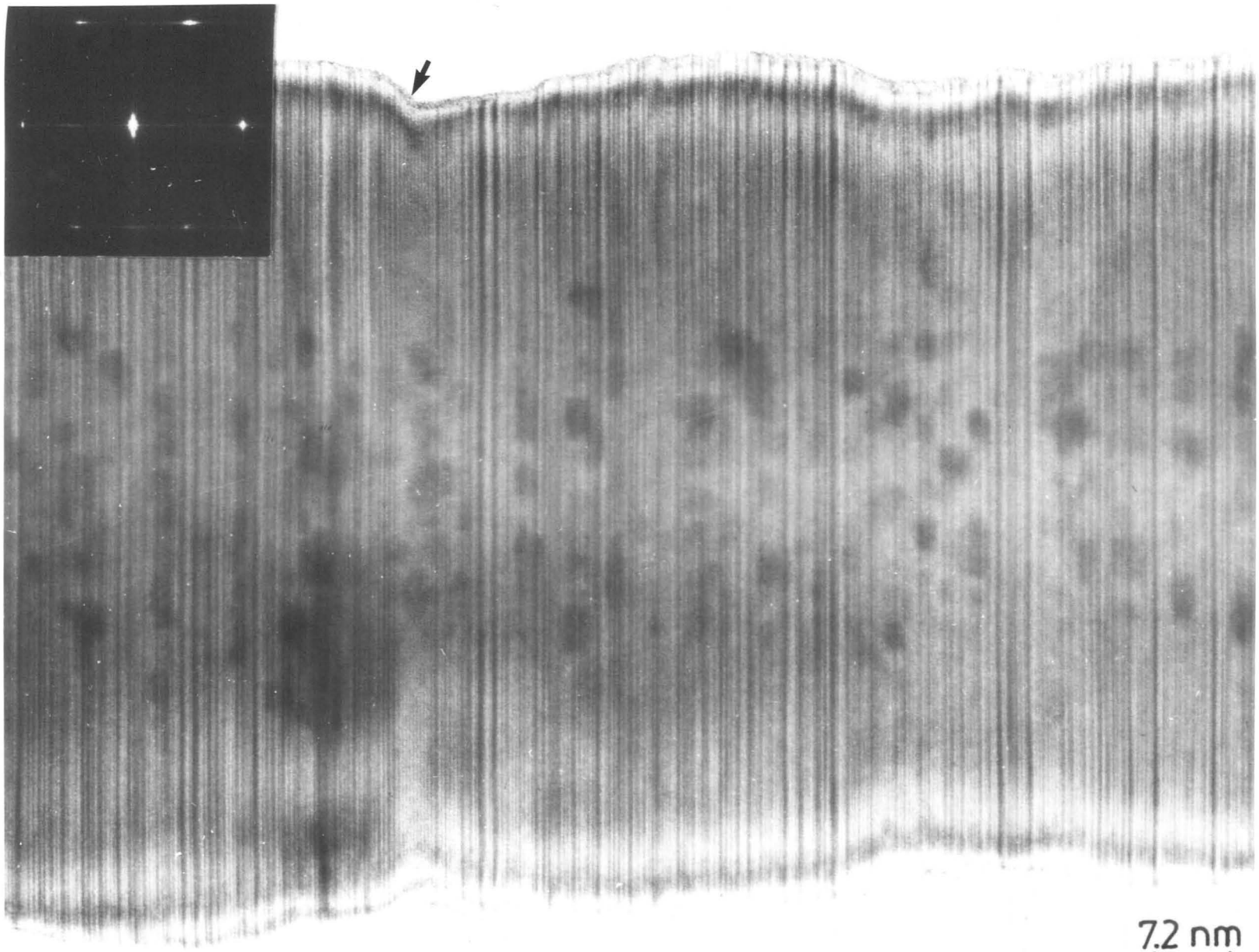
7.2 nm

the occurrence of continuous streaks along the reciprocal lattice rows have been considered as partially due to a one-dimensional disordered arrangement of the close packed planes or, in the case of X-ray studies, to a lack of spatial resolution of reflexions from extremely long-period polytypes. One-dimensional lattice images show that crystals giving X-ray diffraction patterns containing continuous streaks can be resolved into small regions of the common short-period polytypes. If intensity maxima corresponding to larger unit cells appear in the electron diffraction pattern, then it is possible to identify larger unit cell repeats, even though the contents of successive cells are not identical. However, Shinozaki & Kinsman (1978) have observed a random arrangement of very thin lamellae (1-10 nm thick) of the common short period polytypes 3C, 4H, 6H, 15R and 21R. In the case of the elongated crystals observed in the current work, no long period order is apparent and the high degree of faulting occurs in a purely random way, dividing the crystal into small regions of 2H and other short-period polytypes.

Since regions of perfect 2H extend only to ∿5 nm (for other polytypes this value is even smaller), these crystals cannot be expected to contribute intensity to the X-ray diffraction pattern. This implies that the remainder of the specimen i.e. the equiaxed particles, must be responsible for the observed X-ray diffraction intensity. Information from these crystals was more difficult to obtain because of their tendency to agglomerate, and usually, separate crystals were too thick to give useful data. Nevertheless, selected area diffraction patterns were consistent with a mostly unfaulted 2H structure.

VIII.4.2 Intermediate silicon carbide-aluminium nitride alloys

Additional information concerning the structure of the equiaxed crystals was obtained from a SiC-AlN alloy containing nominally 50 m/o AlN and shown by SEM to consist of needles and small equiaxed particles similar to those comprising much of the SiC-rich alloy (see section VII .5). By TEM, it was similar to the 25 m/o AlN alloy, described previously (see section VIII.4.1), in that aggregates of small equiaxed particles (∿0.4 μm in size) formed the majority of the specimen. Suitable crystals gave selected area diffraction patterns of unfaulted 2H; see Figure VIII.12 which is markedly different from the patterns of the heavily faulted needles (cf.Figure VIII.6).

The large differences in the faulting within the two different crystal morphologies, were confirmed by lattice images from suitably oriented equiaxed particles. Figure VIII.12 was obtained by positioning the optical axis at (d) in the diffraction pattern and including the $(10\bar{1}\bar{1})$, $(10\bar{1}1)$, (1000), (0001), $(000\bar{1})$ and undiffracted beams in the objective aperture. The resulting image reveals large areas (>10 nm) of unfaulted 2H polytype. An enlargement of such an area is shown in Figure VIII.13(a) where the chevron-type fringes clearly show the ABAB... stacking sequence in 2H. Part of the faulted region in Figure VIII.12 is shown in Figure VIII.13(b).

The needle shaped crystals, comprising 15-20% of the 50 m/o AlN alloy, were >2 μm long x ∿0.2 μm wide and similar to those in the 25 m/o AlN alloy. Electron diffraction patterns were typical of randomly faulted 2H-SiC, with continuous streaking along reciprocal lattice rows parallel to $[000\bar{1}]$. The growth direction is parallel to $[000\bar{1}]$ and faults occur in the basal planes. By tilting the crystal, so that the faults do not

Figure VIII.12

Tilted illumination lattice fringe

image revealing the almost

perfect 2H structure of an equiaxed crystal

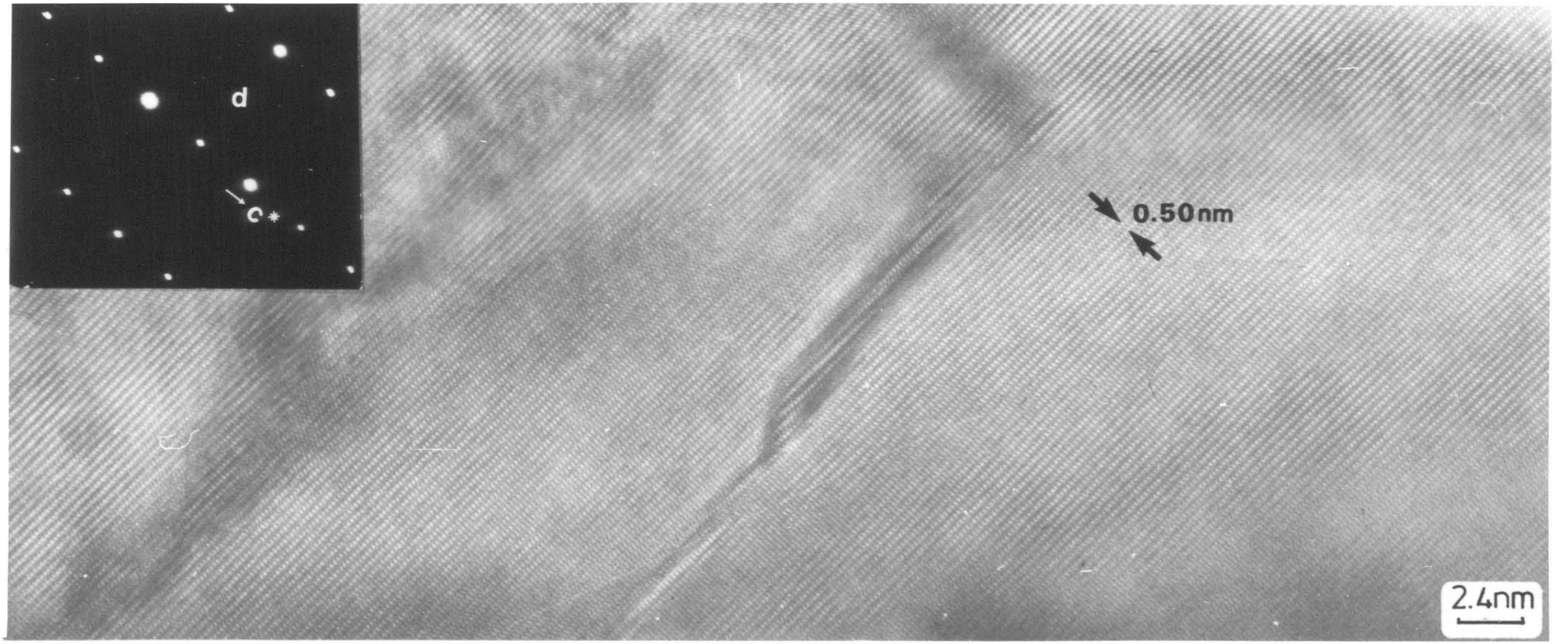
d
c*
0.50nm
2.4nm

Figure VIII.13

(a) Chevron-type $(10\bar{1}1)$ and $(10\bar{\bar{1}}\bar{\bar{1}})$ fringes representing tetrahedral faces in 2H

(b) Enlargement of faulted area in Figure VIII.12

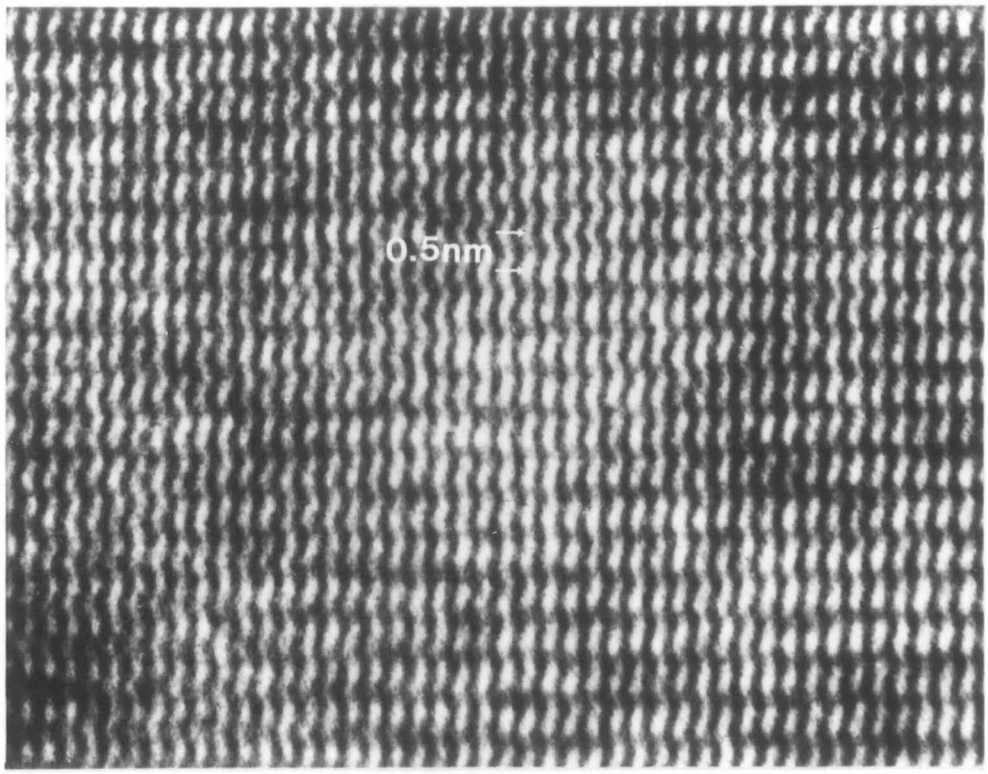

(a)

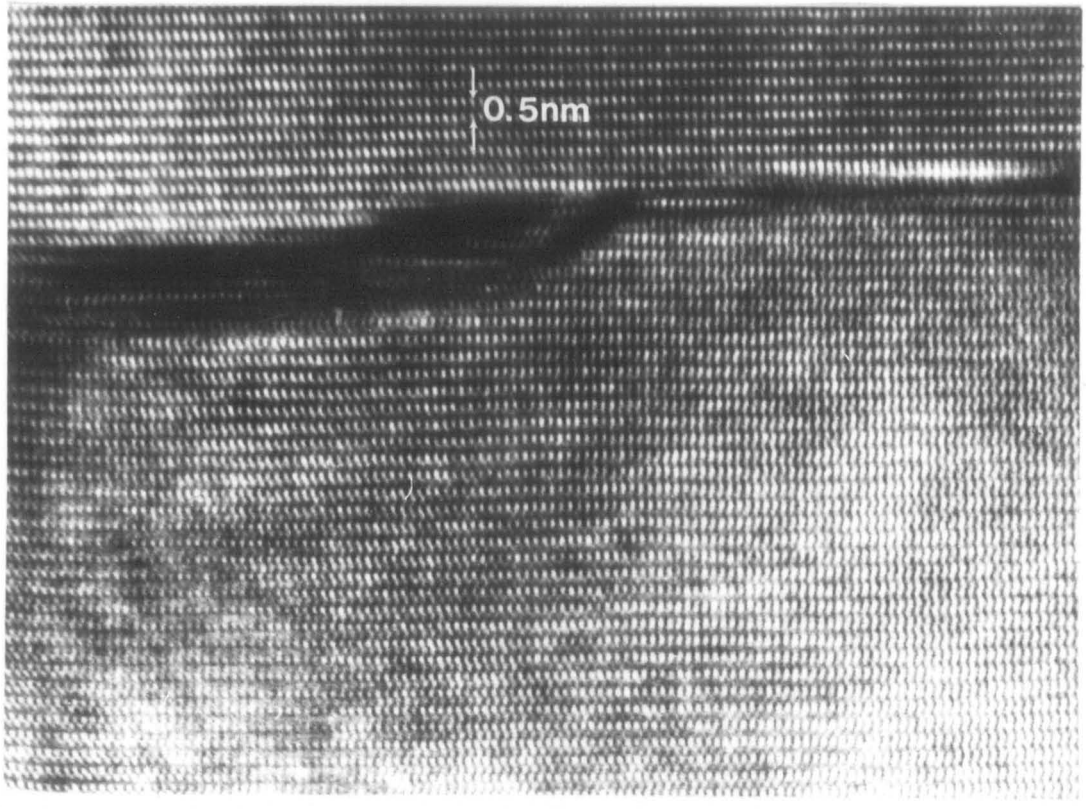

(b)

lie perpendicular to the electron beam, the needles appear to be hexagonal in cross-section; see Figure VIII.14(a). Also visible, are spotty defects similar to those in the 25 m/o AlN specimen. Bearing in mind that EDX analysis indicated that calcium remains in these specimens and that no electron diffraction pattern could be obtained from the precipitates, it is thought that the spotty defects are a calcium-containing glassy phase. n-beam lattice images show small areas of unfaulted 2H, typically 5 nm wide, separated by slightly smaller faulted regions; see Figure VIII.14(b).

A feature of the needles, observed only in the 50 m/o AlN specimen, is the relatively frequent occurrence of additional spots in $[1\bar{0}10]$ zone electron diffraction patterns corresponding to a d-spacing of 3.4 Å. This is apparently due to a surface coating on the crystals as shown in Figure VIII.15(a). A particularly thick coating gave a ring diffraction pattern corresponding to d-spacings of 3.37 , 2.12 , 1.22 , and 1.16 Å's, characteristic of graphite. Moreover, the single spots observed in some patterns correspond with the 002 reflexion of graphite. Figure VIII.15(b) shows the 3.4 Å spacing of fringes arising from the coating, and small regions of 2H are also visible. There seems to be no obvious reason why needles in the 50 m/o AlN alloy have a graphite coating since, in all other respects, they are structurally very similar to those in the 25 m/o AlN alloy; the loss of SiO from the crystal could cause deposition of C on the surface.

The present study of 2H-SiC-AlN alloys shows that a small proportion of each specimen (10-20%) is composed of highly faulted material which, although containing small regions of 2H (~5 nm), cannot contribute to the X-ray diffraction pattern. The latter is due to the

Figure VIII.14

(a) Dark field image of a needle

which is hexagonal in cross-section

(b) Lattice fringes from a needle showing

small areas of 2H

(a)

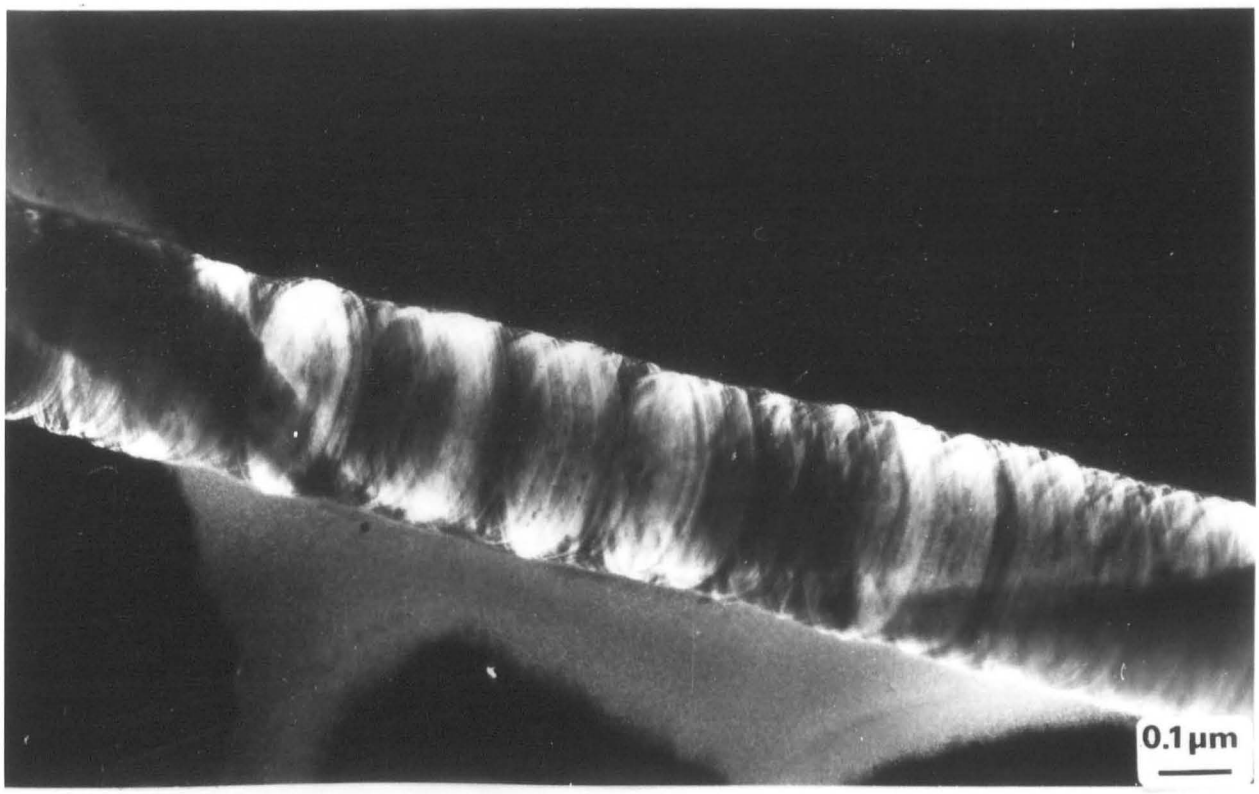

(b)

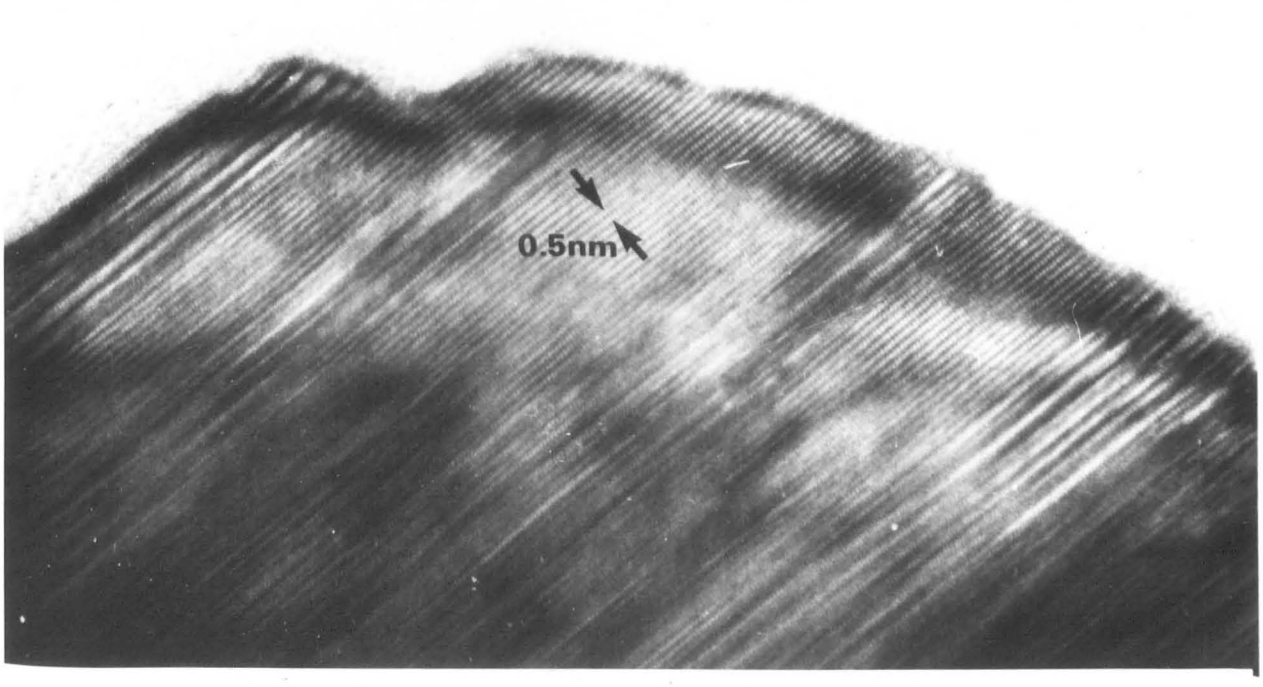

Figure VIII.15

(a) Bright-field image showing needle with surface coating

(b) [$10\bar{1}0$] zone from needle revealing small areas of 2H stacking and the (002) fringes from graphite coating

(a)

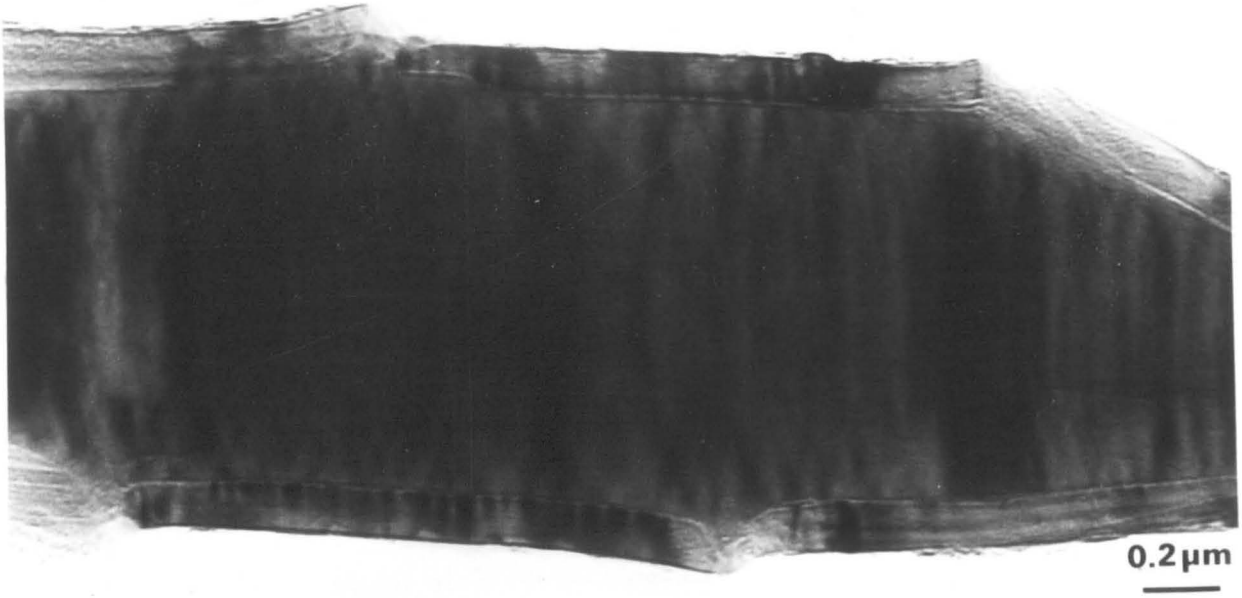

(b)

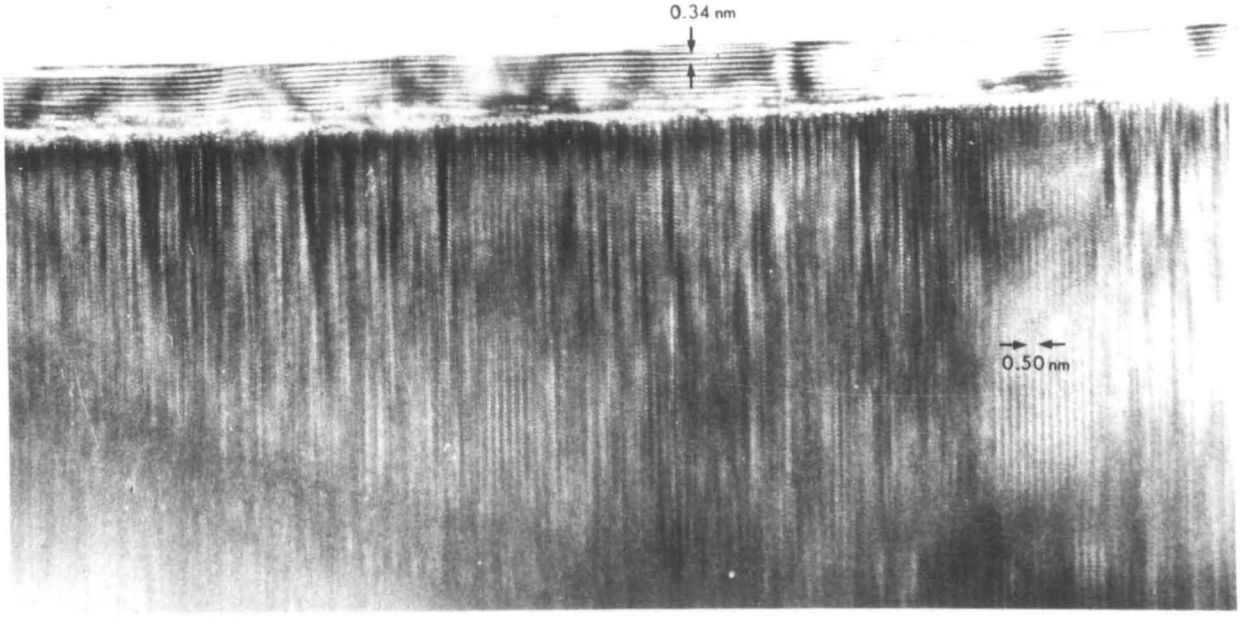

equiaxed crystals which, from lattice images, are almost perfect 2H. These observations are confirmed by calculating the average particle size giving rise to the broadened X-ray reflexions which are observed in the Hägg-Guiner photographs. Intensity data from the specimen showing most line-broadening indicate that the average crystallite size is about 30 $\pm$ 10 nm.

VIII.5 The 2H→3C transformation

VIII.5.1 Introduction

As discussed in Chapter II, the transformation from 2H to 3C-SiC has been observed both in single crystal and polycrystalline specimens, but the transformation mechanisms have been deduced only from X-ray diffraction studies. In the present work, 2H→3C is observed both in nitrogen-2H-SiC and in a silicon carbide alloy containing nominally 25% AlN (see sections VI.6 and VII.4).

VIII.5.2 Nitrogen-2H

The 2H→3C transformation is observed in nitrogen-2H (see section VI.6). As in the other SiC alloys, nitrogen-2H is composed of 10-20% needles heavily disordered in the close-packed (0001) planes and equiaxed particles having a mostly unfaulted 2H structure. After annealing at 2000°C for 30 mins., transformation was observed to give 50-75% conversion to the structure. Electron diffraction patterns from suitably oriented fragments, i.e. $[10\bar{1}0]_{2H}//[1\bar{1}0]_{3C}$ and $[0001]_{2H}//[111]_{3C}$, showed that the rate of transformation varies considerably between fragments. For example, the electron diffraction patterns of Figure VIII.16(a)-(e) are all from the same specimen but clearly the

Figure VIII.16

$[10\bar{1}0]_{2H}$ // $[1\bar{1}0]_{3C}$ zone electron diffraction patterns showing fragments in different stages of transformation from 2H → 3C

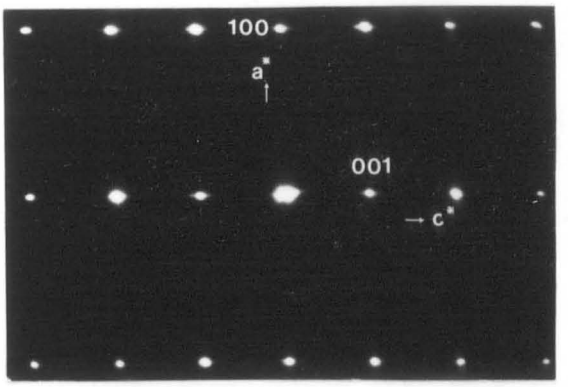

(a)

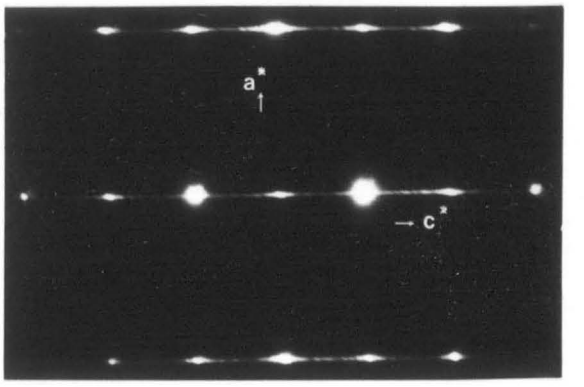

(b)

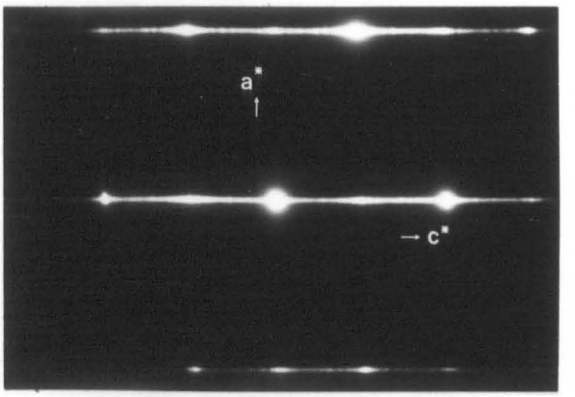

(c)

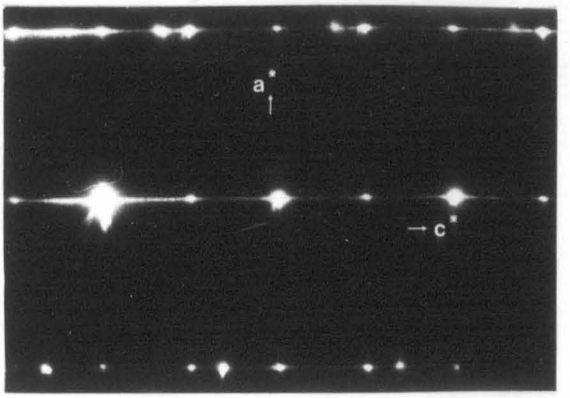

(d)

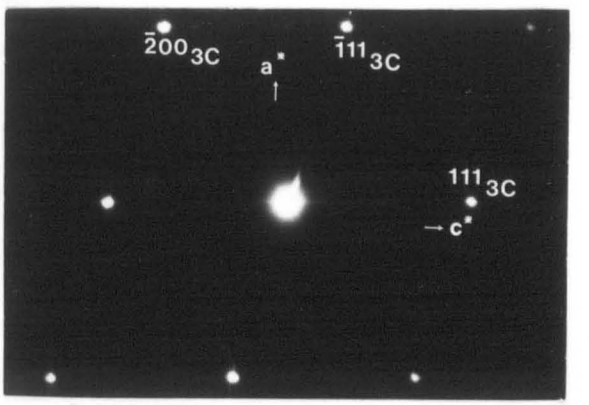

(e)

amount of 2H and 3C in each crystal are different. The transformation from a relatively unfaulted 2H structure (Figure VIII.16(a)) takes place by the random insertion of stacking faults giving a heavily faulted structure (Figure VIII.16(b)) which, in some cases, may almost appear to have a completely random stacking sequence; see Figure VIII.16(c). Nucleation of the stacking faults results in partially transformed structures giving reflexions corresponding to both 2H and 3C polytypes; (see Figure VIII.16(d)) before eventually resulting in a predominantly cubic structure as shown in Figure VIII.16(e).

Crystal fragments at different stages of transformation are shown in the next series of micrographs. Figure VIII.17(b) is typical of an early stage where, although a large number of stacking faults are present (see insert diffraction pattern), areas of 2H still extend to $\sim$15 nm or 30 unit cells in the c direction. Of particular interest in this micrograph are three faults which appear to be joined up, probably as a result of a reaction between the partial dislocations which produce the changes in stacking. These additional faults are perpendicular to the stacking faults and therefore lie on non-close packed $\{10\bar{1}0\}$ planes. It is very unusual to observe such faults in a hexagonal close-packed structure. It is possible that the presence of nitrogen significantly lowers the stacking fault energy which, as indicated by the abundance of SiC polytypes, is already low. Thus, faulting in $\{10\bar{1}0\}$ planes is facilitated.

Micrograph VIII.17(c) shows the stage in the 2H→3C transformation where regions of 2H extend to a maximum of only 2.5 nm. Moreover, no long-period structures are observed and so the crystal has essentially a random arrangement of SiC layers. The inset diffraction pattern of

Figure VIII.17

(a) Dark field electron micrograph showing regions of 2H and 3C within a fragment

(b) A fragment containing faults on the $\{10\bar{1}0\}$ planes

(c) A crystal at the highly disordered stage of the 2H→3C transformation

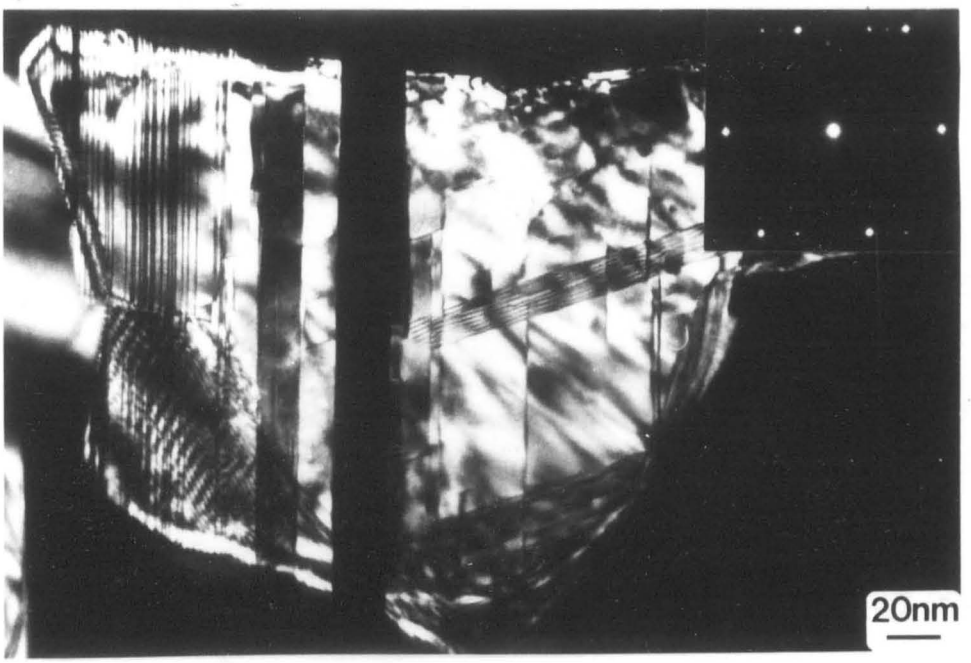

(a)

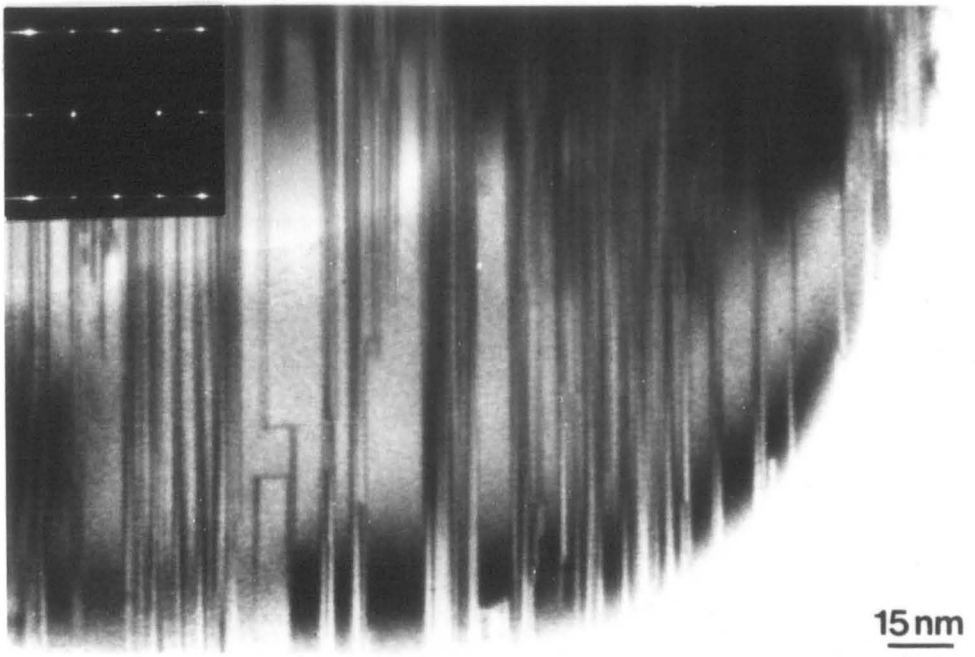

(b)

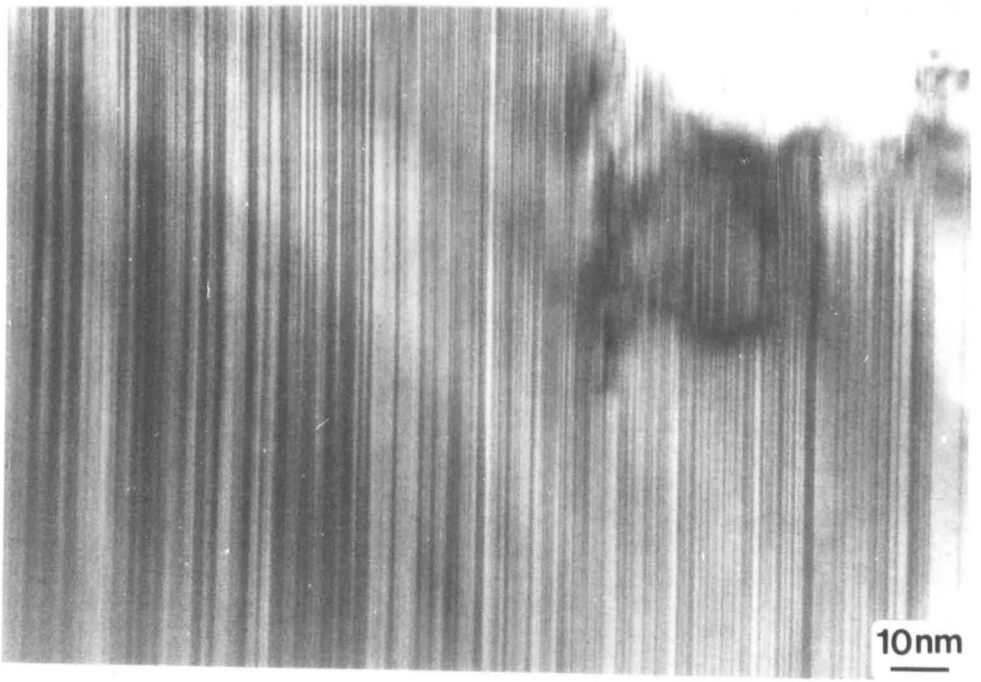

(c)

Figure VIII.17(a) shows that this particular crystal consists of syntactically coalesced regions of 2H and twinned 3C. The bright regions in the dark-field micrograph are 3C formed as a result of complete 2H→3C transformation. The darkest bands in the centre are 3C twins, and a region composed of fine intergrowths of 2H and 3C, representing an area of incomplete transformation, is visible at the left hand side of the micrograph. Frequently the final 3C structure is twinned as shown in Figure VIII.18(a) & (b) where each dark field micrograph was taken using a different twin reflexion. Fine twinning therefore occurs in addition to the large twinned regions.

The changes in stacking sequence which occur during the 2H→3C transformation can be directly observed by lattice imaging the tetrahedral plane faces which for 2H are the $\{10\bar{1}1\}$-type and for 3C the $\{111\}$-type. The micrograph of Figure VIII.19 shows a region where the 2H→3C transformation is occurring and the arrangement of chevron-like fringes illustrates the stacking sequence. The change in stacking required for the transition from hexagonal to cubic packing results in the formation of microregions of the crystal, where one or two unit cells of 2H or 3C are sandwiched between larger areas of untransformed 2H. Frequently, 3C is twinned, giving a single unit cell of 6H. Also seen in the micrograph is an incoherent stacking fault but, because of the increase in crystal thickness, it is not possible to determine the change in sequence which it causes. The transformation zone consists of newly formed 3C and untransformed 2H.

Regions of crystal in a less advanced stage of transformation are shown by Figure VIII.20(a) & (b). The first micrograph shows that the transformation begins with changes in the stacking sequence of a single

Figure VIII.18

Dark field electron micrographs

showing a twinned 3C fragment

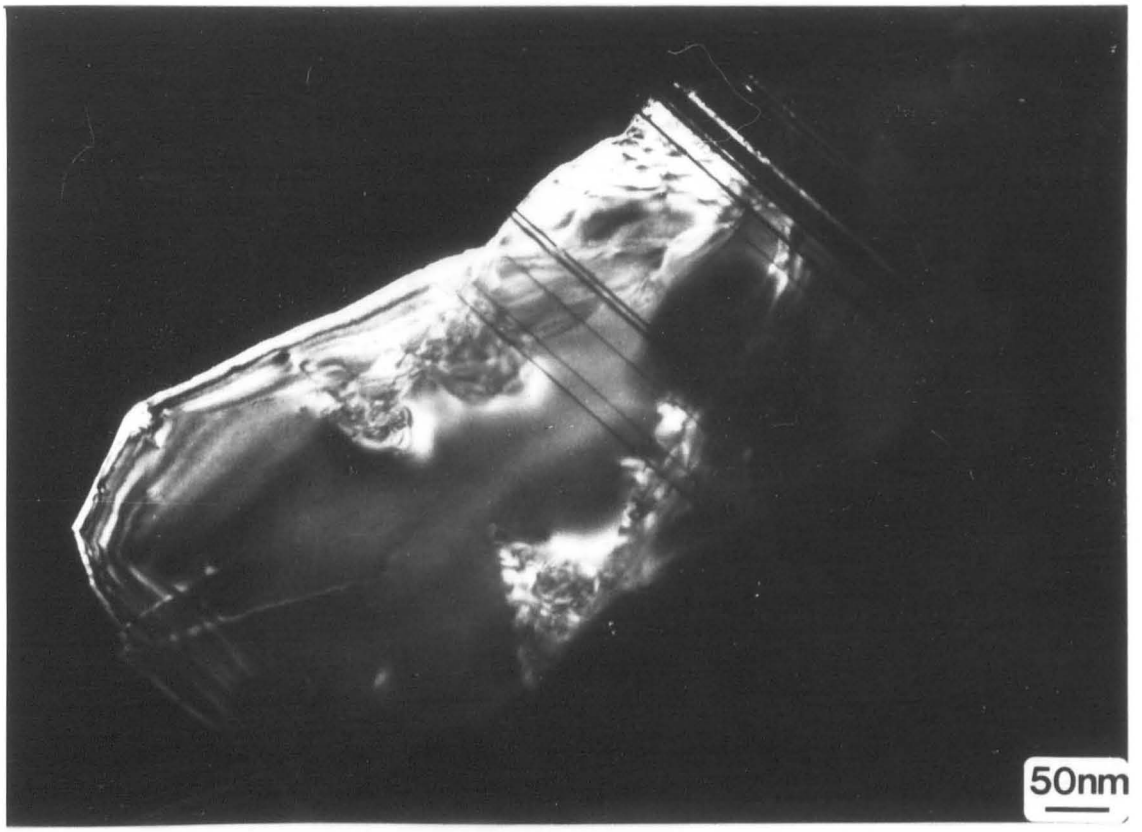

(a)

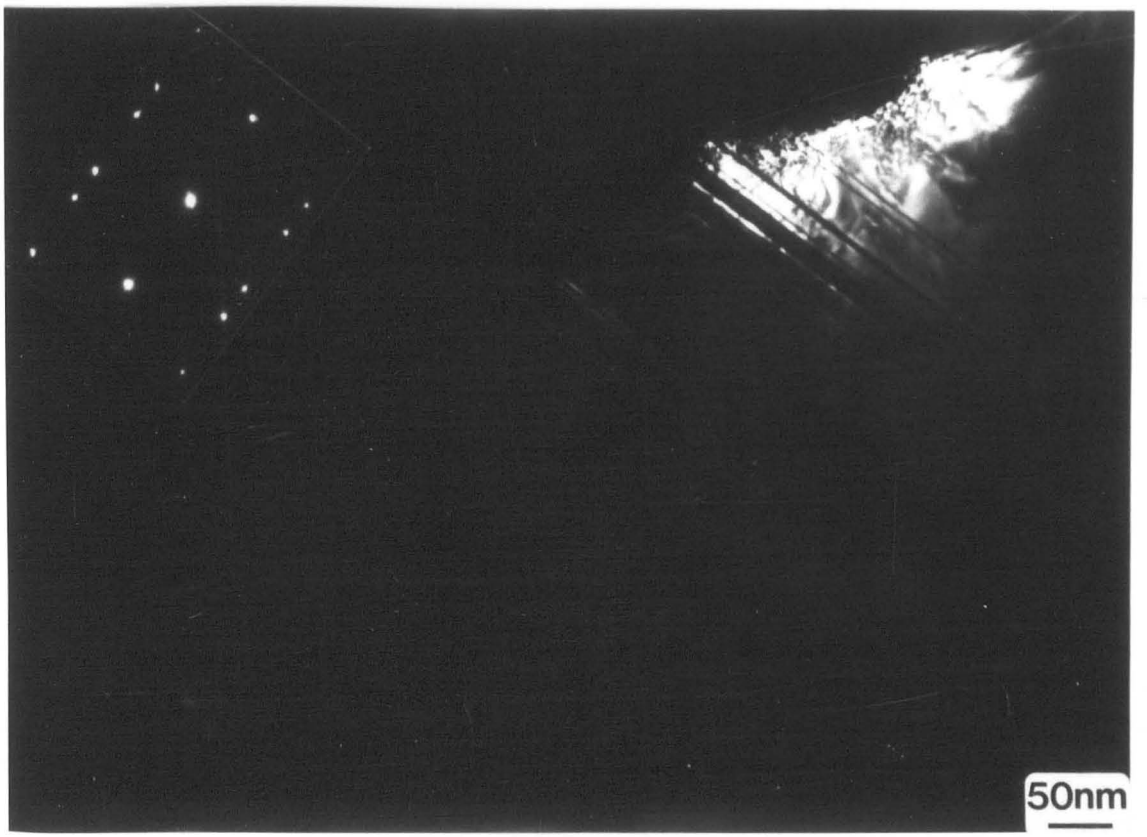

(b)

Figure VIII.19

Lattice fringes from an area

in the process of transformation

from 2H → 3C

zone axis $[10\bar{1}0]_{2H}$ // $[1\bar{1}0]_{3C}$

0.5nm
ABABABABABACABABACBA

Figure VIII.20

$[10\bar{1}0]_{2H}$ // $[1\bar{1}0]_{3C}$ **zone, lattice**

fringe image revealing changes

in the stacking sequence characteristic

of regions of 2H and 3C

(a)

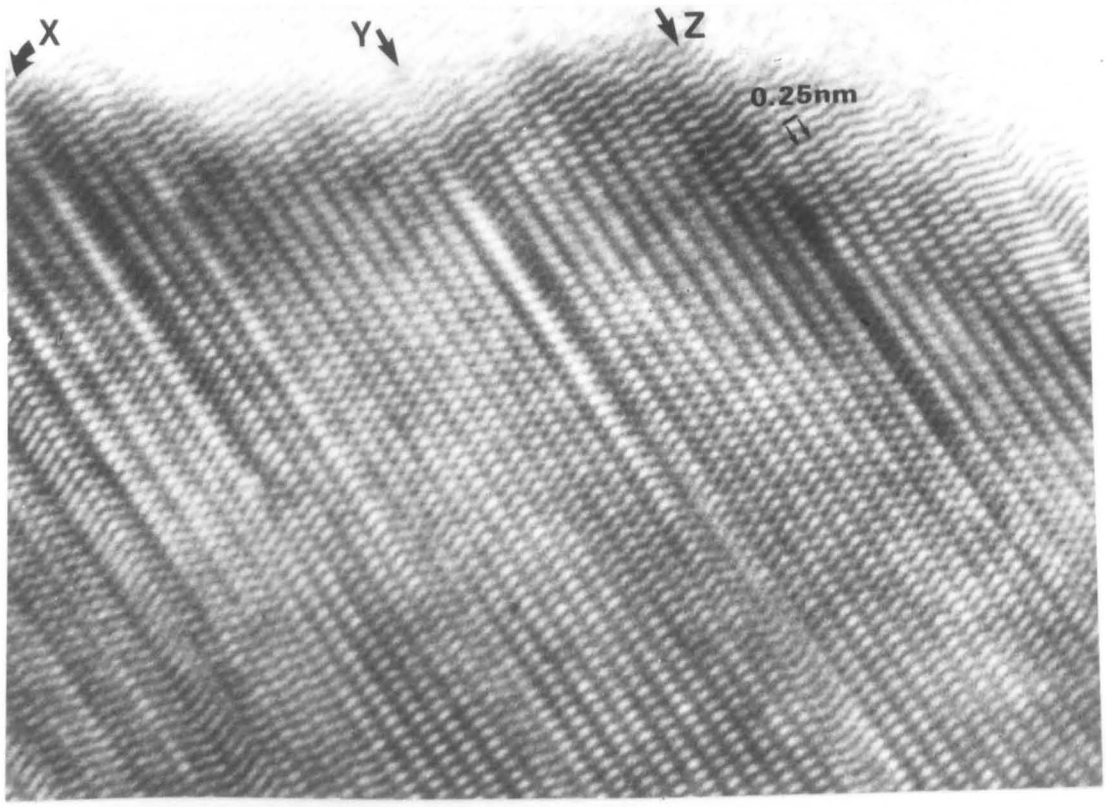

(b)

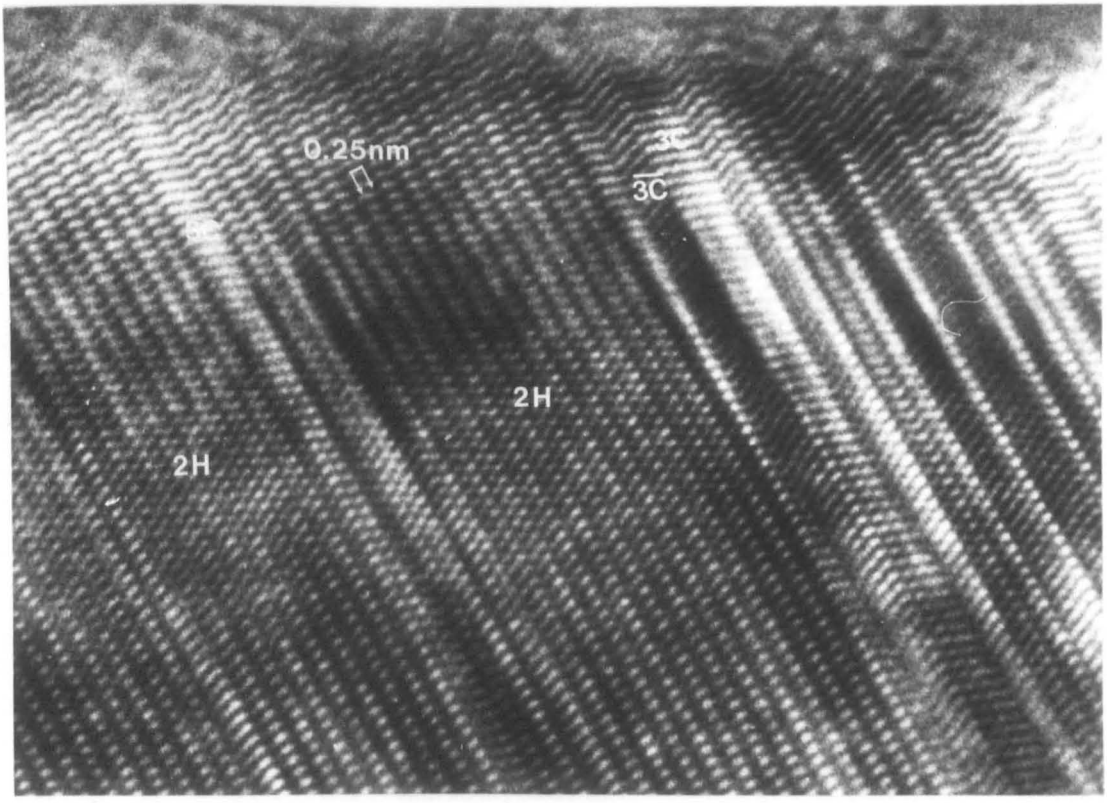

layer, indicated by arrows X, Y and Z. In particular, the dislocations causing the changes in atom positions at Y and Z have advanced the faults further than the area shown in the micrograph. However, at X, the fault ends within the observed area, giving regions of untransformed 2H towards the bottom and new 3C at the top. It is significant that initiation of the fault occurs at the surface of the crystal where the interatomic bonding forces are asymmetric. More changes in the stacking sequence have occurred in Figure VIII.20(b). In particular regions of cubic stacking and twinning occur.

VIII.5.3 Silicon carbide-rich alloys

As for nitrogen-2H, annealing at 2000°C induces partial transformation to 3C in a SiC-AlN alloy containing nominally 25 m/o AlN. The average crystal size increases during annealing, presumably through a vapour or surface diffusion mechanism, but the resulting crystals are still heavily faulted as shown in Figure VIII.21(a) & (b). The largest crystals are of the 3C polytype and are usually well faceted in projection; see Figure VIII.21(a).

One-dimensional lattice images from typical crystals show the high degree of faulting which preceeds formation of 3C (see Figure VIII.22). The largest region from any single polytype is that of 2H and regions of other polytypes are much narrower.

In one particular case, a lath-like crystal 82 nm wide x 140 nm long connected two faulted crystals see Figure VIII.23(a) . n-beam lattice images show an intergrowth of 3C polytype, 10 nm wide, sandwiched in the lath which otherwise is 2H (see Figure VIII.23(b)) and electron diffraction indicates that the polyhedral crystals at either end are 2H

Figure VIII.21

(a) Dark field image of a faceted crystal containing stacking faults

(b) Bright field image showing grain boundaries and stacking faults within grains

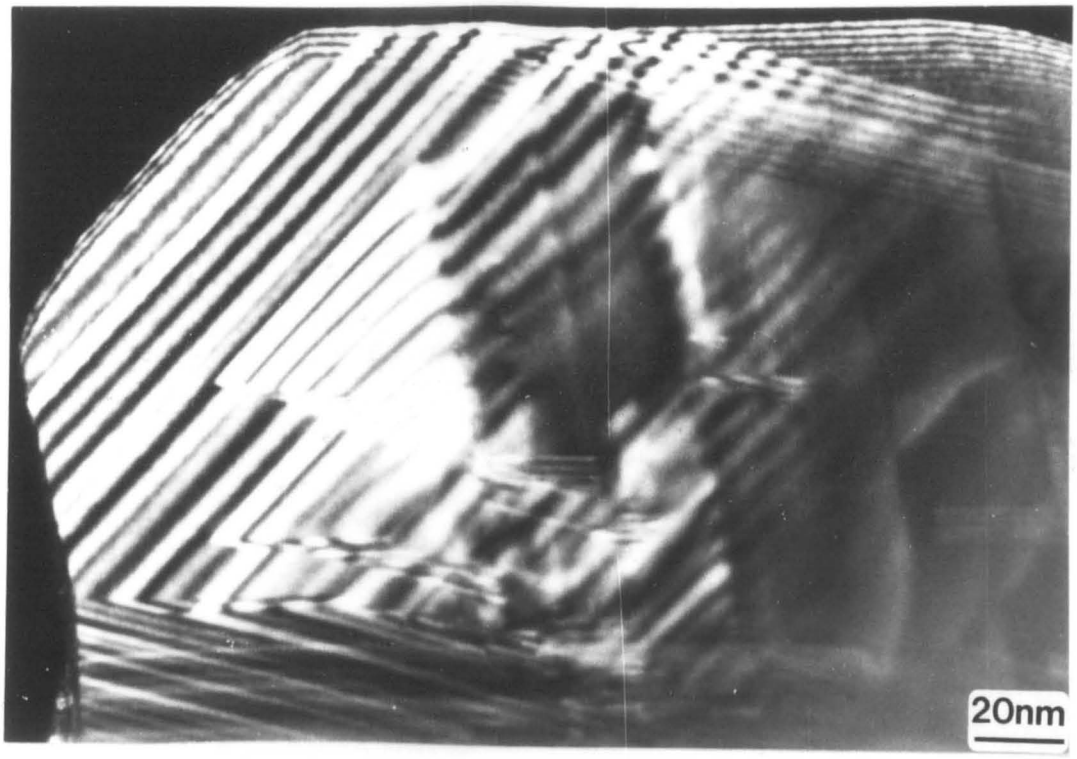

(a)

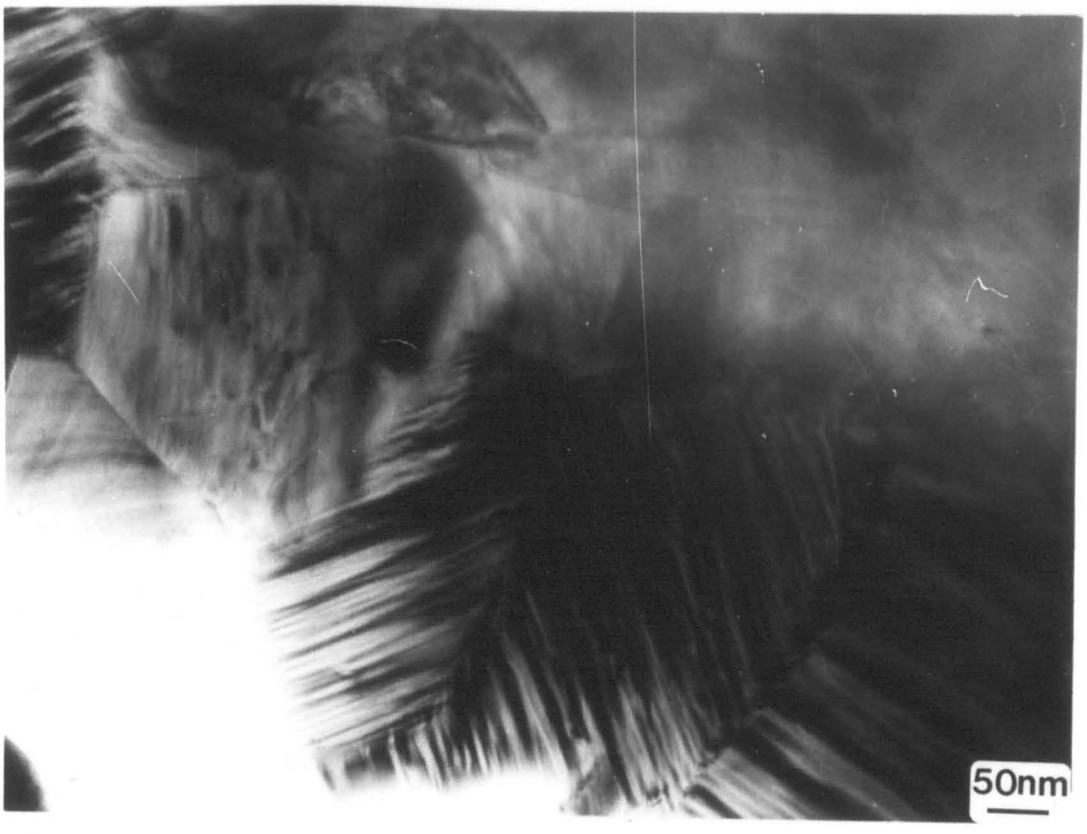

(b)

Figure VIII.22

One dimensional lattice fringes revealing stacking faults as changes in both intensity and spacing of the (000ℓ) fringes

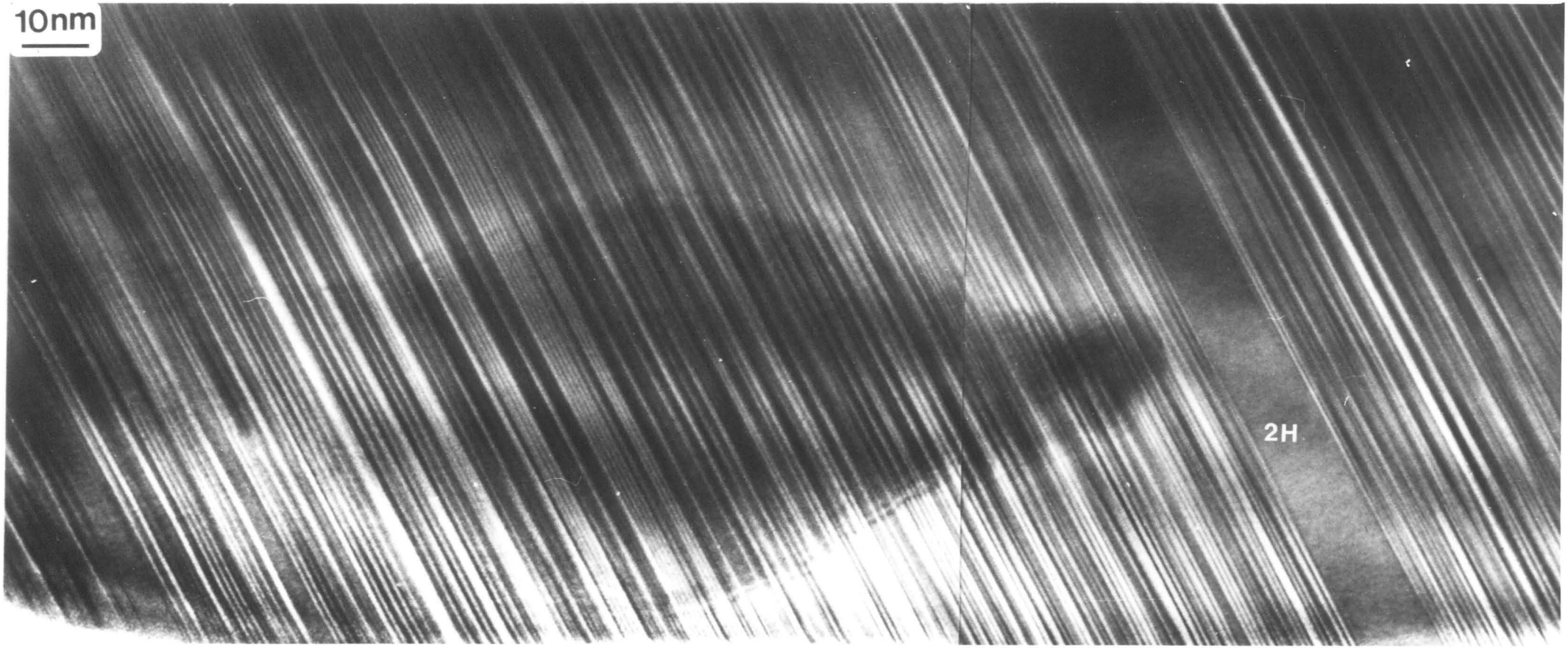
10nm
2H

Figure VIII.23

(a) Lath of predominantly 2H polytype sandwiched between 2 heavily faulted crystals

(b) Lattice fringes of (0001) planes in 2H revealing a region of 3C and several incoherent stacking faults

(a)

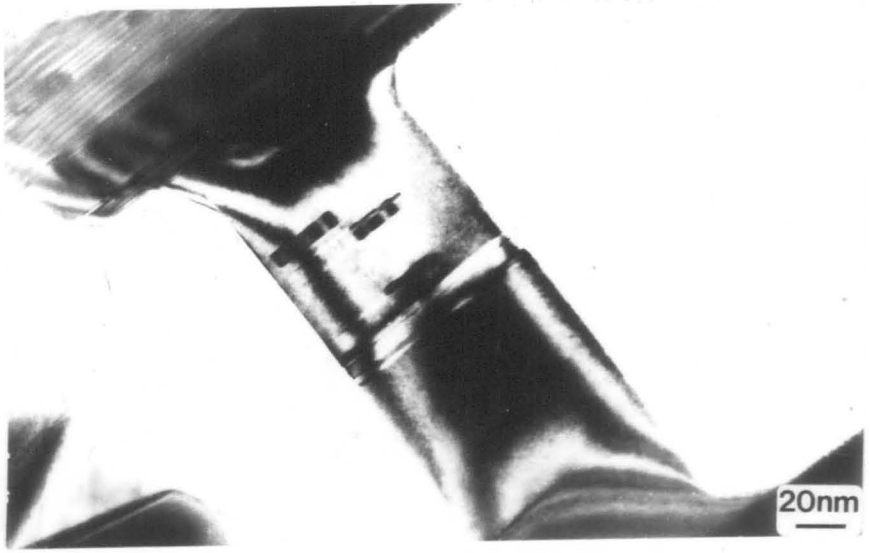

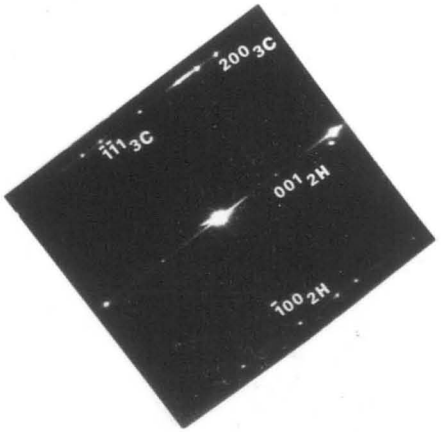

(b)

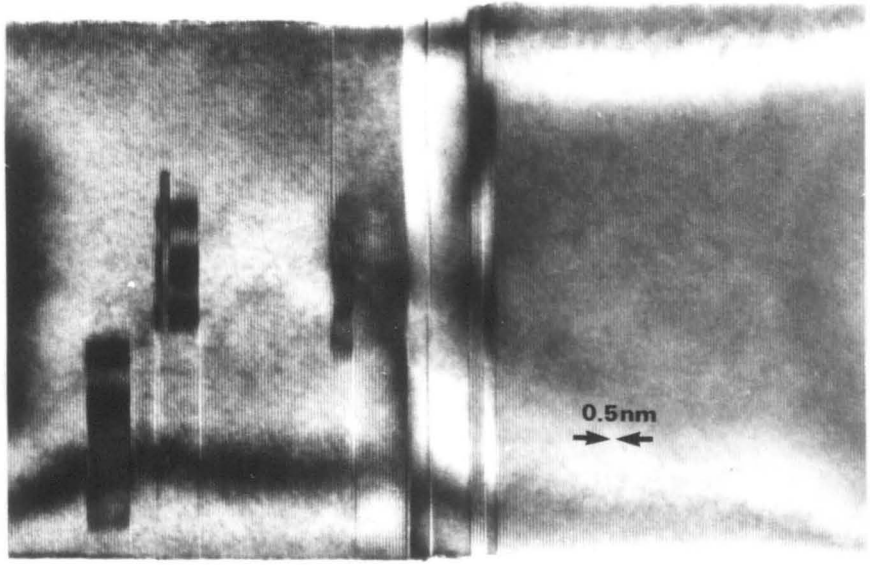

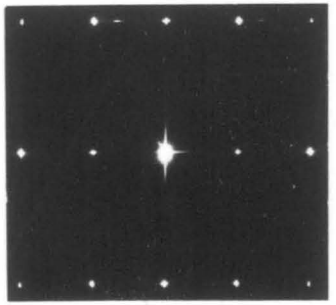

and 3C polytypes in approximately equal amounts. It seems likely that the lath has grown by vapour deposition onto suitable nuclei at the surface of the two faulted crystals but transformation to 3C begins because of the instability of 2H at the annealing temperature. Indeed, in Figure VIII.23(b) visible dislocations are producing changes in the stacking sequence to give localised 3C regions, growth of which results in the final large areas of 3C.

VIII.5.4 Discussion

Two theories attempting to explain the transformation between polytypes of SiC in the solid state have been advanced; namely a basal slip mechanism and a layer displacement mechanism (see section II). The former requires movement of partial dislocations around a screw dislocation to bring about changes in the stacking sequence, whereas the latter is based on diffusional rearrangement to nucleate stacking faults. Pandey & Krishna (1973) have convincingly argued that polytype transformations in SiC take place by the layer displacement mechanism, which is now shown to explain the experimental observations of the present work.

According to Pandey & Krishna, annealing 2H-SiC alloys at 2100^{o}C enables a number of vacancies to come together by thermal diffusion to initiate a fault as neighbouring atoms move into other sites. The partial dislocation, which now bounds the fault is able to glide, causing the fault to expand until the whole layer of atoms is displaced, say, from an A to a C stacking. Other displacements, which occur throughout the crystal in a similar manner, can together produce a new structure which in this case is 3C. Although the stacking faults occur initially in

a random way, an ordered arrangement must eventually result to create the new structure. The layer-displacements which are necessary for 2H→3C are shown in Figure VIII.24(a) together with those for 3C→6H and 2H→6H. As transformation proceeds, the rise in entropy with degree of disorder makes it difficult to arrive at a stable ordered configuration, and consequently, the final structures should exhibit considerable one-dimensional disorder (Pandey & Krishna, 1973). The wide range of transformation rates observed within each specimen in the current work can be explained if transformation occurs by the nucleation of stacking faults which will be different for each fragment.

Although the layer-displacement mechanism explains the solid-state transformations in SiC alloys, the changes in crystal morphology are due to surface-flow and sintering of crystallites caused by grain boundary diffusion at 2100°C. Indeed, for nitrogen-free 2H these observations agree with Bootsma et al. (1971), who observed a similar tendency for the formation of faceted crystals during the 2H→3C transformation.

VIII.6 High temperature vapour growth of 3C crystals

The post-preparative heat-treatment of SiC-AlN alloys containing nominally 25 m/o AlN is described in section VII.4. SEM coupled with EDX and X-ray analyses show that, after annealing at 2000°C, large highly faceted crystals, containing no AlN and having a cubic structure, grow on the surface of the alloy. Crystals from this specimen were carefully removed and examined by HREM.

Selected area diffraction patterns are typical of 3C-SiC and, in most cases, the crystals are twinned; see Figure VIII.25. The bright

Figure VIII.24

Diagrammatic representation of the layer displacements required for the polytypic transformations:

(a) 2H→3C

(b) 3C→6H

(c) 2H→6H

(a) 2H→3C

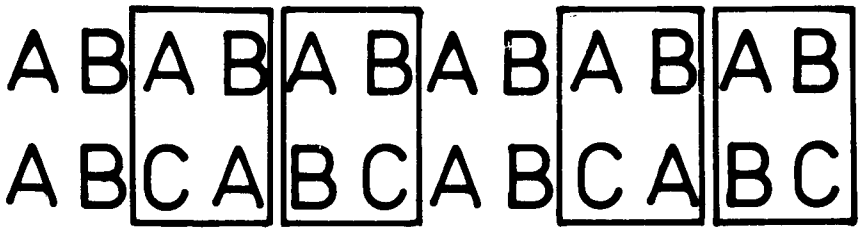

(b) 3C→6H

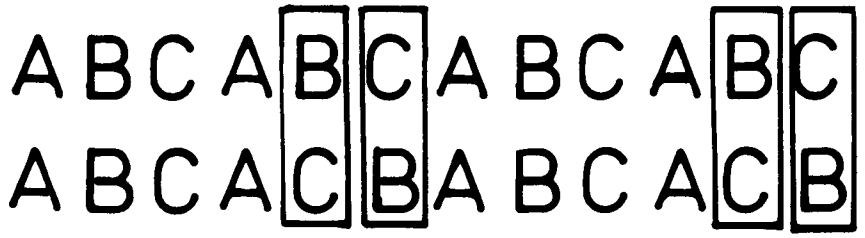

(c) 2H→6H

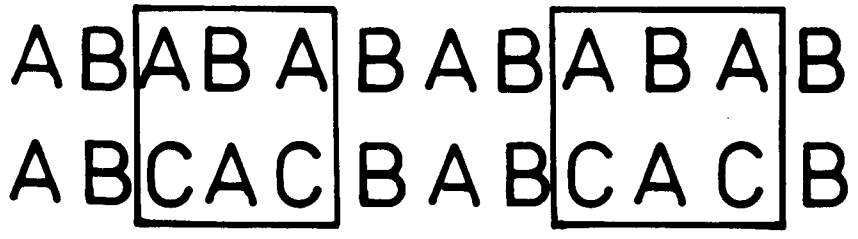

(Pandey & Krishna, 1973)

Figure VIII.25

(a) Bright field image of a fragment showing 2 sets of twins

(b)-(d) Dark field images revealing areas in twin orientation

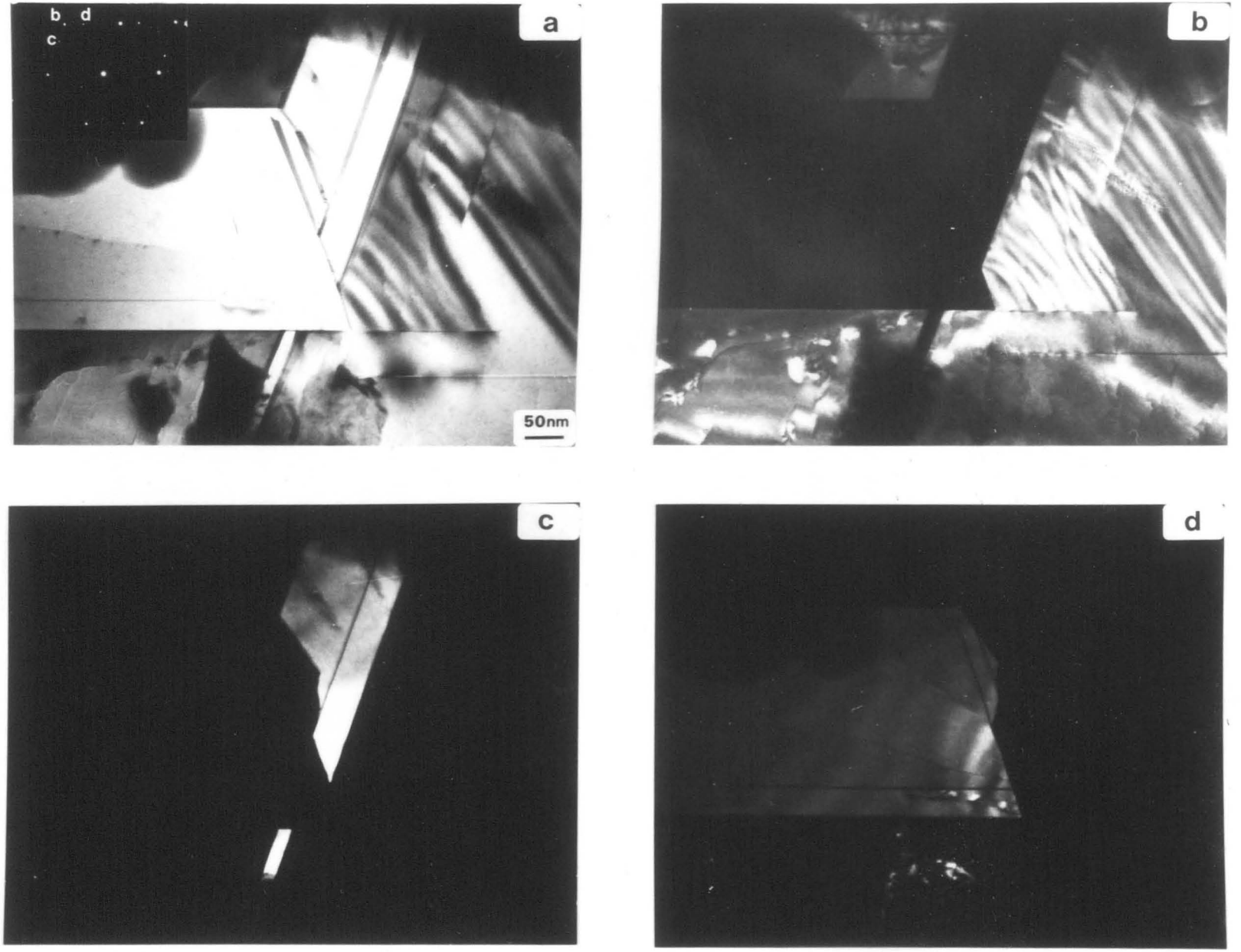
a
b
c
d
50nm

field electron micrograph, Figure VIII.25(a), shows a region containing twins and the inset $\langle 1\bar{1}0 \rangle$ zone diffraction pattern indicates that there are two sets of twins. The dark field micrograph, Figure VIII.25(a) & (b), taken by using the spot labelled b in the diffraction pattern, clearly reveals the matrix, whilst using spots c and d to obtain micrographs VIII.25(c) & (d), the twin orientation relationships become apparent. Twinning occurs about the $[1\bar{1}0]$ direction in the close-packed {111} planes.

The nature of the twin boundary can be observed in detail by orienting the crystal in a $[1\bar{1}0]$ beam direction, which gives a diffraction pattern containing both twin and matrix {111}-type reflexions. Lattice images of the relevant {111} planes may be realised by tilting the beam so that the optical axis lies mid-way between the undiffracted beam and the appropriate twin and matrix reflexions i.e $1\bar{1}\bar{1}$ and $\bar{1}\bar{1}1$ respectively. Including these beams in the aperture, lattice fringes from either side of the (111) twin interface are obtained simultaneously as shown in Figure VIII.26. Here, the image was obtained with tilted illumination, the optical axis being positioned at d in the diffraction pattern. The 0.25 nm spaced fringes show the changes in orientation of the tetrahedra resulting in the twin configuration. The twin interfaces are fully coherent although, in some instances, the twinned region is only a few layers thick.

Apart from the extra spots in the diffraction pattern arising from twins, additional spots and streaking were frequently observed as shown in the inset diffraction pattern of Figure VIII.27. The accompanying lattice image was obtained by positioning the optical axis at d, midway between the twin and matrix spots. The micrograph shows a region

Figure VIII.26

Tilted illumination lattice fringe image showing matrix $(11\bar{1})$ and twin $(\bar{1}\bar{1}1)$ planes

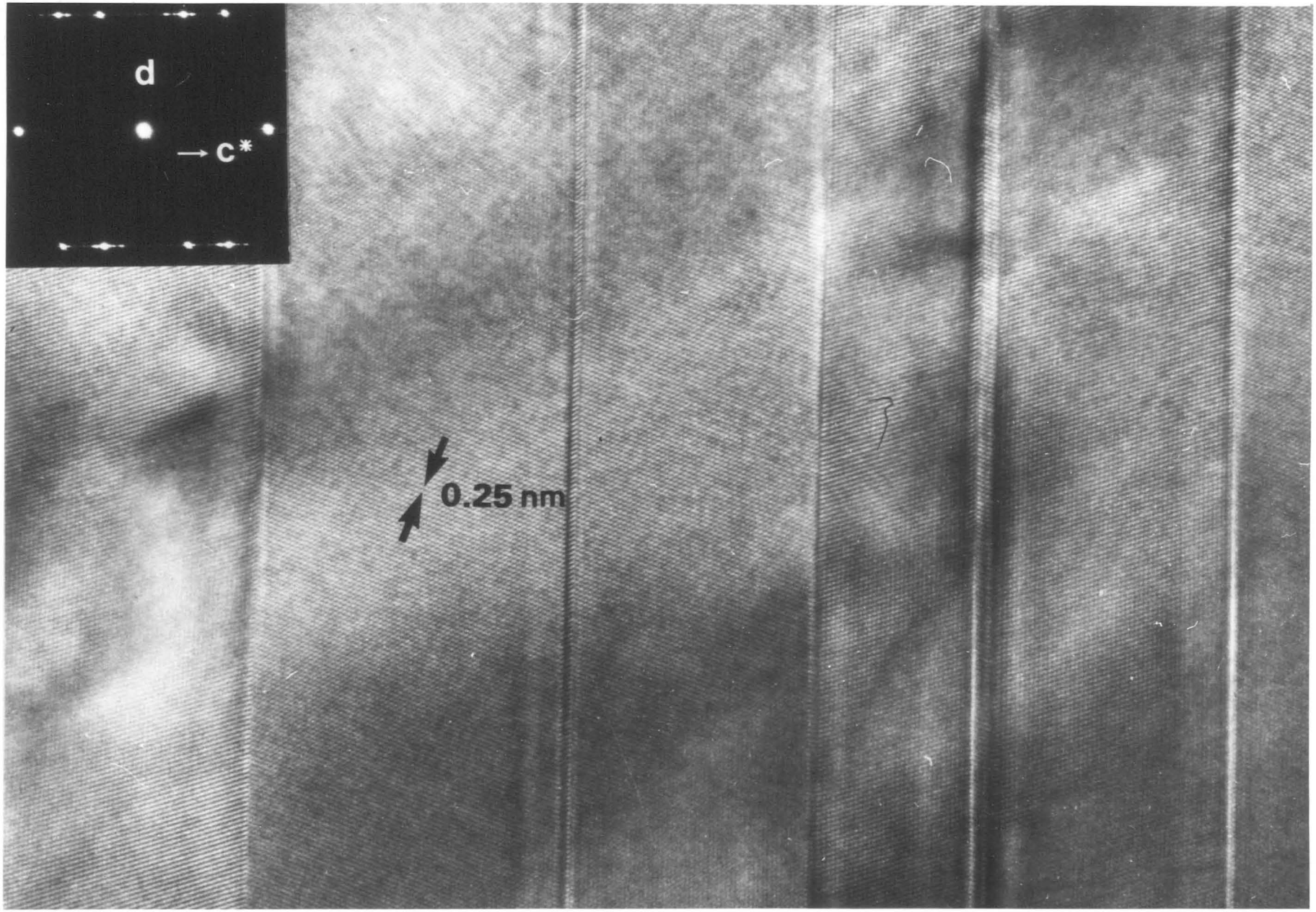
d
c*
0.25 nm

Figure VIII.27

Tilted illumination lattice fringe image showing an α-SiC lamella sandwiched between 3C regions. A unit cell of 15R stacking sequence $(3,2)_3$ and several unit cells of 4H (2,2) can be identified.

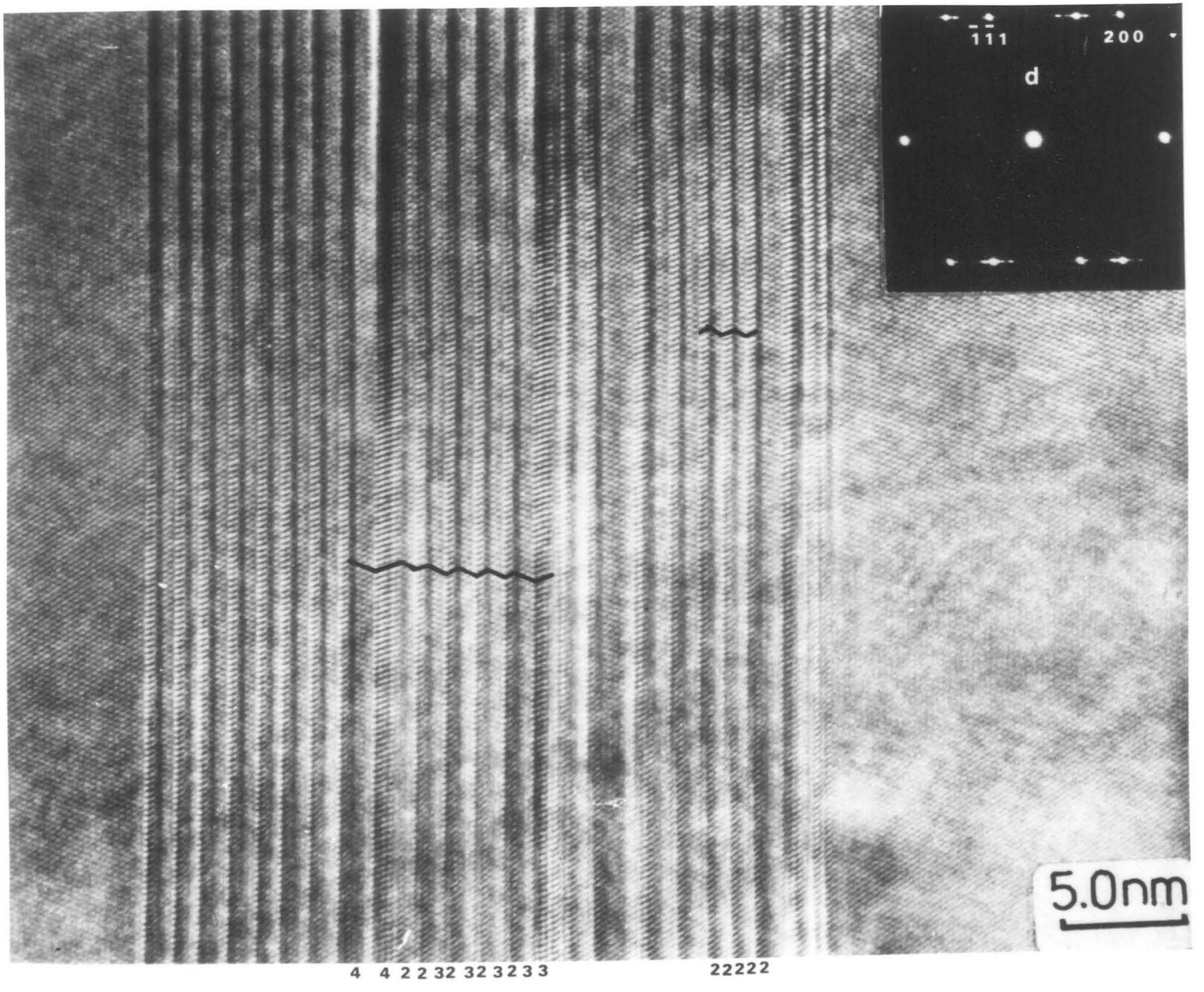
111
200
d
5.0nm
4 4 2 2 32 32 3 2 3 3
22222

of hexagonal material, sandwiched between the matrix and the twin. The stacking sequence across the region is determined and is shown in Figure VIII.27. Single unit cells of 15R, stacking sequence $(32)_3$, and 6H (3,3), as well as several unit cells of 4H (2,2), can be distinguished.

The frequent observation of α lamellae at coherent twin boundaries in these 3C crystals suggests the initial stages of a further transformation to 6H or 15R, both of which have higher temperature stability regions. Ogbuji et al. (1981a) observed a similar preferential nucleation of α at 3C twin boundaries and suggest that the stacking sequence at a coherent twin boundary is an incipient α nucleus. This can be understood from Figure VIII.28; the twin boundary is arrowed and the stacking sequence combinations which are representative of a particular polytype are listed. Thus, as a consequence of the change in stacking sequence across a 3C twin boundary, nuclei for other hexagonal and rhombohedral polytpes are created.

VIII.7 Conclusions

High resolution electron microscopy shows that SiC-AlN alloys are not as homogeneous as indicated by X-ray analysis but consist partly of well ordered material and partly of highly disordered crystals, which do not contribute to the X-ray diffraction patterns. Crystals of pure 2H have been identified using HREM, as have intergrowth structures containing both 2H and 3C. The transformation 2H→3C, is studied by HREM for the first time and changes in the stacking sequence of individual layers have been identified. The transformation is thought to occur by the diffusion-controlled layer-displacement mechanism outlined by Pandey & Krishna (1973).

Figure VIII.28

Diagrammatic representation of stacking sequence across a coherent twin boundary

...A B C A B C A C B A C B..

1 2 3 4 5 6 7 8

Layers: 1-7 6H(33)

1-6 15R(32)

2-7 15R(23)

2-6 4H(22)

1-8 21R(34)

(Ogbuji et al., 1981)

IX GENERAL CONCLUSIONS AND SUGGESTIONS FOR FURTHER WORK

The present work has confirmed that α'-sialons have structures based on α-Si_3N_4 with a general unit-cell formula $M_x(Si,Al)_{12}(O,N)_{16}$ where a maximum of two metal atoms (M; $x \leqslant 2$) occupy the interstices in the structure. The expansion of the unit cell accompanying the incorporation of M atoms is due mainly to the substitution of silicon by aluminium.

The 2H polytype of SiC has been prepared at 1650°C by the reaction of Si_3N_4 and C in the presence of a Ca-containing liquid phase and is stabilized relative to 3C by combination with up to 12 a/o nitrogen. This high level of nitrogen substitution is approximately ten times that observed previously and is achieved by the novel method of preparation from Si_3N_4.

Decreases in the unit-cell dimensions of both the 2H and 3C polytypes are due to the nitrogen substitution. In nitrogen 2H the transformation to 3C begins at ~1900°C, i.e. about 300°C above the normal transformation temperature and the transition to the cubic structure occurs with the loss of nitrogen and a corresponding increase in cell dimensions. It is thought that the ability to dissolve nitrogen plays an important part in polytype stabilization and in particular it is proposed that 6H is unable to accommodate nitrogen and consequently has never been observed in the current work. However, further experiments are required to substantiate any relationship between polytype stability and nitrogen content.

Alloying 2H-SiC with AlN via the reaction of Si_3N_4, AlN, C and CaO at 1800°C has produced a solid solution series isostructural with the two end members and with a miscibility gap extending from ∿40 to ∿84m/o AlN at 1800°C; this does not contract appreciably at higher temperatures. SiC-AlN alloys on annealing at 2100°C transform to a 3C structure which contains between 10 and 20m/o AlN. At still higher temperatures, transformation to other polytypes might occur as in the case of SiC and this would be an interesting area for future research.

Scanning electron microscopy coupled with chemical analysis shows that SiC alloyed with nitrogen and/or aluminium is inhomogeneous in both microstructure and, in some cases composition, but after post-preparative heat-treatment specimens appear homogeneous. The transformation 2H→3C is accompanied by decomposition of needle shaped crystals and the growth of large highly faceted crystals. Lattice images show that 2H→3C transformation in nitrogen-2H-SiC and in SiC-AlN alloys takes place by a layer-displacement mechanism through a disordered intermediate stage before the nucleation of stacking faults results in the new ordered arrangement.

APPENDIX 1

In the calculation of "$\underline{a}_{cubic}$" parameters from the hexagonal 2H unit-cell, the distance of closest approach of like atoms in the wurtzite-type structure is equal to the $\underline{a}_{hex}$ dimension; see Figure A.1(b), whereas in a f.c.c. zinc blend structure the same atoms touch across the face diagonal as shown in Figure A.1(a). Thus the $\underline{a}_{hex}$ and $\underline{a}_{cubic}$ parameters are related by:

$$\underline{a}_{cubic} = \underline{a}_{hex} \times \sqrt{2} \qquad \ldots A.1$$

Also, the atom at position (2/3, 1/3, 1/2) in the wurtzite unit-cell touches like atoms in the basal plane as shown in Figure A.1(c). Another estimate for "$\underline{a}_{cubic}$" can therefore be calculated from both the $\underline{a}_{hex}$ and $\underline{c}_{hex}$ parameters according to the equation:

$$\underline{a}_{cubic} = \left[\left(\frac{\underline{c}_{hex}}{2} \right)^2 + \left(\frac{\underline{a}_{hex}}{\sqrt{3}} \right)^2 \right]^{\frac{1}{2}} \times \sqrt{2} \qquad \ldots A.2$$

The final "$\underline{a}_{cubic}$" was taken as an average of the two values obtained from equations A.1 and A.2.

Figure A.1

Calculation of '$\underline{a}_{cubic}$' from

the wurtzite $\underline{a}$ and $\underline{c}$ parameters

(a)

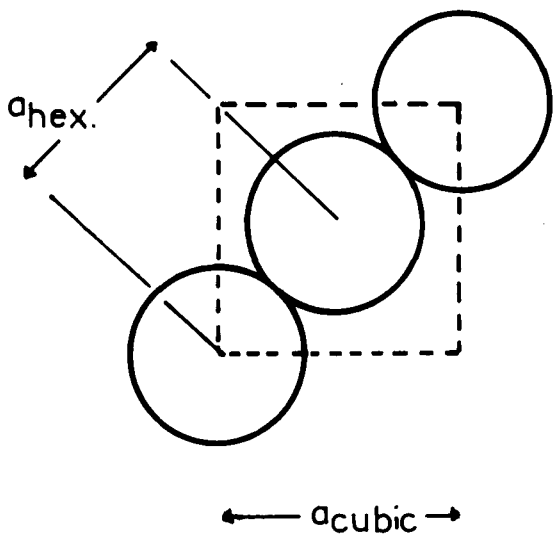

Projection down
[110]

(b)

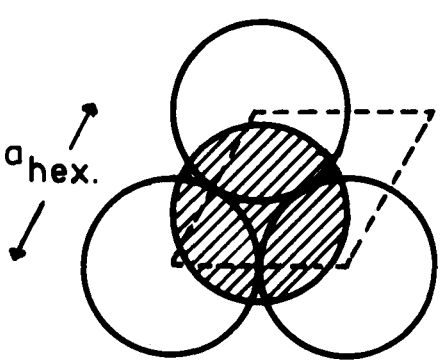

Projection down
[001]

(c)

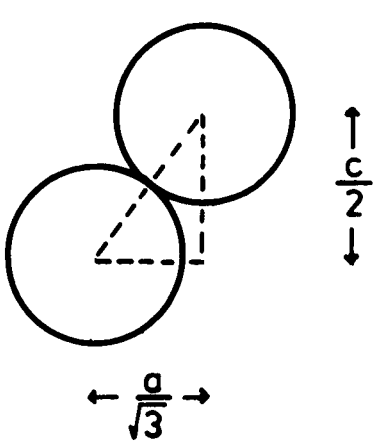

Projection down
[110]

REFERENCES

Acheson, E.G., 1892, Brit. Pat. 17,911.

Adamsky, R.F. & Merz, K.M., 1959, Z. Krist., 111, 350.

Addamiano, A.& Staikoff, L.S., 1965, J.Phys. Chem. Solids, 26, 669.

Amato, I., Mortorana, D. & Rossi, M., 1975, Powder Met., 18, 339.

Ashworth, D.R., 1969, J. Brit. Ceram. Soc., 6, 70.

Batha, H.D. & Hardy, L.H., 1973, "Silicon Carbide - 1973", Proc. III Int. Conf. 1973, 198,(Ed. Marshall R.C., Faust, Jr., J.W. & Ryan, C.E.) University South Carolina Press.

Bauer, J., Fiala, J. & Hrichova, R., 1963, Am. Min., 48, 620.

Baumhauer, H.,1912, Z. Krist., 50, 33.

Berzelius, J.J., 1824, Ann. Phys. Leipzig. 1, 169.

Bird, J.M., 1978, Mat. Res. Bull., 13, 91.

Bobrievich, A.P., Kalyuzhnyi, V.A. & Smirnov, G.I., 1957, Proc. Acad. Sci. USSR Sect. Geol. Sci., 115, 757

Bootsma, G.A., Knippenberg, W.F. & Verspui, G., 1971, J. Cryst. Growth, 8, 341.

Buang, K.B., 1979, Ph.D. Thesis, University of Newcastle upon Tyne.

Carrol, P., 1960, "Silicon Carbide - 1960", 1959 Conf. Proc. (eds. O'Connor, J.R. & Smittens, J.) Permagon Press, New York.

Colquhoun, I., Wild, S., Grieveson, P. & Jack, K.H., 1973, Proc. Brit. Ceram. Soc., 22, 207.

Cowless, A.H. & Cowless, E.H., 1885, U.S. Pat. 319,945.

Cowley, J.M. & Moodie, A.F., 1957a-c, Proc. Phys. Soc., 70, 486, 497, 505.

Cowley, J M. & Moodie, A.F., 1957d, Proc. Phys. Soc., 76, 378.

Cutler, I.B., 1978, Personal Communication to Prof. K. H. Jack.

Cutler, I.B., Miller, P.D., Rafaniello, W., Park, H.K., Thompson, D. P. & Jack, K.H., 1978, Nature, 275, 434.

Deville, H. & Wohler, F., 1857, Liebigs Ann., 104, 256.

Dubey, M.& Singh, G., 1977, Acta. Cryst., A33, 276.

Dubey, M. & Singh, G., 1978, Acta. Cryst., A34, 116.

Feld, H., Ettmayer, P., & Petzehauser, I., 1974, Ber. Dtsch. Keram. Ges., 51, 127.

Foster, L.M., Long, G.& Hunter, M.S., 1956, J. Am. Ceram. Soc., 39, 1.

Frank, F.C., 1951, Phil. Mag., 42, 1014.

Garvon, J.R. & Tilley, R.J.D., 1976, J. Microsc., 106, 59.

Gaukler, L.J., Lukas, H.L. & Petzow, G., 1975, J. Am. Ceram. Soc., 58, 347.

Goeuriot, P., Torre, J.P. & Demit, J., 1977, Paper presented at 3 ième Journées d'Etudes sur les Nitrures, Fontainbleau, June.

Gribkov, V.N., Silaev, V.A., Shchetanov, B.V., Umantsev, E.L. & Isaikin, A.S., 1972, Sov. Phys. Cryst., 825.

Grinton, G.R. & Cowley, J.M., 1971, Optik, 34, 221.

Hampshire, S., 1977, Progress Report Crystallography Laboratory, University Newcastle upon Tyne.

Hampshire, S., 1980, Ph.D. Thesis, University of Newcastle upon Tyne.

Hampshire, S., Park, H.K., Thompson, D.P. & Jack, K.H., 1978, Nature, 274, 880.

Hardie, D. & Jack, K.H., 1957, Nature, 180, 332.

Hendry, A., 1975, "Nitrogen Ceramics", 183 (ed. Riley, F.L.) Proc. NATO Adv. Study Inst., E23, Noordhoff, (Leyden).

Hendry, A., Perera, D.S., Thompson, D.P. & Jack, K.H., 1975, "Special Ceramics 6", (ed. Popper, P.) Brit. Ceram. Res. Assn. (Stoke on Trent).

Heuer, A.H., Fryburg, G.A., Ogbuji, T.E., Mitchell, T.E. & Shinozaki, S., 1978, J. Am. Ceram. Soc. 61, 406.

Hull, A.W., 1919, Phys. Rev., 13, 292.

Hull, A.W., 1920, Phys. Rev., 15, 545.

Inomata, Y. & Inoue, Z., 1970, Yogyo-Kyokai-Shi, 78, 133.

Inomata, Y., Inoue, Z. & Kijima, K., 1969a, Yogyo-Kyokai-Shi, 77, 313.

Inomata, Y., Inoue, Z., Mitomo, M. & Tanaka, H., 1969b, Yogyo-Kyokai-Shi, 77, 83.

Inomata, Y., Mitomo, M., Inoue, Z. & Tanaka, H., 1969c, Yogyo-Kyokai-Shi, 77, 130.

Jack, K.H., 1976, J. Mat. Sci., 11, 1135.

Jack, K.H. & Wilson, W.I., 1972, Nature, 231, 28.

Jagodzinski, H., 1949, Acta. Cryst., 2, 201 & 298.

Jagodzinski, H., 1954, Acta. Cryst., 8, 279.

Jagodzinski, H., 1971, Kristallografiya, 16, 1235.

Jama, S.A.B., Thompson, D.P. & Jack, K.H., 1975, "Special Ceramics 6", (Ed. Popper, P.) Brit. Ceram. Res. Assn., (Stoke on Trent).

Jänecke, E., 1907, Z. Inorg. Chem., 53, 319.

Jennings, H.M. & Richman, M.H., 1976, J. Mat. Sci., 11, 2087.

Jepps, N.W., 1979, Ph.D. Thesis, University of Cambridge.

Jepps, N.W. & Page, T.F., 1979, J. Microsc., 116, 159.

Jepps, N.W., & Page, T.F., 1980, J. Microsc., 119, 177.

Jepps, N.W. Smith, D.J. & Page, T.F., 1979, Acta. Cryst., A35, 916.

Kamm, R., Steinberg, M.A., Y Wuff, J., 1949, Trans. A.I.M.E., 180, 694.

Kato, K., Inowe, Z., Kijima, K., Kawada, H. & Yamane, T., 1975, J. Am. Ceram. Soc., 58, 90.

Kieffer, A., Ettmayer, P., Gugel, E. & Schmidt, A., 1969, Mat. Res. Bull., 4, 3153.

Kijima, K., Kato, K., Inowe, A & Tanaka, H., 1975, J. Mat. Sci., 10, 362.

Knippenberg, W.F., 1963, Philips Research Reports, 18, 161.

Knippenberg, W.F. & Verspui, G., 1968, Mat. Res. Bull., 4, S33.

Knippenberg, W.F. & Verspui, G., 1973, "Silicon Carbide-1973", Proc. III. Int. Conf., 1973, 108, (Ed. Marshall, R.C., Faust, Jr., J.W. & Ryan, C.E.) University South Carolina Press.

Komeya, K. & Inoue, H., 1975, J. Mat. Sci., 10, 1243.

Korgul, P. & Thompson, D.P., 1982, Personal communication.

Krishna, P. & Marshall, R.C., 1971a, J. Cryst. Growth, 11, 147.

Krishna, P. & Marshall, R.C., 1971b, J. Cryst. Growth, 9, 319.

Krishna, P., Marshall, R.C. & Ryan, C.E., 1971, J. Cryst. Growth, 8, 129.

Kroko, L.J. & Milnes, A.G., 1966, Sol. Stat. Electron., 9, 1125.

Kuo, C.L., Zitou, J., Ye, H.Q. & Kuo, K.H., 1982, J. Appl. Cryst. 15, 199.

Landuyt, Van J. & Amelinckx, S., 1971, Mat. Res. Bull., 6, 613.

Laurent, Y., Lang, J. & Bihan, M.T.L., 1968, Acta. Cryst., B24, 494.

Lee, J.G. & Cutler, I.B., 1975, Am. Cerem. Soc. Bull., 54, 195.

Lee, J.G. & Cutler, I.B., 1977, "Nitrogen Ceramics", 175, (ed. Riley, F.L.) Proc. NATO Adv. Study Inst., E23, Noordhoff, (Leyden).

Lilov, S.K., Tairov, Yu, M., Tsvetkov, V.F. & Chernov, M.A., 1976, Phys. Stat. Sol., 37, 143.

Lumby, R.J., North, B. & Taylor, A.J., 1975, "Special Ceramics 6", 283, (ed. Popper, P.) Brit. Ceram. Res. Assn., (Stoke on Trent).

Lundquist, D., 1948, Acta. Chem. Scand., 2, 177.

Martin, S., 1979, Ph.D. Thesis, University of Cambridge.

Masaki, H., Oyama, Y. & Kamigaito, O., 1975, Japan. J. Appl. Phys., 14, 301.

Merz, K.M., 1959, "Silicon Carbide - 1960", 1959 Conf. Proc., 73, (eds. O'Connor, J.R. & Smittens, J.) Pergamon Press, New York.

Mitchell, R.S., 1957, Z. Krist., 109, 1.

Mitchell, T.E., Ogbuji, L.U. & Heuer, A.H., 1978, J. Am. Ceram. Soc., 61, 412.

Mitomo, M., 1977, Yogyo-Kyokai-Shi, 85, 50.

Mitomo, M., Inomata, Y. & Kumanomido, M., 1970, Yogyo-Kyokai-Shi, 78, 18.

Mitomo, M., Inomata, Y. & Tanaka, H., 1971, Mat. Res. Bull., 6, 759.

Moissan, H., 1905, Compt. Rend., 140, 405.

Murata, Y. & Smoak, R.H., 1978, Proceedings of International Symposium of Factors in Densification and Sintering of Oxide and Non-Oxide Ceramics, 382, Japan.

Ogbuji, L.U., Mitchell, T.E. & Heuer, A.H., 1981a, J. Am. Ceram. Soc., 64, 91.

Ogbuji, L.U., Mitchell, T.E., Heuer, A.H. & Shinozaki, S., 1981b, J. Am. Ceram. Soc., 64, 100.

Ott, H., 1925a, Z. Krist., 61, 515.

Ott, H., 1925b, Naturwissenschaften, 13, 76.

Oyama, V. & Kamigaito, O., 1971, Jap. J. Appl. Phys., 10, 1637.

Pandey, D. & Krishna, P., 1973, "Silicon Carbide - 1973", Proc. III, Int. Conf. on Silicon Carbide, Florida, 198, (eds. Marshall, R.C., Faust, Jr., J.W., & Ryan, C.E.) University of South Carolina Press.

Pandey, D. & Krishna, P., 1975, Mat. Sci. Eng., 20, 243.

Pandey, D. & Krishna, P., 1976, Mat. Sci. Eng., 26, 53.

Pandey, D., Lele, S. & Krishna, P., 1980, Proc. R. Soc. Lond., A369, 463.

Park, H.K., 1977 & 1978, Progress Report, Crystallography Laboratory, University of Newcastle upon Tyne.

Peibst, H., 1963, Z. Physik, Chem., 223, 193.

Perara, D.S., 1976, Ph.D. Thesis, University of Newcastle upon Tyne.

Powell, J.A. & Will, H.A., 1972, J. Appl. Phys. 43, 1400.

Prochazka, S., 1973, Sintering of Silicon Carbide, General Electric Company, Corporate Research & Development, Schenectady, New York, Report No. 73CRD325.

Prochazka, S., Johnson, C.A. & Giddings, R.A., 1978, Proc. Int. Sym. Factors in Densification & Sintering of Oxide and Non-Oxide Ceramics, 366, Japan.

Rafaniello, W., Cho, K. & Virkar, A.V., 1981, J. Mat. Sci. 16, 3479.

Rafaniello, W., Plichta, M.R., & Virkar, A.V., 1983, J. Am. Ceram. Soc. 66, 272.

Ramsdell, L.S., 1945, Am. Min., 30, 519.

Ramsdell, L.S., 1947, Am. Min.,32, 64.

Regis, A.J. & Sand, L.B., 1958, Bull. Geol. Soc. Am., 69, 1633.

Roebuck, P. & Thompson, D.P., 1977, "High Temperature Chemistry of Inorganic & Ceramic Materials", 222, (eds. Glasser, F.P. & Potter, R.E.) The Chemical Soc., London.

Ruh, R. & Zangvil, A., 1982, J. Am. Ceram. Soc., 65, 260.

Ruska, J., Gauckler, L.I., Lorenz, J. & Rexer, H.U., 1979, J. Mat. Sci., 14, 2013.

Sas, W.H. & De Wolff, P.M., 1966, Acta. Cryst., 21, 826.

Sato, H. & Shinozaki, S., 1974a, Mat. Res. Bull., 9, 679.

Sato, H., Shinozaki, S. & Yessik, M., 1974, J. Appl. Phys., 45, 1630.

Sato, H. & Shinozaki, S., 1975, Mat. Res. Bull., 10, 257.

Schneer, C.J., 1955, Acta. Cryst., 8, 279.

Schutzenberger, P. & Colson, A., 1881, Compt. Rend., 92, 1508.

Shaffer, P.T.B., 1969a, Mat. Res. Bull., 4, S97.

Shaffer, P.T.B., 1969b, Mat. Res. Bull., 4, 213.

Shaffer, P.T.B., 1969c, Mat. Res. Bull., 4, S13.

Shinozaki, S. & Kinsman, K.R., 1978, Acta. Met., 26. 769.

Sheldrick, G., 1975, "SHELX - a program for crystal structure determination". Unpublished work.

Siddiqui, S.A., 1980, MSc. Thesis, University of Newcastle upon Tyne.

Singh, S.R. & Singh, G., 1980, Acta. Cryst., 36, 779.

Singh, S.R. & Singh, G., 1981, Bull. Mat. Sci., 3, 235.

Skarnulis, A.J., 1976, Ph.D. Thesis, Arizona State University.

Slack, G.A. & Scace, R.I., 1965, J. Chem. Phys., 42, 805.

Smith, D.J., Jepps, N.W. & Page, T.F., 1978, J. Microsc., 114, 1.

Sokhov, M.I. & Glukhov, V.P., 1965, Soc. Phys. Cryst., 10, 341.

Szweda, A., 1980, Ph.D. Thesis, University of Newcastle upon Tyne.

Tagai, T., Sueno, S. & Sadanaga, R., 1971, Mineral.J., 6, 240.

Tairov, Yu. M. & Tsvetkov, V.F., 1981, J. Cryst. Crowth, 52, 146.

Tajima, Yo & Kingery, W.D., 1982, J. Am. Ceram. Soc., C-27.

Taylor, A. & Laidler, D.S., 1950, Brit. J. Appl. Phys., 1, 174.

Taylor, A., 1951, J. Sci. Instr., 28, 200.

Thibault, N.W., 1944, Am. Min. 29, 249.

Thompson, D.P., 1974, Progress Report, Crystallography Laboratory, University of Newcastle upon Tyne.

Thompson, D.P., 1977, J. Mat. Sci., 12, 2344.

Thompson, D.P., 1978, Progress Report, Crystallography Laboratory, University of Newcastle Upon Tyne.

Trigunayat, G.C., & Chadha, G.K., 1971, Phys. Stat. Sol. 4, 9.

Tsukuma, K., Shimada, M. & Koizumi, M., 1982, J. Mat. Sci., Letters, 1, 9.

Verma, A.R., 1951a, Phil. Mag., 42, 1005.

Verma, A.R., 1951b, Nature, 167, 939.

Verma, A.R. & Krishna, P., 1966, "Polymorphism and Polytypism in Crystals", Wiley, New York.

Vodakov, Yu. A. & Mokhov, E.N., 1973, "Silicon Carbide 508 - 1973", Proc. III, Int. Conf. on Silicon Carbide, Florida, (eds. Marshall, R.C., Faust, Jr., J.W. & Ryan, C.E.) University of South Carolina Press.

Wild, S., Grieveson, P & Jack, K.H., 1972a, "Special Ceramics 5", 385, (ed. Popper, P.) Brit. Ceram. Res. Assn., (Stoke on Trent).

Wild, S., Grieveson, P. & Jack, K.H., 1972b, "Special Ceramics 5", 271, (ed. Popper, P.) Brit. Ceram. Res. Assn., (Stoke on Trent).

Woodbury, H.H. & Ludwig, G.W., 1961, Phys. Rev., 124, 1083.

Wyckoff, R.W.G., 1948, "Crystal Structures", 1, Interscience Publishers, New York.